

The automated computation of tree-level and next-to-leading order differential cross sections, and their matching to parton shower simulations

J. Alwall^a, R. Frederix^b, S. Frixione^b, V. Hirschi^c, F. Maltoni^d, O. Mattelaer^d,
H.-S. Shao^e, T. Stelzer^f, P. Torrielli^g, M. Zaro^{hi}

^a *Department of Physics, National Taiwan University, Taipei 10617, Taiwan*

^b *PH Department, TH Unit, CERN, CH-1211 Geneva 23, Switzerland*

^c *SLAC National Accelerator Laboratory, 2575 Sand Hill Road,
Menlo Park, CA 94025-7090 USA*

^d *CP3, Université Catholique de Louvain, B-1348 Louvain-la-Neuve, Belgium*

^e *Department of Physics and State Key Laboratory of Nuclear Physics and Technology,
Peking University, Beijing 100871, China*

^f *University of Illinois, Urbana, IL 61801-3080, USA*

^g *Physik-Institut, Universität Zürich, Winterthurerstrasse 190, 8057 Zurich, Switzerland*

^h *Sorbonne Universités, UPMC Univ. Paris 06, UMR 7589, LPTHE,
F-75005, Paris, France*

ⁱ *CNRS, UMR 7589, LPTHE, F-75005, Paris, France*

ABSTRACT: We discuss the theoretical bases that underpin the automation of the computations of tree-level and next-to-leading order cross sections, of their matching to parton shower simulations, and of the merging of matched samples that differ by light-parton multiplicities. We present a computer program, MADGRAPH5_AMC@NLO, capable of handling all these computations – parton-level fixed order, shower-matched, merged – in a unified framework whose defining features are flexibility, high level of parallelisation, and human intervention limited to input physics quantities. We demonstrate the potential of the program by presenting selected phenomenological applications relevant to the LHC and to a 1-TeV e^+e^- collider. While next-to-leading order results are restricted to QCD corrections to SM processes in the first public version, we show that from the user viewpoint no changes have to be expected in the case of corrections due to any given renormalisable Lagrangian, and that the implementation of these are well under way.

KEYWORDS: QCD, NLO Computations, Automation.

Contents

1. Introduction	2
2. Theoretical bases and recent progress	4
2.1 Methodology of computation	5
2.2 General features for SM and BSM physics	6
2.2.1 Complex mass scheme	7
2.2.2 BSM-specific capabilities	8
2.3 LO computations	9
2.3.1 Generation of tree-level matrix elements	10
2.3.2 Width calculator	12
2.3.3 Event reweighting	13
2.3.4 Tree-level merging	16
2.4 NLO computations	18
2.4.1 NLO cross sections and FKS subtraction: MadFKS	22
2.4.2 One-loop matrix elements: MadLoop	27
2.4.3 Integration of one-loop contributions	40
2.4.4 Matching to showers: MC@NLO	44
2.4.5 Merging samples at the NLO: FxFx	52
2.5 Spin correlations: MadSpin	57
3. How to perform a computation	61
3.1 LO-type generation and running	62
3.2 NLO-type generation and running	64
3.2.1 (N)LO+PS results	66
3.2.2 f(N)LO results	69
3.3 Possibilities for LO simulations	71
4. Illustrative results	72
4.1 Total cross sections	72
4.2 Differential distributions	85
4.3 One-loop SM and BSM results: a look ahead	103
5. Conclusions and outlook	109
A. Technical prerequisites, setup, and structure	112

B. Advanced usage	116
B.1 Models, basic commands, and extended options	116
B.2 Setting the hard scales at the NLO	122
B.3 Scale and PDF uncertainties: the NLO case	124
B.4 Scale and PDF uncertainties: the LO case	128
B.5 Other LO reweighting applications	129
B.6 Output formats and standalone libraries	130
C. Features of one-loop computations	131
C.1 TIR and IREGI	131
C.2 Quantitative profile of MadLoop performances	133
C.3 Computation of the integrand polynomial coefficients	135
D. Third-party codes included in MADGRAPH5_AMC@NLO	137

1. Introduction

Quantum Chromo Dynamics is more than forty years old [1, 2], and perturbative calculations of observables beyond the leading order are almost as old, as is clearly documented in several pioneering works (see e.g. refs. [3–9]), where the implications of asymptotic freedom had been quickly understood. The primary motivation for such early works was a theoretical one, stemming from the distinctive features of QCD (in particular, the involved infrared structure, and the fact that its asymptotic states are not physical), which imply the need of several concepts (such as infrared safety, hadron-parton duality, and the factorisation of universal long-distance effects) that come to rescue, and supplement, perturbation theory. On the other hand, the phenomenological necessity of taking higher-order effects into account was also acknowledged quite rapidly, in view of the structure of jet events in e^+e^- collisions and of the extraction of α_s from data.

Despite this very early start, the task of computing observables beyond the Born level in QCD has remained, until very recently, a highly non-trivial affair: the complexity of the problem, due to both the calculations of the (tree and loop) matrix elements and the need of cancelling the infrared singularities arising from them, has generated a very significant theoretical activity by a numerous community. More often than not, different cases (observables and/or processes) have been tackled in different manners, with the introduction of ad-hoc solutions. This situation has been satisfactory for a long while, given that beyond-Born results are necessary only when precision is key (and, to a lesser extent, when large K factors are relevant), and when many hard and well-separated jets are crucial for the definition of a signature; these conditions have characterized just a handful of cases in the past, especially in hadronic collisions (e.g., the production of single vector bosons, jet pairs, or heavy quark pairs).

The advent of the LHC has radically changed the picture since, in a still relatively short running time, it has essentially turned hadronic physics into a high-precision domain, and one where events turning up in large- p_T tails are in fact not so rare, in spite of being characterised by small probabilities. Furthermore, the absence so far of clear signals of physics beyond the Standard Model implies an increased dependence of discovery strategies upon theoretical predictions for known phenomena. These two facts show that presently the phenomenological motivations are extremely strong for higher-order and multi-leg computations of all observables of relevance to LHC analyses.

While a general solution is not known for the problem of computing exactly the perturbative expansion for any observable up to an arbitrarily large order in α_s , if one restricts oneself to the case of the first order beyond the Born one (next-to-leading order, NLO henceforth), then such a solution does actually exist; in other words, there is no need for ad-hoc strategies, regardless of the complexity of the process under study. This remarkable fact results from two equally important theoretical achievements. Namely, a universal formalism for the cancellation of infrared singularities [10–14], and a technique for the algorithmic evaluation of renormalised one-loop amplitudes [15–23], both of which must work in a process- and observable independent manner. At the NLO (as opposed to the NNLO and beyond) there is the further advantage that fixed-order computations can be matched to parton-shower event generators (with either the MC@NLO [24] or the POWHEG [25] method – see also refs. [26–35] for early, less-developed, or newer related approaches), thus enlarging immensely the scope of the former, and increasing significantly the predictive power of the latter.

It is important to stress that while so far we have explicitly considered the case of QCD corrections, the basic theoretical ideas at the core of the subtraction of infrared singularities, of the computation of one-loop matrix elements, and of the matching to parton showers will require no, or minimal, changes in the context of other renormalisable theories, QCD being essentially a worst-case scenario. This is evidently true for tree-level multi-leg computations, as is proven by the flexibility and generality of tools such as MADGRAPH5 [36], that is able to deal with basically any user-defined Lagrangian.

In summary, there are both the phenomenological motivations and the theoretical understanding for setting up a general framework for the computation of (any number of) arbitrary observables in an arbitrary process at the tree level or at the NLO, with or without the matching to parton showers. We believe that the most effective way of achieving this goal is that of automating the whole procedure, whose technological challenges can be tackled with high-level computer languages capable of dealing with abstract concepts, and which are readily available.

The aim of this paper is that of showing that the programme sketched above has been realised, in the form of a fully automated and public computer code, dubbed MADGRAPH5_AMC@NLO. As the name suggests, such a code merges in a unique framework all the features of MADGRAPH5 and of AMC@NLO, and thus supersedes both of them (and must be used in their place). It also includes several new capabilities that were not available in these codes, most notably those relevant to the merging of event samples with different light-parton multiplicities. We point out that MADGRAPH5_AMC@NLO contains

all ingredients (the very few external dependencies that are needed are included in the package) that are necessary to perform an NLO, possibly plus shower (with the MC@NLO formalism), computation: it thus is the first public (since Dec. 16th, 2013) code, and so far also the only one, with these characteristics. Particular attention has been devoted to the fact that calculations must be doable by someone who is not familiar with Quantum Field Theories, and specifically with QCD. We also show, in general as well as with explicit examples, how the construction of our framework lends itself naturally to its extension to NLO corrections in theories other than QCD, in keeping with the fact that such a flexibility is one of the standard features of the tree-level computations which were so far performed by MADGRAPH, and that has been inherited by MADGRAPH5_AMC@NLO.

It is perhaps superfluous to point out that approaches to automated computations constitute a field of research which has a long history, but which has had an exponential growth in the past few years, out of the necessities and possibilities outlined above. The number of codes which have been developed, either restricted to leading order (LO henceforth) predictions [36–51], or including NLO capabilities [52–79] is truly staggering. The level of automation and the physics scope of such codes, not to mention other, perhaps less crucial, characteristics, is extremely diverse, and we shall make no attempt to review this matter here.

We have organized this paper as follows. In sect. 2, we review the theoretical bases of our work, and discuss new features relevant to future developments. In sect. 3 we explain how computations are performed. Section 4 presents some illustrative results, relevant to a variety of situations: total cross sections at the LHC and future e^+e^- colliders, differential distributions in pp collisions, and benchmark one-loop pointwise predictions, in the Standard Model and beyond. We finally conclude in sect. 5. Some technicalities are reported in appendices A to D.

2. Theoretical bases and recent progress

At the core of MADGRAPH5_AMC@NLO lies the capability of computing tree-level and one-loop amplitudes for arbitrary processes. Such computations are then used to predict physical observables with different perturbative accuracies and final-state descriptions. Since there are quite a few possibilities, we list them explicitly here, roughly in order of increasing complexity, and we give them short names that will render their identification unambiguous in what follows.

1. fLO: this is a tree- and parton-level computation, where the exponents of the coupling constants are the smallest for which a scattering amplitude is non zero. No shower is involved, and observables are reconstructed by means of the very particles that appear in the matrix elements.
2. fnLO: the same as fLO, except for the fact that the perturbative accuracy is the NLO one. As such, the computation will involve both tree-level and one-loop matrix elements.

3. LO+PS: uses the matrix elements of an fLO computation, but matches them to parton showers. Therefore, the observables will have to be reconstructed by using the particles that emerge from the Monte Carlo simulation.
4. NLO+PS: same as LO+PS, except for the fact that the underlying computation is an NLO rather than an LO one. In this paper, the matching of the NLO matrix elements with parton showers is done according to the MC@NLO formalism.
5. MLM-merged: combines several LO+PS samples, which differ by final-state multiplicities (at the matrix-element level). In our framework, two different approaches, called k_T -jet and shower- k_T schemes, may be employed.
6. FxFx-merged: combines several NLO+PS samples, which differ by final-state multiplicities.

We would like to stress the fact that having all of these different simulation possibilities embedded in a single, process-independent framework allows one to investigate multiple scenarios while being guaranteed of their mutual consistency (including that of the physical parameters such as coupling and masses), and while keeping the technicalities to a minimum (since the majority of them are common to all types of simulations). For example, one may want to study the impact of perturbative corrections with (NLO+PS vs LO+PS) or without (fNLO vs fLO) the inclusion of a parton shower. Or to assess the effects of the showers at the LO (LO+PS vs fLO) and at the NLO (NLO+PS vs fNLO). Or to check how the inclusion of different-multiplicity matrix elements can improve the predictions based on a fixed-multiplicity underlying computation, at the LO (MLM-merged vs LO+PS) and at the NLO (FxFx-merged vs NLO+PS).

In the remainder of this section we shall review the theoretical ideas that constitute the bases of the computations listed above in items 1–6. Since such a background is immense, we shall sketch the main characteristics in the briefest possible manner, and rather discuss recent advancements that have not yet been published.

2.1 Methodology of computation

The central idea of MADGRAPH5_AMC@NLO is the same as that of the MADGRAPH family. Namely, that the *structure* of a cross section, regardless of the theory under consideration and of the perturbative order, is essentially independent of the process, and as such it can be written in a computer code once and for all. For example, phase spaces can be defined in full generality, leaving only the particle masses and their number as free parameters (see e.g. ref. [80]). Analogously, in order to write the infrared subtractions that render an NLO cross section finite, one just needs to cover a handful of cases, which can be done in a universal manner. Conversely, matrix elements are obviously theory- and process-dependent, but can be computed starting from a very limited number of formal instructions, such as Feynman rules or recursion relations. Thus, MADGRAPH5_AMC@NLO is constructed as a meta-code, that is a (Python) code that writes a (Python, C++, Fortran) code, the latter being the one specific to the desired process. In order to do so, it needs two ingredients:

- a theory model;
- a set of process-independent building blocks.

A theory model is equivalent to the Lagrangian of the theory plus its parameters, such as couplings and masses. Currently, the method of choice for constructing the model given a Lagrangian is that of deriving its Feynman rules, that `MADGRAPH5_AMC@NLO` will eventually use to assemble the matrix elements. At the LO, such a procedure is fully automated in `FEYNRULES` [81–86]. NLO cross sections pose some extra difficulties, because Feynman rules are not sufficient for a complete calculation – one needs at least UV counterterms, possibly plus other rules necessary to carry out the reduction of one-loop amplitudes (we shall generically denote the latter by R_2 , adopting the notation of the Ossola-Papadopoulos-Pittau method [18]). These NLO-specific terms are presently not computed by `FEYNRULES`¹ and have to be supplied by hand², as was done for QCD corrections to SM processes. Therefore, while the details are unimportant here, one has to bear in mind that there are “LO” and “NLO” models to be employed in `MADGRAPH5_AMC@NLO` – the former being those that could also be adopted by `MADGRAPH5`, and the latter being the only ones that permit the user to exploit the NLO capabilities of `MADGRAPH5_AMC@NLO`.

Given a process and a model, `MADGRAPH5_AMC@NLO` will build the process-specific code (which it will then proceed to integrate, unweight, and so forth) by performing two different operations. *a)* The writing of the matrix elements, by computing Feynman diagrams in order to define the corresponding helicity amplitudes, using the rules specified by the model. *b)* Minimal editing of the process-independent building blocks. In the examples given before, this corresponds to writing definite values for particles masses and the number of particles, and to select the relevant subtraction terms, which is simply done by assigning appropriate values to particle identities. The building blocks modified in this manner will call the functions constructed in *a)*. Needless to say, these operations are performed automatically, and the user will not play any role in them.

We conclude this section by emphasising a point which should already be clear from the previous discussion to the reader familiar with recent `MADGRAPH` developments. Namely that, in keeping with the strategy introduced in `MADGRAPH5` [36], we do *not* include among the process-independent building blocks the routines associated with elementary quantities (such as vertices and currents), whose roles used to be played by the `HELAS` routines [88] in previous `MADGRAPH` versions [37, 49]. Indeed, the analogues of those routines are now automatically and dynamically created by the module `ALOHA` [89] (which is embedded in `MADGRAPH5_AMC@NLO`), which does so by gathering directly the relevant information from the model, when this is written in the Universal `FEYNRULES` Output (UFO [90]) format. See sect. 2.3.1 for more details on this matter.

2.2 General features for SM and BSM physics

Since the release of `MADGRAPH5` a significant effort, whose results are now included in

¹We expect they will in the next public version [87], since development versions exist that are already capable of doing so – see e.g. sect. 4.3.

²Note that these are a finite and typically small number of process-independent quantities.

MADGRAPH5_AMC@NLO, went into extending the flexibility of the code at both the input and the output levels. While the latter is mostly a technical development (see appendix B.6), which allows one to use different parts of the code as standalone libraries and to write them in various computer languages, the former extends the physics scope of MADGRAPH5_AMC@NLO w.r.t. that of MADGRAPH5 in several ways, and in particular for what concerns the capability of handling quantities (e.g., form factors, particles with spin larger than one, and so forth) that are relevant to BSM theories. Such an extension, to be discussed in the remainder of this section and partly in sect. 2.3.1, goes in parallel with the analogous enhanced capabilities of FEYNRULES, and focuses on models and on their use. Thus, it is an overarching theme of relevance to both LO and NLO simulations, in view of the future complete automation of the latter in theories other than the SM. Some of the topics to which significant work has been lately devoted in MADGRAPH5_AMC@NLO, and which deserve highlighting, are the following:

1. Complex mass scheme (sect. 2.2.1).
2. Support of various features, of special relevance to BSM physics (sect. 2.2.2).
3. Improvements to the FEYNRULES/UFO/ALOHA chain (sect. 2.3.1).
4. Output formats and standalone libraries (appendix B.6).
5. Feynman gauge in the SM (sect. 2.4.2).
6. Improvements to the front-end user interface (the MADGRAPH5_AMC@NLO shell – appendix A).
7. Hierarchy of couplings: models that feature more than one coupling constant order them in terms of their strengths, so that for processes with several coupling combinations at the cross section level only the assumed numerically-leading contributions will be simulated (unless the user asks otherwise) – sect. 2.4 and appendix B.1.

We would finally like to emphasise that in the case of LO computations, be they fLO, LO+PS, or merged, one can always obtain from the short-distance cross sections a set of *physical* unweighted events. The same is not true at the NLO: fNLO cross sections cannot be unweighted, and unweighted MC@NLO events are not physical if not showered. This difference explains why at the LO we often adopt the strategy of performing computations with small, self-contained modules whose inputs are Les Houches event (LHE henceforth) files [91, 92], while at the NLO this is typically not worth the effort – compare e.g. appendices B.3 and B.4, where the computation of scale and PDF uncertainties at the NLO and LO, respectively, is considered. Further examples of modules relevant to LO simulations are given in sect. 2.3.3.

2.2.1 Complex mass scheme

In a significant number of cases, the presence of unstable particles in perturbative calculations can be dealt with by using the Narrow Width Approximation (NWA)³. However,

³See sect. 2.5 for a general discussion of the NWA and of other related approaches.

when one is interested in studying either those kinematical regions that correspond to such unstable particles being very off-shell, or the production of broad resonances, or very involved final states, it is often necessary to go beyond the NWA. In such cases, one needs to perform a complete calculation, in order to take fully into account off-shell effects, spin correlations, and interference with non-resonant backgrounds in the presence of possibly large gauge cancellations. Apart from technical difficulties, the inclusion of all resonant and non-resonant diagrams does not provide one with a straightforward solution, since the (necessary) inclusion of the widths of the unstable particles – which amounts to a resummation of a specific subset of terms that appear at all orders in perturbation theory – leads, if done naively, to a violation of gauge invariance. While this problem can be evaded in several ways at the LO (see e.g. refs. [93–98]), the inclusion of NLO effects complicates things further. Currently, the most pragmatic and widely-used solution is the so-called complex mass scheme [99, 100], that basically amounts to an analytic continuation in the complex plane of the parameters that enter the SM Lagrangian, and which are related to the masses of the unstable particles. Such a scheme can be shown to maintain gauge invariance and unitarity at least at the NLO, which is precisely our goal here.

In MADGRAPH5_AMC@NLO it is possible to employ the complex mass scheme in the context of both LO and NLO simulations, by instructing the code to use a model that includes the analytical continuation mentioned above (see the **Setup** part of appendix B.1 for an explicit example). For example, at the LO this operation simply amounts to upgrading the model that describes SM physics in the following way [99]:

- The masses m_k of the unstable particles are replaced by $\sqrt{m_k^2 - im_k\Gamma_k}$.
- The EW scheme is chosen where $\alpha(m_Z)$, m_Z , and m_W (the former a real number, the latter two complex numbers defined as in the previous item) are input parameters.
- All other parameters (e.g., G_F and θ_W) assume complex values. In particular, Yukawa couplings are defined by using the complex masses introduced in the first item.

At the NLO, the necessity of performing UV renormalisation introduces additional complications. At present, the prescriptions of ref. [100] have been explicitly included and validated. As was already mentioned in sect. 2.1, this operation will not be necessary in the future, when it will be replaced by an automatic procedure performed by FEYNRULES.

2.2.2 BSM-specific capabilities

One of the main motivations to have very precise SM predictions, and therefore to include higher order corrections, is that of achieving a better experimental sensitivity in the context of New Physics (NP) searches. At the same time, it is necessary to have as flexible, versatile, and accurate simulations as is possible not only for the plethora of NP models proposed so far, but for those to be proposed in the future as well. These capabilities have been one of the most useful aspects of the MADGRAPH5 suite; they are still available in MADGRAPH5_AMC@NLO and, in fact, have been further extended.

As was already mentioned, the required flexibility is a direct consequence of using the UFO models generated by dedicated packages such as FEYNRULES or SARAH [101], and of

making MADGRAPH5_AMC@NLO compatible with them. Here, we limit ourselves to listing the several extensions recently made to the UFO format and the MADGRAPH5_AMC@NLO code, which have a direct bearing on BSM simulations.

- The possibility for the user to define the analytic expression for the propagator of a given particle in the model [102].
- The implementation of the analytical formulae for two-body decay widths [103], which allows one to save computing time when the knowledge of the widths of all unstable particles in the model is needed (see sect. 2.3.2).
- The possibility to define form factors (i.e., coupling constants depending on the kinematic of the vertex) directly in the UFO model. Note that, since form factors cannot be derived from a Lagrangian, they cannot be dealt with by programs like FEYNRULES, and have therefore to be coded by hand in the models. In order to be completely generic, the possibility is also given to go beyond the format of the current UFO syntax, and to code the form factors directly in Fortran⁴.
- Models and processes are supported that feature massive and massless particles of spin $3/2$ [102]. This implies that all spins are supported in the set $\{0, 1/2, 1, 3/2, 2\}$.
- The support of multi-fermion interactions, including the case of identical particles in the final state, and of UFO models that feature vertices with more than one fermion flow. Multi-fermion interactions with fermion-flow violation, such as in the presence of Majorana particles, are not supported. Such interactions, however, can be implemented by the user by splitting the interaction in multiple pieces connected via heavy scalar particles, a procedure that allows one to define unambiguously the fermion flow associated with each vertex.

While not improved with respect to what was done in MADGRAPH5, we remind the reader that the module responsible for handling the colour algebra is capable of treating particles whose $SU_c(3)$ representation and interactions are non-trivial, such as the sextet and ϵ^{ijk} -type vertices respectively.

2.3 LO computations

The general techniques and strategies used in MADGRAPH5_AMC@NLO to integrate a tree-level partonic cross section, and to obtain a set of unweighted events from it, have been inherited from MADGRAPH5; the most recent developments associated with them have been presented in ref. [36], and will not be repeated here. After the release of MADGRAPH5, a few optimisations have been introduced in MADGRAPH5_AMC@NLO, in order to make it more efficient and flexible than its predecessor. Here, we limit ourselves to listing the two which have the largest overall impact.

⁴Which obviously implies that this option is not available should other type of outputs be chosen (see appendix B.6). Further details are given at:
<https://cp3.irmp.ucl.ac.be/projects/madgraph/wiki/FormFactors>.

1. The phase-space integration of decay-chain topologies has been rewritten, in order to speed up the computations and to deal with extremely long decay chains (which can now easily extend up to sixteen particles). In addition, the code has also been optimised to better take into account invariant-mass cuts, and to better handle the case where interference effects are large.
2. It is now possible to integrate matrix elements which are not positive-definite⁵. This is useful e.g. when one wants to study a process whose amplitude can be written as a sum of two terms, which one loosely identifies with a “signal” and a “background”. Rather than integrating $|S + B|^2$, one may consider $|S|^2 + 2\Re(SB^*)$ and $|B|^2$ separately, which is a more flexible approach (e.g. by giving one the possibility of scanning a parameter space, in a way that affects S while leaving B invariant), that also helps reduce the computation time by a significant amount. One example of this situation is the case when $|B|^2$ is numerically dominant, and thus corresponds to a very large sample of events which can however be generated only once, while smaller samples of events, that correspond to $|S|^2 + 2\Re(SB^*)$ for different parameter choices, can be generated as many times as necessary. Another example is that of an effective theory where a process exists (S) that is also present in the SM (B). In such a case, it is typically $|B|^2 + 2\Re(SB^*)$ which is kept at the lowest order in $1/\Lambda$ (with Λ being the cutoff scale). Finally, this functionality is needed in order to study the large- N_c expansion in multi-parton amplitudes, where beyond the leading $1/N_c$ terms the positive definiteness of the integrand is not guaranteed.

In the following sections, we shall discuss various topics relevant to the calculation of LO-accurate physical quantities. Sect. 2.3.1 briefly reviews the techniques employed in the generation of tree-level amplitudes, emphasising the role of recent UFO/ALOHA developments. Sect. 2.3.2 presents the module that computes the total widths of all unstable particles featured in a given model. Sect. 2.3.3 describes reweighting techniques. Finally, in sect. 2.3.4 we review the situation of MLM-merged computations.

2.3.1 Generation of tree-level matrix elements

The computation of amplitudes at the tree level in MADGRAPH5_AMC@NLO has a scope which is in fact broader than tree-level physics simulations, since *all* matrix elements used in both LO and NLO computations are effectively constructed by using tree-level techniques. While this is obvious for all amplitudes which are not one-loop ones, in the case of the latter it is a consequence of the L-cutting procedure, which was presented in detail in ref. [66] and which, roughly speaking, stems from the observation that any one-loop diagram can be turned into a tree-level one by cutting one of the propagators that enter the loop. Furthermore, as was also explained in ref. [66] and will be discussed in sect. 2.4.2, all of the companion operations of one-loop matrix element computations (namely, UV renor-

⁵We stress that this statement is non-trivial just because it applies to LO computations. In the context of NLO simulations this is the standard situation, and AMC@NLO has obviously been always capable of handling it.

malisation and R_2 counterterms) can also be achieved through tree-level-like calculations, which are thus very central to the whole MADGRAPH5_AMC@NLO framework.

The construction of tree-level amplitudes in MADGRAPH5_AMC@NLO is based on three key elements: Feynman diagrams, helicity amplitudes, and colour decomposition. Helicity amplitudes [104–110] provide a convenient and effective way to evaluate matrix elements for any process in terms of complex numbers, which is quicker and less involved than one based on the contraction of Lorentz indices. As the name implies, helicity amplitudes are computed with the polarizations of the external particles fixed. Then, by employing colour decompositions [111–113], they can be organised into gauge-invariant subsets (often called dual amplitudes), each corresponding to an element of a colour basis. In this way, the complexity of the calculation grows linearly with the number of diagrams instead of quadratically; furthermore, the colour matrix that appears in the squared amplitude can be easily computed automatically (to any order in $1/N_c$) once and for all, and then stored in memory. If the number of QCD partons entering the scattering process is not too large (say, up to five or six), this procedure is manageable notwithstanding the fact that the number of Feynman diagrams might grow factorially. Otherwise, other techniques that go beyond the Feynman-diagram expansion have to be employed [43, 47, 50, 114]. The algorithm used in MADGRAPH5_AMC@NLO for the determination of the Feynman diagrams has been described in detail in ref. [36]. There, it has been shown that it is possible to efficiently “factorise” diagrams, such that if a particular substructure shows up in several of them, it only needs to be calculated once, thus significantly increasing the speed of the calculation. In addition, a not-yet-public version of the algorithm can determine directly dual amplitudes by generating only the relevant Feynman diagrams, thereby reducing the possible factorial growth to less than an exponential one.

The diagram-generation algorithm of MADGRAPH5_AMC@NLO is completely general, though it needs as an input the Feynman rules corresponding to the Lagrangian of a given theory. The information on such Feynman rules is typically provided by FEYNRULES, in a dedicated format (UFO). We remind the reader that FEYNRULES is a MATHEMATICA-based package that, given a theory in the form of a list of fields, parameters and a Lagrangian, returns the associated Feynman rules in a form suitable for matrix element generators. It now supports renormalisable as well as non-renormalisable theories, two-component fermions, spin-3/2 and spin-2 fields, superspace notation and calculations, automatic mass diagonalization and the UFO interface. In turn, a UFO model is a standalone Python module, that features self-contained definitions for all classes which represent particles, parameters, and so forth. With the information from the UFO, the dedicated routines that will actually perform the computation of the elementary blocks that enter helicity amplitudes are built by ALOHA. Amplitudes are then constructed by initializing a set of external wavefunctions, given their helicities and momenta. The wavefunctions are next combined, according to the interactions present in the Lagrangian, to form currents attached to the internal lines. Once all of the currents are determined, they are combined to calculate the complex number that corresponds to the amplitude for the diagram under consideration. Amplitudes associated with different diagrams are then added (as complex numbers), and squared by making use of the colour matrix calculated previously, so as to give the final result. We

point out that versions of MADGRAPH earlier than MADGRAPH5 used the HELAS [88,115] library instead of ALOHA. By adopting the latter, a significant number of limitations inherent to the former could be lifted. A few examples follow here. ALOHA is not forced to deal with pre-coded Lorentz structures; although its current implementation of the Lorentz algebra assumes four space-time dimensions, this could be trivially generalised to any even integer, as the algebra is symbolic and its actual representation enters only at the final stage of the output writing; its flexibility has allowed the implementation of the complex mass scheme (see sect. 2.2.1), and of generic UV and R_2 computations (see sect. 2.4.2); it includes features needed to run on GPU's, and the analogues of the HEGET [116,117] libraries can be automatically generated for any BSM model; finally, it caters to matrix-element generators other than MADGRAPH, such as those now used in HERWIG++ [118,119] and PYTHIA8 [120]. Since its release in 2011 [89], several important improvements have been made in ALOHA. On top of the support to the complex mass scheme and to the Feynman gauge, and of specific features relevant to one-loop computations (which are discussed in sects. 2.2.1 and 2.4.2), we would like to mention here that there has been a conspicuous gain in speed, both at the routine-generation phase as well as in the actual evaluation, thanks to the extensive use of caching. In addition, the user is now allowed to define the form of a propagator (which is not provided by FEYNRULES), while previously this was determined by the particle spin: non-trivial forms, such as those relevant to spin-2 particles in ADD models [121], or to unparticles, can now be used.

2.3.2 Width calculator

Among the basic ingredients for Monte Carlo simulations of new-physics models are the masses and widths of unstable particles; which particle is stable and which unstable may depend on the particular parameter benchmark chosen. Masses are typically obtained by going to the mass eigenbasis and, if necessary, by evolving boundary conditions from a large scale down to the EW one. Very general codes exist that perform these operations starting from a FEYNRULES model, such as ASPERGE [86]. The determination of the corresponding widths, on the other hand, requires the explicit calculation of all possible decay channels into lighter (SM or BSM) states. The higher the number of the latter, the more daunting it is to accomplish this task by hand. Furthermore, depending on the mass hierarchy and interactions among the particles, the computation of two-body decay rates could be insufficient, as higher-multiplicity decays might be the dominant modes for some of the particles. The decay channels that are kinematically allowed are highly dependent on the mass spectrum of the model, so that the decay rates need to be re-evaluated for every choice of the input parameters. The program MADWIDTH [103] has been introduced in order to address the above issues. In particular, MADWIDTH is able to compute partial widths for N -body decays, with arbitrary values of N , at the tree-level and by working in the narrow-width approximation⁶. The core of MADWIDTH is based on new routines

⁶Even if those two assumptions are quite generic, there are particles for which they do not give sufficiently-accurate results, such as the Standard Model Higgs, which has significant loop-induced decay modes.

for diagram generation that have been specifically designed to remove certain classes of diagrams:

- **Diagrams with on-shell intermediate particles.** If the kinematics of an $A \rightarrow n$ -particles decay allows an internal particle B , that appears in an s -channel, to be on shell, the corresponding diagram can be seen as a cascade of two decays, $A \rightarrow B + (n - k)$ -particles followed by $B \rightarrow k$ -particles. It is thus already taken into account in the calculation of lower-multiplicity decay channels, and the diagram is discarded.
- **Radiative diagrams.** Roughly speaking, if one or more zero-mass particles are radiated by another particle, the diagram is considered to be a radiative correction to a lower-multiplicity decay – the interested reader can find the precise definition in ref. [103]. Such a diagram is therefore discarded, because it should be considered only in the context of a higher-order calculation. Furthermore, all diagrams with the same coupling-constant combination and the same external states are also discarded, so that gauge invariance is preserved.

MADWIDTH begins by generating all two-body decay diagrams, and then iteratively adds extra final state particles with the condition that any diagram belonging to either of the classes above is forbidden. This iterative procedure stops when all $N = 4$ modes have been considered, or estimated to be numerically irrelevant⁷. All diagrams thus generated are integrated numerically. MADWIDTH uses several methods to reduce significantly the overall computation time. Firstly, it features two fast (and conservative) estimators, one for guessing the impact of adding one extra final-state particle *before* the actual diagram-generation phase, and another one for evaluating the importance of a single integration channel. Both of these estimators are used to neglect parts of the computation which are numerically irrelevant. Secondly, if the model is compatible with the recent UFO extension of ref. [103], and thus includes the analytical formulae for two-body decays, then the code automatically uses those formulae and avoids the corresponding numerical integrations.

We conclude this section by remarking that, although essential for performing BSM cross-section computations, MADWIDTH should be seen as a *complement* for the existing tools that generate models. This is because the information it provides one with must be available before the integration of the matrix elements is carried out but, at the same time, really cannot be included in a model itself, since it depends on the chosen benchmark scenario. For more details on the use of this model-complementing feature in MADGRAPH5_AMC@NLO, and of its mass-matrix diagonalisation analogue to which we have alluded above, see the **Setup** part of appendix B.1.

2.3.3 Event reweighting

The generation of large samples of events for experimental analyses can be a very time-consuming operation, especially if it involves a full simulation of the detector response.

⁷Both of these conditions can be controlled by the user.

It is therefore convenient, whenever possible, to apply corrections, or to study systematics of theoretical or modelling nature, by using reweighting techniques. The reweighting of either one-dimensional distributions or that performed on an event-by-event basis are equally-common practices in experimental physics. Although the basic idea (that a non-null function can be used to map any other function defined in the same domain) behind these two procedures is the same, one must bear in mind that they are not identical, and in particular that the former can never be proven to be formally correct, since correlations (with other, non-reweighted variables) may be lost or modified, while the latter is correct in general, at least in the limit of a large number of events. For this reason, we consider only event-by-event reweighting approaches in what follows.

Thanks to its flexibility and the possibility of accessing a large amount of information in a direct and straightforward manner (model and running parameters, matrix elements, PDFs, and so forth) MADGRAPH5_AMC@NLO provides one with an ideal framework for the implementation of such approaches. The strategy is rather simple: one starts with a set of hard events, such as those contained in an LHE file, and rescales their weights:

$$w_{\text{new}} = r w_{\text{old}} \quad (2.1)$$

without modifying their kinematics. The rescaling factor r is not a constant, and may change on an event-by-event basis. This implies that, even when the original sample of events is unweighted (i.e., the w_{old} 's are all equal), the reweighted one will be in general weighted (i.e., the w_{new} 's may be different), and therefore degraded from a statistical point of view. If, however, the spread of the new weights is not too large (i.e., the r 's are close to each other, and feature a small number of outliers), the reweighting is typically advantageous with respect to generating a new independent sample from scratch.

While eq. (2.1) is completely general, its practical implementation depends on the kind of problems one wants to solve. We shall consider three of them in this section, two of which constitute a direct application of the basic formula (2.1), and a third one which is more sophisticated. Since these procedures address different types of physics, they are conveniently associated with different modules in MADGRAPH5_AMC@NLO, but they are all fully embedded into our framework and easily accessible through it, as we shall briefly explain in what follows and in appendices B.4 and B.5.

The simplest example is that of the evaluation of the uncertainties through to the variations of the renormalisation and factorisation scales, and of the PDFs. In such a case r is easily determined by using the identities i and j of the initial-state partons, and the power (b) of α_S in the Born matrix elements⁸:

$$r = \frac{f_i^{\text{new}}(x_1, \mu_F^{\text{new}}) f_j^{\text{new}}(x_2, \mu_F^{\text{new}}) \alpha_S^b(\mu_R^{\text{new}})}{f_i^{\text{old}}(x_1, \mu_F^{\text{old}}) f_j^{\text{old}}(x_2, \mu_F^{\text{old}}) \alpha_S^b(\mu_R^{\text{old}})} \quad (2.2)$$

It should be stressed that, although scale and PDF systematics can also be computed with reweighting techniques at the NLO (see ref. [122]), in general they cannot be written in the

⁸There may be cases where such matrix elements do not factorise a single α_S factor – see e.g. sect. 2.4. We limit ourselves to discussing the simplest, and more common, situation here.

very simple form of eq. (2.1), which is that of an overall rescaling. For a direct comparison of the NLO and LO techniques employed in this context by MADGRAPH5_AMC@NLO, and for fuller details about them, see appendices B.3 and B.4 respectively.

Another rather simple example is that of the case where one is interested in studying the implications of changing the modelling of a process, with the sole constraint that its initial and final states be the same. Such a situation can for example occur when the numerical values of the coupling constants are modified, or when the contributions of classes of diagrams are included or eliminated (e.g., Higgs exchange in EW vector boson scattering). The common feature of all examples of this kind is that they are associated with changes to matrix elements, all computed with the same kinematic configuration. Therefore, one can simply write:

$$r = |\mathcal{A}_{\text{new}}|^2 / |\mathcal{A}_{\text{old}}|^2, \quad (2.3)$$

which for obvious reasons is dubbed matrix-element reweighting. Despite its simplicity, this method has very many different applications, from parameter scanning in new-physics models (where one starts with a single sample of events, that corresponds to a given benchmark point, and generates as many new ones as the number of parameter configurations of interest), to more advanced approaches, such as the inclusion of exact loop effects (\mathcal{A}_{new}) in processes that can be also, and more simply, described by effective theories (\mathcal{A}_{old}) – see refs. [123, 124] for recent results of the latter type that make use of MADGRAPH5 and MADGRAPH5_AMC@NLO. Some further comments on matrix-element reweighting and its practical usage in MADGRAPH5_AMC@NLO are given in appendix B.5.

We finally turn to discussing the matrix-element method [125–127], which can be seen as a reweighting one because the weights determined at the parton level through matrix-element computations are possibly modified by a convolution to take into account a variety of blurring effects (such as those due to a detector). On the other hand, from the practical point of view it turns out to be more convenient, rather than talking about reweighting factors, to introduce a likelihood $P(\mathbf{q}|\alpha)$ for the observation of a given kinematic configuration (\mathbf{q}) given a set of theoretical assumptions (α). By doing so, one can just re-express eq. (2.3) in a different language:

$$P(\mathbf{q}|\alpha) = \frac{\mathcal{V}}{\hat{\sigma}_\alpha} |\mathcal{A}_\alpha(\mathbf{q})|^2, \quad (2.4)$$

with \mathcal{V} a suitable volume factor, and $\hat{\sigma}_\alpha$ the total rate associated with the given assumptions α . The advantage of eq. (2.4) is that it is suitable to handle cases which are much more complicated than the purely-theoretical exercise of eq. (2.3), which has led to its introduction here. For example, in the first approximation one may think of \mathbf{q} as the actual kinematic configuration measured by an experiment, whose accuracy is such that it can be directly used as an argument of the matrix elements, as is done in eq. (2.4). Note that this is a rather strong assumption, that in practice identifies hadron-level with parton-level quantities, and assumes that the knowledge of the final state is complete (such as that which one can ideally obtain in Drell-Yan production, $pp \rightarrow Z \rightarrow \ell^+ \ell^-$). It is clear that there are many ways in which this simple approximation (which is used, for example,

in refs. [128–132]) can break down: the effects of radiation, of the imperfect knowledge of the detector, of the impossibility of a strict identification of parton- with hadron-level quantities, the uncertainties that plague the latter, the fact that all the relevant four-momenta cannot in general be measured, are but a few examples. It is therefore necessary to generalise eq. (2.4), which one can do as follows:

$$P(\mathbf{q}|\alpha) = \frac{1}{\sigma_\alpha} \int dx_1 dx_2 d\phi(\mathbf{p}) f^{(1)}(x_1) f^{(2)}(x_2) |\mathcal{A}_\alpha(\mathbf{p})|^2 W(\mathbf{q}, \mathbf{p}). \quad (2.5)$$

In eq. (2.5), we have denoted by \mathbf{p} the parton kinematic configuration. All effects that may turn \mathbf{p} into the detector-level quantity \mathbf{q} (whose dimensionality therefore need not coincide with that of \mathbf{p}) are parametrised by $W(\mathbf{q}, \mathbf{p})$, called transfer function. As for any hadron-collision measurable quantity, eq. (2.5) features the convolution with the PDFs. The likelihood introduced in this way can be used in the context e.g. of an hypothesis test in order to determine which among various choices of α is the most probable.

Although this method is both conceptually simple and very attractive, the numerical evaluation of $P(\mathbf{q}|\alpha)$ is difficult because the transfer function $W(\mathbf{q}, \mathbf{p})$ behaves in a way which cannot be probed efficiently by phase-space parametrisations that work well for just the matrix elements. In order to address this issue, a dedicated program, dubbed MADWEIGHT [133], has been introduced that includes an optimised phase-space treatment specifically designed for eq. (2.5). The new version of the code [134] embedded in MADGRAPH5_AMC@NLO features several improvements w.r.t. that of ref. [133]. It includes the method for the approximate description of higher-order effects due to initial-state radiation, as proposed in ref. [135]. Furthermore, several optimizations have been achieved that render the computations much faster (sometimes by orders of magnitude); this allows one to use this approach also in the case of very involved final states, such as those relevant to Higgs production in association with a $t\bar{t}$ pair [136]. Further details on MADWEIGHT and its use within MADGRAPH5_AMC@NLO can be found in appendix B.5.

2.3.4 Tree-level merging

The goal of merging is that of combining samples associated with different parton multiplicities in a consistent manner, that avoids double counting after showering, thus allowing one to effectively define a single fully-inclusive sample. The tree-level merging algorithms implemented in MADGRAPH5_AMC@NLO are a hybrid version of those available in ALPGEN [43] and SHERPA [137]; they work for both SM and BSM hard processes, but are fully automated only when the shower phase is performed with either PYTHIA6 [138] or PYTHIA8 [120] (however, there are no reasons in principle which prevents these schemes from working with HERWIG6 [139, 140] or HERWIG++ [118, 119]). They are based on the use of a k_T -measure [141] to define hardness and to separate processes of different multiplicities, and do not perform any analytic-Sudakov reweighting of events; rather, this operation is effectively achieved by rejecting showered events under certain conditions (see later), which implies a direct use of the well-tuned showering and hadronization mechanisms of the parton shower Monte Carlos.

There are two merging schemes that can be used in conjunction with PYTHIA6 and PYTHIA8; in the case of the latter, one is also given the possibility of considering CKKW-L approaches [142–144] (after having generated the samples relevant to various parton multiplicities with MADGRAPH5_AMC@NLO); in what follows, we shall limit ourselves to briefly describe the former two methods. Firstly, one has the k_T -jet MLM scheme [145], where final-state partons at the matrix-element level are clustered according to a k_T jet algorithm to find the “equivalent parton shower history” of the event. In our implementation the Feynman diagram information from MADGRAPH5_AMC@NLO is used to retain only those clusterings that correspond to actual Feynman diagrams. In order to mimic the behaviour of the parton shower, the k_T value for each clustering vertex associated with a QCD branching is used as the renormalisation scale for α_s in that vertex. All factorisation scales squared, and the renormalisation scale squared for the hard process (the process with the zero-extra-parton multiplicity), are constructed by clustering back to the irreducible $2 \rightarrow 2$ system and by using the transverse mass in the resulting frame: $\mu^2 = p_T^2 + m^2$. The smallest k_T value found in the jet-reconstruction procedure is restricted to be larger than some minimum cutoff scale, which we denote by $Q_{\text{cut}}^{\text{ME}}$; if this condition is not satisfied, the event is rejected. The hard events are then showered by PYTHIA: at the end of the perturbative-shower phase, final-state partons are clustered into jets, using the very same k_T jet algorithm as before, with the jets required to have a transverse momentum larger than a given scale Q_{match} , with $Q_{\text{match}} > Q_{\text{cut}}^{\text{ME}}$. The resulting jets are compared to the partons at the hard subprocess level (i.e., those that result from the matrix-element computations): a jet j is said to be matched to a parton p if the distance between the two, defined according to ref. [141], is smaller than the minimal jet hardness: $k_T(j, p) < Q_{\text{match}}$. The event is then rejected unless each jet is matched to a parton, except in the case of the largest-multiplicity sample, where extra jets are allowed if softer than the k_T of the softest matrix-element parton in the event, $Q_{\text{softest}}^{\text{ME}}$. Secondly, and with the aim to give one a non-parametric way to study merging systematics, one has the shower- k_T scheme, which can be used only with PYTHIA’s p_T -ordered shower. In this case, events are generated by MADGRAPH5_AMC@NLO as described above and then showered, but information is also retained on the hardest (which is also the first, in view of the p_T -ordered nature of PYTHIA here) emission in the shower, $Q_{\text{hardest}}^{\text{PS}}$; furthermore, one sets $Q_{\text{match}} = Q_{\text{cut}}^{\text{ME}}$, which cannot be done in the context of the k_T -jet MLM scheme. For all samples but the largest-multiplicity one, events are rejected if $Q_{\text{hardest}}^{\text{PS}} > Q_{\text{match}}$, while in the case of the largest-multiplicity sample events are rejected when $Q_{\text{hardest}}^{\text{PS}} > Q_{\text{softest}}^{\text{ME}}$. This merging scheme is simpler than the k_T -jet MLM one, but it rather effectively mimics it. Furthermore, it probes the Sudakov form factors used in the shower in a more direct manner. Finally, the treatment of the largest-multiplicity sample is fairly close to that used in the CKKW-inspired merging schemes. In both the k_T -jet MLM and shower- k_T methods, merging systematics are associated with variations of Q_{match} ; in the former case, changes to Q_{match} must be done by keeping $Q_{\text{match}} - Q_{\text{cut}}^{\text{ME}}$ a constant. For applications of the two schemes described here, see e.g. refs. [123, 145–148].

2.4 NLO computations

When discussing the problem of perturbative corrections, one should bear in mind that one usually considers an expansion in terms of a single quantity (which is a coupling constant for fixed-order computations). However, this is just a particular case of the more general scenario in which that expansion is carried out simultaneously in two or more couplings, all of which are thus treated as “small” parameters – we shall refer to such a scenario as mixed-coupling expansion. Despite the fact that there is typically a clear numerical hierarchy among these couplings, a mixed-coupling situation is far from being academic; in fact, as we shall show in the following, there are cases when one is obliged to work with it. In order to study a generic mixed-coupling expansion without being too abstract, let us consider an observable Σ which receives contributions from processes that stem from both QCD and QED interactions. The specific nature of the interactions is in fact not particularly relevant (for example, QED here may be a keyword that also understands the pure-EW contributions); what matters, for the sake of the present discussion, is that Σ may depend on more than one coupling constant. We assume that the regular function

$$\Sigma(\alpha_S, \alpha) \quad (2.6)$$

admits a Taylor representation:

$$\Sigma(\alpha_S, \alpha) = \sum_{n=0}^{\infty} \sum_{m=0}^{\infty} \frac{\alpha_S^n \alpha^m}{n!m!} \left[\frac{\partial^{n+m} \Sigma}{\partial^n \alpha_S \partial^m \alpha} \right]_{(\alpha_S, \alpha)=(0,0)}, \quad (2.7)$$

which is by definition the perturbative expansion of Σ . The first few terms of the sums in eq. (2.7) will be equal to zero, with the number of such vanishing terms increasing with the complexity of the process under consideration – this is because n and m are directly related to the number of vertices that enter a given diagram. In general, it is clear that for a given pair (n, m) which gives a non-vanishing contribution to eq. (2.7), there may exist another pair (n', m') , with $n \neq n'$, $m \neq m'$, and $n + m = n' + m'$ whose contribution to eq. (2.7) is also non zero. It appears therefore convenient to rewrite eq. (2.7) with a change of variables:

$$k = n + m, \quad l = n - m, \quad (2.8)$$

whence:

$$\Sigma(\alpha_S, \alpha) = \sum_{k=0}^{\infty} \sum_{l=-k}^k \frac{\mathcal{P}_{k,l} \alpha_S^{(k+l)/2} \alpha^{(k-l)/2}}{((k+l)/2)!((k-l)/2)!} \left[\frac{\partial^k \Sigma}{\partial^{(k+l)/2} \alpha_S \partial^{(k-l)/2} \alpha} \right]_{(\alpha_S, \alpha)=(0,0)}, \quad (2.9)$$

where

$$\mathcal{P}_{k,l} = \delta(\text{mod}(k, 2), \text{mod}(l, 2)), \quad (2.10)$$

which enforces the sum over l to run only over those integers whose parity is the same as that of k (therefore, there are $k+1$ terms in each sum over l for a given k). Equation (2.9) implies that we need to call *Born* the sum (over l) of all the contributions with the smallest $k \equiv k_0$ which are non-vanishing. Hence, the *NLO corrections* will correspond to the sum

over l of all terms with $k = k_0 + 1$. This notation is compatible with the usual one used in the context of the perturbation theory of a single coupling: the QCD- or QED-only cases are recovered by considering $l = k$ or $l = -k$ respectively. In a completely general case, for any given k there will exist two integers $l_m(k)$ and $l_M(k)$ which satisfy the following conditions:

$$-k \leq l_m(k) \leq l_M(k) \leq k, \quad (2.11)$$

and such that all contributions to eq. (2.9) with

$$l < l_m(k) \quad \text{or} \quad l > l_M(k) \quad (2.12)$$

vanish, and $l = l_m(k)$, $l = l_M(k)$ are both non-vanishing. This implies that in the range

$$l_m(k) \leq l \leq l_M(k), \quad (2.13)$$

there will be at least one (two if $l_m(k) \neq l_M(k)$) non-null contribution(s) to eq. (2.9) (the typical situation being actually that where all the terms in eq. (2.13) are non-vanishing). Given eq. (2.13), one can re-write eq. (2.9) in the following way:

$$\Sigma(\alpha_S, \alpha) = \sum_{k=k_0}^{\infty} \alpha_S^{c_s(k)} \alpha^{c(k)} \sum_{q=0}^{\Delta(k)} \Sigma_{k,q} \alpha_S^{\Delta(k)-q} \alpha^q, \quad (2.14)$$

where

$$c_s(k) = \frac{1}{2} (k + l_m(k)), \quad (2.15)$$

$$c(k) = \frac{1}{2} (k - l_M(k)), \quad (2.16)$$

$$\Delta(k) = \frac{1}{2} (l_M(k) - l_m(k)). \quad (2.17)$$

The coefficients $\Sigma_{k,l}$ of eq. (2.14) can be expressed in terms of the quantities that appear in eq. (2.9), but this is unimportant here. A typical situation is where:

$$l_M(k+1) = l_M(k) + 1, \quad (2.18)$$

$$l_m(k+1) = l_m(k) - 1, \quad (2.19)$$

so that:

$$c_s(k+1) = c_s(k), \quad (2.20)$$

$$c(k+1) = c(k), \quad (2.21)$$

$$\Delta(k+1) = \Delta(k) + 1, \quad (2.22)$$

whence:

$$\Sigma(\alpha_S, \alpha) = \alpha_S^{c_s(k_0)} \alpha^{c(k_0)} \sum_{p=0}^{\infty} \sum_{q=0}^{\Delta(k_0)+p} \Sigma_{k_0+p,q} \alpha_S^{\Delta(k_0)+p-q} \alpha^q, \quad (2.23)$$

where the Born and NLO contributions correspond to $p = 0$ and $p = 1$ respectively. Note that eq. (2.23) is the most general form of the observable $\Sigma(\alpha_S, \alpha)$ if one allows

the possibility of having $\Sigma_{k_0+p,0} = 0$ or $\Sigma_{k_0+p,\Delta(k_0)+p} = 0$ (or both) for $p > k_0$, since this renders eqs. (2.18) and (2.19) always true. Equation (2.23) has the advantage of a straightforward interpretation of the role of NLO corrections.

An example may help make the points above more explicit. Consider the contribution to dijet production due to the partonic process $uu \rightarrow uu$; the corresponding lowest-order t - and u -channel Feynman diagrams feature the exchange of either a gluon or a photon (or a Z , but we stick to the pure- $U(1)$ theory here). The Born matrix elements will therefore be the sum of terms that factorise the following coupling combinations:

$$\alpha_s^2, \quad \alpha_s \alpha, \quad \alpha^2, \quad (2.24)$$

which implies $k_0 = 2$, $\Delta(2) = 2$, and $c_s(2) = c(2) = 0$. Therefore, according to eq. (2.23), the NLO contribution $p = 1$ will feature the following coupling combinations:

$$\alpha_s^3, \quad \alpha_s^2 \alpha, \quad \alpha_s \alpha^2, \quad \alpha^3. \quad (2.25)$$

From the procedural point of view, it is convenient to identify QCD and QED corrections according to the relationship between one coupling combination in eq. (2.24) and one in eq. (2.25), as follows:

$$\alpha_s^n \alpha^m \xrightarrow{\text{QCD}} \alpha_s^{n+1} \alpha^m, \quad (2.26)$$

$$\alpha_s^n \alpha^m \xrightarrow{\text{QED}} \alpha_s^n \alpha^{m+1}, \quad (2.27)$$

which has an immediate graphic interpretation, depicted in fig. 1. Such an interpretation

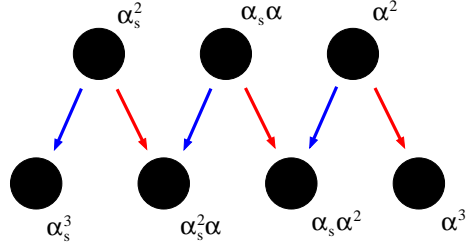


Figure 1: QCD (blue, right-to-left arrows) corrections and QED (red, left-to-right arrows) corrections to dijet production. See the text for details.

has a Feynman-diagram counterpart in the case of real-emission contributions, which is made explicit once one considers cut-diagrams, like those presented in fig. 2. Loosely speaking, one can indeed identify the diagram on the left of that figure as representing QED (since the photon is cut) real-emission corrections to the α_s^2 Born contribution. On the other hand, the diagram on the right represents QCD (since the gluon is cut) real-emission corrections to the $\alpha_s \alpha$ Born contribution. This immediately shows that, in spite of being useful in a technical sense, QCD and QED corrections are not physically meaningful if taken separately: in general, one must consider them both in order to arrive at a sensible, NLO-corrected result. This corresponds to the fact that a given coupling combination in

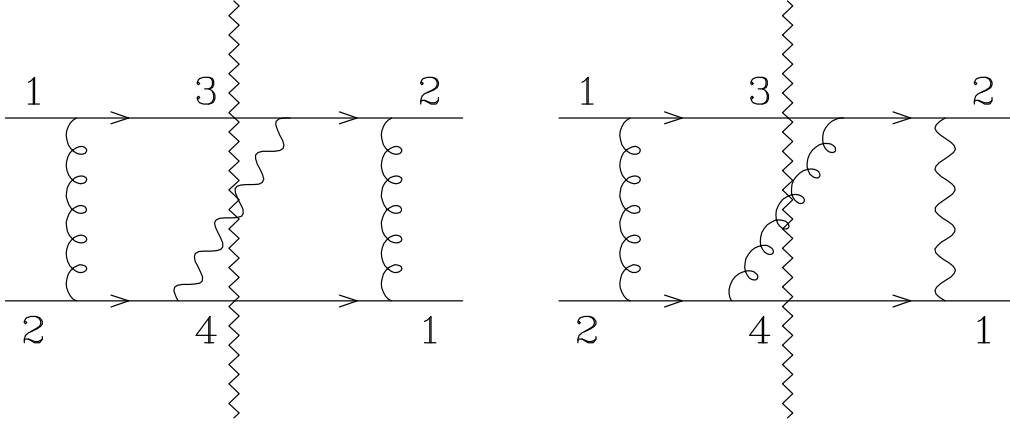


Figure 2: Real-emission contributions to dijet production at the NLO and $\mathcal{O}(\alpha_s^2\alpha)$. The saw-shaped lines represent Cutkosky cuts.

the bottom row of fig. 1 can be reached by means of two different arrows when starting from the top row (i.e., the Born level). Therefore, fig. 1 also immediately shows that when one considers *only* the Born term associated with the highest power of α_s (α), then QCD-only (QED-only) corrections are sensible (because only a right-to-left or left-to-right arrow is relevant, respectively): they coincide with the NLO corrections as defined above (see the paragraph after eq. (2.10)). It also should be clear that the above arguments have a general validity, whatever the values of $c_s(k_0)$, $c(k_0)$, and $\Delta(k_0)$ in eq. (2.23) – the former two quantities never play a role in the analogues of fig. 1, while by increasing $\Delta(k_0)$ one simply inserts more blobs (i.e., coupling combinations) in both of the rows of fig. 1. Finally, note that reading eqs. (2.26) and (2.27) in terms of diagrams, as has been done for those of fig. 2, becomes much harder when one considers virtual contributions. For example, the one whose $\mathcal{O}(\alpha_s^2\alpha)$ cut-diagram is shown in fig. 3 (and its analogues) can indeed be equally well interpreted as a QED loop correction to a QCD \times QCD $\mathcal{O}(\alpha_s^2)$ Born cut-diagram, or as a QCD loop correction to a QCD \times QED $\mathcal{O}(\alpha_s\alpha)$ Born cut-diagram.

MADGRAPH5_AMC@NLO has been constructed by having eq. (2.23) in mind; although the majority of the relevant features are not yet available in the public version of the code, all of them have already been thoroughly tested in the module responsible for computing one-loop matrix elements (see sects. 2.4.2 and 4.3), which is by far the hardest from this point of view, and the checks on the real-emission part are also at quite an advanced stage. The basic idea is that of giving the user the choice of which coupling combinations to retain either at the Born or at the NLO level; this corresponds to choosing a set of blobs in the upper or lower row of fig. 1, respectively. MADGRAPH5_AMC@NLO will then automatically also consider the blobs in the row not involved in the selection by the user, in order to construct a physically-meaningful cross section, compatible with both the user’s choices, and the constraints due to a mixed-coupling expansion (the arrows in fig. 1). It should be stressed that, although the results for the coefficients $\Sigma_{k_0+p,q}$ can be handled separately by MADGRAPH5_AMC@NLO, such coefficients are not (all) independent from each other from a

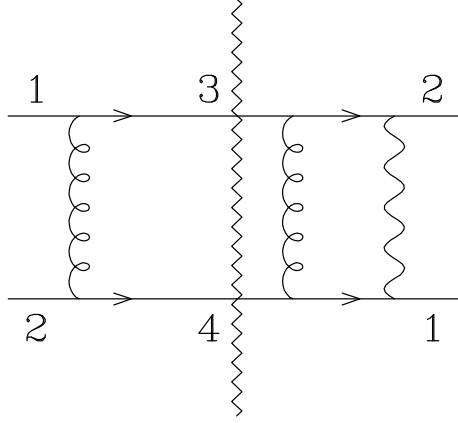


Figure 3: Virtual contribution to dijet production at the NLO and $\mathcal{O}(\alpha_s^2\alpha)$. The saw-shaped line represents a Cutkosky cut.

computational viewpoint, because a single Feynman diagram (an amplitude-level quantity) may contribute to several $\Sigma_{k_0+p,q}$'s (the latter being amplitude-squared quantities). For this reason, as far as the CPU load is concerned the choice of which coupling combinations to consider can be equivalently made at the amplitude level. Indeed, this is the only option presently available in the public version of MADGRAPH5_AMC@NLO; more detailed explanations are given in appendix B.1.

2.4.1 NLO cross sections and FKS subtraction: MadFKS

In this section, we briefly review the FKS subtraction [10,12] procedure, and emphasise the novelties of its implementation in MADGRAPH5_AMC@NLO w.r.t. its previous automation in MADFKS [59], the dedicated module included in AMC@NLO.

We shall denote by n the number of final-state particles relevant to the Born contributions to a given cross section. The set of all the partonic $2 \rightarrow n$ subprocesses that correspond to these contributions will be denoted by \mathcal{R}_n ; each of these subprocesses can be represented by the ordered list of the identities of its $2 + n$ partons, thus:

$$r = (\mathcal{I}_1, \dots, \mathcal{I}_{n+2}) \in \mathcal{R}_n. \quad (2.28)$$

The first operation performed by MADGRAPH5_AMC@NLO is that of constructing \mathcal{R}_n , given the process and the theory model. For example, if one is interested in the hadroproduction of a W^+Z pair in association with a light jet

$$pp \longrightarrow W^+Zj \quad (2.29)$$

as described by the SM, MADGRAPH5_AMC@NLO will obtain:

$$\mathcal{R}_3 = \{(u, \bar{d}, W^+, Z, g), \dots (u, g, W^+, Z, d), \dots\}. \quad (2.30)$$

Since the processes in \mathcal{R}_n are tree-level, MADGRAPH5_AMC@NLO will construct them very efficiently using the dedicated algorithms (see sect. 2.3.1). Beyond the Born level, an NLO

cross section receives contributions from the one-loop and real-emission matrix elements. As is well known, the set of the former subprocesses coincides⁹ with that of the Born, \mathcal{R}_n . Real-emission processes are by nature tree-level, and can therefore be obtained by using the very same algorithms as those employed to generate the Born contributions. This is achieved by making the code generate all tree-level processes that have the same final-state as the Born's, plus one light jet – using the example of eq. (2.29), these would correspond to:

$$pp \longrightarrow W^+ Z jj. \quad (2.31)$$

Such was the strategy adopted in the original MADFKS implementation [59]. There is however an alternative procedure, which we have implemented in MADGRAPH5_AMC@NLO because it is more efficient than the previous one in a variety of ways. Namely, for any given $r_0 \in \mathcal{R}_n$, one considers all possible $a \rightarrow bc$ branchings for each non-identical $a \in r_0$ with a strongly-interacting (i.e., $g \rightarrow gg$, $g \rightarrow q\bar{q}$, and $q \rightarrow qg$, but also $Q \rightarrow Qg$, with Q a quark with non-zero mass). For each of these branchings, a new list is obtained by removing a from r_0 , and by inserting the pair (b, c) in its place. By looping over r_0 one thus constructs the set¹⁰ of real-emission processes \mathcal{R}_{n+1} . As a by-product, one also naturally obtains, for each $r \in \mathcal{R}_{n+1}$, the pairs of particles which are associated with a soft and/or a collinear singularity of the corresponding matrix element (which we denote by $\mathcal{M}^{(n+1,0)}(r)$); by definition [59], these pairs form the set of FKS pairs, $\mathcal{P}_{\text{FKS}}(r)$, which is central in the FKS subtraction procedure. We point out, finally, that regardless of the type of strategy adopted to construct \mathcal{R}_{n+1} and \mathcal{P}_{FKS} , it is immediate to apply it in MADGRAPH5_AMC@NLO to theories other than QCD, such as QED.

After having obtained $\mathcal{P}_{\text{FKS}}(r)$, MADGRAPH5_AMC@NLO constructs the \mathcal{S} functions that are used by FKS in order to achieve what is effectively a dynamic partition of the phase space: in each sector of such a partition, the structure of the singularities of the matrix elements is basically the simplest possible, amounting (at most) to one soft and one collinear divergence. The properties of the \mathcal{S} functions are:

$$\mathcal{S}_{ij}(r) \longrightarrow 1 \quad i, j \text{ collinear}, \quad (2.32)$$

$$\sum_{(i,j) \in \mathcal{P}_{\text{FKS}}(r)} \mathcal{S}_{ij}(r) \longrightarrow 1 \quad i \text{ soft}, \quad (2.33)$$

$$\mathcal{S}_{ij}(r) \longrightarrow 0 \quad \text{all other IR limits}, \quad (2.34)$$

$$\sum_{(i,j) \in \mathcal{P}_{\text{FKS}}(r)} \mathcal{S}_{ij}(r) = 1. \quad (2.35)$$

One exploits eq. (2.35) by rewriting the real matrix elements as follows:

$$\mathcal{M}^{(n+1,0)}(r) = \sum_{(i,j) \in \mathcal{P}_{\text{FKS}}(r)} \mathcal{S}_{ij}(r) \mathcal{M}^{(n+1,0)}(r) \equiv \sum_{(i,j) \in \mathcal{P}_{\text{FKS}}(r)} \mathcal{M}_{ij}^{(n+1,0)}. \quad (2.36)$$

⁹This is because we are considering here only those cases where one-loop matrix elements are obtained by multiplying the one-loop amplitudes times the Born ones. Loop-induced processes, in which the LO contribution is a one-loop amplitude squared, are not to be treated as part of an NLO computation.

¹⁰The exceedingly rare cases of non-singular real-emission contributions can be obtained by crossing; one example is $q\bar{q} \rightarrow Hg$, which is the crossed process of $qg \rightarrow Hq$.

Thanks to eqs. (2.32)-(2.34), $\mathcal{M}_{ij}^{(n+1,0)}$ has the very simple singularity structure mentioned above. Furthermore, the terms in the sum on the r.h.s. of eq. (2.36) are independent of each other, and MADGRAPH5_AMC@NLO is thus able to handle them in parallel.

The FKS method exploits the fact that phase-space sectors associated with different \mathcal{S}_{ij} functions are independent of each other by choosing different phase-space parametrisations in each of them. There is ample freedom in such a choice, bar for two integration variables: the rescaled energy of parton i (denoted by ξ_i), and the cosine of the angle between partons i and j (denoted by y_{ij}), both defined in the incoming-parton c.m. frame. The idea is that these quantities are in one-to-one correspondence with the soft ($\xi_i \rightarrow 0$) and collinear ($y_{ij} \rightarrow 1$) singularities respectively, which renders it particularly simple to write the subtracted cross section. The $(n+1)$ -body phase space is then written as follows:

$$d\phi_{n+1} = \Phi_{ij}^{(n+1)} \left(\mathcal{K}_{n+1}(\chi_{n+1}^{(ij)}) \right) d\chi_{n+1}^{(ij)}, \quad (2.37)$$

where $\chi_{n+1}^{(ij)}$ collectively denote the $3n-1$ independent integration variables, with

$$\{\xi_i, y_{ij}\} \subset \chi_{n+1}^{(ij)}, \quad (2.38)$$

and where

$$\mathcal{K}_{n+1} = \{k_3, k_4, \dots, k_{n+3}\} \quad (2.39)$$

is the set of final-state momenta. Given eq. (2.38), MADGRAPH5_AMC@NLO chooses the other $3n-3$ integration variables and thus determines $\Phi_{ij}^{(n+1)}$ and the functional dependence $\mathcal{K}_{n+1}(\chi_{n+1}^{(ij)})$ according to the form of the integrand, gathered from the underlying Feynman diagrams. In general, this implies splitting the computation in several integration channels, which are independent of each other and can be dealt with in parallel. Such multi-channel technique is irrelevant here, and will be understood in the following. More details can be found in refs. [149, 150] and [59]. Implicit in eq. (2.37) are the maps that allow one to construct soft and collinear kinematic configurations starting from a non-special configuration (i.e., one where no parton is soft, and no two partons are collinear). This we shall denote as follows. Given:

$$\mathcal{K}_{n+1}^{(E)} = \{k_3, k_4, \dots, k_{n+3}\} \quad \text{non special} \quad (2.40)$$

MADGRAPH5_AMC@NLO constructs its soft, collinear, and soft-collinear limits with:

$$\mathcal{K}_{n+1}^{(S)} = \mathcal{K}_{n+1}^{(E)}(\xi_i = 0), \quad (2.41)$$

$$\mathcal{K}_{n+1}^{(C)} = \mathcal{K}_{n+1}^{(E)}(y_{ij} = 1), \quad (2.42)$$

$$\mathcal{K}_{n+1}^{(SC)} = \mathcal{K}_{n+1}^{(E)}(\xi_i = 0, y_{ij} = 1). \quad (2.43)$$

Furthermore, all the phase-space parametrisations employed by MADGRAPH5_AMC@NLO are such that¹¹:

$$\mathcal{K}_{n+1}^{(S)} = \mathcal{K}_{n+1}^{(C)} = \mathcal{K}_{n+1}^{(SC)}, \quad (2.44)$$

¹¹Equation (2.44) holds for all particles except the FKS-pair partons; for the latter, it is the sum of their four-momenta that is the same in the three configurations. This is sufficient owing to the underlying infrared-safety conditions.

which is beneficial from the point of view of the numerical stability of observables computed at the NLO, and is necessary in view of matching with the parton shower according to the MC@NLO formalism. As is usual in the context of NLO computations, we call the non-special and the IR-limit configurations (and, by extension, the corresponding cross-section contributions) the event and the soft, collinear, and soft-collinear counterterms respectively.

Given a real-emission process $r_R \in \mathcal{R}_{n+1}$ and an \mathcal{S}_{ij} contribution, the FKS-subtracted cross section consists of four terms:

$$d\sigma_{ij}^{(\text{NLO})}(r_R) \longleftrightarrow \left\{ d\sigma_{ij}^{(\text{NLO},\alpha)}(r_R) \right\}_{\alpha=E,S,C,SC} \quad (2.45)$$

$$d\sigma_{ij}^{(\text{NLO},\alpha)}(r_R) = \mathcal{L}^{(\alpha)}\left(r_R; \chi_{Bj}^{(ij)}\right) W_{ij}^{(\alpha)}(r_R) d\chi_{Bj}^{(ij)} d\chi_{n+1}^{(ij)}, \quad (2.46)$$

where $d\chi_{Bj}^{(ij)}$ is the integration measure over Bjorken x 's, $\mathcal{L}^{(\alpha)}$ is the corresponding parton-luminosity factor¹², and the short-distance weights $W_{ij}^{(\alpha)}$ are reported in refs. [59, 122]. In ref. [59], in particular, an extended proof is given that all contributions to an NLO cross section which are *not* naturally $(n+1)$ -body ones (such as the Born, virtual, and initial-state collinear remainders) can be cast in a form formally identical to that of the soft or collinear counterterms, and can thus be dealt with simultaneously with the latter. The fully differential cross section that emerges from eqs. (2.45) and (2.46) is:

$$\begin{aligned} \frac{d\sigma_{ij}^{(\text{NLO})}(r_R)}{d\mathcal{K}} &= \delta\left(\mathcal{K} - \mathcal{K}_{n+1}^{(E)}\right) \frac{d\sigma_{ij}^{(\text{NLO},E)}(r_R)}{d\chi_{Bj}^{(ij)} d\chi_{n+1}^{(ij)}} d\chi_{Bj}^{(ij)} d\chi_{n+1}^{(ij)} \\ &+ \delta\left(\mathcal{K} - \mathcal{K}_{n+1}^{(S)}\right) \sum_{\alpha=S,C,SC} \frac{d\sigma_{ij}^{(\text{NLO},\alpha)}(r_R)}{d\chi_{Bj}^{(ij)} d\chi_{n+1}^{(ij)}} d\chi_{Bj}^{(ij)} d\chi_{n+1}^{(ij)}, \end{aligned} \quad (2.47)$$

where we have understood the complete integration over the measures on the r.h.s.. MADGRAPH5_AMC@NLO scans the phase space by generating randomly $\{\chi_{Bj}^{(ij)}, \chi_{n+1}^{(ij)}\}$. For each of these points, an event kinematic configuration $\mathcal{K}_{n+1}^{(E)}$ and its weight, and a counterterm kinematic configuration $\mathcal{K}_{n+1}^{(S)}$ and its weight are given in output; with these, any number of (IR-safe) observables can be constructed. As can be seen from eq. (2.47), the weight associated with the single counterterm kinematics is the sum of the soft, collinear, soft-collinear, Born, virtual, and initial-state collinear remainders contributions, which reduces the probability of mis-binning and thus increases the numerical stability of the result.

In order for the results of eq. (2.47) to be physical, they must still be summed over all processes $r_R \in \mathcal{R}_{n+1}$ and all FKS pairs $(i, j) \in \mathcal{P}_{\text{FKS}}(r_R)$. As far as the latter sum is concerned, it is easy to exploit the symmetries due to identical final-state particles, and thus to arrive at the set [59]:

$$\overline{\mathcal{P}}_{\text{FKS}} \subseteq \mathcal{P}_{\text{FKS}}, \quad (2.48)$$

whose elements give non-identical contributions to the sum over FKS pairs. Therefore:

$$\sum_{r_R \in \mathcal{R}_{n+1}} \sum_{(i,j) \in \mathcal{P}_{\text{FKS}}(r_R)} \frac{d\sigma_{ij}^{(\text{NLO})}(r_R)}{d\mathcal{K}} = \sum_{r_R \in \mathcal{R}_{n+1}} \sum_{(i,j) \in \overline{\mathcal{P}}_{\text{FKS}}(r_R)} \varsigma_{ij}^{(n+1)} \frac{d\sigma_{ij}^{(\text{NLO})}(r_R)}{d\mathcal{K}}, \quad (2.49)$$

¹²Whose dependence on α is a consequence of eq. (2.44) when $j = 1, 2$ – see ref. [24] for more details.

with $\varsigma_{ij}^{(n+1)}$ a suitable symmetry factor. The sum on the r.h.s. of eq. (2.49) is obviously more convenient to perform than that on the l.h.s.; it is customary to include the symmetry factor in the short-distance weights (see e.g. ref. [122]). The number of elements in $\overline{\mathcal{P}}_{\text{FKS}}(r_R)$ can indeed be much smaller than that in $\mathcal{P}_{\text{FKS}}(r_R)$. For example, when r_R is a purely gluonic process, we have $\#(\overline{\mathcal{P}}_{\text{FKS}}(r_R)) = 3$ (i.e., independent of n), while $\#(\mathcal{P}_{\text{FKS}}(r_R)) = (n+1)(n+2)$. While the former figure typically increases when quarks are considered, it remains true that, for asymptotically large n 's, $\#(\overline{\mathcal{P}}_{\text{FKS}})$ is a constant while $\#(\mathcal{P}_{\text{FKS}})$ scales as n^2 .

The sum on the r.h.s. of eq. (2.49) is what has been originally implemented in MADFKS. It emphasises the role of the real-emission processes, which implies that for quantities which are naturally Born-like (such as the Born matrix elements themselves) one needs to devise a way to map unambiguously \mathcal{R}_n onto \mathcal{R}_{n+1} . The interested reader can find the definition of such a map in sect. 6.2 of ref. [59], which we summarise here using the Born cross section $d\sigma^{(\text{LO})}$ as an example:

$$d\sigma^{(\text{LO})}(r_R) = \sum_{(i,j) \in \overline{\mathcal{P}}_{\text{FKS}}(r_R)} \delta_{g\mathcal{I}_i} \mathcal{S}_{ij}(\xi_i = 0) d\sigma^{(\text{LO})}(r_R^{\mathfrak{X}}), \quad (2.50)$$

where

$$r_R = (\mathcal{I}_1, \dots, \mathcal{I}_i, \dots, \mathcal{I}_j, \dots, \mathcal{I}_{n+3}) \implies r_R^{\mathfrak{X}} = (\mathcal{I}_1, \dots, \mathfrak{I}_i, \dots, \mathcal{I}_j, \dots, \mathcal{I}_{n+3}). \quad (2.51)$$

In other words, through the r.h.s. of eq. (2.50) one is able to define a Born-level quantity as a function of a real-emission process. In MADGRAPH5_AMC@NLO we have followed the opposite strategy, namely that of defining real-emission level quantities as functions of a Born process. The proof that this can indeed be done is given in appendix E of ref. [59]; here, we limit ourselves to summarising it as follows, using the event contribution $d\sigma_{ij}^{(\text{NLO},E)}$ to the NLO cross section as an example. One has the identity:

$$\sum_{r_R \in \mathcal{R}_{n+1}} \sum_{(i,j) \in \overline{\mathcal{P}}_{\text{FKS}}(r_R)} \varsigma_{ij}^{(n+1)} d\sigma_{ij}^{(\text{NLO},E)}(r_R) = \sum_{r_B \in \mathcal{R}_n} d\sigma^{(\text{NLO},E)}(r_B). \quad (2.52)$$

Here we have defined:

$$d\sigma^{(\text{NLO},E)}(r_B) = \sum_{r_R \in \mathcal{R}_{n+1}} \sum_{(i,j) \in \overline{\mathcal{P}}_{\text{FKS}}(r_R)} \delta(r_B, r_R^{j \oplus i, \mathfrak{X}}) \varsigma_{ij}^{(n+1)}(r_R) d\sigma_{ij}^{(\text{NLO},E)}(r_R), \quad (2.53)$$

where the generalised Kronecker symbol $\delta(\dots)$ is equal to one if its arguments are equal, and to zero otherwise, and

$$r_R^{j \oplus i, \mathfrak{X}} = (\mathcal{I}_1, \dots, \mathfrak{I}_i, \dots, \mathcal{I}_{j \oplus i}, \dots, \mathcal{I}_{n+3}). \quad (2.54)$$

Although the first sum in eq. (2.53) might seem to involve a very large number of terms, MADGRAPH5_AMC@NLO knows immediately which terms will give a non-zero contribution, thanks to the procedure used to construct \mathcal{R}_{n+1} which was outlined at the beginning of this section. On top of organising the sums over processes and FKS pairs in a different way

w.r.t. the first version of MADFKS, MADGRAPH5_AMC@NLO also performs some of these (and, specifically, those in eq. (2.53)) using MC techniques (whereas all sums are performed explicitly in ref. [59]). In particular, for any given $r_B \in \mathcal{R}_n$, one real-emission process and one FKS pair are chosen randomly among those which contribute to eq. (2.53); these choices are subject to importance sampling, and are thus adaptive. In summary, while the procedure adopted originally in MADFKS takes a viewpoint from the real-emission level, that adopted in MADGRAPH5_AMC@NLO emphasises the role of Born processes. The two are fully equivalent, but the latter is more efficient in the cases of complicated processes, and it offers some further advantages in the context of matching with parton showers.

2.4.2 One-loop matrix elements: MadLoop

Both MADGRAPH5_AMC@NLO and its predecessor AMC@NLO are capable of computing the virtual contribution to an NLO cross section in a completely independent manner (while still allowing one to interface to a third-party one-loop provider if so desired), through a module dubbed MADLOOP [66]. However, there are very significant differences between the MADLOOP embedded in AMC@NLO (i.e., the one documented in ref. [66]), and the MADLOOP currently available in MADGRAPH5_AMC@NLO; hence, in order to avoid confusion between the two, we shall call the former MADLOOP4, and the latter MADLOOP5. The aim of this section is that of reviewing the techniques for automated one-loop numerical computations, and of giving the first public documentation of MADLOOP5.

As the above naming scheme suggests, core functionalities relevant to the handling of tree-level amplitudes were inherited from MADGRAPH4 in MADLOOP4, while MADLOOP5 uses MADGRAPH5. This was a necessary improvement in view of the possibility of computing virtual corrections in arbitrary renormalisable models (i.e., other than the SM). More in general, one can identify the following three items as strategic capabilities, that were lacking in MADLOOP4, and that are now available in MADLOOP5¹³:

- A. The adoption of the procedures introduced with MADGRAPH5, and in particular the UFO/ALOHA chain for constructing amplitudes starting from a given model.
- B. The possibility of switching between two reduction methods for one-loop integrals, namely the Ossola-Papadopoulos-Pittau (OPP [18]) and the Tensor Integral Reduction (TIR [151, 152]) procedures.
- C. The organization of the calculation in a way consistent with the mixed-coupling expansion described in sect. 2.4, and in particular with eq. (2.23).

It should be clear that these capabilities induce an extremely significant broadening of the scope of MADLOOP (in particular, extending it beyond the SM). As a mere by-product, they have also completely lifted the limitations affecting MADLOOP4, which were described in sect. 4 of ref. [66]. It is instructive to see explicitly how this has happened. Item A. is responsible for lifting MADLOOP4 limitation #1 (MADLOOP4 cannot generate a process whose Born contains a four-gluon vertex, because the corresponding R_2 routines necessary

¹³Some of them are not yet public, but are fully tested.

in the OPP reduction were never validated, owing to the technically-awkward procedure for handling them in MADGRAPH4; this step is now completely bypassed thanks to the UFO/ALOHA chain). Limitation #2 (MADLOOP4 cannot compute some loops that feature massive vector bosons, which is actually a limitation of CUTTOOLS [153], in turn due to the use of the unitary gauge) is now simply absent because of the possibility of adopting the Feynman gauge, thanks again to item *A*. Limitation #4 (MADLOOP4 cannot handle finite-width effects in loops) is removed thanks to the implementation of the complex mass scheme, a consequence of item *A*. Finally, item *C*. lifts MADLOOP4 limitation #3 (MADLOOP4 cannot generate a process if different contributions to the Born amplitudes do not factorise the same powers of all the relevant coupling constants).

The advances presented in items *A.–C.* above are underpinned by many technical differences and improvements w.r.t. MADLOOP4. Here, we limit ourselves to listing the most significant ones:

- MADLOOP5 is written in Python, the same language which was adopted for MADGRAPH5 (MADLOOP4 was written in C++).
- The UV-renormalisation procedure has been improved and rendered fully general (that of MADLOOP4 had several hard-coded simplifying solutions, motivated by QCD).
- An extensive use is made of the optimisations proposed in ref. [71] (OPENLOOPS).
- The self-diagnostic numerical-stability tests, and the procedures for fixing numerically-unstable loop-integral reductions, have been redesigned.

More details on these points will be given in what follows. Before turning to that, we shall discuss the basic principles used by MADLOOP5 for the automation of the computation of one-loop integrals.

Generalities

Given a $2 \rightarrow n$ partonic process r (see eq. (2.28)), MADLOOP computes the quantity:

$$V(r) = \sum_{\substack{\text{colour} \\ \text{spin}}} 2\Re \left\{ \mathcal{A}^{(n,1)}(r) \mathcal{A}^{(n,0)}(r)^* \right\}, \quad (2.55)$$

with $\mathcal{A}^{(n,0)}$ and $\mathcal{A}^{(n,1)}$ being the relevant tree-level and UV-renormalised one-loop amplitudes respectively; the averages over initial-state colour and spin degrees of freedom are understood. The result for $V(r)$ is given as a set of three numbers, corresponding to the residues of the double and single IR poles, and the finite part, all in the 't Hooft-Veltman scheme [154]. In the case of a mixed-coupling expansion, each of these three numbers is replaced by a set of coefficients, in the form given by eq. (2.23). There may be processes for which $\mathcal{A}^{(n,0)}$ is identically equal to zero, and $\mathcal{A}^{(n,1)}$ is finite; for these processes (called loop-induced), MADLOOP computes the quantity:

$$V_{\text{LI}}(r) = \sum_{\substack{\text{colour} \\ \text{spin}}} \left| \mathcal{A}^{(n,1)}(r) \right|^2. \quad (2.56)$$

Only eq. (2.55) is relevant to NLO computations proper, and we shall mostly deal with it in what follows. In the current version of MADGRAPH5_AMC@NLO, the loop-induced $V_{\text{LI}}(r)$ cannot be automatically integrated (for want of an automated procedure for multi-channel integration), and hence in this case the code output by MADLOOP5 must be interfaced in an ad-hoc way to any MC integrator (including MADGRAPH5_AMC@NLO – see e.g. ref. [124] for a recent application).

The basic quantity which MADLOOP needs to compute and eventually renormalise in order to obtain $\mathcal{A}^{(n,1)}$ that enters eq. (2.55) is the one-loop UV-unrenormalised amplitude:

$$\mathcal{A}_{\text{U}}^{(n,1)} = \sum_{\text{diagrams}} \mathcal{C}, \quad (2.57)$$

where \mathcal{C} denotes the contribution of a single Feynman diagram after loop integration, whose possible colour, helicity, and Lorentz indices need not be specified here, and are understood; they will be re-instated later. A standard technique for the evaluation of \mathcal{C} is a so-called reduction procedure, pioneered by Passarino and Veltman [151], which can be written as follows:

$$\mathcal{C} = \text{Red}[\mathcal{C}] = \sum_i c_i(\mathcal{C}) \mathcal{J}_i^{(\text{Red})} + R(\mathcal{C}). \quad (2.58)$$

The quantities $\mathcal{J}_i^{(\text{Red})}$ are one-loop integrals, independent of \mathcal{C} . The essence of any reduction procedure is that it is an *algebraic* operation that determines the coefficients c_i and R (which are functions of external momenta and of masses, and some of which may be equal to zero); the intricacies of loop integration are dealt once and for all in the computations of the $\mathcal{J}_i^{(\text{Red})}$'s (which are much simpler than any \mathcal{C}). As the leftmost equality in eq. (2.58) indicates, from the operator point of view $\text{Red}[\]$ is the identity; its meaning is that of replacing \mathcal{C} with the linear combination in the rightmost member of eq. (2.58). As the notation $\{\mathcal{J}_i^{(\text{Red})}\}$ suggests, different reduction procedures can possibly make use of different sets of one-loop integrals.

Equation (2.58) is basically what one would do if one were to compute \mathcal{C} in a non-automated manner. In automated approaches, however, additional problems arise, for example due to the necessity of relying on numerical methods, which have obvious difficulties in dealing with the non-integer dimensions needed in the context of dimensional regularisation, and with the analytical information on the integrand of \mathcal{C} , which is extensively used in non-automated reductions. In order to discuss how these issues can be solved, let us write \mathcal{C} in the following form:

$$\mathcal{C} = \int d^d \bar{\ell} \bar{C}(\bar{\ell}), \quad \bar{C}(\bar{\ell}) = \frac{\bar{N}(\bar{\ell})}{\prod_{i=0}^{m-1} \bar{D}_i}, \quad (2.59)$$

where $d = 4 - 2\epsilon$, and we have assumed the diagram to have m propagators in the loop and have defined:

$$\bar{D}_i = (\bar{\ell} + p_i)^2 - m_i^2, \quad 0 \leq i \leq m-1, \quad (2.60)$$

with m_i the mass of the particle relevant to the i^{th} loop propagator, and p_i some linear combination of external momenta. For any four-dimensional quantity x , its $(4 - 2\epsilon)$ -dimensional counterpart is denoted by \bar{x} , and its (-2ϵ) -dimensional one by \tilde{x} . The fact

that p_i , rather than \bar{p}_i , enters eq. (2.60) is a consequence of the use of the 't Hooft-Veltman scheme. The loop momentum is decomposed as follows:

$$\bar{\ell} = \ell + \tilde{\ell} \quad \text{with} \quad \ell \cdot \tilde{\ell} = 0, \quad (2.61)$$

with similar decompositions holding for the Dirac matrices $\bar{\gamma}^\mu$ and metric tensor $\bar{g}^{\mu\nu}$. One can thus define [155] the purely four-dimensional part of the numerator that appears in eq. (2.59):

$$N(\ell) = \lim_{\epsilon \rightarrow 0} \bar{N}(\bar{\ell} = \ell; \bar{\gamma}^\mu = \gamma^\mu, \bar{g}^{\mu\nu} = g^{\mu\nu}), \quad (2.62)$$

from whence one can obtain its (-2ϵ) -dimensional counterpart:

$$\tilde{N}(\ell, \tilde{\ell}) = \bar{N}(\bar{\ell}) - N(\ell). \quad (2.63)$$

The quantity defined in eq. (2.62), not involving non-integer dimensions, can be treated by a computer with ordinary techniques. By using eq. (2.63) in eq. (2.59) one obtains:

$$\mathcal{C} = \mathcal{C}_{\text{non-}R_2} + R_2, \quad (2.64)$$

where

$$\mathcal{C}_{\text{non-}R_2} = \int d^d \bar{\ell} \frac{N(\ell)}{\prod_{i=0}^{m-1} \bar{D}_i}, \quad (2.65)$$

$$R_2 = \int d^d \bar{\ell} \frac{\tilde{N}(\ell, \tilde{\ell})}{\prod_{i=0}^{m-1} \bar{D}_i}. \quad (2.66)$$

Both integrals in eq. (2.65) and eq. (2.66) still depend on $(4-2\epsilon)$ -dimensional quantities, but they do so in a way that allows one to further manipulate and cast them in a form suitable for a fully numerical treatment. In particular, one can show [155] that the computation of R_2 is equivalent to that of a tree-level amplitude, constructed with a universal set of theory-dependent rules (see ref. [156], refs. [157–159], and refs. [160–162] for the QCD, QED+EW, and some BSM cases respectively), analogous to the Feynman ones and that can be derived once and for all (for each model) by just considering the one-particle-irreducible amplitudes with up to four external legs [163]. On the other hand, eq. (2.65) is still potentially divergent in four dimensions. The details of how this is dealt with may vary, but the common characteristic is that all of them are entirely defined by a reduction procedure. In other words, we shall use the following identity:

$$\mathcal{C} = \text{Red}[\mathcal{C}_{\text{non-}R_2}] + R_2, \quad (2.67)$$

which is a consequence of eqs. (2.58) and (2.64). The general idea is that all things that are inherently $(4-2\epsilon)$ -dimensional in $\text{Red}[\mathcal{C}_{\text{non-}R_2}]$ can be parametrized in terms of the one-loop integrals $\mathcal{J}_i^{(\text{Red})}$, so that any piece of computation that would require an analytical knowledge of the integrand and an analytical treatment of the (-2ϵ) -dimensional terms is indeed treated analytically, but in a universal manner through $\mathcal{J}_i^{(\text{Red})}$.

We emphasise that, although the decomposition of eq. (2.64) is inspired by the OPP reduction method, it is universal, in the sense that the operator $\text{Red}[\]$ in eq. (2.67) does not

need to be OPP-inspired, and that the definition of R_2 has nothing to do with the OPP procedure as such, but rather with the interplay of $(4 - 2\epsilon)$ -dimensional quantities and their four-dimensional counterparts. There are of course several alternative approaches, but the majority of them do not lend themselves to the *numerical* computation of the rational part $R(\mathcal{C}_{\text{non-}R_2}) + R_2$. The two methods which have been used for complicated numerical simulations are bootstrap [17] and D -dimensional unitarity [19,20,23]. However, they also involve rather non-trivial issues, such as the presence of spurious singularities (for bootstrap), or the necessity of performing additional computations in 6 and 8 dimensions (for D -dimensional unitarity). The latter problem can be bypassed by means of a mass shift [164], which however might imply additional complications in the case of axial couplings in massive theories. In summary, while it is true that there are advantages and disadvantages in each of these approaches, we point out that R_2 must not really be seen as an extra issue in the context of a complete calculation, simply because one has to carry out UV renormalisation anyhow, which is similar to R_2 but more involved.

Integral reduction in MadLoop

We now turn to discussing the way in which the previous formulae are handled by MAD-LOOP. In order to do so, we shall re-instate in the notation the dependence of the amplitudes on the relevant quantities; in particular, we work with scalar sub-amplitudes that have definite helicities (i.e., all Lorentz indices are contracted away, and all Dirac matrices are sandwiched between spinors), and that factorise a single colour factor. The latter condition implies that, in general, our sub-amplitudes are not in one-to-one correspondence with Feynman diagrams (typically when these feature at least a four-gluon vertex), but that they can be written as follows:

$$\mathcal{A}_h^{(n,0)} = \sum_b \lambda_b^{(0)} \mathcal{B}_{h,b}, \quad (2.68)$$

for the Born amplitude. Here, h denotes a given helicity configuration, and b runs over all possible single-colour factors. The quantity $\lambda_b^{(0)}$ is one such colour factor, that collects all the colour indices, which are understood. Hence, $\mathcal{B}_{h,b}$ is a scalar quantity which does *not* contain any colour index. In the case of one-loop diagrams, we shall use a similar notation, thus replacing the quantities that appear in eqs. (2.65) and (2.66) with:

$$N(\ell) \longrightarrow \lambda_l^{(1)} \mathcal{N}_{h,l}(\ell), \quad (2.69)$$

$$\bar{D}_i \longrightarrow \bar{D}_{i,l}, \quad (2.70)$$

$$R_2 \longrightarrow R_{2,h,l}. \quad (2.71)$$

The quantity $\lambda_l^{(1)}$ in eq. (2.69) has the same meaning as $\lambda_b^{(0)}$ in eq. (2.68), but is relevant to one-loop amplitudes rather than tree-level ones, hence the different notation. Since the index l unambiguously identifies a single-colour-structure subamplitude, and the latter has a non-trivial kinematic dependence, different l 's may correspond to different one-loop Feynman diagrams, and thus the necessity of inserting a dependence on l on the r.h.s. of eq. (2.70). Finally, we did not factor out the colour structure in eq. (2.71), since this will

not be relevant in the following. We remark that decompositions such as those on the r.h.s.'s of eqs. (2.68) and (2.69) are easily handled by `MADGRAPH5_AMC@NLO`, which has inherited the treatment of the colour algebra from `MADGRAPH5` (see sect. 2.3 of ref. [36]). It should be stressed that such a treatment is symbolic and that, although introduced to deal with tree-level quantities, is perfectly capable of computing one-loop ones such as $\lambda_l^{(1)}$. Furthermore, the colour algebra is internally decomposed in terms of colour flows (for which several different representations are available); although this information is presently not used in the integral-reduction procedure, it will be trivial to exploit it in the future, should this need arise. By using eqs. (2.68)–(2.71) one obtains:

$$\mathcal{A}_U^{(n,1)} \mathcal{A}^{(n,0)*} = \sum_{\text{colour}} \sum_h \left(\sum_l \lambda_l^{(1)} \int d^d \bar{\ell} \frac{\mathcal{N}_{h,l}(\ell)}{\prod_{i=0}^{m_l-1} \bar{D}_{i,l}} + \sum_l R_{2,h,l} \right) \left(\sum_b \lambda_b^{(0)} \mathcal{B}_{h,b} \right)^* . \quad (2.72)$$

As was already mentioned, the R_2 term gives rise to what is effectively a tree-level computation; therefore, we shall drop it in what follows, and just deal with:

$$\mathcal{A}_U^{(n,1)} \mathcal{A}^{(n,0)*} \Big|_{\text{non-}R_2} = \sum_h \sum_l \sum_b \int d^d \bar{\ell} \frac{\mathcal{N}_{h,l}(\ell)}{\prod_{i=0}^{m_l-1} \bar{D}_{i,l}} \Lambda_{lb} \mathcal{B}_{h,b}^* , \quad (2.73)$$

$$\Lambda_{lb} = \sum_{\text{colour}} \lambda_l^{(1)} \lambda_b^{(0)*} . \quad (2.74)$$

The integral-reduction procedure of `MADLOOP4` [66] can be read directly from eq. (2.73), and is as follows:

$$\mathcal{A}_U^{(n,1)} \mathcal{A}^{(n,0)*} \Big|_{\text{non-}R_2} = \sum_h \sum_l \sum_b \text{Red} \left[\int d^d \bar{\ell} \frac{\mathcal{N}_{h,l}(\ell)}{\prod_{i=0}^{m_l-1} \bar{D}_{i,l}} \right] \Lambda_{lb} \mathcal{B}_{h,b}^* , \quad (2.75)$$

where $\text{Red} \equiv \text{OPP}$, since in `MADLOOP4` only OPP reduction has been considered. Equation (2.75) is not particularly satisfactory from an efficiency point of view, for two reasons, both of which have to do with the fact that the integral-reduction operation is quite time-consuming. Firstly, the $\text{Red}[]$ operator is called $\#h \times \#l$ number of times (we recall that, by construction, $\#l$ is equal to or larger than the number of loop diagrams). Secondly, each of these calls involves the recomputation of $\mathcal{N}_{h,l}(\ell)$ a large number of times (determined by the OPP procedure), but which involve only changing the numerical value of ℓ , without affecting any other quantity entering it. The first issue is solved by reducing the number of integral-reduction operations, while the second by rendering more efficient the computation of $\mathcal{N}_{h,l}(\ell)$. The strategies adopted in `MADLOOP5` are the following. One begins by observing that the operator $\text{Red}[]$ acts on the “space” of one-loop integrals. Therefore, Born amplitudes must be seen as c-numbers as far as this operator is concerned. One can thus exploit the fact that $\text{Red}[]$ is linear. Furthermore, what really drives integral reduction is the structure of the denominators (numerators are just numbers computed with suitable values of ℓ , specific to the given $\text{Red}[]$ operator). Hence, one can organize loop integrals in sets of *topologies*, the latter being defined as subsets of integrals with the same

denominator combinations:

$$\prod_{i=0}^{m_l-1} \bar{D}_{i,l} = \prod_{i=0}^{m_p-1} \bar{D}_{i,p}, \quad \forall l, p \in t, \quad t \in \text{topologies}. \quad (2.76)$$

By exploiting eq. (2.76), one can rewrite eq. (2.75) as follows:

$$\mathcal{A}_U^{(n,1)} \mathcal{A}^{(n,0)*} \Big|_{\text{non-}R_2} = \sum_t \text{Red} \left[\int d^d \bar{\ell} \frac{\sum_h \sum_{l \in t} \sum_b \mathcal{N}_{h,l}(\ell) \Lambda_{lb} \mathcal{B}_{h,b}^*}{\prod_{i=0}^{m_{l_t}-1} \bar{D}_{i,l_t}} \right], \quad (2.77)$$

for any $l_t \in t$. Eq. (2.77) is optimal from the viewpoint of reducing the number of calls to $\text{Red}[\cdot]$, and thus addresses the first of the issues mentioned before. As far as the second of those issues is concerned, MADLOOP5 makes a systematic use of the fact that any numerator $\mathcal{N}_{h,l}(\ell)$ admits the following representation:

$$\mathcal{N}_{h,l}(\ell) = \sum_{r=0}^{r_{\max}} C_{\mu_1 \dots \mu_r; h, l}^{(r)} \ell^{\mu_1} \dots \ell^{\mu_r}, \quad (2.78)$$

where the coefficients $C^{(r)}$ are independent of the loop momentum; when $r = 0$, we understand that no Lorentz indices and no loop momenta appear on the r.h.s. of eq. (2.78). The quantity r_{\max} is the largest rank in $\mathcal{N}_{h,l}$, and in the Feynman gauge in renormalisable theories is always lower than or equal to the number of loop propagators. However, since different $\mathcal{N}_{h,l}$ functions appear in the inner sums in eq. (2.77), it is actually convenient (just for the sake of using the present simplified notation) to regard it as the largest rank in the whole one-loop amplitude; for a given $\mathcal{N}_{h,l}$, this simply implies that some of the $C^{(r)}$ coefficients will be equal to zero. Equation (2.78) can be exploited in two ways. One starts by determining the $C^{(r)}$'s once and for all. Then, in the context of the OPP reduction, the numerical computation of $\mathcal{N}_{h,l}(\ell)$ becomes much faster, as suggested originally in OPENLOOPS (see ref. [71]), because for each new value of ℓ generated within the OPP reduction one simply needs to perform the sums and multiplications explicit in eq. (2.78), without recomputing the $C^{(r)}$'s. Furthermore, when eq. (2.78) is symbolically (as opposed to numerically) replaced in eq. (2.77), the structures of tensor integrals naturally emerge. Thus, eq. (2.78) paves the way to performing a Tensor Integral Reduction (TIR) as well. Therefore, regardless of whether an OPP or TIR procedure will be applied, the inputs to the $\text{Red}[\cdot]$ operator in MADLOOP5 are the sets:

$$\left\{ \int d^d \bar{\ell} \frac{\ell^{\mu_1} \dots \ell^{\mu_r}}{\prod_{i=0}^{m_{l_t}-1} \bar{D}_{i,l_t}}, \sum_h \sum_{l \in t} \sum_b C_{\mu_1 \dots \mu_r; h, l}^{(r)} \Lambda_{lb} \mathcal{B}_{h,b}^* \right\}_{r=0}^{r_{\max}}. \quad (2.79)$$

Then, when using OPP the Lorentz indices of the two members of these sets are contracted in order to give OPP the scalar functions it needs. On the other hand, when using TIR the first members in eq. (2.79) are all that is needed for this type of reduction to work. It is clear that the practical success of the decomposition in eq. (2.78) relies on the capability of a fast and efficient computation of the coefficients $C^{(r)}$. MADLOOP5 has a fully independent implementation of the recursion-construction procedure presented in ref. [71] (thanks to a

dedicated treatment by ALOHA), and its own internal system of caching and retrieving the $C^{(r)}$'s. At variance with what is done in ref. [71], MADLOOP5 does not assume r_{\max} to be less than or equal to the number of loop propagators, i.e. it admits the possibility that the contribution of any given vertex to the rank of $\mathcal{N}_{h,l}(\ell)$ be larger than one. This is useful, for example, in the context of the computation of QCD corrections to processes stemming from a Higgs EFT Lagrangian. See appendix C.3 for more details.

We conclude this part with a few diverse observations. Firstly, given the advantages of an efficient caching and recycling of the coefficients $C^{(r)}$, in the case of a mixed-coupling expansion MADLOOP5 starts from determining all of the coefficients that will contribute to $\Sigma_{k_0+1,0}$ (we recall that we always associate the largest power of the dominant coupling constant, as defined by the hierarchy of the model, with the terms $q = 0$: see sect. 2.4). Some of the $C^{(r)}$'s thus computed will also contribute to $\Sigma_{k_0+1,1}$, for which MADLOOP5 will only calculate those $C^{(r)}$'s not yet found, and just recycle the others. This procedure is then iterated till necessary, in the sense that it can be stopped when reaching the largest q 's among those selected by the user; it is maximally efficient when the smallest user-selected q is equal to zero, which is justified from a physics viewpoint given the coupling hierarchy of the model. Secondly, in general the kinematic configurations which are potentially unstable in TIR are rather different than with OPP; therefore, the possibility of using TIR as an alternative to OPP before turning to quadruple-precision calculations (see below) is very beneficial for reducing the overall computing time when numerically-unstable situations are encountered. Finally, since TIR essentially performs integral reduction at the level of amplitudes, rather than at that of amplitude squared as OPP, it allows one to use efficiently the decomposition of eq. (2.78) and its caching-and-recycling system also in the case of loop-induced matrix elements, eq. (2.56).

UV renormalisation and R_2 contribution

In order to obtain $V(r)$ as defined in eq. (2.55), MADLOOP must sum to the result of the integral-reduction procedure, eq. (2.77), the R_2 (see eq. (2.72)) and the UV-renormalisation contributions. Both of these can be cast in the form of a tree-level-like amplitude $\mathcal{A}^{(n,x)}$ times the Born amplitude, whose contribution to eq. (2.55) will therefore be:

$$\sum_{\substack{\text{colour} \\ \text{spin}}} 2\Re \left\{ \mathcal{A}^{(n,x)}(r) \mathcal{A}^{(n,0)}(r)^* \right\}, \quad X = R_2, \text{ UV}. \quad (2.80)$$

In an automated approach, the computation of $\mathcal{A}^{(n,x)}$ may be performed in the same manner as that of $\mathcal{A}^{(n,0)}$, provided that the usual Feynman rules are supplemented by new UV and R_2 rules, and by imposing that $\mathcal{A}^{(n,x)}$ contain one and only one UV- or R_2 -type vertex¹⁴. This was indeed the procedure adopted by MADLOOP4 for the R_2 computation. As far as UV renormalisation was concerned, the fact that MADLOOP4 was limited to considering QCD corrections to SM processes allowed significant simplifications, and eq. (2.80) was effectively computed in a simpler way, by taking the Born amplitude squared multiplied by suitable UV factors. Mass insertions cannot be accounted for in this way; however,

¹⁴Note that in this context a “vertex” can have two external legs.

their structure being identical to that of the R_2 two-point vertex, the two could always be treated together (see ref. [66] for more details).

The above solution is not tenable when considering an arbitrary renormalisable theory, and therefore MADLOOP5 must explicitly compute eq. (2.80) for both the UV and R_2 contributions. This is not the only significant difference between MADLOOP4 and MADLOOP5. According to the general philosophy of the current MADGRAPH5_AMC@NLO approach, the UV and R_2 rules are part of the NLO theory model¹⁵ chosen by the user, and that MADLOOP adopts when performing a computation: they are not (as opposed to what happened with MADLOOP4) hard-coded UV or R_2 computer routines corresponding to n -point counterterms, but a set of instructions in UFO, that ALOHA will dynamically translate into the latter routines.

After including the UV and R_2 rules into a UFO model (an operation that, we remind the reader, has to be performed once and for all per theory and per type of corrections, and which FEYNRULES will soon be able to perform automatically), it should be clear that the computation by MADGRAPH5_AMC@NLO of $\mathcal{A}^{(n,X)}$ becomes identical to that of a regular tree-level amplitude for which only Feynman rules are relevant; thus, we shall call this a tree-matching construction. In order to increase the flexibility of MADLOOP5, in particular for what concerns the exclusion of the contributions of certain loop integrals, and to allow developers more freedom when debugging, an alternative but fully equivalent procedure has been implemented, which we shall call loop-matching construction. The tree-matching and loop-matching constructions (an explanation of which will be given below) can be understood by considering the physics contents of the generic UV and R_2 counterterm G , which we shall denote as follows:

$$G = \left\{ \left\{ \mathcal{I}_1^{(e)}, \dots, \mathcal{I}_m^{(e)} \right\}; \left\{ \mathcal{I}_1^{(l_k)}, \dots, \mathcal{I}_{n_k}^{(l_k)} \right\}_{k=1}^{k_{loop}}; \mathcal{W}, L, \lambda, c, X \right\}. \quad (2.81)$$

The quantity X determines the kind of counterterm one is working with – UV wavefunction, or internal n -point UV and R_2 functions; it also allows the builder of the model to specify whether G will be used in the context of a tree-matching or loop-matching construction. In other words, and in order to stress this point again: MADLOOP5 can handle both types of construction, which are simply seen as attributes of the model used for the computation. This flexibility is important for example because models constructed “by hand” are set up in a different way w.r.t. that adopted by FEYNRULES. The quantity c is symbolically (i.e., not numerically) set equal to a coupling constant, with that implying that G is a counterterm relevant to NLO corrections in the theory whose perturbative expansion is governed by that coupling. Note that in a model there may be several subsets of counterterms, each associated with a different type of correction; in the example of the mixed QCD-QED case discussed at the beginning of sect. 2.4, when $c = \alpha_s$ one has counterterms for QCD corrections (eq. (2.26)), and when $c = \alpha$ one has counterterms for QED corrections (eq. (2.27)). The quantities L and λ in eq. (2.81) denote the Lorentz and colour structures of G respectively. The set $\{\mathcal{I}_1^{(e)}, \dots, \mathcal{I}_m^{(e)}\}$ is the list of “external” particle identities associated with G . For example, if G is the contribution to α_s renormalisation

¹⁵In fact, it is their very presence that tells NLO and LO models apart. See also sect. 2.1.

due to the $gu\bar{u}$ vertex, then this set is equal to $\{g, u, \bar{u}\}$; if G corresponds to the mass insertion for the top quark, then one has¹⁶ $\{t, \bar{t}\}$. The counterterm G in general receives contributions from $k_{loop} \geq 1$ different types of loop diagrams, and $\{\mathcal{I}_1^{(l_k)}, \dots, \mathcal{I}_{n_k}^{(l_k)}\}$ is called the k^{th} loop topology, i.e. the set of the identities of the particles circulating in the k^{th} type of loop¹⁷. When counting these loops, one needs to take into account the physical meaning of G . By using again the example of the $gu\bar{u}$ vertex, one may be tempted to conclude that $k_{loop} = 1$, which corresponds to the triangle corrections to such a vertex. This would be incorrect: in fact, since G is a contribution to α_s renormalisation, it must include wave-function renormalisation factors; therefore, in the k_{loop} types of loops one must include the bubble diagrams relevant to the g , u , and \bar{u} external legs. Thus, in this example one will need to consider both $\{g, u\}$ (for triangles and the u self-energy) and $\{g\}$, $\{q\}$, $\{b\}$, $\{t\}$ (for the gluon self-energy; q is a massless quark, and b and t are heavy quarks). It should be clear that this complication (there are more loop topologies that contribute to G than the list of its external particles would suggest) is basically due to wave-function renormalisation, which physically corresponds to the fact that renormalised couplings are defined in terms of renormalised Green functions. When this is not the case, and notably for mass insertions, and for R_2 contributions (because the latter are directly defined in terms of specific loop integrals – see eq. (2.66)), loop topologies are indeed in one-to-one correspondence with those naively deduced from the list of external particles. Finally, in eq. (2.81) \mathcal{W} represents the actual value of the counterterm G . By following the usual textbook procedure which makes use of renormalised coupling constants, and by ignoring the Lorentz and colour structures, one may e.g. have:

$$\mathcal{W} \propto 1 - Z_{\text{coupling}}^{-1} = 1 - Z_{\text{vertex}}^{-1} \prod_i Z_{\text{wf},i}, \quad \mathcal{W} = 0, \quad (2.82)$$

for coupling and internal 2-point (bubble) renormalisation respectively, and

$$\mathcal{W} \propto \delta m, \quad \mathcal{W} \propto W_{R_2, \text{vertex}}, \quad (2.83)$$

for UV mass insertions and an R_2 correction, respectively. From the discussion presented before, it follows that the Z and δm terms in eqs. (2.82) and (2.83) will be related to the sets $\{\mathcal{I}_1^{(l_k)}, \dots, \mathcal{I}_{n_k}^{(l_k)}\}$. On the other hand, MADLOOP5 leaves the model builder the possibility of implementing coupling-constant renormalisation by directly working at the level of vertex renormalisation. This can be simply done for example by adopting:

$$\mathcal{W} \propto 1 - Z_{\text{vertex}}^{-1}, \quad \mathcal{W} \propto 1 - Z_{\text{wf},i}, \quad (2.84)$$

instead of the settings of eq. (2.82). One may (slightly improperly, since the physics contents are exactly the same) refer to the procedures induced by eq. (2.82) and eq. (2.84) as

¹⁶A mass insertion is treated in a similar manner as vertices; therefore, all external particles must be outgoing, whence the \bar{t} .

¹⁷The term “set” implies that two or more identical particles contribute *one* particle identity to this set, as opposed to the case of external particles, which are all explicitly present in the *list* $\{\mathcal{I}_1^{(e)}, \dots, \mathcal{I}_m^{(e)}\}$. Note that, when circulating in a loop, a quark and its antiquark can be identified. Furthermore, it should be clear that the present “topology” has nothing to do with that introduced in eq. (2.76).

coupling-constant and vertex renormalisation respectively. The latter is the current method of choice for the extension of FEYNRULES to NLO. Note that, when working with vertex renormalisation, wave-function factors for external legs need not be included (as opposed to the usual case of coupling-constant renormalisation), which can be easily specified in the model definition. Again, no assumption is made in MADLOOP5 on the treatment of external legs, and full flexibility is maintained by reading the relevant information from the model.

Now we suppose that an NLO model is given, and thus eq. (2.81) is fully specified for all counterterms relevant to all types of corrections dealt with by the model. We shall now discuss how MADLOOP5 exploits such information. First of all, one may want to exclude some loops from the calculation (this can be motivated by physics requirements, for example when leaving out heavy-flavour contributions, or done for debugging purposes); we call this operation *loop-content filtering* (not to be confused with diagram filtering, which discards over-counting L-cut diagrams at generation time – see sect. 3.2.1 of ref. [66]). This filtering is basically trivial in the generation of diagrams: one simply does not include the undesired particles in the list of L-cut particles. The presence of $\{\mathcal{I}_1^{(l_k)}, \dots, \mathcal{I}_{n_k}^{(l_k)}\}$ in eq. (2.81) allows one to do the same when computing the UV and R_2 contributions: if this set contains the particle(s) to be discarded, the corresponding contributions are not included in eqs. (2.82)–(2.84). Apart from loop-content filtering, eq. (2.81) can be exploited in the context of the tree-matching construction in the same way as all other elementary building blocks derived from ordinary Feynman rules, by using the information on external particles, and Lorentz and colour structures. As far as the loop-matching construction is concerned, one starts from a given loop integral \mathcal{C} , and determines what we call its associated tree topology:

$$\mathcal{C} \longrightarrow \Gamma^{(\mathcal{C})} = \left(\{\mathcal{T}_1, \dots, \mathcal{T}_{T(\mathcal{C})}\}, \{\mathcal{I}_1^{(l_{\mathcal{C}})}, \dots, \mathcal{I}_n^{(l_{\mathcal{C}})}\} \right). \quad (2.85)$$

The notation understands that there are $T(\mathcal{C})$ trees \mathcal{T}_α attached to the loop¹⁸ (see fig. 2 of ref. [66] for a graphical example of such trees); $\{\mathcal{I}_1^{(l_{\mathcal{C}})}, \dots, \mathcal{I}_n^{(l_{\mathcal{C}})}\}$ is the set of particles that flow in the loop. Since different loops can have the same associated tree topology, MADLOOP5 first collects all of the different tree topologies relevant to the computation being performed. Next, for each of these, all counterterm vertices G (that have survived loop-content filtering) are found that fulfill the following equation:

$$\{\mathcal{I}_1^{(e)}, \dots, \mathcal{I}_m^{(e)}\} = \{\mathcal{R}(\mathcal{T}_1), \dots, \mathcal{R}(\mathcal{T}_{T(\mathcal{C})})\}, \quad (2.86)$$

where by $\mathcal{R}(\mathcal{T}_\alpha)$ we have denoted the root of the α^{th} tree \mathcal{T}_α (the root being obviously the single particle that stems from the loop, and branches into the tree); note that eq. (2.86) implies $m = T(\mathcal{C})$. Among the counterterms thus found, one further considers the UV mass insertion and R_2 ones, and discards those that do not fulfill the equation:

$$\{\mathcal{I}_1^{(l_k)}, \dots, \mathcal{I}_{n_k}^{(l_k)}\} = \{\mathcal{I}_1^{(l_{\mathcal{C}})}, \dots, \mathcal{I}_n^{(l_{\mathcal{C}})}\}. \quad (2.87)$$

¹⁸A four-gluon vertex, with two gluons belonging to the loop, gives rise to two trees, both of which are attached to the loop at the same point.

Equation (2.87) guarantees a rather strict correlation between a generated diagram and its UV and R_2 counterterms, which is quite useful for example when establishing the correctness of a model. It should be pointed out, however, that such a correlation can never be turned into a one-to-one map, because of coupling-constant or vertex renormalisation, in which case eq. (2.87) cannot be imposed (since vertex corrections and wave-function renormalisation are always strictly related, and this is true also when carrying out a vertex-renormalisation procedure). Finally, for each counterterm G selected as explained above, MADLOOP5 builds the corresponding tree amplitude by attaching to G the off-shell currents relevant to the tree structures $\{\mathcal{T}_1, \dots, \mathcal{T}_{T(C)}\}$. When performing coupling-constant renormalisation, MADLOOP5 also constructs additional tree-amplitude counterterms by multiplying each Born amplitude by the suitable combination of external wave-function factors.

We conclude this part by re-iterating its main message: MADLOOP5 has a fully-flexible structure that allows it to handle on equal footing several different strategies, such as tree-matching vs loop-matching construction, or coupling vs vertex renormalisation, thanks to its capability of obeying the relevant instructions encoded in the model. This includes the prescription for the renormalisation scheme, which now must be simply seen as one of the model characteristics.

Checks, stability, and recovery of numerically-unstable integral reductions

MADLOOP4 featured many self-consistency checks, that served to establish the correctness of any one-loop matrix element generated by the code; they are described extensively in sect. 3.3 of ref. [66], and all of them are inherited by MADLOOP5. On top of those, in MADLOOP5 we have included two new checks: firstly, we verify that the matrix elements are Lorentz scalars, by recomputing them using a kinematic configuration obtained by boosting and rotating the original one; and secondly, in the case of QCD corrections we test whether the matrix elements computed in the unitary gauge are identical to those computed in the Feynman gauge¹⁹. The experience with MADLOOP4 and MADLOOP5 has shown that there is a vast amount of redundancy in all of these checks; therefore, in MADLOOP5 we have decided to perform only one of them before proceeding to integrate the matrix elements. We have chosen the most complete one, namely that on the residues of the infrared poles (where the numerical values of such residues as returned by MADLOOP are compared to those known analytically from the subtraction of real-emission singularities), which has the virtue of being an indirect test on the UV-renormalisation procedure as well. The other checks can still be performed if need be, by simply executing a single command from the MADGRAPH5_AMC@NLO interactive shell²⁰.

Integral-reduction procedures are fairly involved, and some kinematic configurations may give rise to numerically-unstable results. Any automated approach must therefore have solid self-diagnostic and recovery strategies: those of MADLOOP4 have been presented in sect. 3.4 of ref. [66]. In view of the extended scope of MADLOOP5 w.r.t. that of MADLOOP4, both of these strategies have been completely redesigned, for the technical reasons which

¹⁹Incidentally, these tests can also be performed in the context of tree-level matrix-element computations.

²⁰Apart from that on the dependence on the mass of a heavy quark, which is still available but too process-specific to be worth automating.

we shall now discuss. Firstly, MADLOOP4 based the instability diagnostics on the results of tests performed within CUTTOOLS, on a loop-by-loop basis. Therefore, the capability of MADLOOP5 to exploit both the OPP and TIR methods has forced us to set up a CUTTOOLS-independent diagnostic tool. Furthermore, a loop-by-loop method is in any case not ideal, because it is never trivial to determine the threshold that decides when a computation is flagged as unstable (e.g., a single loop integral may be unstable, but give a totally negligible contribution to the full amplitude). This problem is exacerbated when increasing the final-state multiplicity, and indeed suggests to use an “inclusive” (i.e., at the level of the amplitude, rather than of the individual loop integral) type of test in MADLOOP5, which can handle more complicated processes than MADLOOP4. Secondly, the recovery strategy used by MADLOOP4 (which involved a small deformation of the kinematics) is on the one hand related to the loop-by-loop diagnostic (because when one considers two or more integrals simultaneously, the deformation of the kinematics that renders stable an unstable integral can turn a stable integral into an unstable one), and on the other hand not particularly satisfactory when increasing the process multiplicity (because it becomes more difficult to obtain a stable result out of the deformed kinematic configuration).

The diagnostic procedure of MADLOOP5 works as follows. Let us write the result of eq. (2.55), obtained by MADLOOP after integral reduction and UV renormalisation, as follows:

$$V(r) = \frac{(4\pi)^\epsilon}{\Gamma(1-\epsilon)} \left(\frac{\mu_F^2}{Q^2} \right)^\epsilon \left(\frac{c_{-2}}{\epsilon^2} + \frac{c_{-1}}{\epsilon} + c_0 \right). \quad (2.88)$$

For any given kinematic configuration, the coefficients c_j of eq. (2.88) are evaluated $1 + n_{test}$ times (in a way specified below), which we denote as follows:

$$c_j \longrightarrow c_j^{(i)}, \quad i = 0, \dots, n_{test}, \quad \text{for } j = -2, -1, 0. \quad (2.89)$$

These coefficients are used to define the following quantities:

$$\bar{c}_j = \frac{1}{2} \left(\max \left\{ |c_j^{(i)}| \right\}_{i=0}^{n_{test}} + \min \left\{ |c_j^{(i)}| \right\}_{i=0}^{n_{test}} \right), \quad (2.90)$$

$$\Delta c_j = \max \left\{ |c_j^{(i)}| \right\}_{i=0}^{n_{test}} - \min \left\{ |c_j^{(i)}| \right\}_{i=0}^{n_{test}}, \quad (2.91)$$

which in turn enter the definition of the relative accuracy of the MADLOOP evaluation:

$$\chi = \frac{\sum_{j=-2}^0 \Delta c_j}{\sum_{j=-2}^0 \bar{c}_j}. \quad (2.92)$$

A computation is deemed unstable, and the corresponding kinematic configuration called an Unstable Phase-Space point (UPS), when:

$$\chi > \varepsilon, \quad (2.93)$$

with ε a quantity which can be defined by the user, but whose default value is 10^{-3} . The $c_j^{(i=0)}$ results in eqs. (2.89)–(2.91) are those obtained by applying the OPP reduction

with the given kinematic configuration. The $c_j^{(i>0)}$ are obtained in two different ways, by performing again the integral reduction either: *a)* by using a kinematic configuration obtained by rotating the original one (hence, by following the same procedure as is used in one of the self-consistency checks previously discussed); or *b)* by using a different ordering of the loop propagators \bar{D}_i as input to OPP (this changes the inner workings of the reduction procedure, and is thus numerically different from, although physically completely equivalent to, what one does with the original ordering). These two re-computation procedures are called *Lorentz test* and *Direction test* respectively. By default, MADLOOP5 sets $n_{test} = 2$, and performs one Lorentz test and one Direction test. Both n_{test} and the type of tests performed can be controlled by the user. Note that any Direction test re-uses the coefficients $C^{(r)}$ of eq. (2.78) computed in the context of the first evaluation ($c_j^{(i=0)}$), and is thus less time-consuming than Lorentz tests, despite the fact that both require the integral reduction to be performed from scratch. In the case of a mixed-coupling expansion, each of the $c_j^{(i)}$ is expanded as is done in eq. (2.23), so that it will correspond to a set $\{c_{j,q}^{(i)}\}$. By fixing q (which is associated with a given combination of coupling constants, see sect. 2.4), one defines χ_q as in eqs. (2.90)–(2.92); a kinematic configuration is a UPS if, following eq. (2.93), $\chi_q > \varepsilon$ for any q .

When a UPS is found, MADLOOP5 has two main methods for recovery, which are attempted in turn. It starts by changing the integral-reduction procedure, from OPP to TIR. The results of TIR depend on the specific TIR library MADLOOP5 is linked to. In principle, any library might be used; in practice, so far we have considered IREGI [165] and PJFRY++ [166, 167]. A given TIR library has a maximal number of propagators it can handle (presently, up to hexagons for IREGI and up to pentagons for PJFRY++); in the case one particular loop integral exceeds that number, OPP is used again for it and only for it²¹. More than one TIR library can be linked to MADLOOP5 at the same time. After having found a UPS with OPP, MADLOOP5 switches to the first of such TIR libraries, and repeats the diagnostic tests mentioned above. If the result is again classified as a UPS, the next TIR library is used, and so forth. If none of the available TIR libraries is able to give a numerically-stable reduction, MADLOOP5 resorts to the second method of recovery, namely the OPP integral reduction with all relevant quantities ($\mathcal{N}_{h,l}$ and the internal CUTTOOLS algebra) computed in quadruple precision. This is usually extremely effective, but has the disadvantage of being extremely slow. In the case when the recovery in quadruple precision fails as well, MADLOOP5 gives up, sets $c_0 = 0$, and proceeds to the next kinematic configuration; the user is warned when this happens. We emphasise that the order in which the various integral-reduction procedures are used in the context of UPS recovery (OPP, TIR library #1 to TIR library # n) can be controlled through an input card. So in the present public version of MADGRAPH5_AMC@NLO, where TIR reduction is not yet included, only OPP and quadruple-precision calculations are employed.

2.4.3 Integration of one-loop contributions

The way in which the virtual contributions are integrated by MADGRAPH5_AMC@NLO in

²¹This being a single integral, it should be clear that this procedure will not necessarily result again in being classified as a UPS – the original UPS was due to *all* integrals being reduced with OPP.

either an fNLO or an NLO+PS computation is quite different w.r.t. what was done in AMC@NLO. In the latter, one-loop matrix elements were integrated separately from the other contributions, and eventually combined with them at the level of either distributions (in the case of fNLO), or unweighted events (in the case of NLO+PS); on the other hand, in MADGRAPH5_AMC@NLO all contributions are integrated simultaneously. The original strategy of AMC@NLO had been adopted because it allowed one to control, in a very direct manner, the number of phase-space points for which the virtual corrections were computed, and by doing so to reduce such a number, without this implying a degradation of the overall accuracy of the physical results²². The fact that the accuracy of the final result does not change significantly despite the reduction mentioned above stems from the following two observations. *a)* n -body phase-space integrals are significantly simpler than $(n + 1)$ -body ones, and therefore require to be sampled a smaller number of times than the latter. *b)* Virtual corrections are usually smaller than the Born, which implies that a smaller number of phase-space points has to be used to integrate the former than the latter, in order to obtain the same absolute precision for the two resulting integrals. The possibility of exploiting observation *a)* in a flexible manner was the main reason why in AMC@NLO the virtual contributions were integrated separately. In fact, without a separate integration, n -body matrix elements were previously evaluated the same number of times as $(n + 1)$ -body ones (see eq. (2.50) for an explicit example, relevant to the Born). This could of course be bypassed in several ways, none of which however is simpler than a separate treatment, and better suited to an adaptive multi-channel integration. As explained in sect. 2.4.1, MADGRAPH5_AMC@NLO combines n - and $(n + 1)$ -body contributions in the opposite way w.r.t. that of AMC@NLO, taking an n -body viewpoint. This is what allows MADGRAPH5_AMC@NLO to naturally use observation *a)* while integrating one-loop matrix elements together with all other contributions.

The simultaneous versus separate integration is only one of the differences between the current treatment in MADGRAPH5_AMC@NLO and what was done previously. While the former has several advantages over the latter²³, if applied straightforwardly it implies that the same number of evaluations are performed for the one-loop as for the Born matrix elements, which is not ideal in view of observation *b)*. In order to amend this situation, and thus to increase the speed of MADGRAPH5_AMC@NLO without a loss of accuracy, several

²²The reduction of the number of evaluations of the one-loop matrix elements was (and still is) highly desirable because virtual contributions are typically the numerical bottleneck in our NLO computations (owing to the efficiency of the FKS subtraction, which leads to a relatively fast convergence of the real-emission contributions).

²³On top of item *a)* discussed above: all other things being equal, two or more contributions integrated together lead to a better accuracy than when integrated separately, in the case of cancellation among them, as it often happens with NLO cross sections; also, a smaller number of integration channels implies a reduction of negative-weighted NLO+PS events.

solutions have been devised. They are based on the properties of the following quantity²⁴:

$$\frac{V_h}{|\mathcal{A}_h^{(n,0)}|^2} \equiv \frac{2\Re\{\mathcal{A}_h^{(n,1)}\mathcal{A}_h^{(n,0)*}\}}{|\mathcal{A}_h^{(n,0)}|^2}, \quad (2.94)$$

where $\mathcal{A}_h^{(n,0)}$ has been introduced in eq. (2.68), and V_h can be obtained e.g. from eq. (2.72) by not performing the sum over h there (and similarly for the corresponding UV counter-terms). The ratio in eq. (2.94) is a slowly-varying function over the phase space (behaving essentially as logarithms or dilogarithms), and is to a good extent independent of the helicity configuration h (note that the same helicity configuration h is used in the numerator and in the denominator): in other words, one-loop and Born matrix elements have very similar dependencies on helicity configurations and, in particular, there are no helicity configurations for which $\mathcal{A}_h^{(n,0)}$ is null while V_h is not. This also implies that the ratio of eq. (2.94) is numerically of the same order as its helicity-summed counterpart:

$$\frac{V}{|\mathcal{A}^{(n,0)}|^2} \equiv \frac{\sum_h V_h}{\sum_{h'} |\mathcal{A}_{h'}^{(n,0)}|^2}. \quad (2.95)$$

In MADGRAPH5_AMC@NLO we exploit the behaviour w.r.t. to h of eq. (2.94) by performing the sum over helicities implicit in V by means of MC methods: for each phase-space point, a single helicity configuration is chosen, according to the relative weights of $|\mathcal{A}_h^{(n,0)}|^2$. What has been said above guarantees the efficiency and the fast convergence of this procedure, as well as a reduction of the time spent in computing the one-loop contribution (see eq. (2.79) – such a reduction is due to the fact that the numerator is simpler and therefore less time-consuming: the time spent carrying out the integral reduction is not affected).

Let us finally see how the fact that the quantity in eq. (2.95) is a slowly-varying function of the kinematics helps reduce further the CPU load necessary to compute the integral of V . In order to shorten the notation introduced in sect. 2.4.1, we symbolically write the integral of the NLO cross section as follows:

$$\int d\phi_n (E_V + V), \quad (2.96)$$

where E_V denotes all contributions other than V (the integration over the extra degrees of freedom relevant to the real matrix elements plays no role here, and is understood). Integrals such as that of eq. (2.96) are performed by adaptive methods, which entail successive estimates (called iterations) of quantities relevant to the integrals. For the generic integral:

$$\int d\phi_n F \quad (2.97)$$

we shall denote by

$$I_k(F), \quad \sigma_k(F), \quad (2.98)$$

²⁴With some abuse of notation, V here denotes only the finite part of the one-loop contribution, i.e. the coefficient c_0 of eq. (2.88) up to overall factors, which are irrelevant for the present discussion.

the results of the k^{th} iteration for the mean (i.e., the integral itself) and the standard deviation. One expects that:

$$\lim_{k \rightarrow \infty} I_k(F) = \int d\phi_n F, \quad \lim_{k \rightarrow \infty} \sigma_k(F) = 0. \quad (2.99)$$

It will be convenient for what follows to have an explicit expression for the mean:

$$I_k(F) = \frac{1}{p_k} \sum_{i=1}^{p_k} \Phi_n \left(\phi_n^{(k,i)} \right) F \left(\phi_n^{(k,i)} \right). \quad (2.100)$$

Here, we have denoted by $\phi_n^{(k,i)}$ the i^{th} phase-space point, generated at random during the course of the k^{th} iteration; a total of p_k points are considered. The quantity Φ_n collects all normalisation and jacobian factors. We point out that, when applying eqs. (2.97)–(2.100) to the case of interest, eq. (2.96), one is able to obtain not only the integral of the sum $E_V + V$, but also those of E_V and V individually, by keeping track of $I_k(E_V)$ and $I_k(V)$ respectively (despite the fact that the two terms are still integrated simultaneously). This is useful in view of the following manipulation: we introduce an approximant of V , that we denote by \tilde{V}_k , which we use in the identity:

$$\int d\phi_n V = \int d\phi_n \left[\tilde{V}_k + (V - \tilde{V}_k) \right]. \quad (2.101)$$

As the notation suggests, the approximant \tilde{V}_k is a function of the adaptive-integration iteration, where it is used according to the following formula:

$$I_k(V) = \frac{1}{p_k} \sum_{i=1}^{p_k} \Phi \left(\phi_n^{(k,i)} \right) \tilde{V}_k \left(\phi_n^{(k,i)} \right) + \frac{1}{p_k f_k} \sum_{i=1}^{p_k f_k} \Phi \left(\phi_n^{(k,i)} \right) \left[V \left(\phi_n^{(k,i)} \right) - \tilde{V}_k \left(\phi_n^{(k,i)} \right) \right]. \quad (2.102)$$

A number $0 < f_k \leq 1$ has been introduced in eq. (2.102), which implies that the difference $V - \tilde{V}_k$ is computed only in a fraction f_k of the total number of point thrown²⁵. For an explicit evaluation of eq. (2.102), we need to define what enters it. We have:

$$\tilde{V}_k = c_k \left| \mathcal{A}^{(n,0)} \right|^2, \quad (2.103)$$

with c_k a quantity to be determined iteration-by-iteration, similarly to what happens for f_k . The initial conditions are:

$$f_1 = 1, \quad c_1 = 0, \quad (2.104)$$

and for $k > 1$ we define:

$$c_k = \frac{\text{grid} \{ I_{k-1}(V) \}}{\text{grid} \left\{ I_{k-1} \left(\left| \mathcal{A}^{(n,0)} \right|^2 \right) \right\}}, \quad (2.105)$$

$$f_k = f_{k-1} \max \left\{ \min \left\{ \frac{2\sigma_{k-1}(V - \tilde{V}_{k-1})}{\sigma_{k-1}(E_V + V)}, 2 \right\}, \frac{1}{4} \right\}. \quad (2.106)$$

²⁵Although eq. (2.102) literally implies that these are the first $p_k f_k$ points, in the actual computation they are chosen randomly in the whole set of the p_k points, so that biases are avoided.

The value of f_k obtained from eq. (2.106) is further constrained to be in the range

$$0.005 \leq f_k \leq 1. \quad (2.107)$$

A few explanations are in order. Firstly, c_k and f_k are dynamically constructed, using the information that the numerical integrator (we use a modified version of MINT [168]) has gathered during the previous iteration. One such piece of information is a grid, which among other things stores the averages of the function that is being integrated in non-overlapping phase-space regions which cover the whole phase space. Therefore, c_k as defined in eq. (2.105) is a piecewise-constant function. Because of the properties of eq. (2.95), we expect it to be close to an overall constant, and \tilde{V}_k defined in eq. (2.103) to be a good approximant of V . Secondly, if indeed \tilde{V}_k is an increasingly (with k) good approximant of V , we expect the quantity $\sigma_{k-1}(V - \tilde{V}_{k-1})$ that appears in eq. (2.106) to decrease faster than the estimated error on the integral of $E_V + V$, thus inducing the values of f_k to decrease. On the other hand, eq. (2.106) prevents the series of f_k 's to be fluctuating: w.r.t. the preceding value f_{k-1} , f_k can be at most a factor of 2 larger, or a factor 1/4 smaller – these values are simply sensible, but can of course be changed, as the absolute minimum for f_k given in eq. (2.107).

The rationale behind eqs. (2.101)–(2.107) should now be clear, and it has to do with the fact that one can compute \tilde{V}_k much faster than V . One starts in the first iteration by always computing V ; while doing so, MADGRAPH5_AMC@NLO gathers the information that will allow it to construct the approximant \tilde{V}_2 to be used in the next iteration. While this procedure is iterated, the relative²⁶ number of times V (\tilde{V}_k) is computed is decreased (increased). The procedure is exact, being based on the *local* identity (2.101). Furthermore, the code is protected against any pathological behaviour: if, for example, \tilde{V}_k does not turn out to be a good approximant of V , one will have $f_k \simeq 1$ for all k 's, so that \tilde{V}_k will not play any role (see eq. (2.102)). In practice, this situation has not been encountered so far.

2.4.4 Matching to showers: MC@NLO

In this section, we review the MC@NLO formalism [24] and its implementation in MADGRAPH5_AMC@NLO, making extensive use of the results given in sect. 2.4.1. We start by considering the formulation where the short-distance cross sections are defined for a given real-emission process $r_R \in \mathcal{R}_{n+1}$, which also allows one to symplify the notation, since the dependence on r_R can thus be easily understood. We shall eventually arrive at expressions which lend themselves to the same manipulations as those carried out at the end of sect. 2.4.1, which MADGRAPH5_AMC@NLO exploits in order to deal with MC@NLO cross sections defined at given Born processes, precisely as for their NLO counterparts.

In essence, MC@NLO defines two short-distance cross sections, associated with real-emission-type kinematics (i.e., $(n + 1)$ -body) and Born-type kinematics (i.e., n -body),

²⁶MADGRAPH5_AMC@NLO, following MADGRAPH, starts with a relatively small number of points $p_1 \simeq 80N_{dim}$, and doubles it at each iteration.

dubbed \mathbb{H} - and \mathbb{S} -event contributions respectively. Their forms are written as follows:

$$d\sigma^{(\mathbb{H})} = \sum_{(i,j) \in \mathcal{P}_{\text{FKS}}} d\sigma_{ij}^{(\text{NLO}, E)} - d\sigma^{(\text{MC})}, \quad (2.108)$$

$$d\sigma^{(\mathbb{S})} = d\sigma^{(\text{MC})} + \sum_{(i,j) \in \mathcal{P}_{\text{FKS}}} \sum_{\alpha=S, C, SC} d\sigma_{ij}^{(\text{NLO}, \alpha)}, \quad (2.109)$$

where $d\sigma_{ij}^{(\text{NLO}, E)}$ and $d\sigma_{ij}^{(\text{NLO}, \alpha)}$ are *exactly* the same quantities (eqs. (2.45) and (2.46)) that appear in the NLO cross section (eq. (2.47)). The only new (w.r.t. the NLO) ingredient in MC@NLO is thus $d\sigma^{(\text{MC})}$, which is the cross section one obtains from the parton shower Monte Carlo (PSMC) one interfaces to by truncating the perturbative expansion at $\mathcal{O}(\alpha_s^{b+1})$ (the Born matrix elements being of $\mathcal{O}(\alpha_s^b)$), in the case of resolved emission (eq. (2.108)) and of no resolved emission (eq. (2.109)) – indeed, as is implicit in the notation these two cases result in the same cross section, up to a sign. The crucial point is that, since the leading IR behaviour of any PSMC must be the same as that resulting from an exact matrix-element computation in QCD, eqs. (2.108) and (2.109) are locally finite²⁷. This is the reason why the $d\sigma^{(\text{MC})}$ terms are called the MC counterterms, and the MC@NLO cross section, contrary to the NLO one, can be unweighted.

The definition of the MC counterterms immediately implies that their actual expressions depend on the specific PSMC one interfaces to. These expressions have therefore to be worked out case-by-case, which has been done for the following PSMCs, whose matching with NLO calculations has been fully validated in MADGRAPH5_AMC@NLO: PYTHIA8 [120], HERWIG++ [118, 119], HERWIG6 [139, 140], and PYTHIA6 [138] (in the case of p_T -ordered PYTHIA6, only processes with no strongly-interacting particles in the final state are supported). The details of the construction of the MC counterterms for some of these PSMCs are given in refs. [24, 169–172]. On the other hand, the general structure of the MC counterterms is actually PSMC-independent, and it is easy to convince oneself that they can always be written in the following way:

$$d\sigma^{(\text{MC})} = \sum_{(i,j) \in \mathcal{P}_{\text{FKS}}} d\sigma_{ij}^{(\text{MC})}, \quad (2.110)$$

since FKS pairs are in one-to-one correspondence with IR singularities, which in turn are at the core of the shower mechanism. It is important to bear in mind that this implies that eq. (2.110) is therefore valid not only for those PSMCs based on a $1 \rightarrow 2$ branching picture (such as those just mentioned), but more generally for any PSMC consistent with QCD (in particular, those that adopt a dipole picture [32, 173–179]). The functional form of the terms $d\sigma_{ij}^{(\text{MC})}$ is the same for all of the PSMCs considered here²⁸, and we shall briefly describe its construction in what follows. One starts with the PSMC cross section that

²⁷In fact, this locality property may be spoiled by certain approximations inherent in the PSMC. It is not difficult to restore it [24], as we shall briefly discuss later.

²⁸Different classes of PSMCs may be conceived, for example dipole-shower-based or by going beyond the leading- N_c approximation (see e.g. refs. [180–183]), which could induce a different form. However, the idea of MC counterterms in general, and of eq. (2.110) in particular, would still be valid.

results from a single branching²⁹:

$$d\sigma_{ij}^{(\text{MC},0)} = \sum_c \sum_{l \in c} d\sigma_{ij,cl}^{(\text{MC},0)}, \quad (2.111)$$

$$d\sigma_{ij,cl}^{(\text{MC},0)} = \mathcal{L}^{(\text{MC})} \left(x_{1,2}^{(l)} \right) \frac{\delta_{i \oplus j \in l}}{N_{i \oplus j}} \frac{\alpha_s}{2\pi} \frac{P_{\mathcal{I}_j \mathcal{I}_{i \oplus j}}(z_{ij}^{(l)})}{\xi_{ij}^{(l)}} \mathcal{M}_c^{(n,0)} \Theta^{(\text{MC})} d\xi_{ij}^{(l)} dz_{ij}^{(l)} \frac{d\varphi}{2\pi} d\phi_n. \quad (2.112)$$

As the notation suggests, although $d\sigma_{ij}^{(\text{MC},0)}$ does not necessarily coincide with $d\sigma_{ij}^{(\text{MC})}$ (the possible differences between the two will be explained below), it does fully include its physics contents, which we now turn to describing.

The sums in eq. (2.111) run over all possible planar colour configurations (c), and the individual colour lines belonging to them (l). In `MADGRAPH5_AMC@NLO` we represent a colour configuration as a list, $c = \{l_1, \dots, l_m\}$, where the individual colour line is represented as an ordered pair, $l_k = (s(k), e(k))$, whose meaning is that of a connection between particle $\mathcal{I}_{s(k)}$ (the starting point of the line) and particle $\mathcal{I}_{e(k)}$ (the end point of the line). This implies that, for any given c , a quark or an antiquark will belong to a single colour line (through its colour or anticolour respectively), while a gluon will belong to two colour lines (one for colour and one for anticolour). This is the reason for the factor $N_{i \oplus j}$ in eq. (2.112), which is equal to 1(2) if $i \oplus j$ is a quark or an antiquark (a gluon). `MADGRAPH5_AMC@NLO` constructs the colour configurations during an initialisation phase, by gathering the relevant information from the underlying matrix elements. $\xi_{ij}^{(l)}$ and $z_{ij}^{(l)}$ are the PSMC shower variables; as the notation indicates, in general their forms depend on the branching particle $i \oplus j$ (in particular, on whether it is in the final or initial state), and on the colour line (which determines the colour partner of $i \oplus j$). The actual shower variables are very PSMC-dependent, and they are coded in `MADGRAPH5_AMC@NLO` for all the PSMCs one may match with. The colour connections in general also determine the choice of Bjorken x 's made by the PSMC (see e.g. ref. [24]), which is the reason for the dependence on l in the argument of the luminosity factor $\mathcal{L}^{(\text{MC})}$ in eq. (2.112). $P_{ba}(z)$ is the Altarelli-Parisi one-loop kernel [184], for parton b emerging from the branching of parton a with momentum fraction z . $\mathcal{M}_c^{(n,0)}$ is the Born matrix element multiplied by a factor determined by the colour configuration c , according to the prescription of ref. [185]. Finally, $\Theta^{(\text{MC})}$ symbolically denotes all kind of kinematics constraints, such as generation-level cuts (an n -body Born must have n well-separated partons), possible dead-zone conditions, and so forth.

Implicit in eq. (2.112) is the choice of a shower scale, which roughly speaking sets an upper bound for the hardness of each branching. Since PSMCs are based on a small-scale approximation, it is clear that the larger the shower scale, the worse the description of physics by any PSMC. While in the context of standalone-PSMC simulations it may be necessary to consider shower scales that stretch that approximation (simply to fill phase-space regions otherwise inaccessible), such an attitude is not justified when PSMC are matched with NLO computations, since the latter provide a much better description of hard-emission

²⁹In order to simplify the notation, we understand the universal, azimuthal-dependent part of the branching (see e.g. appendix B of ref. [10]).

regions. Note that in MC@NLO these undesirable large-shower-scale effects are indeed removed completely at $\mathcal{O}(\alpha_s^{b+1})$ by the MC counterterms (see eqs. (2.108) and (2.109)). However, at $\mathcal{O}(\alpha_s^{b+2})$ and beyond the PSMC may still radiate in the hard regions, potentially giving effects which are simply not sensible from the physics viewpoint. Furthermore, even at $\mathcal{O}(\alpha_s^{b+1})$ it does not make much sense to allow the PSMC to produce radiation only to eventually remove it. Fortunately, it is possible to give the PSMC an external mass scale in input; during the course of the shower, the PSMC will generate branchings after choosing the smallest between this external scale and its internally-generated shower scale. In MADGRAPH5_AMC@NLO, we exploit this possibility in the following way³⁰. Firstly, we introduce a function of a mass scale μ :

$$D(\mu) = \begin{cases} 1 & \mu \leq \mu_1, \\ \text{monotonic} & \mu_1 < \mu \leq \mu_2, \\ 0 & \mu > \mu_2, \end{cases} \quad (2.113)$$

with $\mu_1 \leq \mu_2$ two given mass scales. While we typically regard D as a smooth function, it is perfectly fine to consider its sharp version:

$$D(\mu) = \Theta(\mu_Q - \mu), \quad \mu_Q = \mu_1 = \mu_2, \quad (2.114)$$

which is a particular case of eq. (2.113). Secondly, on an event-by-event basis we determine a mass scale by using:

$$\mu_r = D^{-1}(r), \quad (2.115)$$

with r a flat random number (note that with eq. (2.114) one obtains $\mu_r \equiv \mu_Q$). Thirdly, we give μ_r in input to the PSMC, where it acts as an upper bound to the internally-generated shower scales as explained before. The physical meaning of μ_r (be it a relative transverse momentum, a virtuality, or whatever else) depends on the specific PSMC chosen, but is irrelevant here and need not be specified. The crucial thing is the following: by means of this procedure, we are effectively *changing* the shower w.r.t. what the PSMC would do if left alone. This change must therefore correspond to a change in the MC counterterms, because of the very definition of the latter. This amounts to:

$$d\sigma_{ij}^{(\text{MC}, D)} = D(\mu(\mathcal{K}_{n+1})) d\sigma_{ij}^{(\text{MC}, 0)}. \quad (2.116)$$

Note that the argument of D in eq. (2.116) is computed by using the underlying kinematic configuration (after having taken into account its PSMC-specific form: p_T , $\sqrt{Q^2}$, and so forth), and must not be generated randomly. Equation (2.116) can always be used in place of eq. (2.112), the latter being a particular case of the former, which one can formally obtain by setting $\mu_1 = \mu_2 = \infty$.

As was discussed before, the function D controls perturbative effects higher than NLO; hence, its variations can be used to assess the NLO+PS matching systematics (which is, by definition, the size of terms beyond the formal accuracy of the computation) of the

³⁰This technique has been used sparingly in MC@NLO v3.3 and higher.

MC@NLO method. Although this is expected to be small³¹, its actual size is observable-, process- and (especially) PSMC-dependent³², and it is therefore convenient to be able to study it in a straightforward way. This is the case in MADGRAPH5_AMC@NLO, where one can control the values of the scales μ_i of eq. (2.113) through the external parameters f_i , with $\mu_i = f_i \sqrt{\hat{s}_0}$, and \hat{s}_0 the Born-level partonic c.m. energy squared.

Equation (2.116) would give the desired MC counterterms if the corresponding PSMC behaved as expected in the IR regions, namely if it gave exactly the same result as a QCD matrix-element computation in *both* the collinear and the soft limits, whence the local cancellations in eqs. (2.108) and (2.109). Unfortunately, this is not the case in the soft limit, at least for HERWIG and PYTHIA, where this deficiency is basically a consequence of the necessity of having a Markovian shower. What is true, however, is that the amount of soft radiation predicted by the PSMCs is correct; in other words, only its angular pattern is not consistent with the one required by QCD. Fortunately, such an undesirable feature of certain PSMCs will not have dramatic consequences on physical observables, because of the infrared-safety of the latter (the interested reader can find a fuller discussion of this issue in sect. A.5 of ref. [24]). The technical problem of the local finiteness of the MC@NLO short-distance cross sections can be solved by the following definition of the MC counterterms:

$$d\sigma_{ij}^{(\text{MC})} = (1 - \mathcal{G}) d\sigma_{ij}^{(\text{MC},D)} + \mathcal{G} d\sigma_{ij}^{(\text{NLO},S)}|_{\text{real}}. \quad (2.117)$$

Here, \mathcal{G} is a smooth function defined so that $\mathcal{G} \rightarrow 1$ in the soft limit, and $\mathcal{G} = 0$ outside of the soft region; $d\sigma_{ij}^{(\text{NLO},S)}|_{\text{real}}$ is the soft part of the NLO cross section, eq. (2.46), where only the real-emission matrix element contribution is kept³³.

A few comments concerning eq. (2.117) are in order. Given that what the PSMC is supposed to do is $d\sigma_{ij}^{(\text{MC},D)}$, while what MC@NLO assumes the PSMC does is $d\sigma^{(\text{MC})}$ of eq. (2.117), there is a mismatch of $\mathcal{O}(\alpha_s^{b+1})$ between the two. This mismatch, however, is utterly irrelevant for several reasons. Firstly, because of the properties of \mathcal{G} , it is confined to the soft regions, where effects of all orders in α_s are equally important. Secondly, in practice in the soft region the PSMC does not even correspond to $d\sigma_{ij}^{(\text{MC},D)}$ if not in a fully inclusive sense, since the PSMC is unable to handle emissions below the IR cutoffs, which are of the order of the typical hadron mass (and this for a very fundamental reason: QCD does not have infinite resolution power). Thirdly, because of the previous point *all* NLO+PS matching schemes are liable to have $\mathcal{O}(\alpha_s^{b+1})$ effects in small-scale regions which are not in formal agreement with fixed-order results at the NLO, even if the second term on the r.h.s. of eq. (2.117) were not present (see appendix B.3 of ref. [24] for a discussion specific to the MC@NLO formalism). Ultimately, then, the differences driven by the \mathcal{G} function are power suppressed (see e.g. ref. [186]); eq. (2.117) is nothing but a formal trick

³¹The main reason being that MC@NLO short-distance cross sections have no contributions of $\mathcal{O}(\alpha_s^{b+2})$ or higher; terms of these orders in the physical cross sections can only be generated through MC radiation.

³²On top of being, obviously, matching-method dependent. We stress that the results of D variations in MADGRAPH5_AMC@NLO can not be used, even as a mere indication, of the matching systematics that affects other matching methods, such as POWHEG.

³³An analogous solution is adopted when the azimuthal part of the PSMC branching kernel does not agree with that predicted by the matrix elements.

to render the $\mathcal{O}(\alpha_s^{b+1})$ MC@NLO cross sections non-divergent (which is important in view of their numerical integration) in a region where not even the perturbative predictions of PSMCs are sensible, let alone those of fixed-order computations.

Equation (2.117) also gives us the opportunity of commenting briefly on the alternative implementation of the MC@NLO method presented in ref. [34]. There, the function \mathcal{G} does not appear, for the simple reason that the two short-distance cross sections on the r.h.s. of eq. (2.117) coincide in the soft limit and, as explained above, this is a sufficient condition for not having to introduce \mathcal{G} . In turn, this situation occurs because the shower used in ref. [34], and in subsequent papers, in the context of NLO-matched simulations is *constructed* to have the same soft behaviour of the matrix elements (see, in particular, eq. (2.5) of ref. [187]). Once this is done, the form of the MC counterterms is uniquely determined, lest one has a mismatch of $\mathcal{O}(\alpha_s^{b+1})$ (everywhere in the phase space). One may opt (as is done in ref. [34]) to see this as a choice made at the level of short-distance cross sections (the soft behaviour of the MC counterterms), that forces one to modify the shower in order to preserve the perturbative accuracy. While the point of view of ref. [24] and of this paper is the opposite one (namely that it is the chosen PSMC which determines the MC counterterms), the fundamental idea is just the same, and therefore the MC@NLO subtractions of ref. [34] do not differ in any significant way from those that had been adopted in MC@NLO and are now used in MADGRAPH5_AMC@NLO. What has been changed in the approach of ref. [34] (w.r.t. the previous default) is the *shower* adopted in conjunction with the NLO matching performed there (which happens not to be the same as that used in simulations which are not matched to NLO results). We point out that should a version of the PYTHIA or HERWIG showers become available with a matrix-element-type soft behaviour, the relevant MC counterterms would be constructed without a \mathcal{G} function. Furthermore, we stress that the NLO accuracy of the MC@NLO method (including, in particular, the whole $1/N_c$ expansion) is maintained, and that the $\mathcal{O}(\alpha_s^{b+1})$ results are thus in agreement with those of the corresponding matrix elements (up to power-suppressed effects, as explained above), regardless of the behaviour of the PSMC and thus of the presence of a \mathcal{G} function. On the other hand, if some aspect of the PSMC is deficient (for example the treatment of subleading-colour contributions), the MC@NLO method itself cannot provide an improvement in the MC-dominated kinematic regions – any issue of this kind must be addressed at the level of the PSMC itself.

Equation (2.117) is the final form to be used in eq. (2.110); when the latter is in turn replaced in eqs. (2.108) and (2.109), one immediately realises that it is convenient to define the \mathbb{H} - and \mathbb{S} -event contributions at fixed FKS pair:

$$d\sigma_{ij}^{(\mathbb{H})} = d\sigma_{ij}^{(\text{NLO}, E)} - d\sigma_{ij}^{(\text{MC})}, \quad (2.118)$$

$$d\sigma_{ij}^{(\mathbb{S})} = d\sigma_{ij}^{(\text{MC})} + \sum_{\alpha=S, C, SC} d\sigma_{ij}^{(\text{NLO}, \alpha)}. \quad (2.119)$$

It is easy to see that these quantities are locally finite (by construction of the shower variables $\xi_{ij}^{(l)}$ and $z_{ij}^{(l)}$), precisely as their summed counterparts of eqs. (2.108) and (2.109). Eqs. (2.118) and (2.119) can now be used to define the MC@NLO generating functional. In order to do that we also introduce, for consistency with the standard notation and in view

of the discussion to be given in sect. 2.4.5, the \mathbb{H} - and \mathbb{S} -event kinematic configurations:

$$\mathcal{K}_n^{(\mathbb{H})} \equiv \mathcal{K}_{n+1}^{(E)}, \quad \mathcal{K}_n^{(\mathbb{S})} \equiv \mathcal{K}_{n+1}^{(S)}, \quad (2.120)$$

so that the generating functional finally reads as follows:

$$\mathcal{F}_{\text{MC@NLO}} = \sum_{r_R \in \mathcal{R}_{n+1}} \sum_{(i,j) \in \mathcal{P}_{\text{FKS}}} \left\{ \mathcal{F}_{\text{MC}} \left(\mathcal{K}_n^{(\mathbb{H})} \right) \frac{d\sigma_{ij}^{(\mathbb{H})}(r_R)}{d\chi_{Bj}^{(ij)} d\chi_{n+1}^{(ij)}} + \mathcal{F}_{\text{MC}} \left(\mathcal{K}_n^{(\mathbb{S})} \right) \frac{d\sigma_{ij}^{(\mathbb{S})}(r_R)}{d\chi_{Bj}^{(ij)} d\chi_{n+1}^{(ij)}} \right\}, \quad (2.121)$$

where \mathcal{F}_{MC} is the generating functional of the PSMC one interfaces to, and its argument indicates the parton configuration to be adopted as the starting condition for the shower. In eq. (2.121) we have reinstated the formal dependence of the short-distance cross sections on the real-emission process r_R . In this way, the complete similarity between the MC@NLO and NLO cross sections in terms of sums over partonic processes and FKS pairs (i.e., between the r.h.s. of eq. (2.121) and the l.h.s. of eq. (2.49)) is evident. Thus, as was anticipated at the beginning of this section, all the manipulations performed at the end of sect. 2.4.1 apply to the MC@NLO case as well. In particular, the formulation where the MC@NLO short-distance cross sections are defined by fixing the Born-level process is the one adopted in MADGRAPH5_AMC@NLO. Among other things, this renders it particularly easy to obtain \mathbb{S} events by integrating over ξ_i and y_{ij} before unweighting (which is expected to reduce the number of negative-weight events, as advocated in ref. [24] in the context of the MC@NLO formalism; the same idea, dubbed “folding”, has been independently proposed and implemented in POWHEG).

Before concluding this section, we present two variants of what was discussed so far, that we shall want to consider for future MADGRAPH5_AMC@NLO developments. The first one concerns the definition of the MC counterterms. The advantage of using eqs. (2.118) and (2.119) is a one-to-one correspondence between the shower variables $(z_{ij}^{(l)}, \xi_{ij}^{(l)})$ and the FKS integration variables (ξ_i, y_{ij}) . Apart from a transparent way of identifying the IR singular structure (which in turn is related to $d\sigma_{ij}^{(\mathbb{H})}$ and $d\sigma_{ij}^{(\mathbb{S})}$ being locally finite at fixed (i, j)), this implies that, when the integration measure over the MC variables is expressed in terms of $d\chi_{n+1}^{(ij)}$, as it must according to eq. (2.121), one can factorise the jacobian

$$\frac{\partial \left(z_{ij}^{(l)}, \xi_{ij}^{(l)} \right)}{\partial (\xi_i, y_{ij})}; \quad (2.122)$$

in the current version of MADGRAPH5_AMC@NLO, this jacobian is computed analytically. The definitions of eqs. (2.118) and (2.119) might however have a numerical drawback, due to the presence of the factor \mathcal{S}_{ij} only in the terms $d\sigma_{ij}^{(\text{NLO}, \alpha)}$. Its absence in the MC counterterms could induce differences in the damping of singularities not due to the FKS pair (i, j) , that in turn could result in an unnecessary large fraction of events with negative weights. This situation can be amended as follows: by using eq. (2.35) one obtains the identity:

$$d\sigma^{(\text{MC})} = \sum_{(i,j) \in \mathcal{P}_{\text{FKS}}} d\sigma_{ij}^{(\text{MC})} = \sum_{(i,j) \in \mathcal{P}_{\text{FKS}}} \sum_{(k,p) \in \mathcal{P}_{\text{FKS}}} \mathcal{S}_{kp} d\sigma_{ij}^{(\text{MC})} \quad (2.123)$$

which implies

$$d\sigma^{(\text{MC})} = \sum_{(i,j) \in \mathcal{P}_{\text{FKS}}} d\hat{\sigma}_{ij}^{(\text{MC})}, \quad (2.124)$$

$$d\hat{\sigma}_{ij}^{(\text{MC})} = \mathcal{S}_{ij} \sum_{(k,p) \in \mathcal{P}_{\text{FKS}}} d\sigma_{kp}^{(\text{MC})}. \quad (2.125)$$

By using $d\hat{\sigma}_{ij}^{(\text{MC})}$ in place of $d\sigma_{ij}^{(\text{MC})}$ in eqs. (2.118) and (2.119), one can factor out a term \mathcal{S}_{ij} . The disadvantage of course is that the pair $(z_{kp}^{(l)}, \xi_{kp}^{(l)})$ is not in one-to-one correspondence with (ξ_i, y_{ij}) any longer, which implies that the relevant jacobians will be much more involved than that in eq. (2.122). However, this is clearly only a technical problem, which can be overcome by giving up the requirement that jacobians be computed analytically. With modern routines for the numerical evaluation of derivatives this appears definitely feasible, and it would also pave the way for a leaner interface to new PSMCs.

We now turn to the second variant, which concerns the MC@NLO formulation proper. A good feature of the MC@NLO cross section is that it gives a clear separation of matrix element and Monte Carlo effects. A drawback is that one is forced to ignore the fact that in the MC-dominated region (i.e., at small scales) real-emission matrix elements do not give a good description of the underlying physics, which implies that the contribution of \mathbb{H} events there is important only in terms of total rate, but not in terms of shapes, which indeed are dominated by showered \mathbb{S} events. From the viewpoint of final (physical) results this is irrelevant, but it entails a loss of efficiency, since typically \mathbb{H} events have negative weights in the MC-dominated region. A possible way to address this problem is the following. Consider a function Δ with the properties:

$$\Delta = 1 + \mathcal{O}(\alpha_s), \quad (2.126)$$

$$\Delta \longrightarrow 0 \quad \text{IR limits.} \quad (2.127)$$

It is immediate to see that the following definitions:

$$d\sigma_{ij}^{(\mathbb{H})} = \left(d\sigma_{ij}^{(\text{NLO}, E)} - d\sigma_{ij}^{(\text{MC})} \right) \Delta, \quad (2.128)$$

$$d\sigma_{ij}^{(\mathbb{S})} = d\sigma_{ij}^{(\text{MC})} \Delta + \sum_{\alpha=S, C, SC} d\sigma_{ij}^{(\text{NLO}, \alpha)} + d\sigma_{ij}^{(\text{NLO}, E)} (1 - \Delta). \quad (2.129)$$

result in a generating MC@NLO functional with the *same* formal accuracy as that of eq. (2.121). It is clear that, while this conclusion holds regardless of the form of Δ , provided that the conditions in eqs. (2.126) and (2.127) are satisfied, from the physical viewpoint one would identify Δ with a suitable combination of Sudakovs, whose explicit forms would ideally be extracted from the same PSMC one interfaces to. Although at present there is no straightforward way to obtain (numerically) the Sudakovs from a PSMC, there is no reason of principle which prevents the implementation of such a possibility in future versions of modern PSMCs. In the meanwhile, MADGRAPH5_AMC@NLO will have the means to test eqs. (2.128) and (2.129), by using the analytical expression for the Sudakovs which are currently used in the context of the FxFx NLO merging method (see sect. 2.4.5).

2.4.5 Merging samples at the NLO: FxFx

In this section, we present a brief review of the FxFx procedure [188], whose aim is that of improving, by systematically including PSMC matching at the NLO, the multi-leg tree-level merging techniques established in the course of the past decade, such as CKKW, CKKW-L, and MLM (see refs. [142–145, 189–194]). The key word here is merging, which identifies the following problem. If one obtains hard events from the processes:

$$\mathcal{I}_1 + \mathcal{I}_2 \longrightarrow S + i \text{ partons}, \quad (2.130)$$

where S is a set of p particles which does not contain any QCD massless partons, how does one match them to PSMCs when different i values (i.e., different final-state hard-process multiplicities) are *simultaneously* considered? The core of the problem is the avoidance of double counting; note that this is on top of, and more complicated than, the double-counting problem that one faces when fixing i in eq. (2.130), and which is a matching (not a merging) issue. While the formulation of the problem of merging is independent of the perturbative order (i.e., of the accuracy to which the cross sections of the processes in eq. (2.130) are computed), its solution is not, being strictly connected with the adopted matching strategy. NLO (and beyond) mergings are thus inherently more complicated than LO ones, because LO-matching is basically trivial; they have attracted a significant amount of attention lately [181, 188, 195–204]. The quickest way to realise this is that of considering the tree-level matrix element associated with the process in eq. (2.130); this will give the Born contribution to that process, but at the same time it will also be needed at the NLO as real-emission contribution to a process whose Born features a $S + (i - 1)$ partons final state. Such a double role of a given matrix element is specific to an NLO merging, and is absent at the LO.

This example of the tree-level matrix-element double role suggests a way to tackle the NLO-merging problem. In particular, in view of the fact that, in the context of a given calculation, the perturbative accuracy of the prediction for an observable is larger the more inclusive the observable, one wants to use as much as is possible an i -parton tree-level matrix element as a Born, rather than as a real-emission, contribution. The role of hard emissions will thus be mainly played by the Born’s associated with processes with larger multiplicities, while for any given multiplicity the real-emission contributions will mostly provide the correct (NLO) normalisation. Because the MC@NLO formalism is designed to perturb in a minimal way both the underlying matrix-element description and the PSMC one uses for showering events, the above scheme essentially corresponds to limiting the hardness of \mathbb{H} -event emissions. Technically, this can be achieved by simply exploiting the D function introduced in eq. (2.113), and by applying analogous conditions at the matrix element level. In order to do so, it is convenient (and particularly sensible physics-wise) to re-interpret the parameters μ_i of eq. (2.113) in the following way:

$$\begin{aligned} \mu &\leq \mu_1 && \text{soft (MC – dominated),} \\ \mu_1 &< \mu \leq \mu_2 && \text{intermediate,} \\ \mu &> \mu_2 && \text{hard (ME – dominated).} \end{aligned}$$

Note that in the case of a sharp D function, eq. (2.114), the intermediate region collapses to a zero-measure set. Once one has defined hard and soft mass scales, one needs to define a way to measure the hardness; because of the fact that NLO corrections will be computed, it is mandatory that such a measure be IR-safe. The easiest way to achieve this is that of employing quantities that arise from a jet-reconstruction algorithm. We denote by d_j the scale (with canonical dimension equal to one, i.e. mass) at which a given S +partons configuration passes from being reconstructed as a j -jet one to being reconstructed as a $(j-1)$ -jet one, according to a k_T jet-finding algorithm [141] (in other words, there are j jets of hardness $d_j - \varepsilon$, and $(j-1)$ jets of hardness $d_j + \varepsilon$, with ε arbitrarily small). In general, for n final-state partons one will have

$$d_n \leq d_{n-1} \leq \dots \leq d_2 \leq d_1. \quad (2.131)$$

It will also turn out to be convenient to define

$$d_j = \sqrt{s}, \quad j \leq 0, \quad (2.132)$$

with \sqrt{s} the parton c.m. energy, i.e. the largest energy scale available event-by-event. Since the function D determines rather directly the way in which the various partonic processes of eq. (2.130) are combined, the results of variations of the parameters that enter into it can be associated with the systematics of the merging procedure (and not of the matching one, as is the case for the unmerged cross sections discussed in sect. 2.4.4). This is particularly straightforward, and totally analogous to what is typically done at the LO, when one chooses a sharp D function, in which case μ_Q has to be seen as the merging scale.

We now limit ourselves to reporting the final forms of the short-distance cross sections necessary to implement the FxFx merging scheme; the interested reader can find more details in ref. [188]. We denote by N the largest light-parton multiplicity at the Born level that we consider (therefore, N is the largest value that i can possibly assume in eq. (2.130)). The cross sections given below are the analogues of those in eqs. (2.118) and (2.119), i.e., at fixed real-emission process and FKS pair; in the present section, we understand these quantities, lest we clutter the notation with unnecessary details. On the other hand, each \mathbb{H} - or \mathbb{S} -event contribution or short-distance cross section will carry an index, equal to the number of final-state particles in the corresponding hard process (at the Born level), this information being crucial in all merging procedures. We have:

$$d\bar{\sigma}_{p+i}^{(\mathbb{S})} = \left[\sum_{\alpha=S,C,SC} d\sigma_{p+i}^{(\text{NLO},\alpha)} + d\sigma_{p+i}^{(\text{MC},0)} D(d_{i+1}(\mathcal{K}_{p+i}^{(\mathbb{H})})) \right] \quad (2.133)$$

$$\begin{aligned} & \times \left(1 - D(d_i(\mathcal{K}_{p+i}^{(\mathbb{S})})) \right) \Theta \left(d_{i-1}(\mathcal{K}_{p+i}^{(\mathbb{S})}) - \mu_2 \right), \\ d\bar{\sigma}_{p+i}^{(\mathbb{H})} &= \left[d\sigma_{p+i}^{(\text{NLO},E)} \left(1 - D(d_i(\mathcal{K}_{p+i}^{(\mathbb{H})})) \right) \Theta \left(d_{i-1}(\mathcal{K}_{p+i}^{(\mathbb{H})}) - \mu_2 \right) \right. \\ & \left. - d\sigma_{p+i}^{(\text{MC},0)} \left(1 - D(d_i(\mathcal{K}_{p+i}^{(\mathbb{S})})) \right) \Theta \left(d_{i-1}(\mathcal{K}_{p+i}^{(\mathbb{S})}) - \mu_2 \right) \right] D(d_{i+1}(\mathcal{K}_{p+i}^{(\mathbb{H})})), \end{aligned} \quad (2.134)$$

$$d\bar{\sigma}_{p+N}^{(\mathbb{S})} = \left[\sum_{\alpha=S,C,SC} d\sigma_{p+N}^{(\text{NLO},\alpha)} + d\sigma_{p+N}^{(\text{MC},0)} \right] \quad (2.135)$$

$$\begin{aligned} & \times \left(1 - D(d_N(\mathcal{K}_{p+N}^{(\mathbb{S})})) \right) \Theta \left(d_{N-1}(\mathcal{K}_{p+N}^{(\mathbb{S})}) - \mu_2 \right), \\ d\bar{\sigma}_{p+N}^{(\mathbb{H})} &= d\sigma_{p+N}^{(\text{NLO},E)} \left(1 - D(d_N(\mathcal{K}_{p+N}^{(\mathbb{H})})) \right) \Theta \left(d_{N-1}(\mathcal{K}_{p+N}^{(\mathbb{H})}) - \mu_2 \right) \\ & - d\sigma_{p+N}^{(\text{MC},0)} \left(1 - D(d_N(\mathcal{K}_{p+N}^{(\mathbb{S})})) \right) \Theta \left(d_{N-1}(\mathcal{K}_{p+N}^{(\mathbb{S})}) - \mu_2 \right), \end{aligned} \quad (2.136)$$

where in eqs. (2.133) and (2.134) one has $0 \leq i < N$, and in writing the MC counterterms we have understood the \mathcal{G} dependence as given in eq. (2.117), which is irrelevant for the sake of the present discussion. The MC@NLO cross section defined by eqs. (2.133) and (2.134) (eqs. (2.135) and (2.136)), and its analogue that we shall introduce later, is called the i -parton (N -parton) sample. With the cross sections above, one defines the FxFx generating functional:

$$\mathcal{F}_{\text{FxFx}} = \sum_{n=p}^{p+N} \mathcal{F}_{\text{FxFx}}^{(n)}, \quad (2.137)$$

$$\mathcal{F}_{\text{FxFx}}^{(n)} = \mathcal{F}_{\text{MC}} \left(\mathcal{K}_n^{(\mathbb{H})} \right) \frac{d\bar{\sigma}_n^{(\mathbb{H})}}{d\chi_{Bj} d\chi_{n+1}} + \mathcal{F}_{\text{MC}} \left(\mathcal{K}_n^{(\mathbb{S})} \right) \frac{d\bar{\sigma}_n^{(\mathbb{S})}}{d\chi_{Bj} d\chi_{n+1}}. \quad (2.138)$$

Note that eq. (2.138) and eq. (2.121) are formally identical (as was said above, the sums on the r.h.s. of eq. (2.121) are understood here), the difference being in the form of the short-distance cross sections. Equation (2.137) implies that the FxFx generating functional is the incoherent sum of MC@NLO generating functionals, each of which incorporates FxFx-specific type of cuts but that are otherwise fully analogous to their non-merged counterparts. This renders it straightforward to implement the FxFx merging prescription into MADGRAPH5_AMC@NLO.

As was discussed in ref. [188], the formulation of FxFx according to eq. (2.138) can be supplemented by a Sudakov suppression, in keeping with what is done at the LO in the CKKW(-L) and MLM methods. The modifications of the short-distance cross sections are in fact rather minimal, and amount to what follows:

$$d\hat{\sigma}_{p+i}^{(\mathbb{S})} = \left[d\bar{\sigma}_{p+i}^{(\mathbb{S})} + d\sigma_{p+i}^{(\Delta)} \right] \Delta_i \left(\mu_{i,\min}^{(\mathbb{S})}, \mu_{i,\max}^{(\mathbb{S})} \right), \quad (2.139)$$

$$d\hat{\sigma}_{p+i}^{(\mathbb{H})} = d\bar{\sigma}_{p+i}^{(\mathbb{H})} \Delta_i \left(\mu_{i,\min}^{(\mathbb{H})}, \mu_{i,\max}^{(\mathbb{H})} \right), \quad (2.140)$$

with $d\bar{\sigma}_{p+i}^{(\mathbb{S})}$ and $d\bar{\sigma}_{p+i}^{(\mathbb{H})}$ defined in eq. (2.133) (for $i < N$) or eq. (2.135) (for $i = N$), and in eq. (2.134) (for $i < N$) or eq. (2.136) (for $i = N$) respectively. Δ_i is a suitable combination of Sudakov form factors, the construction of which follows closely the CKKW prescription. Further details, including the definition of the hard scales that enter these formulae can be found in ref. [188]. Here, we limit ourselves to stressing the following fact: while for the processes studied in ref. [188] the flavour structure of Δ_i had been worked out by hand, it has now been fully automated in MADGRAPH5_AMC@NLO. The term $d\sigma_{p+i}^{(\Delta)}$ is necessary in order not to spoil the formal NLO accuracy of the formalism:

$$d\sigma_{p+i}^{(\Delta)} = -d\sigma_{p+i}^{(\text{NLO},S)}|_{\text{Born}} \left(1 - D(d_i(\mathcal{K}_{p+i}^{(\mathbb{S})})) \right) \Theta \left(d_{i-1}(\mathcal{K}_{p+i}^{(\mathbb{S})}) - \mu_2 \right) \Delta_i^{(1)} \left(\mu_{i,\min}^{(\mathbb{S})}, \mu_{i,\max}^{(\mathbb{S})} \right), \quad (2.141)$$

where $d\sigma_{p+i}^{(\text{NLO},S)}|_{\text{Born}}$ is the soft part of the NLO cross section, eqs. (2.45) and (2.46), where only the Born matrix element contribution is kept. By $\Delta_i^{(1)}$ we have denoted the $\mathcal{O}(\alpha_s)$ term in the perturbative expansion of Δ_i . It should be clear that Δ_i satisfies eqs. (2.126) and (2.127); therefore, a by-product of the Sudakov-improved FxFx merging procedure (which we regard as our “best” FxFx scheme, and is thus the default in MADGRAPH5_AMC@NLO) is the possibility of testing the alternative (non-merged) MC@NLO formulation presented in eqs. (2.128) and (2.129).

We conclude this section by discussing two arguments of general relevance to NLO-merging techniques, and which may have significant bearings on their phenomenological predictions: unitarity, and merging systematics. In the context of merging, imposing a unitarity condition means that the fully-inclusive merged cross section (i.e., the sum over all i ’s of the i -parton-sample predictions) is equal to the total rate of the *unmerged* 0-parton sample³⁴. In FxFx unitarity is not imposed, for the reasons we shall now explain. One of the advantages of unitarity is the fact that the merging scale μ_Q can be chosen³⁵ in an arbitrarily-large range, whereas in non-unitary approaches this is not possible, and a sensible choice (which takes into account the hardness of the process, and the fact that μ_Q must itself be hard) is always arbitrary to a certain extent. Such a benefit of unitarity has however a less-pleasant side. Namely, in the general context of resummed computations matched with fixed orders, constraints on total rates contribute to significant modifications of matrix-elements predictions, in shape and absolute value, also in regions where one would expect large-logarithms effects to be suppressed (the Higgs p_T spectrum is a spectacular example of this phenomenon – see e.g. figs. 1 and 2 of ref. [205]). This is of course acceptable, and actually constitutes a defining prediction of a matched formalism, if all contributions to the latter are perturbatively consistent: an example is that of an MC@NLO unmerged cross section, where the total rate is of $\mathcal{O}(\alpha_s^{b+1})$, which is the same perturbative order to which both \mathbb{S} and \mathbb{H} events contribute. When unitarised-merging is considered, the total rate is still imposed to be that of $\mathcal{O}(\alpha_s^{b+1})$; however, \mathbb{S} - and \mathbb{H} -event i -parton samples (and their analogues within any merging formalism) are of $\mathcal{O}(\alpha_s^{b+i+1})$; this mismatch of perturbative orders present for any $i \geq 1$ might result in a bias (uniquely due to the total-rate constraint) at the level of shapes, the stronger the larger i . Note that one could impose the unitarity constraint using an NNLO total-rate prediction ($\mathcal{O}(\alpha_s^{b+2})$), were that available. This would marginally alleviate the problem above, but not solve it: firstly, it merely shifts it to $i \geq 2$, and secondly one still uses NLO-matched (and not NNLO-matched) i -parton samples which thus require, at the very least, to be re-normalised. The counter argument is that, although a bias might indeed be present, it appears at perturbative orders which are in any case beyond accuracy. This is correct, but does not have any implications on the presence of large logarithmic terms, that could enhance such contributions. More importantly, it is also an argument that can be used in the context of a non-unitary approach, where it would apply chiefly to total rates (and, by construction, in non-unitary approaches there is no bias due to total-rate constraints). In fact, the dependence on μ_Q of inclusive results

³⁴We neglect here possible complications due to heavy-flavour thresholds, and to contributions to i -parton samples that cannot be shower-generated starting from a lower multiplicity.

³⁵In principle; in practice, there may be efficiency issues, which are however not of concern here.

can be used effectively in non-unitary mergings as a way to arrive at a sensible μ_Q range, to be employed to assess the merging systematics of differential distributions. Examples of this, and of the fact that FxFx exhibits a rather small μ_Q dependence, will be given in sect. 4.2. In conclusion, the arguments above can be argued in different ways; it should be clear, however, that regardless of whether a merging approach imposes or not unitarity, in those phase-space regions where matrix elements and PSMCs will be vastly different the μ_Q dependence is bound to be large. In order to be able to study such effects as locally as is possible, we prefer not to use unitarity arguments in FxFx.

For what concerns the study of merging-scale systematics, we emphasise that the discussion presented above by no means justifies the practice of not being conservative with the choice of μ_Q in non-unitary approaches. There is a particularly common misconception, relevant when the physics one wants to study features a threshold for jet hardness (that we shall denote by $p_T^{(\text{cut})}$ henceforth): such a misconception entails choosing $\mu_Q < p_T^{(\text{cut})}$. The (implicit) argument for this choice is that a tagged jet is by definition a hard quantity, and by setting $\mu_Q > p_T^{(\text{cut})}$ one might spoil the underlying NLO accuracy³⁶ for the corresponding jet cross section. Several observations are in order here. Firstly, the use of $p_T^{(\text{cut})}$ as a criterion to determine μ_Q is a contradiction in terms: by definition, a merging prescription is what allows one to use samples of hard events without knowing *a priori* for which observables they will be employed, in particular which minimal jet hardness will be imposed. The fact that the merging is not perfect (i.e., it does not have zero systematics) just implies that both $\mu_Q \ll p_T^{(\text{cut})}$ and $\mu_Q \gg p_T^{(\text{cut})}$ are not particularly sensible, and nothing else. Secondly, a criterion based solely on $p_T^{(\text{cut})}$ misunderstands the meaning of hardness, which is not absolute, but relative. For example, a jet with $p_T^{(\text{cut})} = 40$ GeV can rightly be defined to be hard in inclusive W production; the same jet is less hard in Higgs production, basically soft in $t\bar{t}$ production, and certainly soft in the production of a 1-TeV Z' resonance. Indeed, it should be obvious that it is always a ratio of mass scales (one of which is of the order of the intrinsic hardness of the production process, essentially defined by the masses of the final-state particles, and the other of the order of $p_T^{(\text{cut})}$), and never the absolute value of one such scale, that matters: the argument of a logarithm is a dimensionless quantity. Thirdly, and related to the previous item. When choosing $\mu_Q > p_T^{(\text{cut})}$ one might indeed spoil some underlying NLO description, and for a very good reason: such matrix-element-driven prediction may simply be irrelevant in the case of a strong scale hierarchy where $p_T^{(\text{cut})}$ is much smaller than the intrinsic hardness of the process, because there one believes the correct type of prediction for jet observables to be rather a PSMC-dominated one. Even if the presence of Sudakov suppression factors in the merged matrix elements may allow one to employ a merging scale which is smaller than what naive expectations would suggest, still by choosing $\mu_Q < p_T^{(\text{cut})}$ one runs the risk of spoiling the underlying PSMC description of the lowest-multiplicity sample. In conclusion, given that a merging-scale choice necessarily represents a non-perfect compromise between a matrix-element- and a PSMC-dominated prediction, for processes where a scale hierarchy is not overwhelmingly clear (i.e., when

³⁶Or the tree-level matrix element accuracy in the case of LO mergings, where this argument is also applied.

$p_T^{(\text{cut})}$ is a non-negligible fraction of the hardness of the production process), one must not decide beforehand whether it is either a matrix-element or a PSMC description which is suited best: they are in principle both valid alternatives, and a sufficiently large range of μ_Q in the surrounding of $p_T^{(\text{cut})}$ must be probed, lest one underestimates the merging-scale systematics.

A final technical remark: given that the work of ref. [188] has used HERWIG6 as PSMC, and that the FxFx formalism naturally matches a p_T -ordered shower, its use with PYTHIA8 and HERWIG++ does not pose any conceptual problems. In fact, a fully automatic FxFx interface with PYTHIA8 has now been achieved, but is not part of the current public MADGRAPH5_AMC@NLO release (the related, specific routine inside the PYTHIA8 code has become available starting from v8.185). For this reason, the sample FxFx-merged results which will be presented in sect. 4.2 will make use of HERWIG6. The FxFx-PYTHIA8 interface also paves the way for a fully analogous procedure, that will be carried out with HERWIG++. We also remind the reader that the FxFx method has so far been formulated only for processes that do not feature light jets at the Born level of the lowest-multiplicity sample, and that the merging of b -quark production processes has not been explicitly studied. Although we believe that these cases can be treated with only minor modifications (if any) w.r.t. the present implementation, we postpone their discussion to a future work.

2.5 Spin correlations: MadSpin

In both SM physics and BSM searches the role of unstable particles, that are not directly observable but (some of) whose decay products may be seen in detectors, is very prominent. Let us consider the production of p unstable particles u_k ($k = 1, \dots, p$; for example, $u_1 = Z$, $u_2 = t$, $u_3 = \bar{t}$, and so forth), each of which decays into n_k particles $d_{1,k}, \dots, d_{n_k,k}$, in association with l stable particles s_1, \dots, s_l :

$$x + y \longrightarrow u_1(\rightarrow d_{1,1} + \dots d_{n_1,1} + X_1) + \dots u_p(\rightarrow d_{1,p} + \dots d_{n_p,p} + X_p) + s_1 + \dots s_l + X_0. \quad (2.142)$$

It is convenient to regard eq. (2.142) as a parton-level quantity, so that x, y , and all the particles in the sets X_k are gluons or light quarks; the contents of X_k depend on the perturbative order considered³⁷, and need not be specified here. Equation (2.142) does not properly define a process, but has the following intuitive meaning: it corresponds to the contributions to the process

$$x + y \longrightarrow d_{1,1} + \dots d_{n_1,1} + \dots d_{1,p} + \dots d_{n_p,p} + s_1 + \dots s_l + X, \quad (2.143)$$

$$X = \bigcup_{k=0}^p X_k, \quad (2.144)$$

whose Feynman diagrams feature an s -channel propagator for each of the p unstable particles u_k , with one end of the propagator attached to a subdiagram that contains at least the

³⁷And, in general, on the type of corrections. In order to be definite, we consider here the case of QCD.

decay products $d_{1,k}, \dots, d_{n_k,k}$ (such a subdiagram is a tree at the leading order). These diagrams may be called p -resonant diagrams and, by extension, any diagram that features n such propagator-plus-subdiagram structures will be called n -resonant (so that, by including the case $n = 0$, all diagrams contributing to eq. (2.143) can be classified in this way). This implies that it would be natural to associate with eq. (2.142) the matrix elements obtained by considering only the p -resonant diagrams in their computations. Unfortunately, this is not straightforward, since in general it violates gauge invariance. So the only possibility is that of an operative meaning: thus, eq. (2.142) stands for the matrix elements relevant to the process of eq. (2.143), subject to selection cuts whose purpose is that of forcing the p -resonant diagrams to be numerically dominant. While this approach is the cleanest possible from a theoretical viewpoint, it has an obvious problem of efficiency: the non- p -resonant contributions to eq. (2.143) might swamp the p -resonant ones; furthermore, the matrix elements of eq. (2.143) are usually very involved. The difficulties mentioned above can be overcome by observing that a computation that uses only p -resonant diagrams is formally correct in the limit where all the widths of unstable particles vanish, $\Gamma_{u_k} \rightarrow 0, \forall k$ (narrow-width approximation, which can be systematically improved in the context of a pole expansion [98, 206, 207]). An immediate consequence of the narrow-width approximation is that the amplitudes associated with parton emissions (i.e., beyond leading order) from the decay products $d_{i_k,k}$ do not interfere with those associated with emissions either from $d_{i'_{k'},k'}$, for any $k' \neq k$, or from any particle which is not a decay product. Hence, higher-order corrections factorise, and can thus be sensibly considered separately for production and decay. This results in a significant simplification of the calculation, since in the narrow-width approximation one can therefore write:

$$x + y \longrightarrow u_1 + \dots u_p + s_1 + \dots s_l + X_0, \quad (2.145)$$

$$u_k \longrightarrow d_{1,k} + \dots d_{n_k,k} + X_k \quad k = 1, \dots p. \quad (2.146)$$

As this notation suggests, the particles u_k in eqs. (2.145) and (2.146) are regarded as final- and initial-state objects respectively, rather than as intermediate ones as in eq. (2.143). The calculation of amplitudes in the narrow-width approximation can be done by employing well-established spin-density-matrix techniques, which allow one to account for all spin correlations (we remind the reader that the process of eq. (2.143) is said to have decay spin correlations if its matrix elements depend non-trivially on the invariants $d_{i,k} \cdot d_{j,k}$ for some k ; production spin correlations are present in the case of non-trivial dependences on $d_{i_k,k} \cdot d_{i'_{k'},k'}$, for any i_k and $i'_{k'}$ with $k' \neq k$, or on $d_{i_k,k} \cdot s_q$, $d_{i_k,k} \cdot x$, $d_{i_k,k} \cdot y$ and $d_{i_k,k} \cdot X_0$ for some i_k and k).

When spin correlations effects are small or can be neglected, a further simplification can be made, where one replaces the *squared* amplitudes associated with the p -resonant diagrams relevant to eq. (2.143) with those relevant to the production (eq. (2.145)) and decays (eq. (2.146)) separately³⁸. Despite being a priori rather crude, such a simplification

³⁸In other words, the narrow-width approximation allows one to get rid of the non- p -resonant diagrams, whereas the simplification mentioned here gives a prescription for the actual computation of the p -resonant diagrams where one does not use spin-density matrices.

is very widely used in the context of PSMCs, since the narrow-width approximation is more difficult to automate already at LO, and more so beyond LO. Besides, unweighted-event generation is significantly more efficient for the process of eq. (2.145) than it is for that of eq. (2.143). The procedure is therefore that of generating (unweighted) events that correspond to eq. (2.145), and then let the PSMC decay the unstable particles according to eq. (2.146) (with $X_k = \emptyset$, i.e., at the leading order) during the shower phase. Note that the PSMC must know how to handle these decays, which sometimes involve non-trivial matrix elements (e.g., in top decays, or for $H^0 \rightarrow 2\ell 2\nu$). If this is not the case, decay spin correlations are also incorrectly predicted.

In order to retain the advantages of the separation of production from decays at the level of squared amplitudes, such as efficiency and ease of automation, without losing the capability of predicting spin correlations, MADGRAPH5_AMC@NLO uses the method introduced in ref. [208]³⁹, and studied there for top and W decays in the SM, which has been fully automated and extended to generic models in ref. [210]; the corresponding module in the code has been dubbed MADSPIN⁴⁰. The method is based on the following identity:

$$\lim_{\{\Gamma_{u_k}\} \rightarrow 0} \frac{\mathcal{M}(x + y \rightarrow d_{1,1} + \dots d_{n_p,p} + s_1 + \dots s_l + X)}{\mathcal{M}(x + y \rightarrow u_1 + \dots u_p + s_1 + \dots s_l + X)} \prod_{k=1}^p \Delta_{u_k}^{-1} \leq \mathcal{U}(\{u_k\}_{k=1}^p), \quad (2.147)$$

where \mathcal{U} is a universal factor, and the matrix elements at the numerator and denominator on the l.h.s. are the tree-level ones relevant to the processes of eqs. (2.143) (with p -resonant diagrams only) and (2.145) (with $X_0 = X$) respectively, and:

$$\Delta_{u_k}^{-1} = (p_{u_k}^2 - m_{u_k}^2)^2 + (m_{u_k} \Gamma_{u_k})^2. \quad (2.148)$$

Note that the factors $\Delta_{u_k}^{-1}$ in eq. (2.147) cancel exactly the denominators of the unstable-particle propagators, so that the limit is indeed a finite quantity. The fact that the set X of radiated partons is the same at the numerator and denominator in eq. (2.147) implies that the two matrix elements are computed at the same relative order w.r.t. the leading one; this allows one to correctly take into account the effects of hard radiation at the production level. Finally, the factor \mathcal{U} depends only on the identities of the unstable particles (and possibly on the decay kinematics), but is independent of the production process. It is computed by considering the decays of eq. (2.146) at the LO (i.e., with $X_k = \emptyset$), in a fully numerical manner by MADSPIN.

Equation (2.147) is used within a standard hit-and-miss procedure, that determines the kinematics of the decay products $d_{i_k,k}$ given that of the unstable particles u_k . In practice, unweighted events are first obtained for the process in eq. (2.145); then, for each of these the phase-space of the decay products is sampled, and through hit-and-miss unweighted events for the process in eq. (2.143) are obtained. It should be clear that the

³⁹For an alternative method, based on the knowledge of the polarization states of the unstable particles and on spin-density matrices, and which is adopted in HERWIG++, see ref. [209].

⁴⁰When working at the LO, production spin correlations can be recovered not only by using MADSPIN, but also by adopting the so-called decay-chain syntax – see appendix B.1 for more details.

latter events thus correctly incorporate the information on both production and decay spin correlations. Furthermore, there is evidence that, at the NLO, eq. (2.147) gives a general better description of the exact result for eq. (2.143) than that of an NLO narrow-width prediction, in spite of the LO-only treatment of the decays in the former. This has to do with the fact that, in the narrow-width approximation, configurations where the virtuality of an unstable particle (as reconstructed from final-state objects) is larger than the particle mass are suppressed both by α_s (being due to hard NLO corrections) and by a kinematical factor – for a recent discussion relevant to top physics, see sect. 3 of ref. [211]. Furthermore, the NLO origin of these configurations implies that, in the case of the production of more than one unstable particle, such off-shell effects can be possibly included only for one particle at a time in the NWA. On the other hand, eq. (2.147) trivially allows one to include off-shell effects without any kinematics suppression, already at the leading order, and for all unstable particles simultaneously. In particular, one starts by generating the virtualities of u_k according to a Breit-Wigner distribution (rather than using the pole masses), and employs those in the generation of the momenta of the decay particles that enter the hit-and-miss procedure mentioned above. In so doing, one may introduce back into the problem gauge-violating terms formally of $\mathcal{O}(\Gamma_{u_k}/m_{u_k})$, i.e., within the accuracy of the method. So the only potential issue might result from the numerical coefficients in front of such terms not being of $\mathcal{O}(1)$. However, one can use eq. (2.147) to check that this is not the case; indeed, the bound of that equation is a fairly good one, even for configurations where the virtuality of some unstable particle is more than ten widths away from the pole mass.

We have so far tacitly assumed to deal with the most common and numerically-relevant case in the SM, namely that of QCD corrections to the production of weakly-decaying unstable particles. When one starts considering EW NLO effects, one may face a self-consistency problem, due e.g. to the fact that the loop propagators relevant to EW vector bosons would have to feature non-zero widths (through the complex mass scheme prescription), while the same particles would have to be treated as on-shell (owing to the $\Gamma_{u_k} \rightarrow 0$ limits) when appearing in the final state. Hence, in the context of a mixed-coupling expansion, or in general when width effects are induced by the same type of interactions which are responsible for higher-order corrections, the method discussed in this section has to be employed by carefully considering the characteristics of the production process.

The MADSPIN module included in MADGRAPH5_AMC@NLO features a number of upgrades w.r.t. that presented in ref. [210]. The most important of these is that the phase-space generation is now handled by the Fortran code (rather than by a Python routine). The determination of the maximum weight has been fully restructured as well; on top of that, it has been noticed that using more events, but less phase-space points per event, is more efficient (the defaults have changed from 20 and 10^4 to 75 and 400, respectively). These two major improvements have resulted in a dramatic decrease of the running time (by a factor of about 10). Furthermore, the former one has paved the way for lifting the present limitation that restricts the code to dealing only with (a succession of) $1 \rightarrow 2$ decays. From the phenomenology viewpoint, two important novelties are the following. Firstly, MADSPIN now always writes the information on the polarization of final-state par-

ticles, gathered from the matrix elements, onto the LHE files. This implies, in particular, that PSMCs, if equipped with a suitable module, can handle τ decays including exactly all decay spin correlations, and also the production ones due to the diagonal terms of the spin-density matrix. Secondly, one can now use a UFO model in the determination of the decays which can be different from the one adopted in the computation of the short-distance undecayed matrix elements.

3. How to perform a computation

The theoretical background discussed in sect. 2 can be ignored if one is only interested in obtaining phenomenological predictions. This is the attitude that will be taken in this section, whose aim is that of giving the briefest documentation for the basic running of the code, and thus to show its extreme simplicity and level of automation.

The MADGRAPH5_AMC@NLO package is self-contained (third-party codes are included in the tarball – see appendix D for their complete list). The local directory where its tarball is unpacked is called main directory; there is a minimal (and optional) setup to be done, as described in appendix A. In essence, the computation of a cross section by MADGRAPH5_AMC@NLO consists of three steps: *generation*, *output*, and *running*. All three steps are performed by executing on-line commands in the MADGRAPH5_AMC@NLO shell⁴¹, which can be accessed by executing from a terminal shell in the main directory the following command:

```
./bin/mg5_aMC
```

The prompt now reads:

```
MG5_aMC>
```

which signals the fact that one is inside the MADGRAPH5_AMC@NLO shell. The three steps mentioned above correspond to the following commands:

```
MG5_aMC> generate process
```

```
MG5_aMC> output
```

```
MG5_aMC> launch
```

respectively; here, *process* denotes the specific process one is interested into generating (see appendix B.1 for full details on the syntax).

When generating a process, one must decide whether he/she is interested in including or not including NLO effects. In fact, although by definition an NLO cross section does include an LO part (the Born contribution), if NLO effects are not an issue it does not make much sense to include their contributions only to discard them at run time, especially in view of their being much more involved than their Born counterparts. Furthermore, the majority of physics models (see sect. 2.1) have not yet been extended to include NLO corrections, and in these cases the whole procedure could not even be conceived.

For these reasons, we talk about LO-type and NLO-type generations, and we note that these two types of generation give access to different running options. We shall discuss their different merits in the following sects. 3.1 and 3.2 respectively. Before going

⁴¹As in MADGRAPH5, scripting commands is of course possible.

into that, we point out that an LO-type generation produces the same short-distance cross section code (and hence the same type of physics) as that one would have obtained by running MADGRAPH5. All possibilities that were available in MADGRAPH5 are still available in MADGRAPH5_AMC@NLO; at the same time, it should be clear that, even in the context of an LO-type generation, MADGRAPH5_AMC@NLO has a much wider scope than MADGRAPH5.

3.1 LO-type generation and running

◆ *Generation*

In the generation phase, MADGRAPH5_AMC@NLO constructs the cross section relevant to the process given as input by the user, and thus performs the operations sketched in sect. 2.1. For example, if one is interested in $t\bar{t}W^+$ production in pp collisions at the LO, one will need to execute the following command:

```
MG5_aMC> generate p p > t t~ w+
```

When generating a process, MADGRAPH5_AMC@NLO assumes the model to be the SM (with massive b quarks); a different model can be adopted, by “importing” it before the generation (see appendix B.1). For example, the generation of a pair of top quarks in association with a pair of neutralinos (the latter denoted by $n1$) can be achieved as follows:

```
MG5_aMC> import model mssm
```

```
MG5_aMC> generate p p > t t~ n1 n1
```

◆ *Output*

When the process generation is complete, the relevant information is still in the computer memory, and needs to be written on disk in order to proceed. This is done by executing the command:

```
MG5_aMC> output MYPROC
```

where MYPROC is a name chosen by the user⁴² that MADGRAPH5_AMC@NLO will in turn assign to the directory under whose tree the cross section of the process just generated is written. We call such a directory the current-process directory, which is where all subsequent operations will be performed. For more details on this and for an overview of the structure of the current-process directory, see appendix A.

◆ *Running*

The running stage allows one to accomplish a variety of tasks, the most important of which are the production of unweighted events, and the plotting of user-defined physical observables. Regardless of the final product(s) of the run, MADGRAPH5_AMC@NLO will start by integrating the cross section generated and written in the two previous steps. In order to run MADGRAPH5_AMC@NLO, one executes the command:

```
MG5_aMC> launch
```

⁴² Such a name may be omitted; in this case, MADGRAPH5_AMC@NLO will choose one. On the other hand, there are a few names which are reserved, since they are interpreted as options of the `output` command. See appendix B.6 for more details.

What is prompted afterwards opens an interactive talk-to (which, again, can be scripted) that allows the user to choose among various options. This looks as follows:

The following switches determine which programs are run:

```

1 Run the pythia shower/hadronization:      pythia=OFF
2 Run PGS as detector simulator:             pgs=OFF
3 Run Delphes as detector simulator:         delphes=OFF
4 Decay particles with the MadSpin module:    madspin=OFF
5 Add weight to events based on coupling parameters: reweight=OFF
Either type the switch number (1 to 5) to change its default setting,
or set any switch explicitly (e.g. type 'madspin=ON' at the prompt)
Type '0', 'auto', 'done' or just press enter when you are done.
[0, 4, 5, auto, done, madspin=ON, madspin=OFF, madspin, reweight=ON, ... ]

```

We would like to emphasise that the structure of the above prompt will evolve in the near future, and be made more similar to its NLO counterpart (see sect. 3.2); however, the general idea that underpins its use will remain the same, so that what follows has to be regarded as an exemplification of the general features of the MADGRAPH5_AMC@NLO talk-to phase.

By entering 1, 2, 3, 4, or 5 at the prompt one toggles between the two values **ON** and **OFF** of the corresponding feature. For example, by entering 1 one is prompted again with the display above, except for the fact that **pythia=OFF** has now become **pythia=ON**. By entering 1 again, one gets back to **pythia=OFF**. By entering 0, or **done**, or by simply hitting return, the talk-to phase ends, and MADGRAPH5_AMC@NLO starts the actual run. The defaults shown above imply that MADGRAPH5_AMC@NLO will simply limit itself to integrating the cross section, and to producing the required number of unweighted events. On the other hand, by turning the various switches above to **ON**, one enables the following features.

pythia=ON: with such a setting MADGRAPH5_AMC@NLO will steer the showering of the hard events previously generated, by employing PYTHIA6. However, it is crucial to bear in mind that the same hard events can be showered with PSMCs other than PYTHIA6, but in this case MADGRAPH5_AMC@NLO is not capable of steering the shower⁴³ (the steering of PYTHIA8 will soon become available). The user may have an independent installation of PYTHIA6, but also install the code using the MADGRAPH5_AMC@NLO shell, by executing the command `install pythia-pgs`.

pgs=ON: in this case, MADGRAPH5_AMC@NLO will also steer the run of the Pretty Good Simulator (PGS) [212] after that of PYTHIA6 (i.e., first all events are showered and hadronised, and next they are passed through the basic detector simulation as implemented by PGS). For this reason, when **pgs=ON** MADGRAPH5_AMC@NLO automatically sets **pythia=ON**. Note, also, that when the MADGRAPH5_AMC@NLO shell is used to install PYTHIA with the `install pythia-pgs` command, PGS is installed too.

delphes=ON: this allows one to steer the run of DELPHES 3 [213] for a fast detec-

⁴³This is not the case for NLO simulations – see later.

tor simulation. DELPHES can also be installed through the MADGRAPH5_AMC@NLO shell with the command `install Delphes`⁴⁴. As for switch number 2, when `delphes=ON` MADGRAPH5_AMC@NLO sets automatically `pythia=ON`.

madspin=ON: by doing so, one includes production spin correlations by means of MADSPIN (see sect. 2.5). Note that the decay-chain syntax (see appendix B.1) is actually faster and features a better approximation of the exact cross section than MADSPIN, which is thus more conveniently used in the context of NLO simulations.

reweight=ON: instructs MADGRAPH5_AMC@NLO to store in the LHE file information to be used later within the matrix-element reweighting procedure, for example relevant to assessing the impact of different theoretical assumptions (see sect. 2.3.3 and appendix B.5).

When switches 1–5 are set as desired by the user and 0, or `done`, or `<return>` are entered, MADGRAPH5_AMC@NLO proceeds with the run, whose first stage is that of giving the user the possibility of modifying the various inputs relevant to the options selected above. Such inputs, and the `*_card.dat` files where they are stored, have a self-explanatory meaning, and we will not discuss them in detail here.

3.2 NLO-type generation and running

◆ *Generation*

The generation phase of an NLO-type generation has the same conceptual meaning of that relevant to the LO case, described at the beginning of sect. 3.1. The syntax is also *very* similar: adopting again the example of $t\bar{t}W^+$ production in pp collisions, one will need to execute the following command in order to include QCD NLO effects:

```
MG5_aMC> generate p p > t t~ w+ [QCD]
```

As one can see, the only difference w.r.t. the case of the LO-generation is in the presence of the keyword `[QCD]` here. Fuller details on the syntax for NLO-type generation are given in appendix B.1.

◆ *Output*

There is no conceptual or technical difference w.r.t. the case of an LO-type generation in the output phase. Specifically, the command one will need to execute is the same as that described in sect. 3.1:

```
MG5_aMC> output MYPROC
```

The same comments concerning the choice of `MYPROC` as made for LO simulations apply here (see footnote 42).

◆ *Running*

Also in the case of an NLO-type generation, the running phase begins by integrating the cross section generated and written in the two previous steps. There is an important difference w.r.t. the LO case that must be stressed here. Namely, at the LO the short-distance cross sections relevant to LO+PS and to fLO computations are identical. This is not the case at the NLO: the MC@NLO cross sections used in NLO+PS computations

⁴⁴Or `install Delphes2`, if one wanted to use the older DELPHES 2 [214] version.

are different from the fixed-order ones used in fNLO computations (the former contain the MC counterterms, the latter do not; the former can be unweighted, the latter cannot – see sect. 2.4.4 for more details). However, when MADGRAPH5_AMC@NLO generates and outputs a process, it writes *both* cross sections, and in so doing allows the user to choose at runtime which type of computation to perform. In other words, after having generated a process and used it to obtain (say) fNLO results, there is no need to re-generate it to obtain NLO+PS results: it is sufficient to run MADGRAPH5_AMC@NLO again.

In order to run MADGRAPH5_AMC@NLO, one executes the same command as that relevant to the LO-type generation:

```
MG5_aMC> launch
```

However, what is prompted afterwards opens an interactive talk-to which is different from the one of the LO-type generation. In particular, one now obtains what follows:

The following switches determine which operations are executed:

```
1 Perturbative order of the calculation:                order=NLO
2 Fixed order (no event generation and no MC@[N]LO matching): fixed_order=OFF
3 Shower the generated events:                          shower=ON
4 Decay particles with the MadSpin module:               madspin=OFF
```

Either type the switch number (1 to 4) to change its default setting,
or set any switch explicitly (e.g. type 'order=L0' at the prompt)

Type '0', 'auto', 'done' or just press enter when you are done.

```
[0, 1, 2, 3, 4, auto, done, order=L0, order=NLO, ... ]
```

By entering 1, 2, 3, or 4 at the prompt one toggles between the two values of the corresponding feature (which are NLO and L0 for 1, and ON or OFF for 2–4). For example, by entering 2 one is prompted again what is displayed above, except for the fact that `fixed_order=OFF` has now become `fixed_order=ON`. By entering 2 again, one gets back to `fixed_order=ON`. By entering 0, or done, or by simply hitting return, the talk-to phase ends, and MADGRAPH5_AMC@NLO starts the actual runs.

It is the combinations of the values of the switches 1 and 2 that control which kind of computation the program will perform. More explicitly, we have:

<code>(order=NLO,fixed_order=OFF)</code>	→	NLO+PS and FxFx-merged ⁴⁵
<code>(order=NLO,fixed_order=ON)</code>	→	fNLO
<code>(order=L0,fixed_order=OFF)</code>	→	LO+PS
<code>(order=L0,fixed_order=ON)</code>	→	fLO

One need not be surprised by the fact that LO+PS and fLO results can be obtained following an NLO-type generation, since all the LO information is obviously there, being part of the NLO cross section. Rather, one may wonder why these options are not disabled, since they lead to the same physics as a run that follows an LO-type generation. A discussion on this point will be given in sect. 3.3; here, we limit ourselves to giving the shortest answer, which is the following: the access to both LO and NLO results within the same generation

⁴⁵We remind the reader that *i*-parton samples, the contributions to an FxFx cross section of a given multiplicity, are nothing but unmerged NLO+PS samples with some extra damping factors, which are included by MADGRAPH5_AMC@NLO through a parameter (`ickkw`) in an input card.

procedure (i.e., in the same current-directory process) guarantees an extremely easy and swift comparison between them.

Switch 3 controls whether one employs `MADGRAPH5_AMC@NLO` to steer the showering of hard-subprocess events previously generated (`shower=ON`) or not (`shower=OFF`). We shall give a more extended discussion about this point in sect. 3.2.1. Here, we would like to stress one crucial point: if the hard events are relevant to an NLO+PS run, they do not have any physical meaning unless they are showered. Hence, one is free to use or not use `MADGRAPH5_AMC@NLO` for showering them, but shower them he/she must. Note that this is not the case for LO+PS hard events, although of course shower or not shower them leads to different types of physics (in particular, observables constructed with unshowered LO+PS hard events are the same as those resulting from an fLO computation).

Finally, switch 4 allows one to decide whether to include production spin correlations by means of `MADSPIN` (see sect. 2.5). Since the method works starting from unweighted events, `MADSPIN` is disabled when a fixed-order run is selected (in other words, the inputs `fixed_order=ON` and `madspin=ON` are incompatible, and `MADGRAPH5_AMC@NLO` will automatically prevent the user from making such a choice; this is not necessary when `order=LO`, but it is done anyway in order to simplify things).

As in the case of an LO-type generation, after setting switches 1–4 to the desired values and entering 0, or `done`, or `<return>`, `MADGRAPH5_AMC@NLO` proceeds with the run by giving the user the possibility of modifying the various input cards relevant to the options selected.

3.2.1 (N)LO+PS results

The aim of this section is that of giving some details on the (N)LO+PS runs that follow an NLO-type generation. We recall that (N)LO+PS results are obtained by setting `fixed_order=OFF`, and the perturbative order is assigned according to the value of the switch `order` (see sect. 3.2).

There are two types of objects⁴⁶ that may be obtained with an (N)LO+PS run:

1. One or two files of unweighted events at the hard-subprocess level.
2. One file that collects results at the end of the shower, be them in the form of histograms, or n-tuples, or events; we call it `MC.output`.

The first of the files in 1 is the result of the integration of the short-distance partonic cross section performed by `MADGRAPH5_AMC@NLO`. The second file is present only in the case when `MADSPIN` is used (`madspin=ON`), and results from feeding the former file to `MADSPIN`. These two files will be found under the current-process directory tree:

```
MYPROC/Events/run_nn/events.lhe.gz
```

```
MYPROC/Events/run_nn_decayed_mm/events.lhe.gz
```

Although of course `MADSPIN` may not be used (or it may simply be not relevant, if the generated process does not feature particles that decay), the above structure is the most

⁴⁶There are actually several other auxiliary files produced by `MADGRAPH5_AMC@NLO`, whose role is however not important here. See appendix A for more details.

general, and hence we shall discuss it so as to encompass all cases. We shall call the two files above the undecayed and decayed (hard-subprocess) event files, respectively; both files are fully compliant with the recent Les Houches Accord v3.0 [215].

The undecayed event file will contain events whose particle content is the same as that given as input during the generation step (up to one final-state parton at the NLO), i.e., using the example of sect. 3.2:

$$x + y \longrightarrow t + \bar{t} + W^+(+z), \quad (3.1)$$

where x , y , and z are quarks or gluons⁴⁷. The integration of the cross section that results in the actual events is performed once the values of the relevant parameters (such as particles masses, collider energy, PDFs) are given in input by the user. The two primary input cards are:

MYPROC/Cards/run_card.dat

MYPROC/Cards/param_card.dat

One can obtain an undecayed event file with some parameter settings, then change these settings, integrate the cross section again, and obtain a second event file; the procedure can be iterated as many times as one likes. Each run is identified by an integer number, chosen by MADGRAPH5_AMC@NLO, which unambiguously names the directory where the event files will be stored. So, in the example given above, we shall have **nn=01** for the first run, **nn=02** for the second run, and so forth.

Each undecayed event file can be fed to MADSPIN in order to obtain a decayed event file. In order to do so, the user is expected to give in input to MADSPIN the actual decay(s) he/she is interested into, which can be done by means of the input card:

MYPROC/Cards/madspin_card.dat

Using again the generation example given before, and supposing that one wants to study the decays:

$$t \rightarrow b e^+ \nu_e, \quad \bar{t} \rightarrow \bar{b} e^- \bar{\nu}_e, \quad W^+ \rightarrow \mu^+ \nu_\mu, \quad (3.2)$$

then the decayed event file will contain events of the following kind:

$$x + y \longrightarrow b + e^+ + \nu_e + \bar{b} + e^- + \bar{\nu}_e + \mu^+ + \nu_\mu (+z). \quad (3.3)$$

It is possible to run MADSPIN multiple times, by feeding it with the same undecayed event file and by changing the type of decays considered (e.g., semileptonic top decays after the di-leptonic ones of eq. (3.2)). For each MADSPIN run, MADGRAPH5_AMC@NLO will store the decayed event file in a different directory – this is the reason for the integer number **mm** in the example above, which is automatically assigned to each new run: so **mm=1** will identify the first MADSPIN run, **mm=2** the second, and so forth.

In summary, directories that contain undecayed event files are identified by an integer **nn**, which roughly speaking corresponds to a given choice of settings in **run_card.dat** and **param_card.dat**. On the other hand, directories that contain decayed event files are identified by a pair of integers (**nn,mm**), which correspond to a given choice of settings in **run_card.dat**, **param_card.dat**, and **madspin_card.dat**.

⁴⁷The parton z is present in the case of \mathbb{H} events, and absent in \mathbb{S} events [24].

Both undecayed and decayed hard-subprocess event files are non physical (at the NLO), and *must* be showered in order to obtain physical results. Such a showering can be done without using MADGRAPH5_AMC@NLO, since it is nothing but the nowadays typical PSMC run starting from an external (to the PSMC) LH-compliant event file. On the other hand, MADGRAPH5_AMC@NLO can steer PSMC runs: this is convenient for a variety of reasons, among which the most important are probably those of ensuring a full consistency among the parameters used when integrating the cross section and those adopted by the PSMC, and the correct setting of a few control switches in the PSMC itself⁴⁸. As was explained in sect. 3.2, MADGRAPH5_AMC@NLO will steer the shower when `shower=ON`: in this case, several of the features of the PSMC run can be controlled through a MADGRAPH5_AMC@NLO input card:

```
MYPROC/Cards/shower_card.dat
```

The parameters not explicitly included in this card must be controlled directly in the relevant PSMC, in the same way as one would follow in a PSMC standalone run.

The steering of the PSMC by MADGRAPH5_AMC@NLO also guarantees that the PSMC adopted is consistent with that assumed during the integration of the short-distance cross section. Indeed, it is important to keep in mind that NLO+PS events obtained with the MC@NLO formalism are PSMC-dependent, and for this reason one of the input parameters in `run_card.dat` is the name of the PSMC which will be eventually used to shower the hard-subprocess events. This kind of consistency is the user's responsibility in the case of a PSMC not steered by MADGRAPH5_AMC@NLO. Finally, we point out that the most recent versions of the source codes of the Fortran77 PSMCs (HERWIG6 and PYTHIA6) are included in the MADGRAPH5_AMC@NLO tarball⁴⁹. On the other hand, the modern C++ PSMC (PYTHIA8 and HERWIG++) must be installed locally prior to running MADGRAPH5_AMC@NLO. The paths to their executables/libraries have to be included in the setup file `mg5_configuration.txt` (see appendix A).

When steering of the PSMC by MADGRAPH5_AMC@NLO one will obtain, at the end of the PSMC run, the file `MC.output` mentioned in item 2 at the beginning of this section. By default (i.e., if the user does not write his/her own analysis) this file will contain the full event record of each showered event (in `StdHEP` format for Fortran MCs, and in `HepMC` format for C++ PSMCs), and it will be named as follows:

```
MYPROC/Events/run_*/events_MCTYPE_11.hep.gz
```

Here, the `run_*` directory is one of those introduced before; `MC.output` is moved to the same directory where one finds the hard-subprocess event file fed to the PSMC during the course of the run. `MCTYPE` is a string equal to the name of the PSMC used, and `11` is an integer, chosen by MADGRAPH5_AMC@NLO, that allows one to distinguish different files obtained by showering the same hard-event file multiple times (for example by changing

⁴⁸See <http://amcatnlo.cern.ch> → Help and FAQs → Special settings for the parton shower.

⁴⁹These codes are essentially frozen, so we expect no or very minor changes in the future. Should the need arise to use versions different w.r.t. those included here, copy them to `MYPROC/MCatNLO/srcHerwig` and `MYPROC/MCatNLO/srcPythia`, and write their names in `MYPROC/MCatNLO/MCatNLO_MadFKS.inputs`. In the case of PYTHIA6, the routines `UPINIT`, `UPEVNT`, `PDFSET`, `STRUCTP`, and `STRUCTM` need also be commented out of the source code.

the shower parameters). Any other output created by the PSMC (such as its standard output, which would be printed on the screen during an interactive run) will be found in the directory:

`MYPROC/MCatNLO/RUN_MCTYPE_pp`

with `pp` an integer that enumerates the various runs⁵⁰.

While `StdHEP` full event records may be analysed off-line, they have the disadvantage of using a very significant amount of disk space. It is very often more convenient to analyse showered events on-the-fly, using the event kinematics and weight to construct observables and fill the corresponding histograms. This can be done in a very flexible manner in the PSMC runs steered by `MADGRAPH5_AMC@NLO`. The user's analysis can be stored in one of the directories⁵¹

`MYPROC/MCatNLO/XYZAnalyzer`

where the string `XYZ` depends on the PSMC adopted. The name of such an analysis, and those of all its dependencies (be they in the form of either source codes or libraries) can be given in input to `MADGRAPH5_AMC@NLO` at runtime, as parameters in `shower_card.dat`. It is clear that it is the user's analysis that determines the format of `MC.output`. Since `MADGRAPH5_AMC@NLO` cannot know it beforehand, it will treat `MC.output` as any other standard file produced by the PSMC, which will thus be found in the directory `RUN_MCTYPE_pp`. An exception is that of the topdrawer format (which is human readable); in this case, `MC.output` will be named as follows:

`MYPROC/Events/run_*/plot_MCTYPE_kk_*.top`

with again `kk` an integer that allows one to distinguish the outputs relevant to different showering of the same hard-event file.

We conclude this section by mentioning the fact that when the `launch` command is executed with `madspin=ON` and `shower=ON` (i.e., both undecayed and decayed events are produced, the PSMC runs immediately follows the integration of the cross section, and it is steered by `MADGRAPH5_AMC@NLO`) only the decayed event file will be showered. In order to shower the undecayed event file, or to perform other shower runs, one needs to use the `MADGRAPH5_AMC@NLO` shell command `shower`. Please see appendix B.1 for more details.

3.2.2 f(N)LO results

As was discussed in sect. 3.2, fixed-order results can be obtained with `MADGRAPH5_AMC@NLO` by setting `fixed_order=ON`, with the perturbative order assigned according to the value of the switch `order`.

We remind the reader that an NLO computation not matched to a parton shower cannot produce *unweighted* events, since the matrix elements are not bounded from above in the phase space; unweighting events would require the introduction of unphysical cutoffs that would bias predictions, and must therefore be avoided. The only thing one can do is that of considering weighted events, namely parton-level kinematic configurations

⁵⁰Note that in general `pp` \neq 11: for example, a PSMC run may not create an `StdHEP` event record, in which case `pp` would be increased, while 11 would not.

⁵¹Which contain several ready-to-run templates.

supplemented by a weight (which is basically equal to the matrix element times a phase-space factor). Such events, which are readily obtained when sampling the phase space in the course of the integration of the cross section, can be either stored in a file or used on-the-fly to predict physical observables. While we choose the latter option as our default, we remark that the former can be easily implemented by the interested user, as it will become clear in what follows.

The input parameters relevant to f(N)LO runs can be found in the same cards that control NLO+PS runs, namely `run_card.dat` and `param_card.dat`. Since observables will be plotted on the fly, the user is expected to write his/her own analysis (which is a trivial task, in view of the rather small final-state multiplicities of parton-level computations). This analysis must be written in Fortran (or at least it must include a Fortran front-end interface to the user's core analysis, written in a language other than Fortran) and stored in the directory:

`MYPROC/FixedOrderAnalysis`

which contains several templates, meant to be used as examples. As the templates show, MADGRAPH5_AMC@NLO at present supports two output formats for user's analyses – Root and topdrawer (see appendix. A for more details about this). The analysis name and the format of its output must be given in input to MADGRAPH5_AMC@NLO, which is done by including them in the input card:

`MYPROC/Cards/F0_analyse_card.dat`

where the user will also be able to specify any other source file or library needed by the analysis. Upon running, MADGRAPH5_AMC@NLO will produce the final-result file:

`MYPROC/Events/run_nn/MADatNLO.root`

if the Root format has been chosen, and:

`MYPROC/Events/run_nn/MADatNLO.top`

for the topdrawer format; these will contain plots for the observables defined by the user. As in the case of NLO+PS runs, the integer `nn` will be chosen by MADGRAPH5_AMC@NLO in a non-ambiguous way (it should be obvious that both (N)LO+PS and f(N)LO simulations can be performed any number of times starting from a given generation, and `nn` will allow one to distinguish their results). By default, if the user does not write an analysis, MADGRAPH5_AMC@NLO will produce a file which will contain the predictions for the total rate (possibly within the cuts, as specified in `run_card.dat` and `cuts.f`).

In essence, the user's analysis will have to construct the desired observables, given in input the pair composed of a kinematic configuration and its corresponding weight⁵², which are provided by MADGRAPH5_AMC@NLO. These pairs can be read from eq. (2.47): for each choice of the random variables $\{\chi_{Bj}^{(ij)}, \chi_{n+1}^{(ij)}\}$ that scan the phase space and Bjorken

⁵²Such a weight becomes an array of weights when the user asks MADGRAPH5_AMC@NLO to compute scale and PDF uncertainties. See sect. B.3 for more details.

x 's, MADGRAPH5_AMC@NLO will call the user's analysis three times, with input pairs:

$$\left(\mathcal{K}_{n+1}^{(E)}, \frac{d\sigma_{ij}^{(\text{NLO}, E)}}{d\chi_{Bj}^{(ij)} d\chi_{n+1}^{(ij)}} \right), \quad (3.4)$$

$$\left(\mathcal{K}_{n+1}^{(S)}, \sum_{\alpha=S, C, SC} \frac{d\sigma_{ij}^{(\text{NLO}, \alpha)}|_{\text{non-Born}}}{d\chi_{Bj}^{(ij)} d\chi_{n+1}^{(ij)}} \right), \quad (3.5)$$

$$\left(\mathcal{K}_{n+1}^{(S)}, \frac{d\sigma_{ij}^{(\text{NLO}, S)}|_{\text{Born}}}{d\chi_{Bj}^{(ij)} d\chi_{n+1}^{(ij)}} \right), \quad (3.6)$$

where

$$d\sigma_{ij}^{(\text{NLO}, \alpha)}|_{\text{non-Born}} = d\sigma_{ij}^{(\text{NLO}, \alpha)} \quad \alpha = C, SC, \quad (3.7)$$

$$d\sigma_{ij}^{(\text{NLO}, S)}|_{\text{Born}} + d\sigma_{ij}^{(\text{NLO}, S)}|_{\text{non-Born}} = d\sigma_{ij}^{(\text{NLO}, S)}, \quad (3.8)$$

and $d\sigma_{ij}^{(\text{NLO}, S)}|_{\text{Born}}$ is the contribution of the Born matrix elements to the soft-counterevent weight. The user's analysis must treat eqs. (3.4)–(3.6) precisely in the same way: this is an essential condition which guarantees that infrared safety is not spoiled. In particular, to any given histogram all of these weights must contribute (obviously, to the bins and subject to the cuts determined by the respective kinematics configurations, $\mathcal{K}_{n+1}^{(E)}$ and $\mathcal{K}_{n+1}^{(S)}$), if the NLO accuracy is to be maintained. Note, also, that the weights (3.4)–(3.6) are correlated, and thus cannot be individually used in a statistical analysis as they would if they had been the result e.g. of an unweighted-event procedure.

Thanks to the fact that the Born weight, eq. (3.6), is kept separate from the other contributions to the NLO cross section, MADGRAPH5_AMC@NLO allows the user to plot, during the course of the same run, a given observable both at the NLO accuracy (by using eqs. (3.4)–(3.6)) and at the LO accuracy (by using eq. (3.6) only). In order to allow the user's analysis to tell eq. (3.6) apart from eqs. (3.4) and (3.5), MADGRAPH5_AMC@NLO will tag these weights with an integer, equal to 3, 1, and 2 respectively. For explicit examples, see one of the template analyses in `MYPROC/FixedOrderAnalysis`.

We conclude this section by pointing out that the writing of weighted events can be seen as a special type of analysis. The flexibility inherent in the structure sketched above should easily allow a user to write and exploit such an analysis. In this case, we also note that, rather than associating a single weight with each event, one can use all of the scale- and PDF-independent ones defined in ref. [122] (which are available as variables in a common block) in order to be able to compute scale and PDF uncertainties through reweighting. These uncertainties can obviously be included when plotting observables on the fly – see appendix B.3.

3.3 Possibilities for LO simulations

As was mentioned in sect. 3, MADGRAPH5_AMC@NLO offers two ways to obtain LO results. One is through an LO-type generation, where when executing the command `generate` one does not include the keyword `[QCD]`; this is completely equivalent to what one would do

if using MADGRAPH5. The other is accessed through an NLO-type generation, by using `order=L0`.

We stress once again that all of the capabilities of MADGRAPH5 are inherited by MADGRAPH5_AMC@NLO. Therefore, if one is interested *only* in LO physics, there is no reason to simulate it within an NLO-type generation (which in that case would simply be a waste of time). This is also in view of the fact that many of the options available in the context of an LO-type generation are disabled when an LO process is computed after an NLO-type generation. The idea of LO runs in the context of NLO-type generation is that of rendering the comparison between LO and NLO a completely trivial affair. Note, for example, that the input cards relevant to LO- and NLO-type generations are different: many of the cuts that are present in the former would simply not make sense in the latter (owing to the necessity of being compliant with infrared safety). Also, one should bear in mind that the functional form of α_S used by MADGRAPH5_AMC@NLO (i.e., at one or two loops) is determined by the set of PDFs employed in the runs. Therefore, when working with an NLO-type generation, and assuming that fLO (or LO+PS) results are obtained during the same run as their fNLO (or NLO+PS) counterparts, the former will be based on NLO PDFs and two-loop α_S (which is of course fully consistent with perturbation theory, and actually the best option if one is interested in assessing the perturbative behaviour of the partonic short-distance matrix elements).

In summary, both options for LO runs lead to exactly the same physics. However, by running the code at the LO with its default inputs one generally does *not* obtain exactly the same numbers, since the relevant input cards are tailored either to LO-type or to NLO-type generations, which have different necessities and emphases. Hence, we recommend to consider fLO and/or LO+PS results obtained through NLO-type generation mainly in the context of studies that feature fNLO and/or NLO+PS simulations as well.

4. Illustrative results

4.1 Total cross sections

In this section we present benchmark results for total rates (possibly within the cuts which will be specified later), at both the LO and the NLO. These are fLO and fNLO results respectively, with the former computed in the context of an NLO-type generation (see sect. 3.3). On the one hand, the aim of this section is that of showing the extreme flexibility and reach of MADGRAPH5_AMC@NLO: in keeping with our general philosophy, no part of the code has been customised to the computation of any of the processes below. The code has been run as is extracted from the tarball (apart from the occasional necessity of defining some final-state cuts in `cuts.f`, in some cases relevant to $(b\text{-})$ jet production, which are explicitly mentioned in the captions of tables 1–11). We stress that several of these cross sections have never been computed before to NLO accuracy.

We summarise here the main physics parameters used in our runs; the complete list of inputs, in the form of the input cards of MADGRAPH5_AMC@NLO, can be found by visiting http://amcatnlo.cern.ch/cards_paper.htm, which should render it particularly easy to reproduce the results that follow.

- $m_H = 125$ GeV, $m_t = 173.2$ GeV.
- MSTWnlo2008 [216] PDFs with errors at 68%CL, $n_f = 4, 5$. Note that these PDFs are used to obtain the fLO results as well, and that they set the value of $\alpha_s(m_Z)$.
- Central scale choice: $\mu_0 = H_T/2$, with H_T the scalar sum of the transverse masses $\sqrt{p_T^2 + m^2}$ of all final state particles.
- Scale variations: independent, $1/2\mu_0 < \mu_R, \mu_F < 2\mu_0$.
- Diagonal CKM matrix.

Final-state objects are defined as follows:

- Jets: anti- k_T algorithm [217] with $R = 0.5$, $p_T(j) > 30$ GeV, $|\eta(j)| < 4$.
- Photons: Frixione isolation [218] with $R = 0.7$, $p_T(\gamma) > 20$ GeV, $|\eta(\gamma)| < 2$.

While MADGRAPH5_AMC@NLO can handle intermediate resonances by using the complex mass scheme, in this section we consider W 's, Z 's, and top quarks as stable, and thus set their widths equal to zero. Furthermore, although matrix elements for loop-induced processes (e.g. such as $gg \rightarrow ZZ$), can be obtained with MADLOOP, they have not been considered in this section. Apart from reporting the absolute values of the total cross sections, the following tables also show (as percentages) scale and PDF uncertainties. These are computed exactly but without re-running, by exploiting the reweighting method presented in ref. [122]. Following ref. [66], Yukawa's are renormalised with an on-shell scheme.

We tag the processes for which we are not aware of any fNLO result being available in the literature with an asterisk. We stress that, in those cases where an fNLO prediction had been previously obtained, the corresponding matching to PSMCs might not necessarily have been achieved; this is the typical situation for several of the high-multiplicity reactions. On the other hand, for all processes presented in the tables below the corresponding NLO+PS event samples can be obtained with MADGRAPH5_AMC@NLO. Some non-exhaustive examples will be given in sect. 4.2.

The following results are organised into broad classes of processes that share some defining characteristic. In hadroproduction (with a c.m. energy of 13 TeV), we have considered vector bosons plus up to three light jets (table 1), vector boson pairs plus up to two light jets (table 2), three vector bosons plus up to one light jet (table 3), four vector bosons (table 4), light jets, b -jets, and top quarks, possibly in association with each other (table 5), vector bosons in association with top or bottom quarks and light jets (table 6), single top quarks in association with b quarks (four-flavour scheme⁵³) and vector bosons (table 7), Higgs and double-Higgs in association with (possibly multiple) light jets, vector bosons and heavy quarks (tables 8 and 9). In e^+e^- collisions (with a c.m. energy of 1 TeV), we have considered light jets, possibly in association with heavy quarks (table 10), and top quark pairs in association with (possibly multiple) vector or Higgs bosons (table 11).

⁵³Throughout this paper, we adopt standard definitions for the four- and five-flavour schemes. See e.g. sect. 1 of ref. [219] for a recent short review.

Process		Syntax	Cross section (pb)					
Vector boson +jets			LO 13 TeV			NLO 13 TeV		
a.1	$pp \rightarrow W^\pm$	p p > wpm	$1.375 \pm 0.002 \cdot 10^5$	+15.4%	+2.0%	$1.773 \pm 0.007 \cdot 10^5$	+5.2%	+1.9%
a.2	$pp \rightarrow W^\pm j$	p p > wpm j	$2.045 \pm 0.001 \cdot 10^4$	+19.7%	+1.4%	$2.843 \pm 0.010 \cdot 10^4$	+5.9%	+1.3%
a.3	$pp \rightarrow W^\pm jj$	p p > wpm j j	$6.805 \pm 0.015 \cdot 10^3$	+24.5%	+0.8%	$7.786 \pm 0.030 \cdot 10^3$	+2.4%	+0.9%
a.4	$pp \rightarrow W^\pm jjj$	p p > wpm j j j	$1.821 \pm 0.002 \cdot 10^3$	+41.0%	+0.5%	$2.005 \pm 0.008 \cdot 10^3$	+0.9%	+0.6%
a.5	$pp \rightarrow Z$	p p > z	$4.248 \pm 0.005 \cdot 10^4$	+14.6%	+2.0%	$5.410 \pm 0.022 \cdot 10^4$	+4.6%	+1.9%
a.6	$pp \rightarrow Z j$	p p > z j	$7.209 \pm 0.005 \cdot 10^3$	+19.3%	+1.2%	$9.742 \pm 0.035 \cdot 10^3$	+5.8%	+1.2%
a.7	$pp \rightarrow Z jj$	p p > z j j	$2.348 \pm 0.006 \cdot 10^3$	+24.3%	+0.6%	$2.665 \pm 0.010 \cdot 10^3$	+2.5%	+0.7%
a.8	$pp \rightarrow Z jjj$	p p > z j j j	$6.314 \pm 0.008 \cdot 10^2$	+40.8%	+0.5%	$6.996 \pm 0.028 \cdot 10^2$	+1.1%	+0.5%
a.9	$pp \rightarrow \gamma j$	p p > a j	$1.964 \pm 0.001 \cdot 10^4$	+31.2%	+1.7%	$5.218 \pm 0.025 \cdot 10^4$	+24.5%	+1.4%
a.10	$pp \rightarrow \gamma jj$	p p > a j j	$7.815 \pm 0.008 \cdot 10^3$	+32.8%	+0.9%	$1.004 \pm 0.004 \cdot 10^4$	+5.9%	+0.8%

Table 1: Sample of LO and NLO rates for vector-boson production, possibly within cuts and in association with jets, at the 13-TeV LHC; we also report the integration errors, and the fractional scale (left) and PDF (right) uncertainties. Where relevant, the notation understands the sum of the W^+ and W^- cross sections, and `wpm` is a label that includes both W^+ and W^- , defined from the shell with `define wpm = w+ w-`. All cross sections are calculated in the five-flavour scheme. Results at the NLO accuracy for W/Z plus jets are also available in MCFM for up to two jets [220–222], including heavy-flavour identification [223–227], and in POWHEG [228–230]. NLO cross sections for W plus three jets have appeared in refs. [231, 232]. The BLACKHAT+SHERPA collaboration has provided samples and results for up to Z plus four jets and W plus five jets at the NLO [233–237]. NLO+PS merged samples for W plus up to three jets are also available in SHERPA [238]. γ plus up to three jets calculations have been presented in refs. [239, 240]. We do not show cross sections for EW-induced V plus two jets processes with $V = \gamma, Z, W^\pm$, which are available in VBFNLO [241] and have been studied in ref. [242].

Process		Syntax	Cross section (pb)					
Vector-boson pair +jets			LO 13 TeV			NLO 13 TeV		
b.1	$pp \rightarrow W^+W^-$ (4f)	p p > w+ w-	$7.355 \pm 0.005 \cdot 10^1$	+5.0%	+2.0%	$1.028 \pm 0.003 \cdot 10^2$	+4.0%	+1.9%
b.2	$pp \rightarrow ZZ$	p p > z z	$1.097 \pm 0.002 \cdot 10^1$	-6.1%	-1.5%	$1.415 \pm 0.005 \cdot 10^1$	-4.5%	-1.4%
b.3	$pp \rightarrow ZW^\pm$	p p > z wpm	$2.777 \pm 0.003 \cdot 10^1$	+4.5%	+1.9%		+3.1%	+1.8%
b.4	$pp \rightarrow \gamma\gamma$	p p > a a	$2.510 \pm 0.002 \cdot 10^1$	-5.6%	-1.5%		-3.7%	-1.4%
b.5	$pp \rightarrow \gamma Z$	p p > a z	$2.523 \pm 0.004 \cdot 10^1$	+3.6%	+2.0%	$3.695 \pm 0.013 \cdot 10^1$	+4.4%	+1.7%
b.6	$pp \rightarrow \gamma W^\pm$	p p > a wpm	$2.954 \pm 0.005 \cdot 10^1$	-4.7%	-1.5%	$7.124 \pm 0.026 \cdot 10^1$	-4.4%	-1.3%
				+22.1%	+2.4%		+17.6%	+2.0%
				-22.4%	-2.1%		-18.8%	-1.9%
				+9.9%	+2.0%		+5.4%	+1.8%
				-11.2%	-1.6%		-7.1%	-1.4%
				+9.5%	+2.0%		+9.7%	+1.5%
				-11.0%	-1.7%		-9.9%	-1.3%
b.7	$pp \rightarrow W^+W^-j$ (4f)	p p > w+ w- j	$2.865 \pm 0.003 \cdot 10^1$	+11.6%	+1.0%	$3.730 \pm 0.013 \cdot 10^1$	+4.9%	+1.1%
b.8	$pp \rightarrow ZZj$	p p > z z j	$3.662 \pm 0.003 \cdot 10^0$	-10.0%	-0.8%	$4.830 \pm 0.016 \cdot 10^0$	-4.9%	-0.8%
b.9	$pp \rightarrow ZW^\pm j$	p p > z wpm j	$1.605 \pm 0.005 \cdot 10^1$	+10.9%	+1.0%		+5.0%	+1.1%
b.10	$pp \rightarrow \gamma\gamma j$	p p > a a j	$1.022 \pm 0.001 \cdot 10^1$	-9.3%	-0.8%		-4.8%	-0.9%
b.11*	$pp \rightarrow \gamma Zj$	p p > a z j	$8.310 \pm 0.017 \cdot 10^0$	+11.6%	+0.9%	$2.086 \pm 0.007 \cdot 10^1$	+4.9%	+0.9%
b.12*	$pp \rightarrow \gamma W^\pm j$	p p > a wpm j	$2.546 \pm 0.010 \cdot 10^1$	-10.0%	-0.7%		-4.8%	-0.7%
				+20.3%	+1.2%	$2.292 \pm 0.010 \cdot 10^1$	+17.2%	+1.0%
				-17.7%	-1.5%		-15.1%	-1.4%
				+14.5%	+1.0%	$1.220 \pm 0.005 \cdot 10^1$	+7.3%	+0.9%
				-12.8%	-1.0%		-7.4%	-0.9%
				+13.7%	+0.9%	$3.713 \pm 0.015 \cdot 10^1$	+7.2%	+0.9%
				-12.1%	-1.0%		-7.1%	-1.0%
b.13	$pp \rightarrow W^+W^+jj$	p p > w+ w+ j j	$1.484 \pm 0.006 \cdot 10^{-1}$	+25.4%	+2.1%	$2.251 \pm 0.011 \cdot 10^{-1}$	+10.5%	+2.2%
b.14	$pp \rightarrow W^-W^-jj$	p p > w- w- j j	$6.752 \pm 0.007 \cdot 10^{-2}$	-18.9%	-1.5%		-10.6%	-1.6%
b.15	$pp \rightarrow W^+W^-jj$ (4f)	p p > w+ w- j j	$1.144 \pm 0.002 \cdot 10^1$	+25.4%	+2.4%	$1.003 \pm 0.003 \cdot 10^{-1}$	+10.1%	+2.5%
b.16	$pp \rightarrow ZZjj$	p p > z z j j	$1.344 \pm 0.002 \cdot 10^0$	-18.9%	-1.7%		-10.4%	-1.8%
b.17	$pp \rightarrow ZW^\pm jj$	p p > z wpm j j	$8.038 \pm 0.009 \cdot 10^0$	+27.2%	+0.7%	$1.396 \pm 0.005 \cdot 10^1$	+5.0%	+0.7%
b.18	$pp \rightarrow \gamma\gamma jj$	p p > a a j j	$5.377 \pm 0.029 \cdot 10^0$	-19.9%	-0.5%		-6.8%	-0.6%
b.19*	$pp \rightarrow \gamma Zjj$	p p > a z j j	$3.260 \pm 0.009 \cdot 10^0$	+26.6%	+0.7%	$1.706 \pm 0.011 \cdot 10^0$	+5.8%	+0.8%
b.20*	$pp \rightarrow \gamma W^\pm jj$	p p > a wpm j j	$1.233 \pm 0.002 \cdot 10^1$	-19.6%	-0.6%		-7.2%	-0.6%
				+26.7%	+0.7%	$9.139 \pm 0.031 \cdot 10^0$	+3.1%	+0.7%
				-19.7%	-0.5%		-5.1%	-0.5%
				+26.2%	+0.6%	$7.501 \pm 0.032 \cdot 10^0$	+8.8%	+0.6%
				-19.8%	-1.0%		-10.1%	-1.0%
				+24.3%	+0.6%	$4.242 \pm 0.016 \cdot 10^0$	+6.5%	+0.6%
				-18.4%	-0.6%		-7.3%	-0.6%
				+24.7%	+0.6%	$1.448 \pm 0.005 \cdot 10^1$	+3.6%	+0.6%
				-18.6%	-0.6%		-5.4%	-0.7%

Table 2: Sample of LO and NLO rates for vector-boson pair production, possibly within cuts and in association with jets, at the 13-TeV LHC; we also report the integration errors, and the fractional scale (left) and PDF (right) uncertainties. See table 1 for the meaning of **wpm**. All cross sections are calculated in the five-flavour scheme, except for processes b.1, b.7, and b.15, which are obtained in the four-flavour scheme to avoid resonant-top contributions. NLO results for VV production have been known for some time [243–252], are publicly available in MCFM and in VBFNLO [241], and are matched to parton showers in MC@NLO [24] and POWHEG [253]. NLO results for VV with up to an extra jet have been made available in POWHEG [254,255]. NLO corrections to $\gamma\gamma$ plus up to three jets are also known [256–260]. Other available results are: $W^\pm W^\pm jj$ [261], $W^\pm W^\pm jj$ (EW+QCD) [262], $Z\gamma j$ [263], $W\gamma jj$ [264], $WZjj$ [265], $W\gamma j$ [266,267], WZj [268]. We do not show results for NLO corrections to EW-induced production of VV plus two jets, such as $W^\pm W^\mp jj$ [269], $WZjj$ [270], and $ZZjj$ [271], which can also be obtained with POWHEG and VBFNLO.

Process		Syntax	Cross section (pb)					
Three vector bosons +jet			LO 13 TeV			NLO 13 TeV		
c.1	$pp \rightarrow W^+W^-W^\pm$ (4f)	p p > w+ w- wpm	$1.307 \pm 0.003 \cdot 10^{-1}$	+0.0%	+2.0%	$2.109 \pm 0.006 \cdot 10^{-1}$	+5.1%	+1.6%
c.2	$pp \rightarrow ZW^+W^-$ (4f)	p p > z w+ w-	$9.658 \pm 0.065 \cdot 10^{-2}$	-0.3%	-1.5%	$1.679 \pm 0.005 \cdot 10^{-1}$	-4.1%	-1.2%
c.3	$pp \rightarrow ZZW^\pm$	p p > z z wpm	$2.996 \pm 0.016 \cdot 10^{-2}$	+0.8%	+2.1%		+6.3%	+1.6%
c.4	$pp \rightarrow ZZZ$	p p > z z z	$1.085 \pm 0.002 \cdot 10^{-2}$	-1.1%	-1.6%		-5.1%	-1.2%
c.5	$pp \rightarrow \gamma W^+W^-$ (4f)	p p > a w+ w-	$1.427 \pm 0.011 \cdot 10^{-1}$	+1.0%	+2.0%	$2.581 \pm 0.008 \cdot 10^{-1}$	+6.8%	+1.5%
c.6	$pp \rightarrow \gamma\gamma W^\pm$	p p > a a wpm	$2.681 \pm 0.007 \cdot 10^{-2}$	-1.4%	-1.6%		-5.5%	-1.1%
c.7	$pp \rightarrow \gamma ZW^\pm$	p p > a z wpm	$4.994 \pm 0.011 \cdot 10^{-2}$	+0.0%	+1.9%	$1.417 \pm 0.005 \cdot 10^{-2}$	+2.7%	+1.9%
c.8	$pp \rightarrow \gamma ZZ$	p p > a z z	$2.320 \pm 0.005 \cdot 10^{-2}$	-0.5%	-1.5%		-2.1%	-1.5%
c.9	$pp \rightarrow \gamma\gamma Z$	p p > a a z	$3.078 \pm 0.007 \cdot 10^{-2}$	+1.9%	+2.0%	$2.581 \pm 0.008 \cdot 10^{-1}$	+5.4%	+1.4%
c.10	$pp \rightarrow \gamma\gamma\gamma$	p p > a a a	$1.269 \pm 0.003 \cdot 10^{-2}$	-2.6%	-1.5%		-4.3%	-1.1%
				+4.4%	+1.9%	$8.251 \pm 0.032 \cdot 10^{-2}$	+7.6%	+1.0%
				-5.6%	-1.6%		-7.0%	-1.0%
				+0.8%	+1.9%	$1.117 \pm 0.004 \cdot 10^{-1}$	+7.2%	+1.2%
				-1.4%	-1.6%		-5.9%	-0.9%
				+2.0%	+1.9%	$3.118 \pm 0.012 \cdot 10^{-2}$	+2.8%	+1.8%
				-2.9%	-1.5%		-2.7%	-1.4%
				+5.6%	+1.9%	$4.634 \pm 0.020 \cdot 10^{-2}$	+4.5%	+1.7%
				-6.8%	-1.6%		-5.0%	-1.3%
				+9.8%	+2.0%	$3.441 \pm 0.012 \cdot 10^{-2}$	+11.8%	+1.4%
				-11.0%	-1.8%		-11.6%	-1.5%
c.11	$pp \rightarrow W^+W^-W^\pm j$ (4f)	p p > w+ w- wpm j	$9.167 \pm 0.010 \cdot 10^{-2}$	+15.0%	+1.0%	$1.197 \pm 0.004 \cdot 10^{-1}$	+5.2%	+1.0%
c.12*	$pp \rightarrow ZW^+W^- j$ (4f)	p p > z w+ w- j	$8.340 \pm 0.010 \cdot 10^{-2}$	-12.2%	-0.7%	$1.066 \pm 0.003 \cdot 10^{-1}$	-5.6%	-0.8%
c.13*	$pp \rightarrow ZZW^\pm j$	p p > z z wpm j	$2.810 \pm 0.004 \cdot 10^{-2}$	+15.6%	+1.0%		+4.5%	+1.0%
c.14*	$pp \rightarrow ZZZ j$	p p > z z z j	$4.823 \pm 0.011 \cdot 10^{-3}$	-12.6%	-0.7%		-5.3%	-0.7%
c.15*	$pp \rightarrow \gamma W^+W^- j$ (4f)	p p > a w+ w- j	$1.182 \pm 0.004 \cdot 10^{-1}$	+16.1%	+1.0%	$3.660 \pm 0.013 \cdot 10^{-2}$	+4.8%	+1.0%
c.16	$pp \rightarrow \gamma\gamma W^\pm j$	p p > a a wpm j	$4.107 \pm 0.015 \cdot 10^{-2}$	-13.0%	-0.7%		-5.6%	-0.7%
c.17*	$pp \rightarrow \gamma ZW^\pm j$	p p > a z wpm j	$5.833 \pm 0.023 \cdot 10^{-2}$	+14.3%	+1.4%	$6.341 \pm 0.025 \cdot 10^{-3}$	+4.9%	+1.4%
c.18*	$pp \rightarrow \gamma ZZ j$	p p > a z z j	$9.995 \pm 0.013 \cdot 10^{-3}$	-11.8%	-1.0%		-5.4%	-1.0%
c.19*	$pp \rightarrow \gamma\gamma Z j$	p p > a a z j	$1.372 \pm 0.003 \cdot 10^{-2}$	+13.4%	+0.8%	$1.233 \pm 0.004 \cdot 10^3$	+18.9%	+1.0%
c.20*	$pp \rightarrow \gamma\gamma\gamma j$	p p > a a a j	$1.031 \pm 0.006 \cdot 10^{-2}$	-11.2%	-0.7%		-19.9%	-1.5%
				+11.8%	+0.6%	$5.807 \pm 0.023 \cdot 10^{-2}$	+5.8%	+0.7%
				-10.2%	-0.8%		-5.5%	-0.7%
				+14.4%	+0.7%	$7.764 \pm 0.025 \cdot 10^{-2}$	+5.1%	+0.8%
				-12.0%	-0.6%		-5.5%	-0.6%
				+12.5%	+1.2%	$1.371 \pm 0.005 \cdot 10^{-2}$	+5.6%	+1.2%
				-10.6%	-0.9%		-5.5%	-0.9%
				+10.9%	+1.0%	$2.051 \pm 0.011 \cdot 10^{-2}$	+7.0%	+1.0%
				-9.4%	-0.9%		-6.3%	-0.9%
				+14.3%	+0.9%	$2.020 \pm 0.008 \cdot 10^{-2}$	+12.8%	+0.8%
				-12.6%	-1.2%		-11.0%	-1.2%

Table 3: Sample of LO and NLO rates for triple-vector-boson production, possibly within cuts and in association with one jet, at the 13-TeV LHC; we also report the integration errors, and the fractional scale (left) and PDF (right) uncertainties. See table 1 for the meaning of **wpm**. All cross sections are calculated in the five-flavour scheme, except for processes with at least two W bosons, where the four-flavour scheme is adopted to avoid resonant-top contributions. Triple-vector-boson cross sections at the NLO have been computed recently: $Z\gamma\gamma$ [263,272], $\gamma\gamma W^\pm$ [273], γZW^\pm [274], $WW\gamma$ and $ZZ\gamma$ [275], ZZW and WWW [276], $\gamma\gamma\gamma$ [277,278], ZZZ [279]. The complete set of triple-vector-boson cross sections at the NLO is also available in VBFNLO [241]. Except for $\gamma\gamma W^\pm j$ and $W^+W^-W^\pm j$ that have appeared in ref. [280] and ref. [281] respectively, $VVVj$ cross sections at the NLO have been computed here for the first time.

Process	Syntax	Cross section (pb)							
		LO 13 TeV				NLO 13 TeV			
Four vector bosons									
c.21*	$pp \rightarrow W^+ W^- W^+ W^-$ (4f)	p p > w+ w- w+ w-	$5.721 \pm 0.014 \cdot 10^{-4}$	+3.7% +2.3% -3.5% -1.7%	$9.959 \pm 0.035 \cdot 10^{-4}$	+7.4% +1.7% -6.0% -1.2%			
c.22*	$pp \rightarrow W^+ W^- W^\pm Z$ (4f)	p p > w+ w- wpm z	$6.391 \pm 0.076 \cdot 10^{-4}$	+4.4% +2.4% -4.1% -1.8%	$1.188 \pm 0.004 \cdot 10^{-3}$	+8.4% +1.7% -6.8% -1.2%			
c.23*	$pp \rightarrow W^+ W^- W^\pm \gamma$ (4f)	p p > w+ w- wpm a	$8.115 \pm 0.064 \cdot 10^{-4}$	+2.5% +2.2% -2.5% -1.7%	$1.546 \pm 0.005 \cdot 10^{-3}$	+7.9% +1.5% -6.3% -1.1%			
c.24*	$pp \rightarrow W^+ W^- Z Z$ (4f)	p p > w+ w- z z	$4.320 \pm 0.013 \cdot 10^{-4}$	+4.4% +2.4% -4.1% -1.7%	$7.107 \pm 0.020 \cdot 10^{-4}$	+7.0% +1.8% -5.7% -1.3%			
c.25*	$pp \rightarrow W^+ W^- Z \gamma$ (4f)	p p > w+ w- z a	$8.403 \pm 0.016 \cdot 10^{-4}$	+3.0% +2.3% -2.9% -1.7%	$1.483 \pm 0.004 \cdot 10^{-3}$	+7.2% +1.6% -5.8% -1.2%			
c.26*	$pp \rightarrow W^+ W^- \gamma \gamma$ (4f)	p p > w+ w- a a	$5.198 \pm 0.012 \cdot 10^{-4}$	+0.6% +2.1% -0.9% -1.6%	$9.381 \pm 0.032 \cdot 10^{-4}$	+6.7% +1.4% -5.3% -1.1%			
c.27*	$pp \rightarrow W^\pm Z Z Z$	p p > wpm z z z	$5.862 \pm 0.010 \cdot 10^{-5}$	+5.1% +2.4% -4.7% -1.8%	$1.240 \pm 0.004 \cdot 10^{-4}$	+9.9% +1.7% -8.0% -1.2%			
c.28*	$pp \rightarrow W^\pm Z Z \gamma$	p p > wpm z z a	$1.148 \pm 0.003 \cdot 10^{-4}$	+3.6% +2.2% -3.5% -1.7%	$2.945 \pm 0.008 \cdot 10^{-4}$	+10.8% +1.3% -8.7% -1.0%			
c.29*	$pp \rightarrow W^\pm Z \gamma \gamma$	p p > wpm z a a	$1.054 \pm 0.004 \cdot 10^{-4}$	+1.7% +2.1% -1.9% -1.7%	$3.033 \pm 0.010 \cdot 10^{-4}$	+10.6% +1.1% -8.6% -0.8%			
c.30*	$pp \rightarrow W^\pm \gamma \gamma \gamma$	p p > wpm a a a	$3.600 \pm 0.013 \cdot 10^{-5}$	+0.4% +2.0% -1.0% -1.6%	$1.246 \pm 0.005 \cdot 10^{-4}$	+9.8% +0.9% -8.1% -0.8%			
c.31*	$pp \rightarrow Z Z Z Z$	p p > z z z z	$1.989 \pm 0.002 \cdot 10^{-5}$	+3.8% +2.2% -3.6% -1.7%	$2.629 \pm 0.008 \cdot 10^{-5}$	+3.5% +2.2% -3.0% -1.7%			
c.32*	$pp \rightarrow Z Z Z \gamma$	p p > z z z a	$3.945 \pm 0.007 \cdot 10^{-5}$	+1.9% +2.1% -2.1% -1.6%	$5.224 \pm 0.016 \cdot 10^{-5}$	+3.3% +2.1% -2.7% -1.6%			
c.33*	$pp \rightarrow Z Z \gamma \gamma$	p p > z z a a	$5.513 \pm 0.017 \cdot 10^{-5}$	+0.0% +2.1% -0.3% -1.6%	$7.518 \pm 0.032 \cdot 10^{-5}$	+3.4% +2.0% -2.6% -1.5%			
c.34*	$pp \rightarrow Z \gamma \gamma \gamma$	p p > z a a a	$4.790 \pm 0.012 \cdot 10^{-5}$	+2.3% +2.0% -3.1% -1.6%	$7.103 \pm 0.026 \cdot 10^{-5}$	+3.4% +1.6% -3.2% -1.5%			
c.35*	$pp \rightarrow \gamma \gamma \gamma \gamma$	p p > a a a a	$1.594 \pm 0.004 \cdot 10^{-5}$	+4.7% +1.9% -5.7% -1.7%	$3.389 \pm 0.012 \cdot 10^{-5}$	+7.0% +1.3% -6.7% -1.3%			

Table 4: Sample of LO and NLO rates for quadruple-vector-boson production, possibly within cuts, at the 13-TeV LHC; we also report the integration errors, and the fractional scale (left) and PDF (right) uncertainties. See table 1 for the meaning of **wpm**. All cross sections are calculated in the five-flavour scheme, except the processes with at least two W bosons, where the four-flavour scheme is adopted to avoid resonant-top contributions. For all processes in this table NLO QCD corrections have never been computed before.

Process		Syntax	Cross section (pb)					
Heavy quarks and jets			LO 13 TeV			NLO 13 TeV		
d.1	$pp \rightarrow jj$	p p > j j	$1.162 \pm 0.001 \cdot 10^6$	+24.9%	+0.8%	$1.580 \pm 0.007 \cdot 10^6$	+8.4%	+0.7%
d.2	$pp \rightarrow jjj$	p p > j j j	$8.940 \pm 0.021 \cdot 10^4$	-18.8%	-0.9%	$7.791 \pm 0.037 \cdot 10^4$	-9.0%	-0.9%
				+43.8%	+1.2%		+2.1%	+1.1%
				-28.4%	-1.4%		-23.2%	-1.3%
d.3	$pp \rightarrow b\bar{b}$ (4f)	p p > b b~	$3.743 \pm 0.004 \cdot 10^3$	+25.2%	+1.5%	$6.438 \pm 0.028 \cdot 10^3$	+15.9%	+1.5%
d.4*	$pp \rightarrow b\bar{b}j$ (4f)	p p > b b~ j	$1.050 \pm 0.002 \cdot 10^3$	-18.9%	-1.8%	$1.327 \pm 0.007 \cdot 10^3$	-13.3%	-1.7%
				+44.1%	+1.6%		+6.8%	+1.5%
d.5*	$pp \rightarrow b\bar{b}jj$ (4f)	p p > b b~ j j	$1.852 \pm 0.006 \cdot 10^2$	-28.5%	-1.8%	$2.471 \pm 0.012 \cdot 10^2$	-11.6%	-1.8%
				+61.8%	+2.1%		+8.2%	+2.0%
d.6	$pp \rightarrow b\bar{b}b\bar{b}$ (4f)	p p > b b~ b b~	$5.050 \pm 0.007 \cdot 10^{-1}$	-35.6%	-2.4%	$8.736 \pm 0.034 \cdot 10^{-1}$	-16.4%	-2.3%
				+61.7%	+2.9%		+20.9%	+2.9%
				-35.6%	-3.4%		-22.0%	-3.4%
d.7	$pp \rightarrow t\bar{t}$	p p > t t~	$4.584 \pm 0.003 \cdot 10^2$	+29.0%	+1.8%	$6.741 \pm 0.023 \cdot 10^2$	+9.8%	+1.8%
				-21.1%	-2.0%		-10.9%	-2.1%
d.8	$pp \rightarrow t\bar{t}j$	p p > t t~ j	$3.135 \pm 0.002 \cdot 10^2$	+45.1%	+2.2%	$4.106 \pm 0.015 \cdot 10^2$	+8.1%	+2.1%
				-29.0%	-2.5%		-12.2%	-2.5%
d.9	$pp \rightarrow t\bar{t}jj$	p p > t t~ j j	$1.361 \pm 0.001 \cdot 10^2$	+61.4%	+2.6%	$1.795 \pm 0.006 \cdot 10^2$	+9.3%	+2.4%
				-35.6%	-3.0%		-16.1%	-2.9%
d.10	$pp \rightarrow t\bar{t}t\bar{t}$	p p > t t~ t t~	$4.505 \pm 0.005 \cdot 10^{-3}$	+63.8%	+5.4%	$9.201 \pm 0.028 \cdot 10^{-3}$	+30.8%	+5.5%
				-36.5%	-5.7%		-25.6%	-5.9%
d.11	$pp \rightarrow t\bar{t}b\bar{b}$ (4f)	p p > t t~ b b~	$6.119 \pm 0.004 \cdot 10^0$	+62.1%	+2.9%	$1.452 \pm 0.005 \cdot 10^1$	+37.6%	+2.9%
				-35.7%	-3.5%		-27.5%	-3.5%

Table 5: Sample of LO and NLO total rates for the production of heavy quarks and/or jets, possibly within cuts, at the 13-TeV LHC; we also report the integration errors, and the fractional scale (left) and PDF (right) uncertainties. Processes d.1 and d.2, as well as processes involving at least a top pair, are computed in the five-flavour scheme. Processes that explicitly involve b -quarks in the final state are calculated in the four-flavour scheme. For processes d.3–d.6 we require 2 (or 4) b -jets in the final state with $|\eta| < 2.5$. For processes d.1–d.6, we require the (b) -jets to have $p_T > 80$ GeV, with at least one of them with $p_T > 100$ GeV. Calculations of cross sections at the NLO for this class of processes are available in the literature as well as in public codes: from the seminal results for the hadroproduction of a heavy quark pair [282–286], to their NLO+PS implementation in MC@NLO [169] and POWHEG [287], to $t\bar{t}j$ [288] (also including top decays [254,289] and parton shower effects [290]), to the computation of $t\bar{t}jj$ [291]. Merged NLO+PS results for $t\bar{t}$ plus jets are also available [188,292,293]. NLO results for three jets [294], four jets [73], and up to five jets [295,296] have been published. Two- and three-jet event generation is available in POWHEG [297,298]. Calculations for $b\bar{b}b\bar{b}$ [299,300], $t\bar{t}b\bar{b}$ [301–303], and $t\bar{t}t\bar{t}$ [304] production have appeared in the literature.

Process		Syntax	Cross section (pb)					
Heavy quarks+vector bosons			LO 13 TeV			NLO 13 TeV		
e.1	$pp \rightarrow W^\pm b\bar{b}$ (4f)	p p > wpm b b~	$3.074 \pm 0.002 \cdot 10^2$	+42.3% -29.2%	+2.0% -1.6%	$8.162 \pm 0.034 \cdot 10^2$	+29.8% -23.6%	+1.5% -1.2%
e.2	$pp \rightarrow Z b\bar{b}$ (4f)	p p > z b b~	$6.993 \pm 0.003 \cdot 10^2$	+33.5% -24.4%	+1.0% -1.4%	$1.235 \pm 0.004 \cdot 10^3$	+19.9% -17.4%	+1.0% -1.4%
e.3	$pp \rightarrow \gamma b\bar{b}$ (4f)	p p > a b b~	$1.731 \pm 0.001 \cdot 10^3$	+51.9% -34.8%	+1.6% -2.1%	$4.171 \pm 0.015 \cdot 10^3$	+33.7% -27.1%	+1.4% -1.9%
e.4*	$pp \rightarrow W^\pm b\bar{b}j$ (4f)	p p > wpm b b~ j	$1.861 \pm 0.003 \cdot 10^2$	+42.5% -27.7%	+0.7% -0.7%	$3.957 \pm 0.013 \cdot 10^2$	+27.0% -21.0%	+0.7% -0.6%
e.5*	$pp \rightarrow Z b\bar{b}j$ (4f)	p p > z b b~ j	$1.604 \pm 0.001 \cdot 10^2$	+42.4% -27.6%	+0.9% -1.1%	$2.805 \pm 0.009 \cdot 10^2$	+21.0% -17.6%	+0.8% -1.0%
e.6*	$pp \rightarrow \gamma b\bar{b}j$ (4f)	p p > a b b~ j	$7.812 \pm 0.017 \cdot 10^2$	+51.2% -32.0%	+1.0% -1.5%	$1.233 \pm 0.004 \cdot 10^3$	+18.9% -19.9%	+1.0% -1.5%
e.7	$pp \rightarrow t\bar{t}W^\pm$	p p > t t~ wpm	$3.777 \pm 0.003 \cdot 10^{-1}$	+23.9% -18.0%	+2.1% -1.6%	$5.662 \pm 0.021 \cdot 10^{-1}$	+11.2% -10.6%	+1.7% -1.3%
e.8	$pp \rightarrow t\bar{t}Z$	p p > t t~ z	$5.273 \pm 0.004 \cdot 10^{-1}$	+30.5% -21.8%	+1.8% -2.1%	$7.598 \pm 0.026 \cdot 10^{-1}$	+9.7% -11.1%	+1.9% -2.2%
e.9	$pp \rightarrow t\bar{t}\gamma$	p p > t t~ a	$1.204 \pm 0.001 \cdot 10^0$	+29.6% -21.3%	+1.6% -1.8%	$1.744 \pm 0.005 \cdot 10^0$	+9.8% -11.0%	+1.7% -2.0%
e.10*	$pp \rightarrow t\bar{t}W^\pm j$	p p > t t~ wpm j	$2.352 \pm 0.002 \cdot 10^{-1}$	+40.9% -27.1%	+1.3% -1.0%	$3.404 \pm 0.011 \cdot 10^{-1}$	+11.2% -14.0%	+1.2% -0.9%
e.11*	$pp \rightarrow t\bar{t}Zj$	p p > t t~ z j	$3.953 \pm 0.004 \cdot 10^{-1}$	+46.2% -29.5%	+2.7% -3.0%	$5.074 \pm 0.016 \cdot 10^{-1}$	+7.0% -12.3%	+2.5% -2.9%
e.12*	$pp \rightarrow t\bar{t}\gamma j$	p p > t t~ a j	$8.726 \pm 0.010 \cdot 10^{-1}$	+45.4% -29.1%	+2.3% -2.6%	$1.135 \pm 0.004 \cdot 10^0$	+7.5% -12.2%	+2.2% -2.5%
e.13*	$pp \rightarrow t\bar{t}W^-W^+$ (4f)	p p > t t~ w+ w-	$6.675 \pm 0.006 \cdot 10^{-3}$	+30.9% -21.9%	+2.1% -2.0%	$9.904 \pm 0.026 \cdot 10^{-3}$	+10.9% -11.8%	+2.1% -2.1%
e.14*	$pp \rightarrow t\bar{t}W^\pm Z$	p p > t t~ wpm z	$2.404 \pm 0.002 \cdot 10^{-3}$	+26.6% -19.6%	+2.5% -1.8%	$3.525 \pm 0.010 \cdot 10^{-3}$	+10.6% -10.8%	+2.3% -1.6%
e.15*	$pp \rightarrow t\bar{t}W^\pm\gamma$	p p > t t~ wpm a	$2.718 \pm 0.003 \cdot 10^{-3}$	+25.4% -18.9%	+2.3% -1.8%	$3.927 \pm 0.013 \cdot 10^{-3}$	+10.3% -10.4%	+2.0% -1.5%
e.16*	$pp \rightarrow t\bar{t}ZZ$	p p > t t~ z z	$1.349 \pm 0.014 \cdot 10^{-3}$	+29.3% -21.1%	+1.7% -1.5%	$1.840 \pm 0.007 \cdot 10^{-3}$	+7.9% -9.9%	+1.7% -1.5%
e.17*	$pp \rightarrow t\bar{t}Z\gamma$	p p > t t~ z a	$2.548 \pm 0.003 \cdot 10^{-3}$	+30.1% -21.5%	+1.7% -1.6%	$3.656 \pm 0.012 \cdot 10^{-3}$	+9.7% -11.0%	+1.8% -1.9%
e.18*	$pp \rightarrow t\bar{t}\gamma\gamma$	p p > t t~ a a	$3.272 \pm 0.006 \cdot 10^{-3}$	+28.4% -20.6%	+1.3% -1.1%	$4.402 \pm 0.015 \cdot 10^{-3}$	+7.8% -9.7%	+1.4% -1.4%

Table 6: Sample of LO and NLO total rates for the production of heavy quarks in association with vector bosons, possibly within cuts and in association with jets, at the 13-TeV LHC; we also report the integration errors, and the fractional scale (left) and PDF (right) uncertainties. Processes that explicitly involve b -quarks in the final state, and process e.13, are calculated in the four-flavour scheme, while all of the others are in the five-flavour scheme. Results are available in the literature for $Wb\bar{b}$ [66, 305–308], $Zb\bar{b}$ [66, 307, 309], $t\bar{t}\gamma$ [310], $t\bar{t}Z$ [66, 311, 312], $t\bar{t}W$ [66, 312, 313] production. For the majority of the processes in this table, NLO corrections are calculated in this work for the first time.

Process		Syntax	Cross section (pb)					
Single-top			LO 13 TeV			NLO 13 TeV		
f.1	$pp \rightarrow tj$ (t-channel)	p p > tt j \$\$ w+ w-	$1.520 \pm 0.001 \cdot 10^2$	+9.4%	+0.4%	$1.563 \pm 0.005 \cdot 10^2$	+1.4%	+0.4%
f.2	$pp \rightarrow t\gamma j$ (t-channel)	p p > tt a j \$\$ w+ w-	$9.956 \pm 0.014 \cdot 10^{-1}$	+6.4%	+0.9%	$1.017 \pm 0.003 \cdot 10^0$	+1.3%	+0.8%
f.3	$pp \rightarrow tZj$ (t-channel)	p p > tt z j \$\$ w+ w-	$6.967 \pm 0.007 \cdot 10^{-1}$	+3.5%	+0.9%	$6.993 \pm 0.021 \cdot 10^{-1}$	+1.6%	+0.9%
f.4	$pp \rightarrow tbj$ (t-channel, 4f)	p p > tt bb j \$\$ w+ w-	$1.003 \pm 0.000 \cdot 10^2$	+13.8%	+0.4%	$1.319 \pm 0.003 \cdot 10^2$	+5.8%	+0.4%
f.5*	$pp \rightarrow tbj\gamma$ (t-channel, 4f)	p p > tt bb j a \$\$ w+ w-	$6.293 \pm 0.006 \cdot 10^{-1}$	+16.8%	+0.8%	$8.612 \pm 0.025 \cdot 10^{-1}$	+6.2%	+0.8%
f.6*	$pp \rightarrow tbjZ$ (t-channel, 4f)	p p > tt bb j z \$\$ w+ w-	$3.934 \pm 0.002 \cdot 10^{-1}$	+18.7%	+1.0%	$5.657 \pm 0.014 \cdot 10^{-1}$	+7.7%	+0.9%
f.7	$pp \rightarrow tb$ (s-channel, 4f)	p p > w+ > t b~, p p > w- > t~ b	$7.489 \pm 0.007 \cdot 10^0$	+3.5%	+1.9%	$1.001 \pm 0.004 \cdot 10^1$	+3.7%	+1.9%
f.8*	$pp \rightarrow tb\gamma$ (s-channel, 4f)	p p > w+ > t b~ a, p p > w- > t~ b a	$1.490 \pm 0.001 \cdot 10^{-2}$	+1.2%	+1.9%	$1.952 \pm 0.007 \cdot 10^{-2}$	+2.6%	+1.7%
f.9*	$pp \rightarrow tbZ$ (s-channel, 4f)	p p > w+ > t b~ z, p p > w- > t~ b z	$1.072 \pm 0.001 \cdot 10^{-2}$	+1.3%	+2.0%	$1.539 \pm 0.005 \cdot 10^{-2}$	+3.9%	+1.9%

Table 7: Sample of LO and NLO total rates for the production of a single top, possibly in association and within cuts, at the 13-TeV LHC; we also report the integration errors, and the fractional scale (left) and PDF (right) uncertainties. The notation understands the sum of the t and \bar{t} cross sections for all processes, and \mathbf{tt} is a label that includes both t and \bar{t} , defined from the shell with `define tt = t t~` (and analogously for the label \mathbf{bb}). Processes that explicitly involve b -quarks in the final state are calculated in the four-flavour scheme, while all of the others are in the five-flavour scheme. Being an EW-induced process, single-top production requires special care for the MADGRAPH5_AMC@NLO generation syntax: `$$` means excluding particles in the s -channel, while the `> w+ >` (`> w- >`) forces a W^+ (W^-) to be present in the s -channel (see appendix B.1). Total NLO cross sections for t - and s -channel single-top production have been known for some time [314, 315]. All single-top channels are also available in MCFM [316–319], MC@NLO [170, 320], and POWHEG [321, 322]. An NLO calculation for tZj production has appeared in ref. [323].

Process		Syntax	Cross section (pb)					
Single Higgs production			LO 13 TeV			NLO 13 TeV		
g.1	$pp \rightarrow H$ (HEFT)	p p > h	$1.593 \pm 0.003 \cdot 10^1$	+34.8%	+1.2%	$3.261 \pm 0.010 \cdot 10^1$	+20.2%	+1.1%
g.2	$pp \rightarrow H j$ (HEFT)	p p > h j	$8.367 \pm 0.003 \cdot 10^0$	-26.0%	-1.7%	$1.422 \pm 0.006 \cdot 10^1$	-17.9%	-1.6%
g.3	$pp \rightarrow H j j$ (HEFT)	p p > h j j	$3.020 \pm 0.002 \cdot 10^0$	+39.4%	+1.2%		+18.5%	+1.1%
				-26.4%	-1.4%		-16.6%	-1.4%
				+59.1%	+1.4%	$5.124 \pm 0.020 \cdot 10^0$	+20.7%	+1.3%
				-34.7%	-1.7%		-21.0%	-1.5%
g.4	$pp \rightarrow H j j$ (VBF)	p p > h j j \$\$\$ w+ w- z	$1.987 \pm 0.002 \cdot 10^0$	+1.7%	+1.9%	$1.900 \pm 0.006 \cdot 10^0$	+0.8%	+2.0%
g.5	$pp \rightarrow H j j j$ (VBF)	p p > h j j j \$\$\$ w+ w- z	$2.824 \pm 0.005 \cdot 10^{-1}$	-2.0%	-1.4%		-0.9%	-1.5%
				+15.7%	+1.5%	$3.085 \pm 0.010 \cdot 10^{-1}$	+2.0%	+1.5%
				-12.7%	-1.0%		-3.0%	-1.1%
g.6	$pp \rightarrow HW^\pm$	p p > h wpm	$1.195 \pm 0.002 \cdot 10^0$	+3.5%	+1.9%	$1.419 \pm 0.005 \cdot 10^0$	+2.1%	+1.9%
g.7	$pp \rightarrow HW^\pm j$	p p > h wpm j	$4.018 \pm 0.003 \cdot 10^{-1}$	-4.5%	-1.5%		-2.6%	-1.4%
g.8*	$pp \rightarrow HW^\pm j j$	p p > h wpm j j	$1.198 \pm 0.016 \cdot 10^{-1}$	+10.7%	+1.2%	$4.842 \pm 0.017 \cdot 10^{-1}$	+3.6%	+1.2%
				-9.3%	-0.9%		-3.7%	-1.0%
				+26.1%	+0.8%	$1.574 \pm 0.014 \cdot 10^{-1}$	+5.0%	+0.9%
				-19.4%	-0.6%		-6.5%	-0.6%
g.9	$pp \rightarrow H Z$	p p > h z	$6.468 \pm 0.008 \cdot 10^{-1}$	+3.5%	+1.9%	$7.674 \pm 0.027 \cdot 10^{-1}$	+2.0%	+1.9%
g.10	$pp \rightarrow H Z j$	p p > h z j	$2.225 \pm 0.001 \cdot 10^{-1}$	-4.5%	-1.4%		-2.5%	-1.4%
g.11*	$pp \rightarrow H Z j j$	p p > h z j j	$7.262 \pm 0.012 \cdot 10^{-2}$	+10.6%	+1.1%	$2.667 \pm 0.010 \cdot 10^{-1}$	+3.5%	+1.1%
				-9.2%	-0.8%		-3.6%	-0.9%
				+26.2%	+0.7%	$8.753 \pm 0.037 \cdot 10^{-2}$	+4.8%	+0.7%
				-19.4%	-0.6%		-6.3%	-0.6%
g.12*	$pp \rightarrow HW^+ W^-$ (4f)	p p > h w+ w-	$8.325 \pm 0.139 \cdot 10^{-3}$	+0.0%	+2.0%	$1.065 \pm 0.003 \cdot 10^{-2}$	+2.5%	+2.0%
g.13*	$pp \rightarrow HW^\pm \gamma$	p p > h wpm a	$2.518 \pm 0.006 \cdot 10^{-3}$	-0.3%	-1.6%		-1.9%	-1.5%
g.14*	$pp \rightarrow H Z W^\pm$	p p > h z wpm	$3.763 \pm 0.007 \cdot 10^{-3}$	+0.7%	+1.9%	$3.309 \pm 0.011 \cdot 10^{-3}$	+2.7%	+1.7%
g.15*	$pp \rightarrow H Z Z$	p p > h z z	$2.093 \pm 0.003 \cdot 10^{-3}$	-1.4%	-1.5%		-2.0%	-1.4%
				+1.1%	+2.0%	$5.292 \pm 0.015 \cdot 10^{-3}$	+3.9%	+1.8%
				-1.5%	-1.6%		-3.1%	-1.4%
				+0.1%	+1.9%	$2.538 \pm 0.007 \cdot 10^{-3}$	+1.9%	+2.0%
				-0.6%	-1.5%		-1.4%	-1.5%
g.16	$pp \rightarrow H t \bar{t}$	p p > h t t~	$3.579 \pm 0.003 \cdot 10^{-1}$	+30.0%	+1.7%	$4.608 \pm 0.016 \cdot 10^{-1}$	+5.7%	+2.0%
g.17	$pp \rightarrow H t j$	p p > h t t j	$4.994 \pm 0.005 \cdot 10^{-2}$	-21.5%	-2.0%		-9.0%	-2.3%
g.18	$pp \rightarrow H b \bar{b}$ (4f)	p p > h b b~	$4.983 \pm 0.002 \cdot 10^{-1}$	+2.4%	+1.2%	$6.328 \pm 0.022 \cdot 10^{-2}$	+2.9%	+1.5%
				-4.2%	-1.3%		-1.8%	-1.6%
				+28.1%	+1.5%	$6.085 \pm 0.026 \cdot 10^{-1}$	+7.3%	+1.6%
				-21.0%	-1.8%		-9.6%	-2.0%
g.19	$pp \rightarrow H t \bar{t} j$	p p > h t t~ j	$2.674 \pm 0.041 \cdot 10^{-1}$	+45.6%	+2.6%	$3.244 \pm 0.025 \cdot 10^{-1}$	+3.5%	+2.5%
g.20*	$pp \rightarrow H b \bar{b} j$ (4f)	p p > h b b~ j	$7.367 \pm 0.002 \cdot 10^{-2}$	-29.2%	-2.9%		-8.7%	-2.9%
				+45.6%	+1.8%	$9.034 \pm 0.032 \cdot 10^{-2}$	+7.9%	+1.8%
				-29.1%	-2.1%		-11.0%	-2.2%

Table 8: Sample of LO and NLO total rates for the production of a single SM Higgs, possibly in association and within cuts, at the 13-TeV LHC; we also report the integration errors, and the fractional scale (left) and PDF (right) uncertainties. See table 1 for the meaning of wpm , and table 7 for the meaning of tt , bb , and the generation syntax. Processes that explicitly involve b -quarks in the final state are calculated in the four-flavour scheme, while all of the others are in the five-flavour scheme, except for g.12. A complete set of references relevant to NLO rates for Higgs production can be found in refs. [324–326]. The W -boson width is set equal to 2.0476 GeV for process g.17. Cross sections at the NLO for $HVjj$ and HVV production appear in this work for the first time.

Process		Syntax	Cross section (pb)					
Higgs pair production			LO 13 TeV			NLO 13 TeV		
h.1	$pp \rightarrow HH$ (Loop improved)	p p > h h	$1.772 \pm 0.006 \cdot 10^{-2}$	+29.5%	+2.1%	$2.763 \pm 0.008 \cdot 10^{-2}$	+11.4%	+2.1%
h.2	$pp \rightarrow HHjj$ (VBF)	p p > h h j j \$\$ w+ w- z	$6.503 \pm 0.019 \cdot 10^{-4}$	-21.4%	-2.6%	$6.820 \pm 0.026 \cdot 10^{-4}$	-11.8%	-2.6%
h.3	$pp \rightarrow HHW^\pm$	p p > h h wpm	$4.303 \pm 0.005 \cdot 10^{-4}$	+7.2%	+2.3%	$5.002 \pm 0.014 \cdot 10^{-4}$	+0.8%	+2.4%
h.4*	$pp \rightarrow HHW^\pm j$	p p > h h wpm j	$1.922 \pm 0.002 \cdot 10^{-4}$	-6.4%	-1.6%	$2.218 \pm 0.009 \cdot 10^{-4}$	-1.0%	-1.7%
h.5*	$pp \rightarrow HHW^\pm \gamma$	p p > h h wpm a	$1.952 \pm 0.004 \cdot 10^{-6}$	+0.9%	+2.0%	$2.347 \pm 0.007 \cdot 10^{-6}$	+1.5%	+2.0%
h.6	$pp \rightarrow HHZ$	p p > h h z	$2.701 \pm 0.007 \cdot 10^{-4}$	-1.3%	-1.5%	$3.130 \pm 0.008 \cdot 10^{-4}$	-1.2%	-1.6%
h.7*	$pp \rightarrow HHZj$	p p > h h z j	$1.211 \pm 0.001 \cdot 10^{-4}$	+14.2%	+1.5%	$1.394 \pm 0.006 \cdot 10^{-4}$	+2.7%	+1.6%
h.8*	$pp \rightarrow HHZ\gamma$	p p > h h z a	$1.397 \pm 0.003 \cdot 10^{-6}$	-11.7%	-1.1%	$1.604 \pm 0.005 \cdot 10^{-6}$	-3.3%	-1.1%
h.9*	$pp \rightarrow HHZZ$	p p > h h z z	$2.309 \pm 0.005 \cdot 10^{-6}$	+2.4%	+2.2%	$2.754 \pm 0.009 \cdot 10^{-6}$	+2.4%	+2.1%
h.10*	$pp \rightarrow HHZW^\pm$	p p > h h z wpm	$3.708 \pm 0.013 \cdot 10^{-6}$	-2.5%	-1.7%	$4.904 \pm 0.029 \cdot 10^{-6}$	-2.0%	-1.6%
h.11*	$pp \rightarrow HHW^+W^-$ (4f)	p p > h h w+ w-	$7.524 \pm 0.070 \cdot 10^{-6}$	+3.9%	+2.2%	$9.268 \pm 0.030 \cdot 10^{-6}$	+2.3%	+2.3%
h.12	$pp \rightarrow HHt\bar{t}$	p p > h h t t~	$6.756 \pm 0.007 \cdot 10^{-4}$	-3.8%	-1.7%	$7.301 \pm 0.024 \cdot 10^{-4}$	-2.0%	-1.7%
h.13	$pp \rightarrow HHtj$	p p > h h tt j	$1.844 \pm 0.008 \cdot 10^{-5}$	+4.8%	+2.3%	$2.444 \pm 0.009 \cdot 10^{-5}$	+3.7%	+2.2%
h.14*	$pp \rightarrow HHb\bar{b}$	p p > h h b b~	$7.849 \pm 0.022 \cdot 10^{-8}$	-4.5%	-1.7%	$1.084 \pm 0.012 \cdot 10^{-7}$	-3.2%	-1.6%

Table 9: Sample of LO and NLO total rates for Higgs-pair production, possibly in association and within cuts, at the 13-TeV LHC; we also report the integration errors, and the fractional scale (left) and PDF (right) uncertainties. See table 1 for the meaning of **wpm**, and table 7 for the meaning of **tt**. All cross sections are calculated in the five-flavour scheme, except for process h.11 which is obtained in the four-flavour scheme to avoid resonant-top contributions. Processes h.1, h.2, h.3, h.6, h.12, and h.13 have appeared in ref. [124] as NLO+PS results; some of these were already known at the NLO [327]. The W -boson width is set equal to 2.0476 GeV for process h.13. Previous to the release of MADGRAPH5_AMC@NLO, the only available public code for Higgs pair production was HPAIR [328, 329], relevant to process h.1 (see ref. [124] for more details on the different approach adopted by MADGRAPH5_AMC@NLO). Process h.2 has been recently added to VBFNLO.

Process		Syntax	Cross section (pb)			
Heavy quarks and jets			LO 1 TeV		NLO 1 TeV	
i.1	$e^+e^- \rightarrow jj$	$e^+ e^- > j j$	$6.223 \pm 0.005 \cdot 10^{-1}$	$+0.0\%$ -0.0%	$6.389 \pm 0.013 \cdot 10^{-1}$	$+0.2\%$ -0.2%
i.2	$e^+e^- \rightarrow jjj$	$e^+ e^- > j j j$	$3.401 \pm 0.002 \cdot 10^{-1}$	$+9.6\%$ -8.0%	$3.166 \pm 0.019 \cdot 10^{-1}$	$+0.2\%$ -2.1%
i.3	$e^+e^- \rightarrow jjjj$	$e^+ e^- > j j j j$	$1.047 \pm 0.001 \cdot 10^{-1}$	$+20.0\%$ -15.3%	$1.090 \pm 0.006 \cdot 10^{-1}$	$+0.0\%$ -2.8%
i.4	$e^+e^- \rightarrow jjjjj$	$e^+ e^- > j j j j j$	$2.211 \pm 0.006 \cdot 10^{-2}$	$+31.4\%$ -22.0%	$2.771 \pm 0.021 \cdot 10^{-2}$	$+4.4\%$ -8.6%
i.5	$e^+e^- \rightarrow t\bar{t}$	$e^+ e^- > t t \sim$	$1.662 \pm 0.002 \cdot 10^{-1}$	$+0.0\%$ -0.0%	$1.745 \pm 0.006 \cdot 10^{-1}$	$+0.4\%$ -0.4%
i.6	$e^+e^- \rightarrow t\bar{t}j$	$e^+ e^- > t t \sim j$	$4.813 \pm 0.005 \cdot 10^{-2}$	$+9.3\%$ -7.8%	$5.276 \pm 0.022 \cdot 10^{-2}$	$+1.3\%$ -2.1%
i.7*	$e^+e^- \rightarrow t\bar{t}jj$	$e^+ e^- > t t \sim j j$	$8.614 \pm 0.009 \cdot 10^{-3}$	$+19.4\%$ -15.0%	$1.094 \pm 0.005 \cdot 10^{-2}$	$+5.0\%$ -6.3%
i.8*	$e^+e^- \rightarrow t\bar{t}jjj$	$e^+ e^- > t t \sim j j j$	$1.044 \pm 0.002 \cdot 10^{-3}$	$+30.5\%$ -21.6%	$1.546 \pm 0.010 \cdot 10^{-3}$	$+10.6\%$ -11.6%
i.9*	$e^+e^- \rightarrow t\bar{t}t\bar{t}$	$e^+ e^- > t t \sim t t \sim$	$6.456 \pm 0.016 \cdot 10^{-7}$	$+19.1\%$ -14.8%	$1.221 \pm 0.005 \cdot 10^{-6}$	$+13.2\%$ -11.2%
i.10*	$e^+e^- \rightarrow t\bar{t}t\bar{t}j$	$e^+ e^- > t t \sim t t \sim j$	$2.719 \pm 0.005 \cdot 10^{-8}$	$+29.9\%$ -21.3%	$5.338 \pm 0.027 \cdot 10^{-8}$	$+18.3\%$ -15.4%
i.11	$e^+e^- \rightarrow b\bar{b} \text{ (4f)}$	$e^+ e^- > b b \sim$	$9.198 \pm 0.004 \cdot 10^{-2}$	$+0.0\%$ -0.0%	$9.282 \pm 0.031 \cdot 10^{-2}$	$+0.0\%$ -0.0%
i.12	$e^+e^- \rightarrow b\bar{b}j \text{ (4f)}$	$e^+ e^- > b b \sim j$	$5.029 \pm 0.003 \cdot 10^{-2}$	$+9.5\%$ -8.0%	$4.826 \pm 0.026 \cdot 10^{-2}$	$+0.5\%$ -2.5%
i.13*	$e^+e^- \rightarrow b\bar{b}jj \text{ (4f)}$	$e^+ e^- > b b \sim j j$	$1.621 \pm 0.001 \cdot 10^{-2}$	$+20.0\%$ -15.3%	$1.817 \pm 0.009 \cdot 10^{-2}$	$+0.0\%$ -3.1%
i.14*	$e^+e^- \rightarrow b\bar{b}jjj \text{ (4f)}$	$e^+ e^- > b b \sim j j j$	$3.641 \pm 0.009 \cdot 10^{-3}$	$+31.4\%$ -22.1%	$4.936 \pm 0.038 \cdot 10^{-3}$	$+4.8\%$ -8.9%
i.15*	$e^+e^- \rightarrow b\bar{b}b\bar{b} \text{ (4f)}$	$e^+ e^- > b b \sim b b \sim$	$1.644 \pm 0.003 \cdot 10^{-4}$	$+19.9\%$ -15.3%	$3.601 \pm 0.017 \cdot 10^{-4}$	$+15.2\%$ -12.5%
i.16*	$e^+e^- \rightarrow b\bar{b}bbj \text{ (4f)}$	$e^+ e^- > b b \sim b b \sim j$	$7.660 \pm 0.022 \cdot 10^{-5}$	$+31.3\%$ -22.0%	$1.537 \pm 0.011 \cdot 10^{-4}$	$+17.9\%$ -15.3%
i.17*	$e^+e^- \rightarrow t\bar{t}b\bar{b} \text{ (4f)}$	$e^+ e^- > t t \sim b b \sim$	$1.819 \pm 0.003 \cdot 10^{-4}$	$+19.5\%$ -15.0%	$2.923 \pm 0.011 \cdot 10^{-4}$	$+9.2\%$ -8.9%
i.18*	$e^+e^- \rightarrow t\bar{t}bbj \text{ (4f)}$	$e^+ e^- > t t \sim b b \sim j$	$4.045 \pm 0.011 \cdot 10^{-5}$	$+30.5\%$ -21.6%	$7.049 \pm 0.052 \cdot 10^{-5}$	$+13.7\%$ -13.1%

Table 10: Sample of LO and NLO rates for the production of light jets in association with heavy quarks, possibly within cuts, at a 1-TeV e^+e^- collider; we also report the integration errors, and the fractional scale uncertainties. Cross sections for processes i.1–i.10 are calculated in the five-flavour scheme. For processes i.11–i.18 we use the four-flavour scheme, and require the presence of at least two (four in i.15–i.16) b -jets in the final state. b -jets are clustered with the same parameters as light jets. Results at NLO accuracy for up to seven light jets can be found in refs. [9, 68, 330–334], and for a heavy-quark-pair plus up to one jet in refs. [335–341]. All other processes are computed here for the first time at the NLO.

Process		Syntax	Cross section (pb)			
Top quarks +bosons			LO 1 TeV		NLO 1 TeV	
j.1	$e^+e^- \rightarrow t\bar{t}H$	e+ e- > t t~ h	$2.018 \pm 0.003 \cdot 10^{-3}$	+0.0% -0.0%	$1.911 \pm 0.006 \cdot 10^{-3}$	+0.4% -0.5%
j.2*	$e^+e^- \rightarrow t\bar{t}Hj$	e+ e- > t t~ h j	$2.533 \pm 0.003 \cdot 10^{-4}$	+9.2% -7.8%	$2.658 \pm 0.009 \cdot 10^{-4}$	+0.5% -1.5%
j.3*	$e^+e^- \rightarrow t\bar{t}Hjj$	e+ e- > t t~ h j j	$2.663 \pm 0.004 \cdot 10^{-5}$	+19.3% -14.9%	$3.278 \pm 0.017 \cdot 10^{-5}$	+4.0% -5.7%
j.4*	$e^+e^- \rightarrow t\bar{t}\gamma$	e+ e- > t t~ a	$1.270 \pm 0.002 \cdot 10^{-2}$	+0.0% -0.0%	$1.335 \pm 0.004 \cdot 10^{-2}$	+0.5% -0.4%
j.5*	$e^+e^- \rightarrow t\bar{t}\gamma j$	e+ e- > t t~ a j	$2.355 \pm 0.002 \cdot 10^{-3}$	+9.3% -7.9%	$2.617 \pm 0.010 \cdot 10^{-3}$	+1.6% -2.4%
j.6*	$e^+e^- \rightarrow t\bar{t}\gamma jj$	e+ e- > t t~ a j j	$3.103 \pm 0.005 \cdot 10^{-4}$	+19.5% -15.0%	$4.002 \pm 0.021 \cdot 10^{-4}$	+5.4% -6.6%
j.7*	$e^+e^- \rightarrow t\bar{t}Z$	e+ e- > t t~ z	$4.642 \pm 0.006 \cdot 10^{-3}$	+0.0% -0.0%	$4.949 \pm 0.014 \cdot 10^{-3}$	+0.6% -0.5%
j.8*	$e^+e^- \rightarrow t\bar{t}Zj$	e+ e- > t t~ z j	$6.059 \pm 0.006 \cdot 10^{-4}$	+9.3% -7.8%	$6.940 \pm 0.028 \cdot 10^{-4}$	+2.0% -2.6%
j.9*	$e^+e^- \rightarrow t\bar{t}Zjj$	e+ e- > t t~ z j j	$6.351 \pm 0.028 \cdot 10^{-5}$	+19.4% -15.0%	$8.439 \pm 0.051 \cdot 10^{-5}$	+5.8% -6.8%
j.10*	$e^+e^- \rightarrow t\bar{t}W^\pm jj$	e+ e- > t t~ wpm j j	$2.400 \pm 0.004 \cdot 10^{-7}$	+19.3% -14.9%	$3.723 \pm 0.012 \cdot 10^{-7}$	+9.6% -9.1%
j.11*	$e^+e^- \rightarrow t\bar{t}HZ$	e+ e- > t t~ h z	$3.600 \pm 0.006 \cdot 10^{-5}$	+0.0% -0.0%	$3.579 \pm 0.013 \cdot 10^{-5}$	+0.1% -0.0%
j.12*	$e^+e^- \rightarrow t\bar{t}\gamma Z$	e+ e- > t t~ a z	$2.212 \pm 0.003 \cdot 10^{-4}$	+0.0% -0.0%	$2.364 \pm 0.006 \cdot 10^{-4}$	+0.6% -0.5%
j.13*	$e^+e^- \rightarrow t\bar{t}\gamma H$	e+ e- > t t~ a h	$9.756 \pm 0.016 \cdot 10^{-5}$	+0.0% -0.0%	$9.423 \pm 0.032 \cdot 10^{-5}$	+0.3% -0.4%
j.14*	$e^+e^- \rightarrow t\bar{t}\gamma\gamma$	e+ e- > t t~ a a	$3.650 \pm 0.008 \cdot 10^{-4}$	+0.0% -0.0%	$3.833 \pm 0.013 \cdot 10^{-4}$	+0.4% -0.4%
j.15*	$e^+e^- \rightarrow t\bar{t}ZZ$	e+ e- > t t~ z z	$3.788 \pm 0.004 \cdot 10^{-5}$	+0.0% -0.0%	$4.007 \pm 0.013 \cdot 10^{-5}$	+0.5% -0.5%
j.16*	$e^+e^- \rightarrow t\bar{t}HH$	e+ e- > t t~ h h	$1.358 \pm 0.001 \cdot 10^{-5}$	+0.0% -0.0%	$1.206 \pm 0.003 \cdot 10^{-5}$	+0.9% -1.1%
j.17*	$e^+e^- \rightarrow t\bar{t}W^+W^-$	e+ e- > t t~ w+ w-	$1.372 \pm 0.003 \cdot 10^{-4}$	+0.0% -0.0%	$1.540 \pm 0.006 \cdot 10^{-4}$	+1.0% -0.9%

Table 11: Sample of LO and NLO rates for the production of top quarks in association with bosons, possibly within cuts and in association with jets, at a 1-TeV e^+e^- collider, and the fractional scale uncertainties. Cross sections are calculated in the five-flavour scheme; see table 1 for the meaning of **wpm**. Results at NLO accuracy for $t\bar{t}H$ production can be found in ref. [342]. All of the other processes are computed here for the first time at the NLO.

4.2 Differential distributions

In this section we present sample results for differential observables relevant to several processes, which we have simulated at the 8, 13, or 14 TeV LHC. While some of these have never been computed before at the NLO+PS accuracy (or even at fNLO; see sect. 4.1), and appear here for the first time, we do not aim to present a series of phenomenological analyses, which would be out of the scope of this work, but rather at showing yet again the flexibility of MADGRAPH5_AMC@NLO, and the type of results that one can obtain with it. For this reason, the various PSMCs which we shall use have been run with their default parameters, and no underlying events have been generated. Having said that, some of the predictions given here are motivated by recent measurements by ATLAS and CMS. Furthermore, the present section constitutes a complement in particular to sect. 2.4.5, since we shall discuss, using explicit examples, several features of the FxFx merging procedure which have been outlined before in a general fashion. We shall be mainly concerned with (N)LO+PS results, but we shall also consider f(N)LO ones where necessary. As was the case for the total rates presented in sect. 4.1, the computation of scale and PDF uncertainties has been carried out by using the reweighting procedure introduced in ref. [122] (see also appendix B.3). NLO+PS results that have never appeared in the literature are: six-lepton, $t\bar{t}W^+W^-$, and SM Higgs in VBF+1 j production; furthermore, double-Higgs production in association with either a $t\bar{t}$ pair or a Z boson has been solely computed with MADGRAPH5_AMC@NLO, in ref. [124]. Finally, FxFx-merged results for ZZ and $He^+\nu_e$ production are also presented here for the first time.

◆ Six-lepton production

We start by studying the (N)LO+PS production of six leptons:

$$pp \longrightarrow e^+e^-\mu^+\nu_\mu\tau^-\bar{\nu}_\tau, \quad (4.1)$$

which we have computed by using the complex mass scheme; the τ^- lepton is set stable, and its mass is kept at the physical value, while the electron and the muon are treated as massless. On top of the computation carried out with the exact six-lepton matrix elements of eq. (4.1), we have also considered the production of the ZW^+W^- triplet, with the subsequent decays of the vector bosons performed with either MADSPIN or by the PSMC (in this case, HERWIG6):

$$pp \longrightarrow Z(\rightarrow e^+e^-)W^+(\rightarrow \mu^+\nu_\mu)W^-(\rightarrow \tau^-\bar{\nu}_\tau). \quad (4.2)$$

While MADSPIN multiplies the undecayed matrix elements by the branching ratios of the relevant decays, so that the rates resulting from eq. (4.2) are in absolute value directly comparable to those of eq. (4.1), the PSMC does not; in that case, we have therefore manually included such an overall factor. To all samples, we have applied the following cut:

$$M(\ell^+\ell'^{-}) > 30 \text{ GeV}, \quad (4.3)$$

on all opposite-charged lepton pairs; given the lepton flavours considered here, not surprisingly the vastly dominant effect of such a cut is that due to the e^+e^- pair. We shall

call eq. (4.3) the generation cut⁵⁴. On top of eq. (4.3), we have also imposed (also at the analysis level):

$$|M(e^+e^-) - m_Z| < 20 \text{ GeV}, \quad (4.4)$$

$$|M(\mu^+\nu_\mu) - m_W| < 20 \text{ GeV}, \quad (4.5)$$

$$|M(\tau^-\bar{\nu}_\tau) - m_W| < 20 \text{ GeV}, \quad (4.6)$$

which we shall call *V-reco* cuts. Since eq. (4.2) features only 3-resonant contributions (see sect. 2.5 about the notation used here for resonant and non-resonant diagrams), the results of the MADSPIN- and PSMC-decayed samples are basically the same if one considers only the generation cut, or the generation and *V-reco* cuts together; for this reason, we shall discuss only the latter scenario. On the other hand, one of the reasons for comparing eqs. (4.1) and (4.2) is precisely that of assessing the importance of non-3-resonant contributions to six-lepton matrix elements; hence, in this case we shall present both the generation-cut-only and the generation-plus-*V-reco* cuts results.

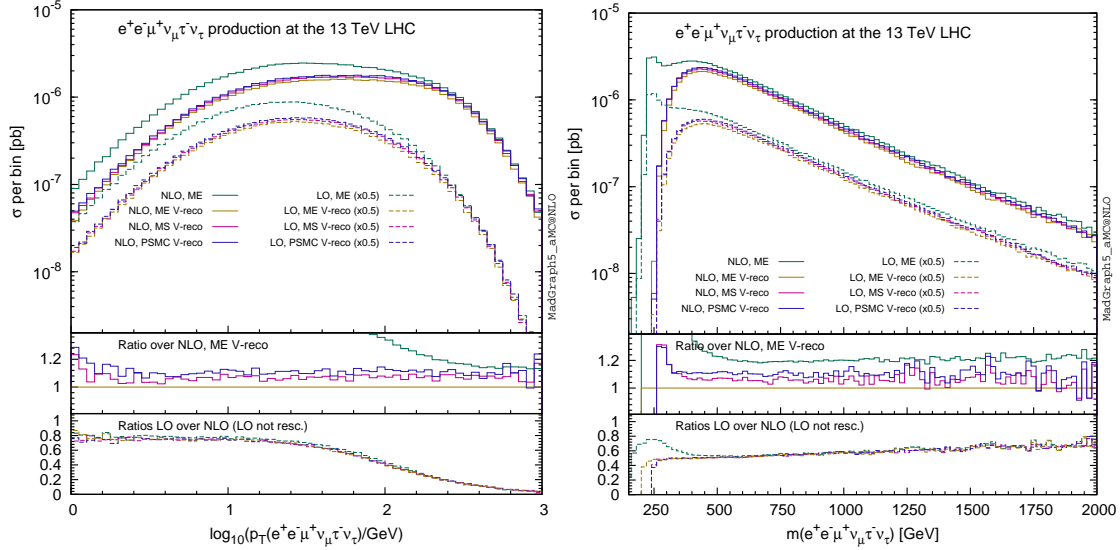


Figure 4: Transverse momentum (left panel) and invariant mass (right panel) of the six-lepton system, for the processes of eqs. (4.1) and (4.2). See the text for details.

In figure 4 we show observables relevant to the six-lepton system, i.e. obtained by summing the four-momenta of the leptons: the transverse momentum (left panel) and the invariant mass (right panel). Both the NLO+PS (solid histograms) and LO+PS (dashed histograms, rescaled as indicated in order to fit into the layout) are displayed. The green histograms are the results of eq. (4.1) with only the generation cut (denoted by “(N)LO ME”); the results for the generation-plus-*V-reco* cuts are shown as yellow (eq. (4.1), denoted by “(N)LO ME *V-reco*”), red (eq. (4.2) with MADSPIN, denoted by “(N)LO MS *V-reco*”),

⁵⁴Despite the fact that it has been imposed at the analysis level, and the true generation cut is marginally lower so as to avoid biases.

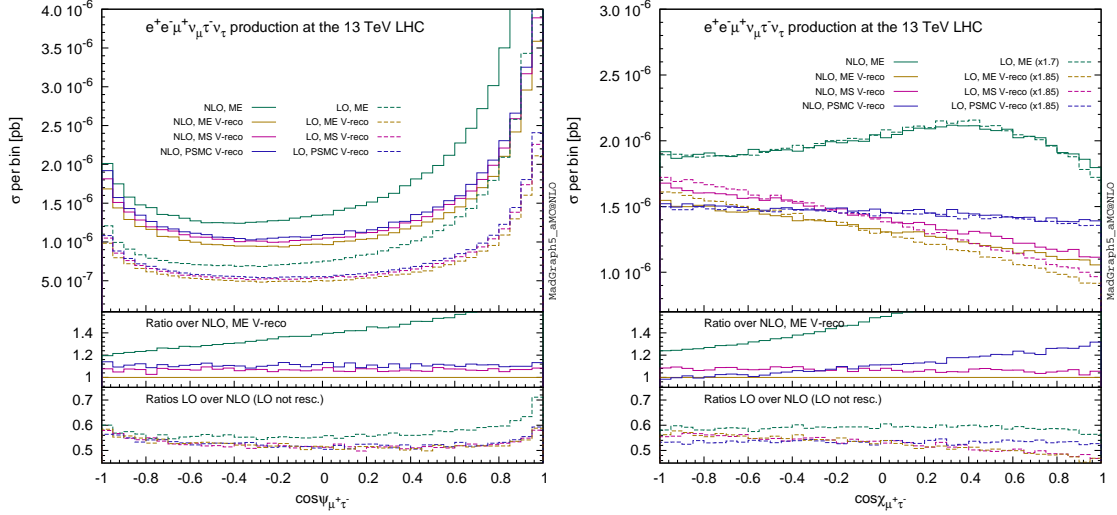


Figure 5: Cosine of correlation angles for the $\mu^+\tau^-$ pair, in six-lepton production, eqs. (4.1) and (4.2). See the text for details.

and blue (eq. (4.2) with PSMC decays, denoted by “(N)LO PSMC V-reco”) histograms respectively. In the middle insets, the ratios of all the NLO results over the NLO ME V-reco ones are presented. Finally, in the lower insets each LO prediction is divided by its NLO counterpart (so these are essentially the inverse of the K factors). The plots show clearly the large impact of non-3-resonant contributions, which induce dramatic shape modifications for $M(6\ell) < 500$ GeV and $10 < p_T(6\ell) < 250$ GeV (the very small p_T region being dominated by PSMC radiation effects). On the other hand, by imposing V-reco cuts the three predictions agree rather well with each other, which is the signal that spin correlations are unimportant for these observables (and, more importantly in view of the aim of this paper, that all is fine from a technical viewpoint, in the context of a very involved production process). We have performed similar comparisons for a large number of observables; here, we limit ourselves to reporting the results for the cosine of the angle defined by the directions of flight of the μ^+ and τ^- leptons, which we denote by $\psi_{\mu^+\tau^-}$ (left panel of fig. 5) when it is computed in the laboratory frame, and by $\chi_{\mu^+\tau^-}$ (right panel of fig. 5) when it is computed by first boosting the four-momentum of the μ^+ and τ^- leptons to the rest frame of the $\mu^+\nu_\mu$ and $\tau^-\bar{\nu}_\tau$ systems respectively (i.e., to the virtual- W^+ and W^- rest frames in the case of resonant contributions); the latter observable is known to be particularly suitable for the study of spin-correlation effects. The same conclusions as for the observables of fig. 4 apply here, bar for the $\chi_{\mu^+\tau^-}$ NLO PSMC V-reco one that is fairly different from both the NLO ME V-reco and NLO MS V-reco predictions, which in turn agree with each other quite well. As it was expected, this is a manifestation of the importance of spin correlations for such an observable, and a direct validation of the MADSPIN procedure.

The overall messages that one can obtain from the present study are the following. Firstly, we did verify that the conclusions reached above are not qualitatively modified

if one replaces the (N)LO ME results with those obtained by imposing the generation cut and eq. (4.4) only – in other words, it is the simultaneous action of the three cuts of eqs. (4.4)–(4.6) that brings the predictions for eq. (4.1) in agreement with those for eq. (4.2) and MADSPIN; this is obviously because it is important that all three vector bosons be near their respective mass shell. Secondly, the effects of NLO corrections are non negligible, in both rate and shape; however, the patterns of comparison among the various calculations are to a large extent independent of the perturbative accuracy of the latter. Thirdly, production spin correlations are present, that can be properly described only by the full six-lepton computation, and by MADSPIN as well *if* one limits oneself to the 3-resonant region. It is clear that the cuts of eqs. (4.5) and (4.6), and the definition of the observables considered here, bar $\psi_{\mu^+\tau^-}$, cannot be achieved experimentally, owing to the presence of the neutrino four-momenta. However, they have helped us reach conclusions which have a general validity, and in particular in the case of a fully realistic analysis: namely, that non-resonant effects in six-lepton production may be quite large and that, for all those cuts that render the 3-resonant contributions dominant, the undecayed-plus-MADSPIN simulation provides one with a very good approximation of the exact calculation.

◆ $t\bar{t}W^-W^+$ production

We now turn to considering the process:

$$pp \longrightarrow t(\rightarrow e^+\nu_e b)\bar{t}(\rightarrow e^-\bar{\nu}_e\bar{b})W^-(\rightarrow \mu^-\bar{\nu}_\mu)W^+(\rightarrow \mu^+\nu_\mu), \quad (4.7)$$

which we have simulated at the (N)LO+PS accuracy, by only considering the undecayed matrix elements with $t\bar{t}W^+W^-$ final states, and by using PYTHIA8 as PSMC and either MADSPIN or the internal PYTHIA8 routine (which correctly accounts for decay spin correlations) for the decays of the top quarks and W bosons. In fig. 6 we present the transverse momentum of the $t\bar{t}W^+W^-$ system, which is the typical observable whose small- p_T behaviour is dominated by MC effects (whose systematics will not be studied here), and which is thus unreliable if computed at fNLO accuracy. Both the NLO+PS (solid histograms) and LO+PS (dashed histograms) results are displayed, with the respective scale-uncertainty bands (in dark and light shades respectively). The very significant reduction of such theoretical systematics when higher-order corrections are included is evident in the whole range considered (see also entry e.13 in table 6 for its total-rate counterpart). While for asymptotically-large transverse momenta one expects the NLO+PS scale dependence to be of LO type (because in that region the computation is dominated by tree-level contributions), for such a massive system these p_T 's are comfortably in the TeV-range. In fig. 7 we show the transverse momenta of the four-hardest charged leptons in the events; the leptons are required to have $p_T(\ell) > 20$ GeV and $|\eta(\ell)| < 2.5$. At variance with those of fig. 6, these plots include the branching ratios of the decays reported in eq. (4.7). The LO+PS results in the main frames are rescaled so as to fit into the layout. Each plot displays four histograms, that correspond to NLO+PS (solid, with MADSPIN decays; dashed, with PYTHIA8 decays) and to LO+PS (dot-dashed, with MADSPIN decays; dotted, with PYTHIA8 decays) results. The ratios of these predictions over the NLO+PS, MADSPIN-decayed ones are shown in the insets. The radiative corrections are large, but relatively flat in the p_T ranges considered

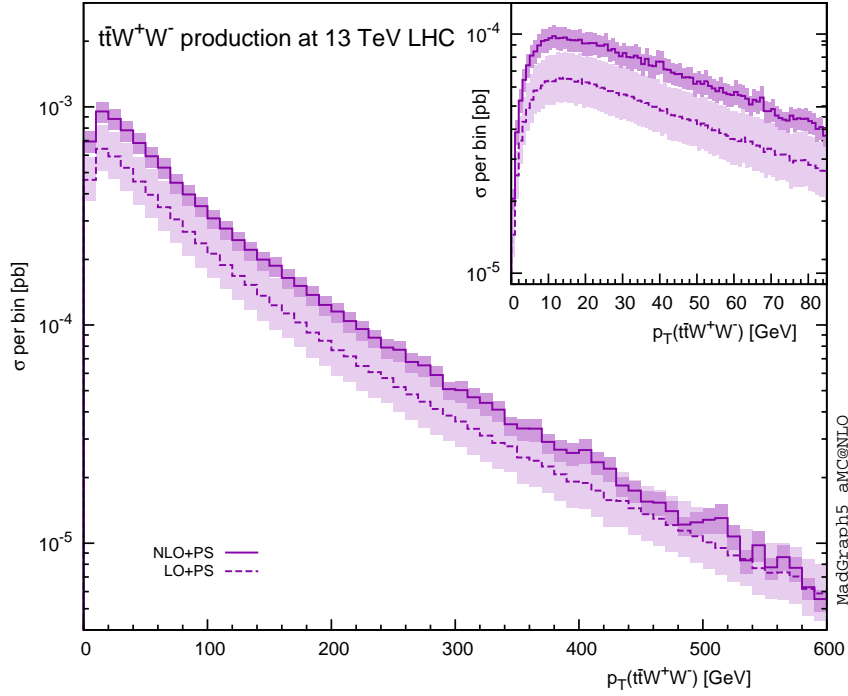


Figure 6: Transverse momentum of the system of the four primary final-state particles in $t\bar{t}W^+W^-$ production.

here; as in the case of the p_T of the system, their inclusion reduces the scale uncertainty in a dramatic manner. Production spin correlations are sizable, so much so that MADSPIN- and PYTHIA8-decayed results have shapes which are barely within, or slightly outside of, the theoretical systematics bands. This is true at the NLO; at the LO, the two predictions are compatible within uncertainties, but this is solely due to the fact that the LO scale dependence is rather large: in fact, the pattern of the inclusion of production spin correlations is basically independent of the perturbative order at which one is working. This is nothing but another manifestation of the benefits inherent to the increased predictive power of simulations that include both NLO and production spin correlation effects.

◆ Double-Higgs production

We now consider double-Higgs production in the SM at the 14 TeV LHC. This process has been investigated recently with MADGRAPH5-AMC@NLO in ref. [124], where all the six dominant channels at the LHC have been computed up to NLO+PS accuracy, some of them for the first time. For all channels, the results of ref. [124] have improved what was available in the literature in at least one respect. In ref. [124] we have only presented (N)LO+PS distributions. Here, we amend this by showing also f(N)LO spectra; we use the transverse momentum of the Higgs pair, and the $t\bar{t}HH$ and ZHH channels, as a definite example; as PSMCs, we adopt PYTHIA8 and HERWIG6. The results are shown in fig. 8, as solid (for NLO-accurate) and dashed (for LO-accurate) histograms. The main frames

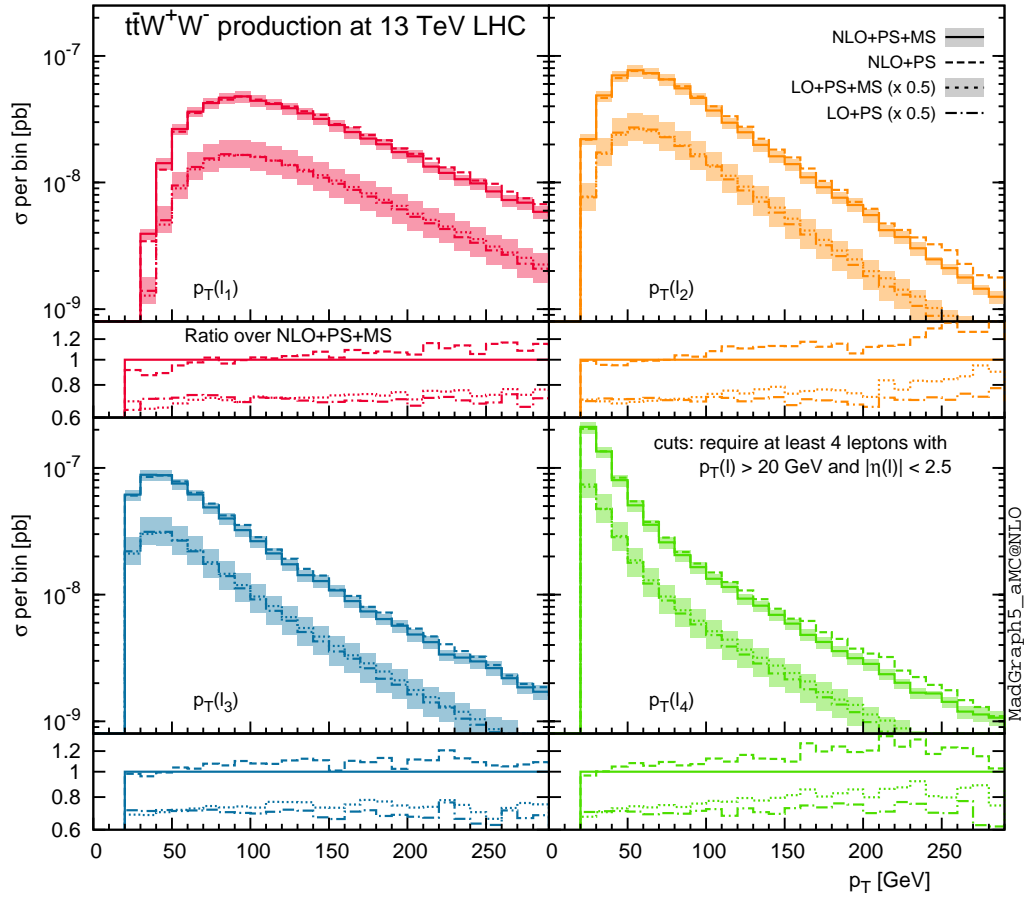


Figure 7: Transverse momentum of the hardest four charged leptons in $t\bar{t}W^+W^-$ production – see eq. (4.7). The LO+PS results that appear in the insets have not been rescaled.

display the NLO predictions in absolute value, while the LO ones are rescaled in order to fit into the layout; the K factors can be read from the insets, where we present the ratios of all results over those at the NLO+PS obtained with PYTHIA8. The common feature of the two plots is that NLO results are mutually closer than the corresponding LO ones; the two NLO+PS predictions are extremely similar for both processes, while the fNLO spectrum in ZHH production is only marginally softer (an overall effect smaller than 20%). It is interesting to see that this stabilisation due to the inclusion of higher-order corrections follows different patterns for the two channels considered here. ZHH is predominantly a $q\bar{q}$ -initiated process: therefore, the difference between the two standalone PSMCs (i.e., LO+PS) is expected to be smaller than in the case of $t\bar{t}HH$ production, which mainly proceeds through gg fusion. This is precisely what we see in fig. 8 (compare the purple and red histograms in the insets). On the other hand, at fLO the Higgs pair recoils against a Z boson and a $t\bar{t}$ -system in ZHH and $t\bar{t}HH$ production respectively; the kinematics of the $t\bar{t}$ pair being non-trivial (at variance with that of a single Z) implies that the fLO prediction

for $p_T(HH)$ is farther away from the corresponding LO+PS ones in the ZHH channel than in the $t\bar{t}HH$ channel (see the green dashed histograms in the insets, and compare the position of the peaks of the fLO and fNLO results).

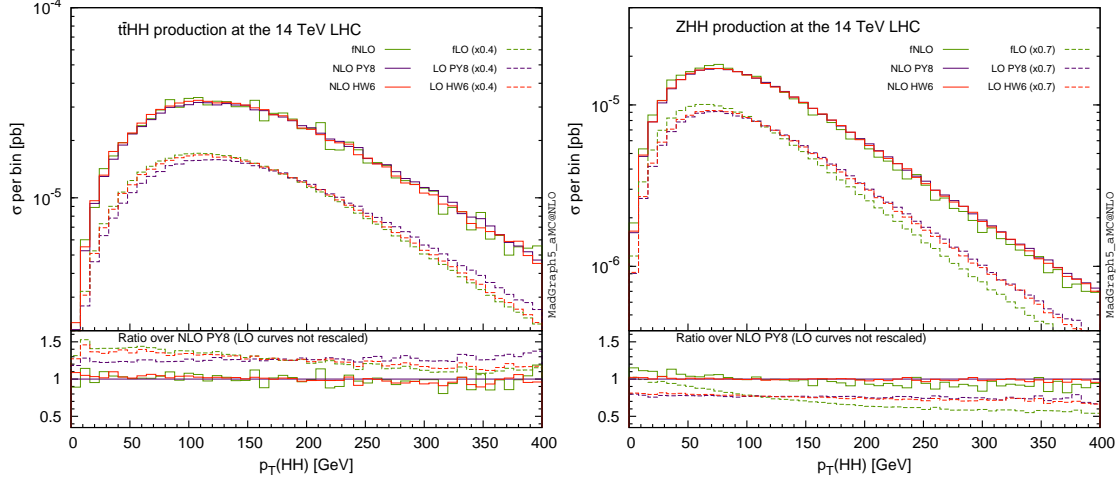


Figure 8: Transverse momentum of the two-Higgs system in $t\bar{t}HH$ (left panel) and ZHH (right panel) production. (N)LO+PS and f(N)LO results are shown. We have used PYTHIA8 and HERWIG6.

◆ Single-Higgs production

We now turn to discussing the production of a single SM Higgs at the 13 TeV LHC. The aims of fig. 9, where we show the Higgs transverse momentum, are twofold. Firstly, we compare LO+PS with NLO+PS predictions; secondly, we present results for all PSMCs which are matched to NLO calculations in MADGRAPH5_AMC@NLO⁵⁵. The comparison between the two panels of the figure shows the two expected behaviours: at large p_T 's, all NLO+PS predictions coincide (and are just on top of the corresponding fNLO result, not displayed here), while the LO+PS are vastly different; on the other hand, at small p_T 's, the relative behaviour of the various PSMCs is the same, regardless of the perturbative order of the underlying matrix-element computations. We point out that all PSMCs are treated on equal footing, i.e. they are given the same numerical values as shower-scales parameters (such scales are equal to m_H at the LO, and controlled by the D function at the NLO); so while different scales for different PSMCs could bring them in better agreement at the LO, this is actually a negative implication of the loss of predictivity at this perturbative order, and it is unnecessary when NLO corrections are included in the simulations; a further example of this pattern will be given below, in the study of Higgs production through VBF. We conclude this part by showing, in fig. 10, the Higgs p_T that results from the five dominant production channels at the 13 TeV LHC (whose total rates are reported in lines g.1, g.4, g.6, g.9, and g.16 of table 8, where one can also find the MADGRAPH5_AMC@NLO shell commands relevant to their generation); the thickness of

⁵⁵We remind the reader that PYTHIA6(p_T) is available for ISR-only processes.

the bands represent the combined scale and PDF uncertainties; all the predictions are obtained at the NLO+PS, with the use of PYTHIA8. This plot is another demonstration of the flexibility of the MADGRAPH5_AMC@NLO framework.

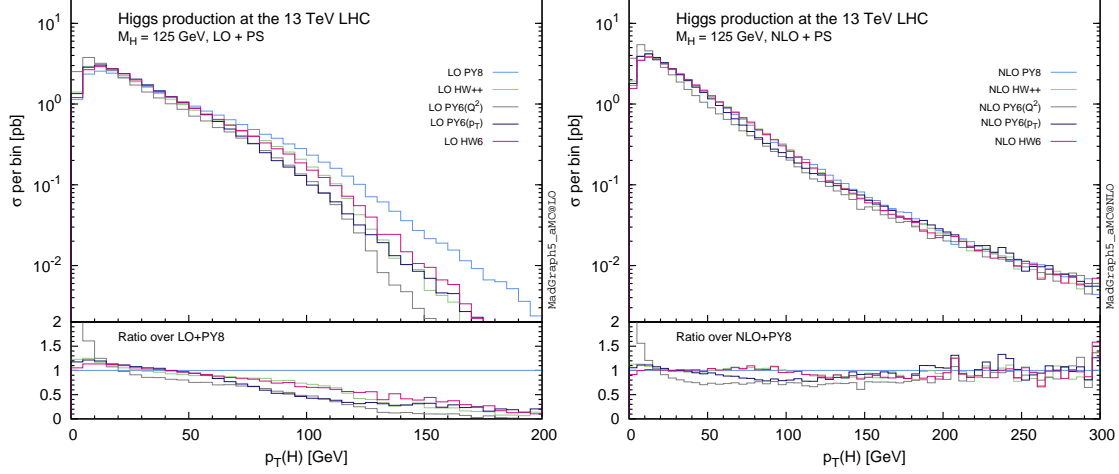


Figure 9: Higgs p_T spectrum in gg fusion (HEFT), for various PSMCs, at the LO+PS (left panel) and NLO+PS (right panel) accuracy. Note the larger p_T range in the right panel.

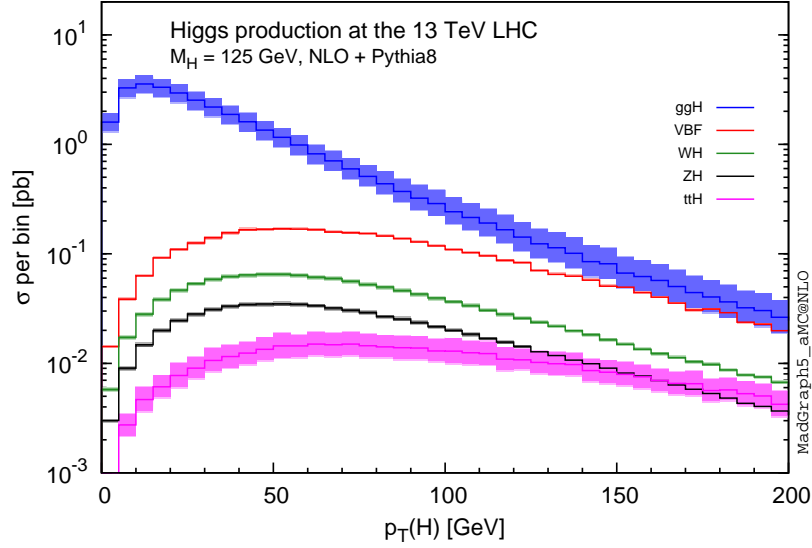


Figure 10: Higgs p_T spectrum for the five dominant production channels at the LHC, at the NLO+PS accuracy with PYTHIA8.

◆ Higgs production in VBF

As a further example of the stabilisation of the predictions that result from including higher-order matrix elements (which in turn serves as a validation exercise for the whole NLO+PS machinery in MADGRAPH5_AMC@NLO), we consider Higgs production in VBF, which we compute in two ways: by considering the process whose Born is of $\mathcal{O}(\alpha^3)$ (which we denote by VBF+0j [343], and whose final state at the Born level thus features a Higgs-plus-two-parton system), and the process whose Born is of $\mathcal{O}(\alpha^3\alpha_s)$ (which we denote by VBF+1j, and whose final state at the Born level thus features a Higgs-plus-three-parton system). These are the processes reported in lines g.4 and g.5 of table 8, where the interested reader can also find the MADGRAPH5_AMC@NLO shell commands that one must use in order to generate them. The only analysis cuts we impose here are on the transverse momenta of the (anti- k_T , $R = 0.5$) jets, by requiring that $p_T(j) > 20$ GeV. The only observables for which a direct comparison between VBF+0j and VBF+1j is sensible, and allow one to assess the impact of perturbative corrections, are those related to the third jet, where one expects to have an effective LO and NLO description respectively. In fig. 11 we present predictions for the transverse momentum spectrum of the third-hardest jet, and for the rate as a function of the transverse momentum of the veto jet:

$$\sigma_{veto}(p_T(j_{veto})) = \int_{p_T(j_{veto})}^{\infty} dp_T \frac{d\sigma}{dp_T}. \quad (4.8)$$

The veto jet is the hardest jet which is not one of the two tagging jet (which are defined to be the two hardest ones overall, and which we denote by j_1 and j_2 respectively), and whose rapidity obeys the condition:

$$\min(y_{j_1}, y_{j_2}) \leq y(j_{veto}) \leq \max(y_{j_1}, y_{j_2}). \quad (4.9)$$

The quantity defined in eq. (4.8) is related to P_{veto} , defined e.g. in eq. (41) of ref. [326], by a simple normalisation factor, $\sigma_{veto} = \sigma_{\text{NLO}} P_{veto}$. For both VBF+0j (dashed histograms) and VBF+1j (solid histograms) the results for three PSMCs (PYTHIA8 (red), PYTHIA6(Q^2) (green), and HERWIG6 (black)) are displayed, with the VBF+0j ones rescaled by a factor 1/5 in order for them to fit into the layout. The ratios of the PYTHIA predictions over the HERWIG6 ones are presented in the insets. In the inset relevant to VBF+1j, we also report the ratio of the HERWIG6 VBF+0j result over the VBF+1j one (black dashed histogram), which is related to the inverse of the K factor – for both observables, the latter is of the order of 1.05–1.15. In the insets we also display the scale uncertainties as gray bands: it is evident that the inclusion of the contributions of relative $\mathcal{O}(\alpha_s)$ in VBF+1j significantly reduces the theoretical systematics. Apart from this, the most striking consequence of such an inclusion is the fact that the three PSMCs in VBF+1j are fairly close to each other; this is not the case in VBF+0j, where PYTHIA8 has a much softer shape than either PYTHIA6 or HERWIG6. We point out that this is a feature of quantities related to the third jet: other observables which have an NLO nature in VBF+0j are much better behaved, with the three PSMCs in good agreement already at $\mathcal{O}(\alpha^3(1 + \alpha_s))$. Therefore, although one could possibly find settings for the PSMCs that would bring the predictions for the $p_T(j_3)$ and σ_{veto} VBF+0j spectra in better agreement than in fig. 11, this would simply be

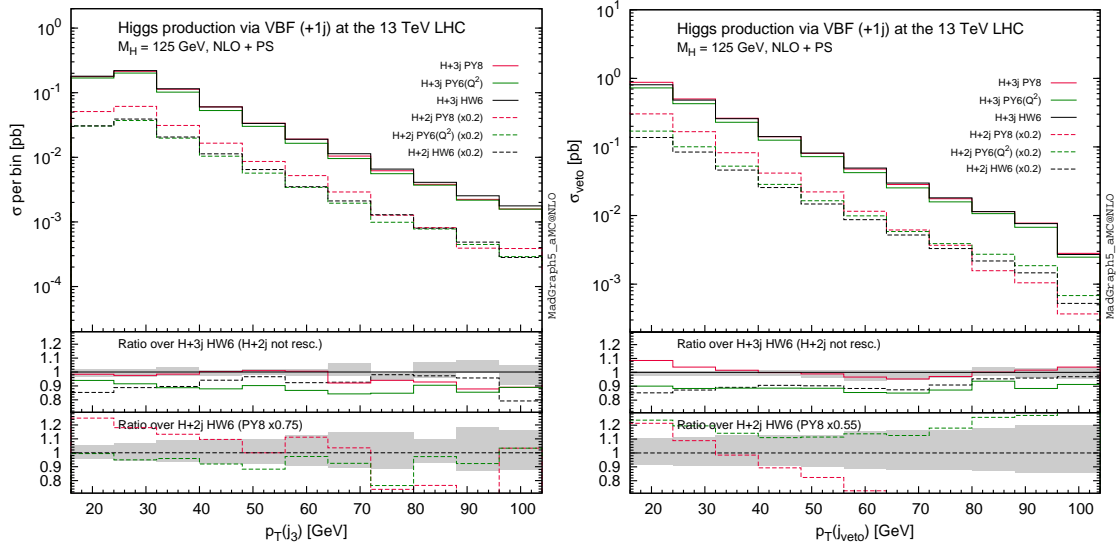


Figure 11: Third-jet observables in Higgs VBF+0j and VBF+1j production, both at the NLO+PS, with PYTHIA8, HERWIG6, and PYTHIA6(Q^2).

the signal of an unsatisfactory predictive capability, which is restored by considering these observables in VBF+1j production.

◆ Top-pair production

While differential distributions relevant to $t\bar{t}$ production measured at the LHC by the ATLAS (at 7 TeV in lepton+jets events [344]) and the CMS (at 7 and 8 TeV, in lepton+jets and dilepton events [345–347]) collaborations are generally in very good agreement with theoretical predictions, the CMS data for the reconstructed transverse momentum of the top quark ($p_T(t)$) are visibly softer than NLO+PS predictions, and in disagreement with those of ATLAS for $p_T(t) < 200$ GeV (ATLAS data are harder). Given this inconsistency between measurements it is premature to speculate on the origin of a possible discrepancy between data and theory; it is however of some interest to discuss the theoretical systematics that affect the NLO+PS spectrum. Among these, those due to scale, PDFs, and choice of top-quark mass have been studied by the experimental collaborations, and shown to be smaller than the disagreement between data and theory [345]. Here, we therefore concentrate on other sources of systematics. One of these is due to missing higher orders, since the NLO+PS predictions used by the experiments include only up to $\mathcal{O}(\alpha_s^3)$ terms, namely $t\bar{t} + 0j$ samples at the NLO. While the impact of missing higher orders in perturbation theory is estimated by scale variations, an important and independent check of this assessment may be obtained by considering NLO-merged predictions. In the left panel of fig. 12 we thus compare the unmerged $t\bar{t} + 0j$ prediction with the FxFx one, where the $t\bar{t} + 0j$ and $t\bar{t} + 1j$ samples are combined with $\mu_Q = 100$ GeV. Both merged and unmerged results have been obtained with HERWIG6, by setting the collider energy equal to 8 TeV; the

latter curve has been rescaled⁵⁶ in order for its visible integral to coincide with that of the former (since in this case we are specifically interested in a shape comparison: in absolute values, the two cross sections differ however by only 2.5%). As one can gather from the plot, the two predictions are close to each other; the FxFx prediction is slightly softer than the unmerged one, but this does not appear to be sufficient to bring it in agreement with the CMS measurement. The variation of the merging scale in a large range (30–155 GeV) does not induce any significant change. It therefore appears that the systematics due to higher-order corrections are fully under control, since scale variations and NLO-merging give consistent results for this observable, and we thus confirm the previous findings that it cannot explain the discrepancy between theory and CMS data. Another source of theo-

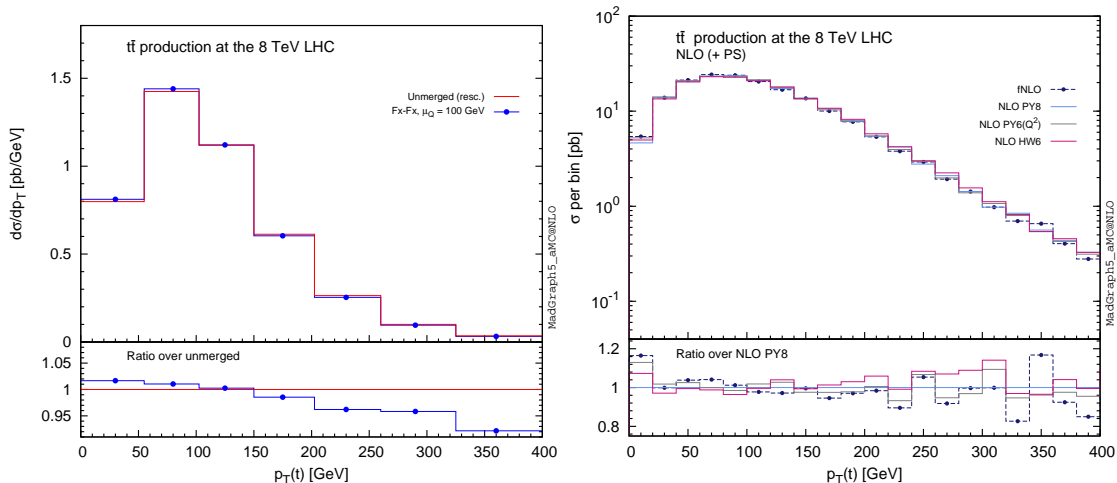


Figure 12: Transverse momentum of the top quark in $t\bar{t}$ production. Left panel: comparison between FxFx-merged (blue) and unmerged (red) predictions; the binning is the same as that of ref. [346]. Right panel: NLO+PS predictions obtained with different PSMCs, compared to the fnLO result.

retical systematics in NLO+PS predictions is that due to the choice of the PSMC. This is presented in the right panel of fig. 12, where we compare the $(t\bar{t} + 0j)$ unmerged predictions obtained with PYTHIA8 (cyan), HERWIG6 (red), and PYTHIA6(Q^2) (grey); the lower inset presents the bin-by-bin ratios of the latter two predictions over that of PYTHIA8. It is clear from the plot that the three PSMCs are amply consistent with each other; this is expected, since the pure-NLO result for $p_T(t)$ must not be dramatically modified by shower effects; such an expectation is confirmed by the fnLO prediction, also reported in the right panel of fig. 12 as the dashed histogram overlaid with full circles, which is in fair agreement with all the other curves. We therefore conclude that it does not seem possible to get NLO+PS predictions to agree with CMS data by changing the PSMC used in the simulations. We also point out that this statement by no means implies that acceptance corrections, which we do not compute here, are PSMC-independent; a careful investigation of these may be

⁵⁶If visually that may not seem to be the case, it is because the bin widths are not equal: note that the cross section is differential.

necessary should the discrepancy discussed here persist, given that $p_T(t)$ is not a quantity that can be measured directly.

Inclusive quantities that stem from either or both tops in $t\bar{t}$ events are an ideal testing ground for NLO+PS predictions, which should give a good description of the data for absolute normalisation as well as for shapes. On the other hand, $t\bar{t}$ events are characterised by large c.m. energies which imply a large amount of QCD radiation (only a tiny fraction of which originate from the top quarks, owing to their being very massive). The study of such radiation and of its topological properties is an interesting subject, particularly in view of the large statistical accuracy that can be obtained at the LHC. At variance with the case of inclusive observables, there is no reason to expect that *all* radiation-related observables will be well described by NLO+PS $t\bar{t} + 0j$ predictions. In particular, those for which large jet multiplicities are important should be sensibly compared only to merged results, or at least to unmerged samples whose underlying matrix elements feature a sufficiently large number of hard partons – the most obvious example is that of N_{jet} . On the other hand, for radiation-related observables which are also inclusive enough, NLO+PS simulations should do relatively well. One such case is that of the so-called gap fractions, which have been measured in the dilepton channel by both ATLAS (at 7 TeV [348]) and CMS (at 7 [349] and 8 TeV [350]), and compared to various theoretical predictions – MC@NLO with HERWIG6, POWHEG with both HERWIG6 and PYTHIA, MADGRAPH with PYTHIA, ALPGEN with HERWIG6, and SHERPA. There are different levels of agreement among generators and with the data, whose discussion is outside the scope of this work; here, we concentrate on MC@NLO, since the relevant formalism is the same as that used in NLO+PS simulations in MADGRAPH5_AMC@NLO. Before going into the details, let us define the main quantity that we shall study, namely the gap fraction for the p_T of the hardest jet. In order to be definite, we shall use the same setup as in ref. [350] (which is CMS’s at the 8 TeV LHC): jets are reconstructed with the anti- k_T algorithm with $R = 0.5$, and the following cuts are imposed:

$$p_T(\ell) \geq 20 \text{ GeV}, \quad |\eta(\ell)| \leq 2.4, \quad p_T(j_b) \geq 30 \text{ GeV}, \quad |\eta(j_b)| \leq 2.4, \quad (4.10)$$

on both charged leptons, and on the two hardest b -jets. Other type of cuts (e.g. lepton isolation) are seen to be unimportant, and are not imposed here. We then define:

$$\text{GF}_{p_T(j_1)}(Q) = \frac{1}{\sigma} \int d\Phi \Theta(Q - \hat{p}_T(j_1)) \frac{d\sigma}{d\Phi}, \quad (4.11)$$

where σ is the cross section within the cuts of eq. (4.10), and for the notation of the argument of the gap fraction we adopt one similar to that of ref. [348], which is not liable to generate confusion. We have also introduced:

$$\hat{p}_T(j_1) = \begin{cases} p_T(j_1) & p_T(j_1) \geq 30 \text{ GeV} \text{ and } \eta_{\min} \leq |\eta(j_1)| \leq \eta_{\max}, \\ 0 & \text{otherwise,} \end{cases} \quad (4.12)$$

with j_1 the hardest jet which is neither of the two b -jets on which the cuts of eq. (4.10) are applied. Note that if there is no jet harder than 30 GeV in the pseudorapidity interval

(η_{\min}, η_{\max}), eq. (4.12) implies that the Θ function in eq. (4.11) is identically equal to one. Therefore, $\text{GF}_{p_T(j_1)}(Q)$ is a constant for $Q < 30$ GeV, equal to the fraction of events which do not have any jet harder than 30 GeV in the relevant pseudorapidity interval: for this reason, gap fractions are not displayed in this range. The quantity $\hat{p}_T(j_1)$ in eq. (4.11) can be replaced by a function, defined analogously to what is done in eq. (4.12) in terms of any observable \mathcal{O} with mass dimension equal to one; in this way, one constructs a different type of gap fraction, $\text{GF}_{\mathcal{O}}(Q)$. The transverse momentum of the second-hardest jet [350], and H_T [348, 350] have been considered in the literature; they are rather strongly correlated with $p_T(j_1)$, and will not be investigated any further here.

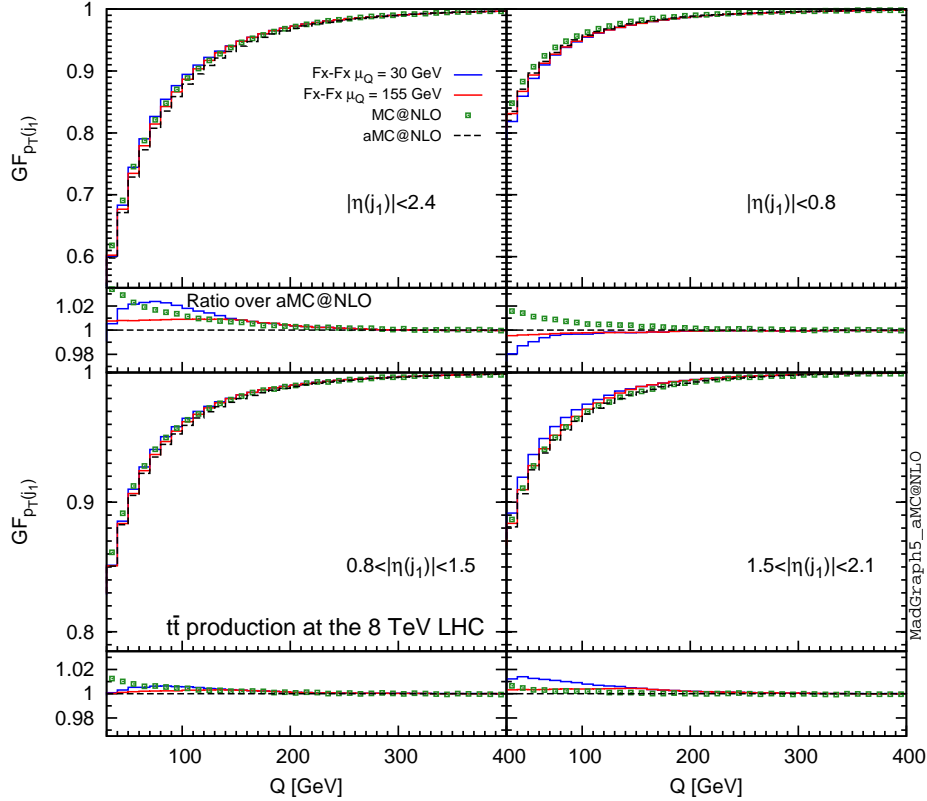


Figure 13: Gap fraction for the p_T of the hardest jet, in four different pseudorapidity intervals, as predicted by FxFx-merged, unmerged (labelled aMC@NLO), and MC@NLO simulations. The setup follows closely that of ref. [350]. See the text for details.

We now aim to compare the NLO+PS predictions of the MC@NLO program (v4.09) with those obtained with MADGRAPH5_AMC@NLO (both NLO+PS and FxFx-merged), which is interesting in two respects. Firstly, the unmerged NLO+PS results of the two codes would be identical, were it not for the fact that in the latter we have included the effect of the function D (see eq. (2.113)); therefore, any difference between the two is the signal of matching systematics⁵⁷. Secondly, the comparison between unmerged $t\bar{t} + 0j$ and FxFx simulations helps assess the impact of the inclusion of matrix elements of

⁵⁷There may be other very tiny differences between MC@NLO and MADGRAPH5_AMC@NLO

higher order in the latter. We have adopted HERWIG6 as PSMC, and the FxFx-merged simulations have been performed for two extreme choices of the merging scale, $\mu_Q = 30$ and 155 GeV. The results for the hardest-jet gap fraction are presented in fig. 13, for the same four pseudorapidity intervals $(\eta_{\min}, \eta_{\max}) = (0, 2.4)$, $(0, 0.8)$, $(0.8, 1.5)$, and $(1.5, 2.1)$ as in ref. [350]; the insets display the ratios of the MC@NLO v4.09 and FxFx-merged results over the unmerged MADGRAPH5_AMC@NLO ones. We first observe that all predictions are quite close to each other, the largest deviation being about 3%. Interestingly, some of the largest relative differences are between the two unmerged predictions, which implies that the matching systematics is not negligible. In general, MADGRAPH5_AMC@NLO predicts more jet activity (i.e., a lower curve) at NLO+PS than MC@NLO v4.09 in the central and widest pseudorapidity regions, this difference decreasing with increasing η_{\min} . This appears to be fairly consistent with what is seen in the 8-TeV CMS data (compare the upper left corner of fig. 13 with fig. 7 in ref. [350], and the other panels of fig. 13 with the upper row of fig. 8 in ref. [350]), whose analysis we have followed here. A similar trend as NLO+PS of MADGRAPH5_AMC@NLO is seen in the FxFx-merged result with $\mu_Q = 155$ GeV, while that obtained with $\mu_Q = 30$ GeV follows a slightly different pattern. Although these findings are encouraging, it is certainly too early to draw any firm conclusions; preliminarily, we can observe that the inclusion of more matrix-elements results into matched predictions seems to be beneficial (be either through an NLO-merging procedure, or because the D function limits the impact of the HERWIG6 shower to smaller scales than it happens in MC@NLO). Furthermore, even by choosing an extremely large range for the merging scale, the FxFx systematics is smaller than that of the MLM-type merging in MADGRAPH5_AMC@NLO (see the results labelled MADGRAPH in ref. [350]). We shall in fact see below another clear example of the pattern of the reduction of the merging systematics when going from the LO to the NLO.

◆ Multi-parton merged predictions

We now turn to illustrate some results of the FxFx merging which are directly relevant to the unitarity and the merging-scale-choice arguments which have been discussed in general at the end of sect. 2.4.5. We shall do so by using an example which one expects to be critical from these viewpoints, namely Higgs production in gluon-gluon fusion (in HEFT) at the 8 TeV LHC, since such a process is characterised by very large higher-order corrections and by a very significant amount of radiation in PSMCs. As was done in ref. [188], we shall also compare to the predictions obtained with ALPGEN, which we shall take as a benchmark for the typical behaviour of LO merging procedures; we have used HERWIG6 as PSMC. We start by presenting in table 12 the results for the fully inclusive rates, both in the absence of cuts (upper two rows), and by imposing the presence of at least two jets (lower two rows): the latter are defined by means of the anti- k_T algorithm with $R = 0.4$, and have to obey the following conditions:

$$p_T(j) \geq 25 \text{ GeV}, \quad |\eta(j)| \leq 5. \quad (4.13)$$

NLO+PS predictions, owing to possibly non-identical choices of parameters, which are negligible for all purposes.

		$\mu_Q = 20 \text{ GeV}$	$\mu_Q = 30 \text{ GeV}$	$\mu_Q = 50 \text{ GeV}$	$\mu_Q = 70 \text{ GeV}$
no cuts	FxFx	14.47(−0.6%)	14.56	14.77(+1.5%)	14.78(+1.5%)
	ALPGEN	8.84(−0.9%)	8.92	9.08(+1.8%)	9.07(+1.7%)
two jets	FxFx	1.65(+0.8%)	1.63	1.60(−2.4%)	1.55(−5.4%)
	ALPGEN	1.27(+13.2%)	1.12	1.01(−9.5%)	0.92(−18.4%)

Table 12: Total rates (in pb) for single-Higgs production in gluon-gluon fusion in HEFT, resulting from FxFx-merged (with up to two extra partons at the NLO) and ALPGEN (with up to three extra partons at the LO) samples. Fractional differences w.r.t. the corresponding results obtained with $\mu_Q = 30 \text{ GeV}$ are also reported.

The rates have been obtained by considering four different values for the merging scale, which cover the very large range $\mu_Q \in (20, 70) \text{ GeV}$. In order to be definite, we shall take $\mu_Q = 30 \text{ GeV}$ as our central value; in table 12, we report in parenthesis the fractional difference of all results obtained with $\mu_Q \neq 30 \text{ GeV}$ w.r.t. those obtained with $\mu_Q = 30 \text{ GeV}$ that appear in the same row. The rates in absence of jet cuts are seen to be extremely stable against merging-scale variations. LO results have an only marginally-larger μ_Q dependence, which is in any case much smaller than the scale uncertainty (not shown here); the same applies to NLO predictions. The NLO fully-inclusive rate for the unmerged $H + 0j$ sample is 13.40 pb: it is therefore from 8% to 10% lower than the FxFx-merged results. Thus, despite the fact that FxFx does not impose any unitarity condition, the merged predictions are “naturally” quite close to the unmerged one. They are not equal, nor they should be – at the end of the day, we are including here contributions up to $\mathcal{O}(\alpha_s^5)$. The increase in the cross section when passing from unmerged to merged results is rather consistent with expectations based on perturbative scaling, and the known large NNLO/NLO K factor that characterises the Higgs-production mechanism we study here. We stress that this feature is not an accident of this process, since we have observed it in all cases studied so far (see later for further examples). When considering rates obtained within the cuts of eq. (4.13), we see that the NLO results are still quite stable, while the merging-scale dependence of the LO ones becomes sizable. In order to further investigate this matter, we present in fig. 14 the Higgs transverse momentum spectra, obtained with FxFx and ALPGEN for the same four merging scales as before; the insets display the ratios of the various curves over the $\mu_Q = 30 \text{ GeV}$ corresponding ones. Obviously, the μ_Q -dependence pattern reflects that of table 12. However, it is interesting to see that when no jet cuts are applied there is a significant compensation in terms of rates in the ALPGEN curves (this can be clearly seen in the ratio plot, with the presence of a crossing point at a $p_T(H)$ of about 70 GeV) – in other words, the very small μ_Q dependence of the LO total rates is partly an artifact, since locally in the phase space the various predictions differ by a larger amount. To some extent, the same is true for the FxFx-merged results, but the effects are much more modest there. Note that, when jet cuts are applied, this phenomenon does not occur any longer, and local and global merging-scale dependences are quite similar:

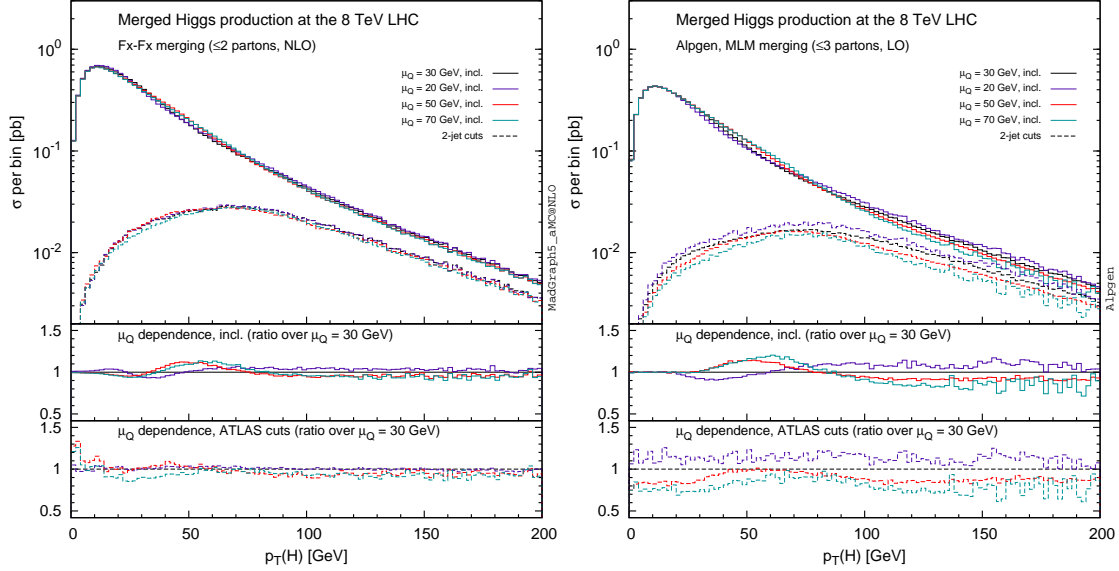


Figure 14: Higgs transverse momentum in single-Higgs production (gluon-gluon fusion in HEFT), as predicted by FxFx (left panel) and ALPGEN (right panel), for various choices of the merging scale μ_Q .

in particular, one sees how all the NLO curves are close to each other also within these cuts. The significance of this (in)dependence is tightly related to the range chosen for the merging scale variation. The function $\log(\mu_Q/m_H)$, which one may take as an indicator of the typical quantity relevant when the merging scale is varied, changes by a factor of 3.16 in the range (20, 70) GeV considered here; we believe that this is a sufficiently-large range to give a sensible indication of merging-scale systematics. As the results presented here clearly show, the supposed spoiling of some underlying NLO accuracy that occurs when “large” values of μ_Q are adopted is simply not an issue if NLO and MC predictions are properly merged, and are reasonably consistent with each other. The latter is in fact a key point: we have observed that, by imposing VBF-type cuts, e.g.:

$$M_{j_1 j_2} \geq 400 \text{ GeV}, \quad |\Delta y_{j_1 j_2}| \geq 2.8, \quad (4.14)$$

the mild dependences shown in table 12 become huge (of the order of 80% and 70% at the LO and NLO respectively). It is clear that the invariant-mass cut of eq. (4.14) introduces a third scale in the game which renders its treatment a complicated matter. Given that such a large merging-scale dependence is basically driven by the largest μ_Q ’s, the problem is likely due to intrinsic differences between the PSMC and matrix-element descriptions of the VBF region. However, we are able to immediately notice this *only* because we have considered a relatively large range of μ_Q , which does not give any issues for sufficiently inclusive quantities, but it does when VBF cuts are applied. We conclude by pointing out that the uncovering of this issue by means of merging-scale systematics does not imply its most naive solution, which would be that of restricting, to small values, the range of μ_Q in this kinematic region, thus relying on a matrix-element-dominated description: in

	$\mu_Q^{(\downarrow)}$	$\mu_Q^{(c)}$	$\mu_Q^{(\uparrow)}$	unmerged
$pp \rightarrow e^+ \nu_e$	7059(−0.9%)	7121	7160(+0.5%)	7067(−0.8%)
$pp \rightarrow ZZ$	7.383(−0.01%)	7.384	7.387(+0.04%)	7.355(−0.4%)
$pp \rightarrow He^+ \nu_e$	0.05180 (+0.9%)	0.05131	0.05117(−0.2%)	0.05066(−1.3%)

Table 13: Total rates (in pb) for three processes, computed with FxFx by using three different merging scales (whose values are process-dependent, see eqs. (4.15)–(4.17)), and with the unmerged lowest-multiplicity samples. Relative differences w.r.t the FxFx results obtained with the central merging scales are also reported.

fact, such a description is not necessarily better than a PSMC one in the context of the multi-scale dynamics induced by eq. (4.13) and (4.14).

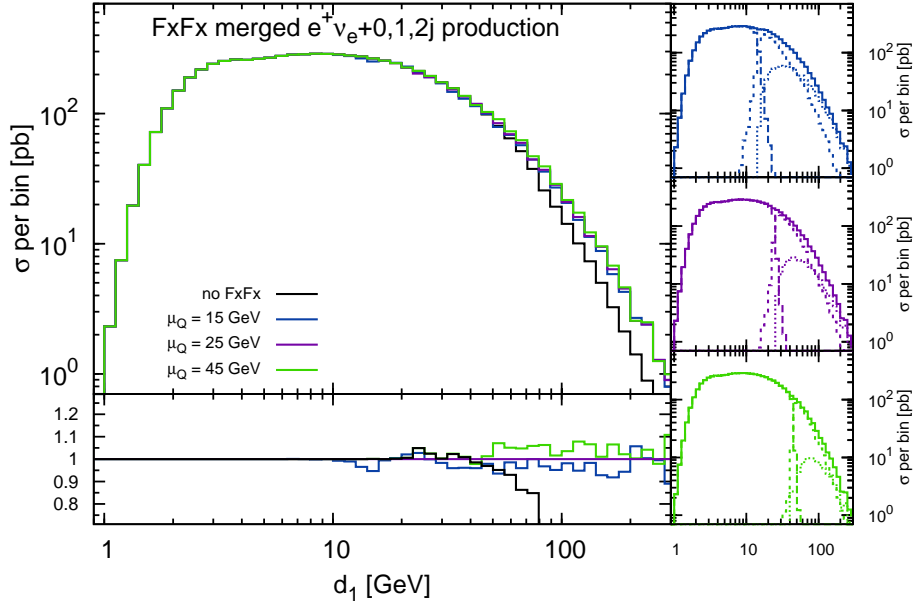


Figure 15: One-jet rate in $e^+ \nu_e$ production. The main frame presents the three FxFx-merged predictions as well as the unmerged one. The lower inset displays the ratios of these curves over the central FxFx-merged one. The insets to the right show the separate contributions of the unphysical 0- (long-dashed), 1- (dashed), and 2-parton (dotted) samples, for the three merging scales.

In order to further the previous arguments, and as a way to validate the FxFx merging procedure with a special attention to cases where the construction of the Sudakovs that enter eqs. (2.139)–(2.141) is involved owing to the flavour structure of the hard process, we consider here three different final states, namely $e^+ \nu_e$, ZZ , and $He^+ \nu_e$, which we simulate at the 8 TeV LHC. In FxFx we include the 0-, 1-, and 2-parton samples for the former process, and the 0- and 1-parton samples for the latter two. In all cases, the unmerged

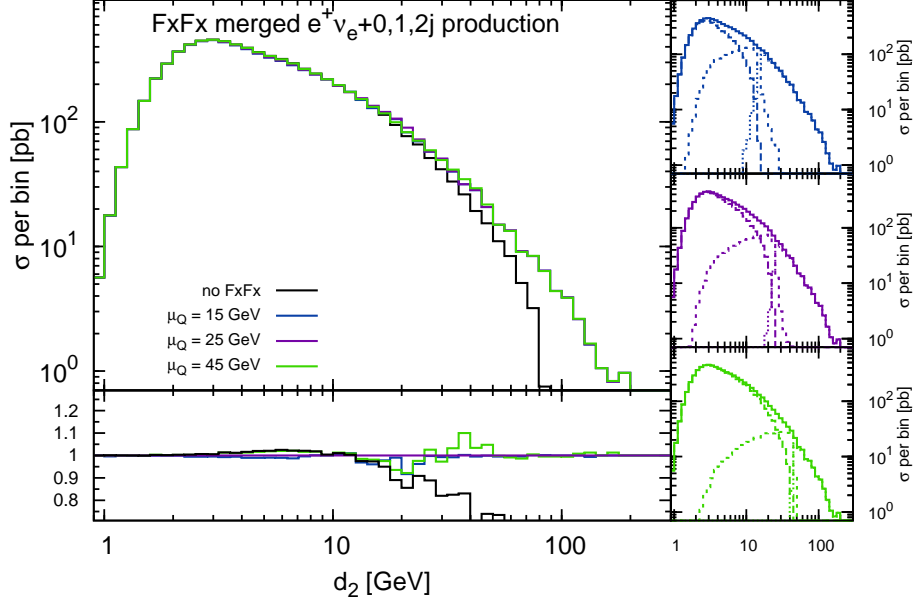


Figure 16: As in fig. 15, for the two-jet rate in $e^+\nu_e$ production.

0-parton results are also presented. All merged and unmerged samples are showered with HERWIG6. We start with the fully-inclusive rates, reported in table 13; the values of the three merging scales are as follows:

$$(\mu_Q^{(\downarrow)}, \mu_Q^{(c)}, \mu_Q^{(\uparrow)}) = (15, 25, 45) \text{ GeV} \quad pp \rightarrow e^+\nu_e, \quad (4.15)$$

$$= (45, 65, 105) \text{ GeV} \quad pp \rightarrow ZZ, \quad (4.16)$$

$$= (50, 75, 100) \text{ GeV} \quad pp \rightarrow He^+\nu_e, \quad (4.17)$$

which cover quite wide ranges. The message emerging from the table is analogous to that relevant to Higgs production, which we have discussed previously: the merging-scale dependence is very small. Furthermore, the unmerged results are extremely close to the merged one, in fact much closer than in the case of $gg \rightarrow H$; this is a natural consequence of the relatively small (compared to Higgs) K factors for the present processes. Again, this fact emerges naturally, without the need to impose any unitarity condition in the merging. We conclude by showing some selected differential distributions, and in particular the j -jet rates of the k_T algorithm (denoted by d_j , see eq. (2.131)); these quantities are known to be critical in the context of merging procedures, since they are very sensitive to artefacts of the latter, which show up as discontinuities in the spectra. Our results are presented in figs. 15–18, where the main frames display the predictions in absolute values. The lower insets display the ratios of the FxFx-merged and unmerged predictions over the FxFx one obtained with the central merging-scale values. The insets at the right of the figures show the way in which the i -parton samples combine in order to give the physical curves. All results for all processes behave as expected.

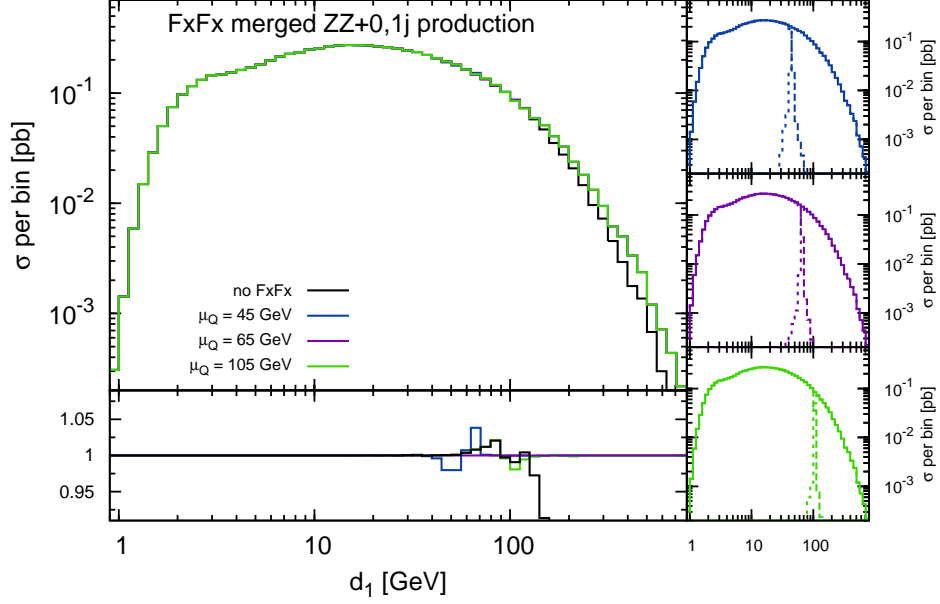


Figure 17: As in fig. 15, for the one-jet rate in ZZ production. Only the 0- and 1-parton samples have been considered here.

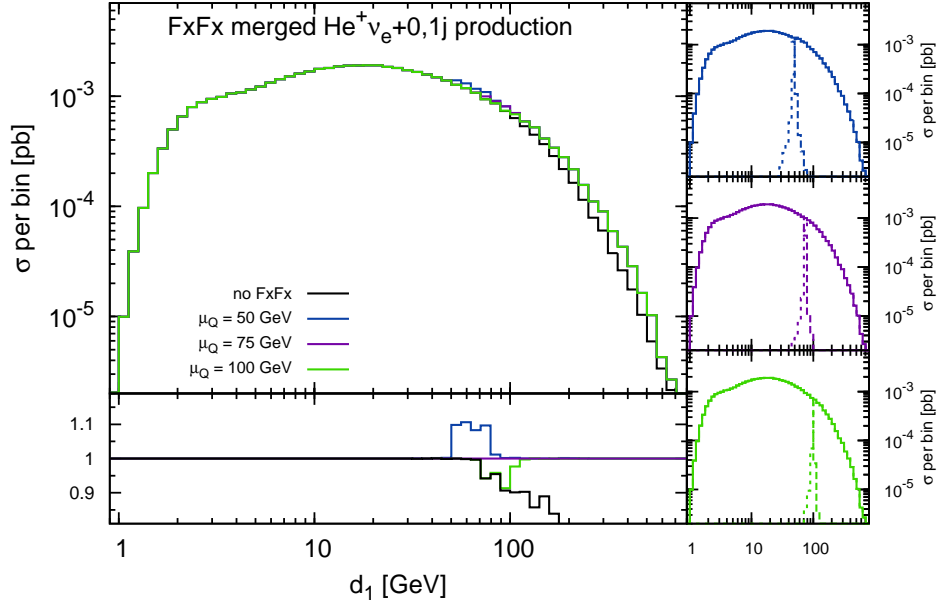


Figure 18: As in fig. 15, for the one-jet rate in $He^+\nu_e$ production. Only the 0- and 1-parton samples have been considered here.

4.3 One-loop SM and BSM results: a look ahead

All the results presented in sects. 4.1 and 4.2 exploit the one-loop computations performed

by the public version of MADLOOP5, which amply demonstrates the reach and flexibility of this code. The aim of this section is on the other hand that of showing that the current, still-private MADLOOP5 program has a much larger scope, being able to handle computations of very high complexity also in the context of a mixed-coupling expansion (see sect. 2.4), and in theories other than the SM. As was already discussed, while the corresponding capabilities on the real-emission side have not yet been fully validated in MADGRAPH5_AMC@NLO, they do not pose any problem of principle, and only minor ones from the technical point of view; therefore, the results presented below constitute the proof that the major obstacles have been cleared which prevent MADGRAPH5_AMC@NLO from performing NLO computations in arbitrary renormalisable theories.

We shall give here benchmark results for given phase-space configurations. They will be presented in the form of the coefficients c_j , $j = -2, -1, 0$, introduced in eq. (2.88) for V , the colour- and helicity-summed virtual amplitude contracted with the corresponding Born one (see eq. (2.55)). We shall also denote by a_0 the Born amplitude squared:

$$a_0 = \sum_{\substack{\text{colour} \\ \text{spin}}} \left| \mathcal{A}^{(n,0)} \right|^2, \quad (4.18)$$

where, similarly to V , the averages over initial-state colour and spin degrees of freedom are understood. Throughout this section, we have set $\mu \equiv Q = \mu_F = \mu_R = \sqrt{s}$, and all particles widths equal to zero for simplicity; the leptons that circulate in the loops are taken to be massless. In order to maximize the numerical accuracy, the computations reported here have been performed by using quadruple-precision arithmetics; the stability tests described in sect. 2.4.2 have shown that these results are numerically stable beyond the seventeen digits quoted below. The coefficients c_j are computed in the 't Hooft-Veltman scheme and, in the case of the pole residues c_{-2} and c_{-1} , compared to their analytically-known forms (see e.g. eq. (B.2) of ref. [59], whose generalisation to cases other than QCD is straightforward). Units for quantities of canonical dimension equal to one are understood to be GeV. The CKM matrix is diagonal. The integral-reduction OPP procedure has been adopted in all cases; processes C) and D) have also been computed with TIR (using IREGI), and perfect agreement with the OPP results has been found. We point out that processes A) and B) feature 8- and 7-point rank-5 loop integrals respectively, and are therefore beyond the present capabilities of any TIR library. Further technical details relevant to the calculations presented in this section are given in appendix C.2. We emphasise that the one-loop results shown here have never been presented in the literature, and can serve as benchmarks for comparisons with future independent computations.

A) High-multiplicity multi-scale QCD process: $gg \rightarrow d\bar{d}b\bar{b}t\bar{t}$

This process involves up to 8-point loop diagrams with three external scales: the top- and bottom-quark masses, and the partonic c.m. energy. A total of 54614 loop diagrams contribute, and all pure-QCD UV renormalisation counterterms are necessary, which makes it an excellent test case for MADLOOP5. The following parameters have been used:

Parameter	value	Parameter	value
α_s	0.118	n_{lf}	4
m_t	173.0	m_b	4.7

The kinematic configuration considered is (we use an (E, p_x, p_y, p_z) notation):

$p_g = ($	500	$,$	0	$,$	0	$,$	500	$)$
$p_{\bar{g}} = ($	500	$,$	0	$,$	0	$,$	-500	$)$
$p_d = ($	159.884957663500	$,$	-100.187853644511	$,$	83.9823400815702	$,$	92.0465111972672	$)$
$p_{\bar{d}} = ($	203.546206153656	$,$	-154.329441032052	$,$	-0.512510195103158	$,$	132.714803257139	$)$
$p_b = ($	81.9036633616240	$,$	4.56741073895954	$,$	-80.4386221767117	$,$	13.9601895942747	$)$
$p_{\bar{b}} = ($	41.5312244194448	$,$	6.99982274816896	$,$	9.96034329509376	$,$	39.4277395334349	$)$
$p_t = ($	239.961310957973	$,$	84.0110736983121	$,$	18.3862699981019	$,$	-142.325385396572	$)$
$p_{\bar{t}} = ($	273.172637443802	$,$	158.938987491122	$,$	-31.3778210029510	$,$	-135.823858185543	$)$

For the $\mathcal{O}(\alpha_s^6)$ Born matrix element and $\mathcal{O}(\alpha_s^7)$ V coefficients we have obtained:

$gg \rightarrow d\bar{d}b\bar{b}t\bar{t}$	
a_0	1.7614866952133752e-14
c_0	7.1888721656398052e-14
c_{-1}	-3.8948541926529643e-15
c_{-2}	-2.8670389920110557e-15

The relevant MADGRAPH5_AMC@NLO-shell generation command is:

```
MG5_aMC> generate g g > d d~ b b~ t t~ [virt=QCD]
```

More details on this syntax can be found in appendix B.1. After the generation phase, the usual `output` and `launch` commands are executed. We point out, however, than in the present context (i.e., when one computes one-loop matrix elements pointwise), `launch` allows the user to specify the kinematic configuration for which the said matrix elements are to be computed.

B) Mixed-coupling expansion: $u\bar{d} \rightarrow d\bar{d}W^+ZH$

The Born matrix elements for this process receive contributions at $\mathcal{O}(\alpha_s^2\alpha^3)$, $\mathcal{O}(\alpha_s\alpha^4)$, and $\mathcal{O}(\alpha^5)$, resulting from $\mathcal{O}(g_s^2e^3)$ and $\mathcal{O}(e^5)$ amplitudes. In the notation of sect. 2.4, this corresponds to $k_0 = 5$, $c_s(k_0) = 0$, $c(k_0) = 3$, and $\Delta(k_0) = 2$. We have considered the full set of NLO corrections, thus obtaining four terms of $\mathcal{O}(\alpha_s^n\alpha^m)$, with $0 \leq n \leq 3$ and $m = 6 - n$ (see eqs. (2.22) and (2.23)). This process features essentially all complications one faces in the case of a mixed QCD-EW expansion, and in particular it tests fully the UV- and R_2 -related machinery, described in sect. 2.4.2, beyond the pure-QCD cases considered so far. From a technical viewpoint, the major challenges are represented by the fact that genuine EW corrections (as opposed to QCD corrections to processes that may feature EW external particles) significantly complicate the flavour structure of the diagrams (whose number therefore grows and which always pose a multi-scale problem),

and by the necessity of keeping separate track of the $\Sigma_{k_0+1,q}$ coefficients of eq. (2.23). We have performed our computation in the Feynman gauge, with an $(\alpha(m_Z), m_Z, m_W)$ input scheme for the EW parameters, and adopted the $\alpha(m_Z)$ renormalisation scheme [351] (we point out that the G_μ scheme [351, 352] is also available in MADLOOP5). The full set of inputs is thus:

Parameter	value	Parameter	value
α_S	0.118	n_{lf}	5
m_t	173.0	y_t	173.0
m_W	80.419	m_Z	91.188
m_H	125.0	α^{-1}	132.507

The kinematical configuration is:

$$\begin{aligned}
p_u &= (500 & , 0 & , 0 & , 500 &) \\
p_{\bar{d}} &= (500 & , 0 & , 0 & , -500 &) \\
p_d &= (77.3867935143263 & , -13.6335837243927 & , 33.7255664483738 & , -68.3039338032245 &) \\
p_{\bar{d}} &= (251.029839835656 & , -74.4940380485791 & , -235.871950829717 & , 42.7906718212678 &) \\
p_{W^+} &= (139.739680522225 & , -81.0565319364851 & , -74.5408139008771 & , 30.5527158347332 &) \\
p_Z &= (382.164100735946 & , 208.038848497860 & , 298.200182616267 & , -74.3682536477996 &) \\
p_H &= (149.679585391847 & , -38.8546947884028 & , -21.5129843340470 & , 69.3287997950232 &)
\end{aligned}$$

The corresponding Born results are:

$u\bar{d} \rightarrow d\bar{d}W^+ZH$	a_0
$\mathcal{O}(\alpha_s^2\alpha^3)$	2.8791434190645365e-16
$\mathcal{O}(\alpha_s\alpha^4)$	-4.2378807039987007e-17
$\mathcal{O}(\alpha^5)$	5.8013051661550053e-18

where the $\mathcal{O}(\alpha_s\alpha^4)$ interference term happens to be negative, while at one loop we obtain:

$u\bar{d} \rightarrow d\bar{d}W^+ZH$	$\mathcal{O}(\alpha_s^3\alpha^3)$	$\mathcal{O}(\alpha_s^2\alpha^4)$
c_0	-4.9670212643498834e-17	3.5197577360529166e-18
c_{-1}	-1.0437771535958436e-16	1.5619709675879874e-17
c_{-2}	-2.8837935481452971e-17	3.9757576347989499e-18
	$\mathcal{O}(\alpha_s\alpha^5)$	$\mathcal{O}(\alpha^6)$
c_0	2.3220780285374270e-18	-1.4592469761033279e-18
c_{-1}	-1.8146075843176133e-18	-5.0799804067050324e-21
c_{-2}	-5.4147748433007504e-19	-5.4195415714279579e-21

The relevant MADGRAPH5_AMC@NLO-shell generation command is:

```
MG5_aMC> generate u d~ > d d~ w+ z h QCD=99 QED=99 [virt=QCD QED]
```

where the `QCD=99 QED=99` bit instructs MADLOOP5 to consider the corrections to all Born-level contributions, and not only to the leading (QCD) $\mathcal{O}(\alpha_s^2\alpha^3)$ one, while the `[virt=QCD QED]` syntax implies that both QCD and QED/EW corrections need to be included. More details on this extended syntax can be found in appendix B.1.

C) Mixed-coupling expansion: $u\bar{u} \rightarrow d\bar{d}t\bar{t}$

Although the one-loop corrections to this process feature a smaller number of diagrams than those relevant to $u\bar{d} \rightarrow d\bar{d}W^+ZH$ studied above, owing to the fact that the corresponding Born amplitudes have three quark lines the mixed-coupling expansion ladder depicted in fig. 1 is wider: we have in fact $\Delta(k_0) = 4$, with $k_0 = 4$, $c_s(k_0) = 0$, $c(k_0) = 0$. The input-parameter and scheme choices are the same as those adopted in the case of $u\bar{d} \rightarrow d\bar{d}W^+ZH$ production, while the kinematic configuration is:

$$\begin{aligned}
p_u &= (500 & , 0 & , 0 & , 500 &) \\
p_{\bar{u}} &= (500 & , 0 & , 0 & , -500 &) \\
p_d &= (77.6887158960956 & , -19.3895923374881 & , 35.1636848900680 & , -66.5063572263756 &) \\
p_{\bar{d}} &= (288.053156184158 & , -91.1103505191485 & , -264.895455921162 & , 67.1112676698377 &) \\
p_t &= (218.623451637725 & , -92.8925122931906 & , -85.7235692614867 & , 43.4702707482150 &) \\
p_{\bar{t}} &= (415.634676282022 & , 203.392455149827 & , 315.455340292580 & , -44.0751811916771 &)
\end{aligned}$$

We thus obtain at the Born level:

$u\bar{u} \rightarrow d\bar{d}t\bar{t}$	a_0
$\mathcal{O}(\alpha_s^4)$	8.0443110796911884e-10
$\mathcal{O}(\alpha_s^3\alpha)$	-4.1964024114099949e-11
$\mathcal{O}(\alpha_s^2\alpha^2)$	3.2368049995513863e-11
$\mathcal{O}(\alpha_s\alpha^3)$	-7.9030872133243511e-13
$\mathcal{O}(\alpha^4)$	1.8667390802029741e-13

while the one-loop coefficients turn out to be:

$u\bar{u} \rightarrow d\bar{d}t\bar{t}$	$\mathcal{O}(\alpha_s^5)$	$\mathcal{O}(\alpha_s^4\alpha)$
c_0	2.7744575300036875e-10	-6.1309409133299879e-11
c_{-1}	-2.4891722473717473e-10	5.1973614496390480e-12
c_{-2}	-8.0573035150936874e-11	3.1296167547367972e-12
	$\mathcal{O}(\alpha_s^3\alpha^2)$	$\mathcal{O}(\alpha_s^2\alpha^3)$
c_0	1.2122291790182845e-11	-4.0611498141889722e-12
c_{-1}	-8.6161115635612362e-12	4.3209683736654367e-15
c_{-2}	-3.1860291930204890e-12	3.5961341456741816e-14
	$\mathcal{O}(\alpha_s\alpha^4)$	$\mathcal{O}(\alpha^5)$
c_0	-3.8642357648130340e-14	-1.1866388556893426e-14
c_{-1}	-3.6050223887148020e-14	-4.7983631557836333e-16
c_{-2}	-1.7642824564621470e-14	-2.4912793041300221e-16

The relevant MADGRAPH5_AMC@NLO-shell generation command is:

```
MG5_aMC> generate u u~ > d d~ t t~ QCD=99 QED=99 [virt=QCD QED]
```

D) A BSM case study: QCD corrections to $gg \rightarrow \tilde{t}_1 \tilde{t}_1^* g$

While MADLOOP has been used to compute one-loop corrections to a very large number of processes in the SM, its applications to other theories have been pretty limited so far. Here, we present the first MADLOOP5 results in a fully-fledged BSM model; namely, we compute QCD corrections to $\tilde{t}_1 \tilde{t}_1^* g$ production in the MSSM. From the technical point of view, the MSSM UFO model at the NLO is immensely complicated, and its writing by hand (which has been the procedure adopted for the SM) is inconceivable: we have therefore obtained it by using a development version of FEYNRULES. All massive modes are subtracted at zero momentum, following the same strategy as e.g. in ref. [353]. It should be pointed out that some of the elementary expressions and structures of such a model (related e.g. to the presence of Majorana fermions) are not featured in any other UFO model employed so far. For this reason, we have double checked our MADLOOP5 results against a completely independent calculation performed with MATHEMATICA. This guarantees that the elementary building blocks are correct, thus rendering analogous tests more and more irrelevant in the future. We have chosen the input parameters as follows:

Parameter	value	Parameter	value
α_S	0.118	n_{lf}	4
m_b	4.75	m_t	175
m_W	79.82901	m_Z	91.1876
$m_{\tilde{g}}$	607.7137	$\tan \beta$	9.748624
$m_{\tilde{u}_1}$	561.119	$m_{\tilde{u}_2}$	549.2593
$m_{\tilde{c}_1}$	561.119	$m_{\tilde{c}_2}$	549.2593
$m_{\tilde{t}_1}$	399.6685	$m_{\tilde{t}_2}$	585.7858
$m_{\tilde{d}_1}$	568.4411	$m_{\tilde{d}_2}$	545.2285
$m_{\tilde{s}_1}$	568.4411	$m_{\tilde{s}_2}$	545.2285
$m_{\tilde{b}_1}$	513.0652	$m_{\tilde{b}_2}$	543.7267

with a diagonal squark-mixing matrix. By using the following kinematic configuration:

$$\begin{aligned}
p_g &= (500 & , 0 & , 0 & , 500) \\
p_g &= (500 & , 0 & , 0 & , -500) \\
p_{\tilde{t}_1} &= (465.457552338590 & , 88.1561012782457 & , 197.510478842819 & , -100.667451003198) \\
p_{\tilde{t}_1^*} &= (442.275748385439 & , -9.53590501776566 & , -180.889189039748 & , 55.3271680251616) \\
p_g &= (92.2666992759711 & , -78.6201962604800 & , -16.6212898030706 & , 45.3402829780365)
\end{aligned}$$

we obtain:

$gg \rightarrow \tilde{t}_1 \tilde{t}_1^* g$	
a_0	2.839872059757065e-4
c_0	-2.081163174420354e-5
c_{-1}	-1.550338075591894e-4
c_{-2}	-4.800024159745521e-5

The relevant MADGRAPH5_AMC@NLO-shell commands are:

```

MG5_aMC> import model loop_MSSM
MG5_aMC> generate g g > t1 t1~ g [virt=QCD]

```

We point out that, similarly to the version of MADLOOP5 used to derive the results presented in this section, the `loop_MSSM` model used here is not yet public.

5. Conclusions and outlook

The motivation for pursuing this project stems from the fact that all aspects of the computations of tree-level and NLO cross sections, including their matching to parton shower simulations, are well understood, in a manner which is fully independent of the process under consideration. Therefore, the best way to make use of this understanding is that of the full automation of such computations. Automation has indeed already proven to be a very successful strategy for obtaining tree-level results, as documented by the theoretical and

experimental activities based on, and spurred by, MADGRAPH. In this paper we have presented the successor of MADGRAPH5, a code that we have named MADGRAPH5_AMC@NLO, which extends the capabilities of the former by giving the user the possibility of computing NLO QCD corrections, if desired in association with parton-shower matching. MADGRAPH5_AMC@NLO is indeed the successor, and not just a plugin, of MADGRAPH5, its main virtue being that of treating tree-level and NLO QCD computations on the very same footing – as far as the user is concerned, the difference between them is a switch in input. In particular, *irrespective* of the perturbative order of the computation, MADGRAPH5_AMC@NLO features the following characteristics: very lean dependencies, simplicity of use, and flexibility. The information that the user has to provide is only related to physics, such as values of masses, couplings, and scales, and the definitions of observables, as well as the hard process one wants to generate.

In the current public version of MADGRAPH5_AMC@NLO the inclusion of higher-order effects is restricted to QCD corrections to SM processes. Such a limitation is mostly due to the fact that, in the context of one-loop computations (performed by MADLOOP or by any other one-loop provider), one needs to take care of the UV renormalisation procedure and (typically, but not always necessarily) of that related to the so-called R_2 counterterms, which are in any case just a simpler version of the former. Both procedures are expressed as a set of rules that can be worked out directly from the Lagrangian, an operation that has to be done only once for a given theory, and that so far has been performed by means of analytical computations. However, all obstacles preventing the automatic computation of the UV and R_2 rules have now essentially been cleared, as hinted by the results we have presented in sect. 4.3. Given that all remaining obstacles are minor and of technical nature, this will allow MADGRAPH5_AMC@NLO to evaluate, in the near future, any type of NLO corrections, starting from the same user-defined Lagrangians that are used in tree-level calculations.

This work shows clearly that automated techniques at the NLO are well past the developmental phase, and are indeed fully established, as was already the case for their tree-level counterparts; we believe that this is amply demonstrated by the results of sect. 4. For the non-trivial cases now of relevance to collider phenomenology, automated computations are more robust, faster by orders of magnitude, and less error-prone than analytical, process-by-process traditional approaches. Furthermore, an increase in complexity generally only requires more CPU power but no conceptually new solutions, one example of such a situation being that of the computation of EW or QCD corrections to supersymmetric processes. As a counterexample, one may mention the calculation of cross sections that feature final states with a very large number of QCD partons, for which dedicated optimisations (such as recursive relations and colour reorganisation, which are being investigated by us) will be needed in order to go beyond what is currently feasible by MADGRAPH5_AMC@NLO.

The ready availability in MADGRAPH5_AMC@NLO of perturbatively-accurate and realistic predictions for an extremely large range of processes of significant complexity should be seen as both solving a few problems, and opening up new and exciting possibilities. Among the former, we would like to mention explicitly the fact that automated tools help free experts in perturbative calculations from spending their resources in the increasingly

involved computations necessary to the experiments, thus allowing them to concentrate on obtaining other, cutting-edge results (such as, to limit oneself to perturbative QCD, calculations of NNLO accuracy with universal subtraction methods, improvements to parton showers, and so forth). As far as future possibilities are concerned, one important characteristic of MADGRAPH5_AMC@NLO to bear in mind is its modularity: we shall be happy to support and help those interested in improving parts of the code and the underpinning physics strategies (such as recursive relations, alternative matching and merging schemes, integral-reduction techniques and libraries). From a phenomenological viewpoint, many different applications of MADGRAPH5_AMC@NLO can be foreseen. The capability of the code to assess systematically and in an easy manner the theoretical uncertainties due to scales, PDFs, and matching and merging methods should be routinely exploited by both theorists and experimentalists. The fact of having a basically unlimited set of processes predicted at the NLO accuracy has two immediate consequences: it gives one the chance of extracting the PDFs by using a much wider set of observables than employed at present, at the same time possibly including EW and parton-shower effects; and that of finally achieving PSMC tunings that properly include NLO results. Exploratory studies at future colliders, such as circular or linear e^+e^- ones, or very-high-energy hadron machines, can also be performed without the need of a dedicated effort. Finally, it is hard to predict the kind of applications that will be relevant to BSM physics. In any case, extending the current flexibility of MADGRAPH5_AMC@NLO for SM processes to new-physics models, be they renormalisable or effective, and thus being able to readily investigate the implications of any theory, will certainly be crucial in current and future analyses.

Acknowledgements

We are grateful to Roberto Pittau for his support of CUTTOOLS, to Stefan Prestel for his dedicated help with the NLO matching to PYTHIA8 and for discussions on related topics, to Matteo Cacciari for his help and support with FASTJET (CORE), to Andreas Papaefstathiou for his dedicated help with HERWIG++, to Simon Badger, Daniel Maitre, and Markus Schulze for clarifications concerning bootstrap and D -dimensional unitarity methods, to Markus Cristinziani and Roberto Chierici for information on top-physics measurements by ATLAS and CMS, to Adam Alloul, Neil Christensen, Celine Degrande, Claude Duhr and Benjamin Fuks for their collaboration to BSM developments and support of FEYNRULES, to Frank Krauss for explanations on the use of the MC@NLO method in SHERPA, to Simon de Visscher for his help with LO merging, to Pierre Artoisenet and Robbert Rietkerk for their work on MADSPIN, to Valery Yundin and Andreas van Hameren for their support of PJFRY++ and ONELOOP, to Diogo Buarque Franzosi for his collaboration on the implementation of the complex mass scheme, to Alexis Kalogeropoulos for his contributions in developing and testing large-scale event production, to Kentarou Mawatari for many fruitful collaborations, to Stefano Pozzorini, Peter Skands and Torbjörn Sjöstrand for useful clarifications, to Josh Bendavid, Vitaliano Ciulli, and Sanjay Padhi for the very useful feedback on the use of the code, and to Michelangelo Mangano for his support and insight. We are thankful to our cluster management team, Jérôme de Favereau, Pavel

Demin, and Larry Nelson, for their help and collaboration over the years. FM and TS are particularly thankful to Kaoru Hagiwara for the constant support and many insightful suggestions since the very beginning of the MADGRAPH project. SF wishes to thank Bryan Webber for his collaboration, over the course of many years, on several of the topics discussed in this paper. The authors not based at CERN are grateful to the PH/TH Unit for the support and hospitality in many different occasions. This work has been supported in part by and performed in the framework of the ERC grant 291377 “LHCtheory: Theoretical predictions and analyses of LHC physics: advancing the precision frontier”, supported in part by the Swiss National Science Foundation (SNF) under contract 200020-149517, by the European Commission through the “LHCPhenoNet” Initial Training Network PITN-GA-2010-264564, by the Research Executive Agency (REA) of the European Union under Grant Agreement number PITN-GA-2012-315877 (MCNet). The work of FM and OM is supported by the IISN “MadGraph” convention 4.4511.10, by the IISN “Fundamental interactions” convention 4.4517.08, and in part by the Belgian Federal Science Policy Office through the Interuniversity Attraction Pole P7/37. OM is “Chercheur scientifique logistique postdoctoral F.R.S.-FNRS”, and wishes to thank the IPPP Durham for the kind hospitality extended to him during his stay there. The work of FM has been supported by the Francqui Foundation via a Francqui Research Professorship. The work of MZ has been partly supported by the ILP LABEX (ANR-10-LABX-63), in turn supported by French state funds managed by the ANR within the “Investissements d’Avenir” programme under reference ANR-11-IDEX-0004-02. VH is supported by the SNF with grant PBELP2_146525. This material is based upon work supported in part by the US National Science Foundation under Grant No. PHY-1068326.

A. Technical prerequisites, setup, and structure

MADGRAPH5_AMC@NLO is being developed and is routinely run on a variety of Linux platforms and on Mac OS-X systems. The basic requirements for running the code are the following:

- A `bash` shell;
- `perl` 5.8 or higher;
- `Python` 2.6 or higher, but lower than 3.0;
- `gfortran/gcc` 4.6 or higher; any other modern Fortran/C++ compiler should work, provided it supports computations in quadruple precision.

After downloading the tarball, and unpacking it in what will be called the *main directory* (which will contain several sub-directories, such as `aloha`, `apidoc`, `bin`, and so forth), the code is ready to run. No installation of external packages is mandatory, thanks to the fact that the tarball includes copies of the third-party codes listed in appendix D.

Setup

From a terminal shell in the main directory, type:

```
./bin/mg5_aMC
```

At this point, one has entered the MADGRAPH5_AMC@NLO shell, which is made evident by the fact that the prompt now reads as follows:

```
MG5_aMC>
```

A minimal setup phase may take place here, before generating and running the first process. This phase, that must be done at most once (i.e., it does not have to be repeated before the generation of any process after the first), consists essentially in defining configuration variables. For example, in the case where a local installation of FASTJET were available⁵⁸, the path to it must be known by MADGRAPH5_AMC@NLO: this is achieved by executing the following command:

```
MG5_aMC> set fastjet /<PATH_TO_FASTJET>/bin/fastjet-config
```

Likewise, for the local installation of LHAPDF [354] to be found, one should execute the command:

```
MG5_aMC> set lhapdf /<PATH_TO_LHAPDF>/bin/lhapdf-config
```

Each of these commands associates the given value with a variable in the file:

```
input/mg5_configuration.txt
```

The user can find a list of all possible configuration variables by visiting that file (or by auto-completion with the <TAB> key after typing **set** in the MADGRAPH5_AMC@NLO shell). We point out that each of these variables can be directly edited in the file, as an alternative to executing the **set** command as shown above. More advanced setup options are described in appendix B.1.

Structure

The various subdirectories of the main directory will be of no interest to the regular user. The only possible exceptions are

```
Template/NLO
```

```
Template/LO
```

a copy (with minor differences) of which is created in the subdirectory

```
MYPROC
```

of the main directory upon executing the command:

```
MG5_aMC> output MYPROC
```

after having executed one of the two following commands:

```
MG5_aMC> generate a b > c_1...c_n [QCD]
```

```
MG5_aMC> generate a b > c_1...c_n
```

for the NLO and LO case respectively (see sect. 3). The minor differences in the copy alluded to before are due to the fact that, after the **generate** command has been issued, the program knows e.g. the number of final-state particles (equal to **n** in the examples given here), which is thus explicitly written in some include files in the directory tree of **MYPROC**. In any case, these include files and their analogues must not be modified by the user.

⁵⁸We point out that FASTJET (CORE) is part of the MADGRAPH5_AMC@NLO tarball.

The directory `MYPROC` will be called the *current-process directory*, and all the operations relevant to the process whose generation gave rise to it are performed somewhere in its directory tree. Such operations can roughly be arranged in two classes: input-type, to be performed by the user before the `launch` command, and output-type, performed by `MADGRAPH5_AMC@NLO` after the `launch` command.

The user may consider input-type operations in the following subdirectory:

`MYPROC/Cards`

which contains the input cards (these are in plain text format, and liberally commented) that steer the `MADGRAPH5_AMC@NLO` run (e.g., `run_card.dat`) or control the physical parameters of the theory (e.g., `param_card.dat`). Contrary to other input-type operations, which will be mentioned below, the values of the entries in the input cards can not only be modified by the user by visiting the appropriate cards before the `launch` command, but can also be accessed *after* the `launch` command through an interactive talk-to within the `MADGRAPH5_AMC@NLO` shell. Both accessing modes can be used in the same run; note that the values of the inputs used in the actual run will be those stored in the input cards at the end of the talk-to phase.

Further input-type operations are specific to NLO-type generations, require a minimal knowledge of Fortran, and must be completed before the `launch` command is issued. They will involve editing files in the following subdirectories:

`MYPROC/FixedOrderAnalysis`

`MYPROC/MCatNLO`

`MYPROC/SubProcesses`

The `FixedOrderAnalysis` subdirectory will need to contain the user's fixed-order analysis file(s) relevant to fLO or fNLO runs. The `MCatNLO` subdirectory is used only in the case when the user chooses to steer the shower phase within the `MADGRAPH5_AMC@NLO` framework; when the LHE files produced by `MADGRAPH5_AMC@NLO` are showered externally, such a subdirectory is ignored. If also the showering is steered by `MADGRAPH5_AMC@NLO`, the user will be able to access the drivers of the various event generators, and to write his/her own analysis inside the `MCatNLO` directory tree (whose structure is analogous to that of the `MC@NLO` package, for those familiar with it). Finally, the subdirectory `SubProcesses` contains the codes necessary for the computation of the cross section proper, and specific to the process that has been constructed in the generation step. Typically, the user will not need to modify any of these files; exceptions are those of `setscales.f`, where one defines the functional forms used for dynamic-scale computations (see sect. B.2), and of `cuts.f`, where one sets any desired parton-level cuts (on top of those accessible through `run_card.dat`); both of these files are amply commented.

As far as output-type operations are concerned, these are by definition dealt with by `MADGRAPH5_AMC@NLO`; we shall mainly describe in what follows those relevant to an NLO-type generation. The relevant directories are

`MYPROC/Events/run_*`

There will be as many `run_*` subdirectories as number of runs⁵⁹; the string `*` will feature a run-identification number. These subdirectories will contain the final outputs of the

⁵⁹Runs may e.g. differ by choices of input parameters, or type of physics simulated, such as f(N)LO vs

corresponding MADGRAPH5_AMC@NLO runs, provided that such outputs are in one of the formats recognised by the code. In particular, one will have:

1. For all types of runs: various plain-text files that summarise the inputs used and the results of the integration of the short-distance cross sections.
2. In (N)LO+PS runs: the Les Houches event file(s) that contain hard-subprocess un-weighted events which are to be showered.
3. In (N)LO+PS runs when MADGRAPH5_AMC@NLO is used to steer the shower phase: the final results after shower, provided that these are either: *a)* an `StdHEP/HepMC` file that contains the event records; or *b)* a topdrawer file that contains histograms defined by the user in his/her analysis.
4. In f(N)LO runs: the histograms defined by the user in his/her analysis, provided that their format be either Root or topdrawer.

There is no problem if the format of the output of the user's analysis relevant to the shower phase (when MADGRAPH5_AMC@NLO is used to steer the shower) is not compliant with either 3.a or 3.b. Simply, such an output will not be moved into `MYPROC/Events/run_*`, but will be kept in the directory where the PSMC run has actually been performed. This directory will be named:

`MYPROC/MCatNLO/RUN_MCTYPE.nn`

with `MCTYPE=PYTHIA8` and so forth (depending on the PSMC used), and `nn` an integer number increased by one unity for each new PSMC run.

On the other hand, the use of formats other than Root or topdrawer in f(N)LO runs is deprecated, since it implies some manual operations and the writing of code by the user. The reason is the following: cross sections are integrated by MADGRAPH5_AMC@NLO through multi-channel techniques – this ensures optimal convergence and high degree of parallelisation, but each channel is non-physical (only their sum is). Analysis routines (regardless of the output format) are used by individual channels; hence, their outputs are to be summed⁶⁰. Summing the results of the individual channels is performed automatically by MADGRAPH5_AMC@NLO for Root and topdrawer outputs, via dedicated auxiliary codes; any new format would thus require the user to write a new such code, and a script that finds all single-channel outputs and feed them to his/her summing code.

We conclude this section by stressing again that the source codes which are compiled after executing the command `launch`, and the input cards used throughout the run, are those in the current-process directory tree, and not in the `Template` directory tree. Therefore, any modifications to files in the `Template` directory tree will have no effect on the current run. However, they will affect *all* subsequent process generations, since as clarified at the beginning of this section it is the files in `Template` that form the core of the contents of each current-process directory. Hence, this procedure is reserved to the very experienced users, and we strongly deprecate it.

(N)LO+PS, or the inclusion of spin correlations as predicted by MADSPIN vs stable-particle production.

⁶⁰This assumes the output is a set of histograms. In case of n-tuples, these will need to be combined, possibly after having rescaled their weights.

B. Advanced usage

This section reports on some of the features of MADGRAPH5_AMC@NLO whose understanding allows the user to exploit the full physics potential of the code. It is not meant to be a usage manual, but only to briefly expand on some of the subjects which have been only touched upon in the main text.

B.1 Models, basic commands, and extended options

We start with the following general comment: within the MADGRAPH5_AMC@NLO shell, the <TAB> key plays the same role as in a normal terminal shell: when hitting it, a list of possible completions (e.g., commands relevant to the current context, or completion of the command syntax) is printed on the screen. Note that the shell commands `help` and `tutorial` can be used as well, and will provide the user with some minimal guidance.

Models

As was explained in sect. 2.1, MADGRAPH5_AMC@NLO needs a model in order to generate a process. When one enters the MADGRAPH5_AMC@NLO shell, the default is that of assuming the SM: however one can choose to work in another theory by loading a new model, by simply executing the command:

```
MG5_aMC> import model ModelName
```

where *ModelName* is the name of the desired model. The list of available models (to which as usual the user can add his/her own) can be obtained by hitting the <TAB> key after `import model`. Each of these models is associated with a directory (under the main directory):

```
models/ModelClass
```

In the directory *ModelClass*, one collects the definition of all those models which are tightly connected with each other, for example by having the same Lagrangian and differing by the choice of some fundamental parameter. To give an explicit example: the default model for the SM in MADGRAPH5_AMC@NLO assumes the charm quark to be massless, but there is a model where the charm quark is massive. For both of these, we have:

```
models/ModelClass  $\equiv$  models/sm
```

The massless-charm or massive-charm SM is explicitly loaded by typing:

```
MG5_aMC> import model sm
```

```
MG5_aMC> import model sm-c_mass
```

respectively. Technically, these two commands are in one-to-one correspondence with the two files:

```
models/sm/restrict_default.dat
```

```
models/sm/restrict_c_mass.dat
```

The user interested in some non-extensive modification of the SM can thus simply create his/her own file `models/sm/restrict_XXX.dat`, which may be eventually loaded by executing `import model sm-XXX`. For more details on these matters, please visit: <https://cp3.irmp.ucl.ac.be/projects/madgraph/wiki/Models/USERMOD>.

We finally stress again that not all models support the computation of NLO corrections. In the first public version of MADGRAPH5_AMC@NLO such corrections are restricted to QCD to SM processes. The relevant models are all found in the directory:

```
models/loop_sm
```

Note that, by default, when performing an NLO-type generation (i.e., by using the [QCD] keyword) the code switches automatically from the LO-type model to the corresponding NLO-type one (i.e., in the SM it switches from `sm` to `loop_sm`). If the latter is not available, a warning is issued and the code proceeds no further.

Setup

A short description of the setup procedure has been already given at the beginning of appendix A. Here, we wish to point out that, on top of the environment variables found in `input/mg5_configuration.txt`, the user can also control other options, which for example affect the physics schemes used by MADGRAPH5_AMC@NLO during the various computations. All such options can be listed with the following command:

```
MG5_aMC> display options
```

which will display all options and their current values. In order to change the latter, one executes the `set` command, whose general syntax is:

```
MG5_aMC> set Option Value
```

For example, MADGRAPH5_AMC@NLO by default does not use the complex mass scheme in its computations. In order to change this, it is sufficient to execute:

```
MG5_aMC> set complex_mass_scheme True
```

Other examples relevant to environment variables have already been given in appendix A.

The operation of computing the widths of the unstable particles present in the imported model can be seen as part of the setup procedure, being a complement to the model itself, independent of the generation procedure, and mandatorily performed before the running phase (see sect. 2.3.2). Such an operation is carried out by issuing the shell command:

```
MG5_aMC> compute_widths [{Options}]
```

which in turn executes the MADWIDTH module; the possible options of the above command can be as usual explored by hitting the <TAB> key. We remind the reader that MADWIDTH works at tree level and in the narrow-width approximation (in other words, the manual setting of widths in the context of an NLO simulation may be necessary).

Finally, another setup-type operation is the diagonalisation of the mass matrix. This is only available in a restricted class of UFO models which include the ASPERGE [86] module, whose inputs are accessible to the user during the interactive talk-to phase.

Generation

The most general form of the `generate` command is the following:

```
MG5_aMC> generate Process {AmpOrders} [{ {Mode} Couplings}]
```

the only mandatory option being *Process*, i.e. the actual process one needs to generate. We shall now comment on the four options above in turn.

The option *Process* is simply the list of initial- and final-state particles, separated by the conventional > sign:

syntax	example	meaning
$\mathbf{x}, \mathbf{x} >$	$\mathbf{p} \mathbf{p} > \mathbf{z} \mathbf{j}, \mathbf{z} > \mathbf{b} \mathbf{b}^{\sim}$	<i>s.1</i>
$\$ \mathbf{x}$	$\mathbf{p} \mathbf{p} > \mathbf{e}^+ \mathbf{e}^- \$ \mathbf{z}$	<i>s.2</i>
$/ \mathbf{x}$	$\mathbf{p} \mathbf{p} > \mathbf{e}^+ \mathbf{e}^- / \mathbf{z}$	<i>s.3</i>
$> \mathbf{x} >$	$\mathbf{p} \mathbf{p} > \mathbf{z} > \mathbf{e}^+ \mathbf{e}^-$	<i>s.4</i>
$\$ \$ \mathbf{x}$	$\mathbf{p} \mathbf{p} > \mathbf{e}^+ \mathbf{e}^- \$ \$ \mathbf{z}$	<i>s.5</i>

Table 14: Process-generation syntax refinements, also exemplified in the case of various processes that involve a Z boson. See the text for the explanation of the keywords *s.1–s.5*. Only syntaxes *s.3–s.5* are supported for NLO-type generations.

Process $\equiv \quad \mathbf{a} \mathbf{b} > \mathbf{c}_1 \dots \mathbf{c}_n$

One can further refine the syntax above in order to include in the computation only some of the contributions that one would normally obtain. Such refinements are reported in table 14, and have the following meaning:

- s.1* A production process is generated that features \mathbf{x} in the final state, with \mathbf{x} subsequently decaying into the list of particles that follow the “ $\mathbf{x} >$ ” string; more in general, there may be p primary particles that play the same role as \mathbf{x} . Only p -resonant diagrams (see sect. 2.5) are included in the computation. In the example of table 14, one has the associated production of a Z and a jet, with the Z further decayed into a $b\bar{b}$ pair. Spin correlations and \mathbf{x} off-shell effects are taken into account exactly, but the virtuality $m_{\mathbf{x}}^*$ of \mathbf{x} is forced to be in the following range:

$$|m_{\mathbf{x}}^* - m_{\mathbf{x}}| \leq \text{bwcutoff} \Gamma_{\mathbf{x}}, \quad (\text{B.1})$$

where $m_{\mathbf{x}}$ is the pole mass of \mathbf{x} , $\Gamma_{\mathbf{x}}$ its width, and **bwcutoff** is a parameter controlled by the user (through **run_card.dat**). Syntax *s.1* thus loosely imposes an on-shell condition; it is called **decay-chain syntax**, and can be iterated: any decay product can be decayed itself by using this syntax (e.g. $\mathbf{x} > \mathbf{y} \mathbf{z}, \mathbf{y} > \mathbf{w} \mathbf{s}$).

- s.2* If \mathbf{x} appears as an intermediate particle in the generated process, its virtuality is forced to be in the range:

$$|m_{\mathbf{x}}^* - m_{\mathbf{x}}| > \text{bwcutoff} \Gamma_{\mathbf{x}}, \quad (\text{B.2})$$

which is the region complementary to that of eq. (B.1), and thus loosely imposes an off-shell condition. All diagrams are kept. In the example of table 14, one has Drell-Yan production with the invariant mass of the e^+e^- pair larger than or smaller than the Z mass by at least **bwcutoff** Γ_Z . A consequence of the complementarity mentioned above is that, while cross sections generated with either *s.1* or *s.2* are **bwcutoff**-dependent, their sum is not (up to interference terms, which are neglected by the process of discarding non-resonant diagrams in *s.1*), and corresponds to the

process generated with the simplest syntax. For example:

$$\frac{d\sigma}{dO}(\text{p p} \rightarrow \text{z}) \simeq \frac{d\sigma}{dO}(\text{p p} \rightarrow \text{z}, \text{z} \rightarrow \text{e} + \text{e}^-) + \frac{d\sigma}{dO}(\text{p p} \rightarrow \text{e} + \text{e}^- \text{ } \text{z}), \quad (\text{B.3})$$

for any observable O .

- s.3 All diagrams that feature (anywhere) the particle \mathbf{x} are discarded.
- s.4 The process is generated by demanding that at least one particle of type \mathbf{x} be in an s -channel.
- s.5 All diagrams that feature the particle \mathbf{x} in an s -channel are discarded.

We stress that all syntaxes but *s.2* produce in general results which are non physical, because gauge invariance might be violated (although there are exceptions: see e.g. ref. [211]), and have therefore to be used with extreme caution. The situation becomes more involved at the NLO, so even more care is required. Syntaxes *s.3*, *s.4*, and *s.5* are supported; more refined selections of individual loop diagrams in MADLOOP5 can be imposed by editing the function `user_filter` in the source code `loop_diagram_generation.py`.

The option *AmpOrders* allows the user to specify the upper bounds on the powers of the coupling constants that enter the scattering *amplitudes* (i.e., not the amplitudes squared); therefore, the coefficients $\Sigma_{k_0+p,q}$ are selected only in an indirect manner – see sect. 2.4. Furthermore, in the case of an NLO-type generation, such amplitudes are the Born ones: the couplings of the one-loop and real-emission amplitudes are then automatically determined according to the type of corrections to be included. The syntax for this option is the following:

$$\text{AmpOrders} \equiv \quad \text{coupling}_1 = p_1 \quad \text{coupling}_2 = p_2 \quad \dots \quad \text{coupling}_n = p_n$$

where `couplingi` is the name of the i^{th} coupling in the model currently used, and p_1 is an integer which represents the upper bound mentioned above. It should be obvious that `couplingi` is an arbitrary name, chosen by the author of the model in use. In order to see the list of all coupling names, one has just to type (after having imported the model):

```
MG5_aMC> display coupling_order
```

For example, by executing this command in the context of the SM, one obtains what follows:

```
QCD : weight = 1
QED : weight = 2
```

which implies that the internal names of the SM couplings g_s and g_w is QCD and QED respectively, with the latter being hierarchically suppressed w.r.t. the former. As an explicit example of the use of the *AmpOrders* option in the SM, let us consider the case of:

$$p + p \longrightarrow W^+ + J_b + J_{\text{light}}, \quad (\text{B.4})$$

where J_b and J_{light} are a b - and a light-jet respectively, and the five-flavour scheme is adopted. Numerically, the dominant contributions to such a process are due to diagrams whose corresponding amplitudes factorise the couplings $g_s^2 g_w$. However, amplitudes of order g_w^3 are more interesting, since they feature diagrams with one top-propagator exchange,

and are thus identified with single-top production (although of course at the same order one has non-resonant diagrams as well). By executing the command (after including the b -quark in the proton)

```
MG5_aMC> generate p p > w+ b j
```

one would obtain only the amplitudes of $\mathcal{O}(g_s^2 g_w)$, the choice being made by the code automatically according to the hierarchy shown above. In order to study single-top production, one can execute what follows instead [211]:

```
MG5_aMC> generate p p > w+ b j QED=3 QCD=0
```

which will force the code to consider only $\mathcal{O}(g_w^3)$ amplitudes. Note that, by entering `QED=3 QCD=2`, one will generate *both* $\mathcal{O}(g_s^2 g_w)$ and $\mathcal{O}(g_w^3)$ amplitudes. In future version of MADGRAPH5_AMC@NLO, the syntax of the option *AmpOrders* will be extended, so as to give the user the possibility of selecting directly cross-section-level quantities ($\Sigma_{k_0+p,q}$'s), at both the leading and the next-to-leading order.

The option *Mode*⁶¹ allows the user to select which contributions to an NLO cross section (on top of that due to the Born, which is always present) will be included in the computation. The possible settings are the following:

<i>Mode</i> \equiv <code>all=</code>	\implies	both one-loop and FKS-subtracted real-emission
<i>Mode</i> \equiv <code>real=</code>	\implies	only FKS-subtracted real-emission
<i>Mode</i> \equiv <code>virt=</code>	\implies	only one-loop

The setting `all=` is equivalent to omitting the option *Mode* altogether, and should be the only one considered by the non-expert user, being the only one that leads to physical results. The setting `real=` instructs MADGRAPH5_AMC@NLO to *not* generate the part of the code relevant to virtual matrix elements with MADLOOP. In this way, the cross section can still be dealt with as explained in sect. 3, but the results will be non-physical, *unless* an external one-loop provider is linked to MADGRAPH5_AMC@NLO (such an external OLP will thus effectively play the same role as MADLOOP). Finally, the setting `virt=` corresponds to the MADLOOP standalone mode. In such a mode, the commands `output` and `launch` will behave differently w.r.t. what is described in sect. 3, the idea being that of using the code so generated in order to obtain the pole residues and finite part of the virtual corrections for user-defined kinematic configurations – see sect. 4.3 for explicit examples.

The option *Couplings* allows the user to specify which kind of NLO corrections MADGRAPH5_AMC@NLO will compute. The general syntax for this option is the following:

```
Couplings  $\equiv$  coupling1 coupling2 ... couplingn
```

However, in the current version only QCD corrections can be computed, and therefore the only valid option read as follows:

```
Couplings  $\equiv$  QCD
```

as already mentioned several times in this paper. For examples of the more general syntax that can be used in a still-private MADGRAPH5_AMC@NLO version, see sect. 4.3.

Output

The most general form of the `output` command is the following:

⁶¹The use of which requires the use of the option *Couplings* as well. The opposite is not true.

```
MG5_aMC> output [OutputForm] [MYPROC]
```

As was already mentioned in sect. 3 (see in particular footnote 42) the target-directory name *MYPROC* may be omitted, in which case *MADGRAPH5_AMC@NLO* will choose automatically a name (and print it out on the screen for the user to know). As the full syntax above implies, however, there are a few names that are reserved because, if used, the code will interpret them as one of the (optional) *OutputForm* keywords. These essentially serve to create executables (or standalone libraries) which are not those typically used for the integration of the cross sections and the unweighting of the events. They are described in appendix B.6.

Running

The most general form of the **launch** command is the following:

```
MG5_aMC> launch {ProcDir} {RunMode} {Options}
```

We cannot possibly describe in this paper all possibilities implied by the syntax above, which we plan to do in a forthcoming user manual; we urge the interested reader to explore them by either using the on-line tutorial, or executing the **help launch** command, or exploiting the <TAB> key.

Here, we limit ourselves to point out that *ProcDir*, if present, must coincide with one of the current-process directories previously generated. The implication is that, after the generation and output phase, a user may not immediately run the process, but rather generate a second one, or also quit the *MADGRAPH5_AMC@NLO* shell. Being saved on disk, the full information of a generated and outputted process can be retrieved at any later time. In order to do this, one needs simply to execute:

```
MG5_aMC> launch MYPROC -i
```

where *MYPROC* is the name of the current-process directory used throughout this paper. It should be clear that, upon executing the command above, one is again dealing with a specific current process. For this reason, many early-stage commands (such as **generate**) are disabled. In order to help the user remind this fact, the prompt itself is actually changed, and reads:

```
MYPROC>
```

In short, we shall call the environment accessed by executing the **launch -i** command the *running mode*. One can re-enter the running mode of a given process an unlimited amount of times. Again, we shall not attempt to give here a full description of the various implications of this fact. However, it is interesting to discuss a specific usage in connection to what has been described in sect. 3.2.1, and namely how to shower hard-subprocess event files previously generated. For example, we have discussed in sect. 3.2.1 how, in the case of a process which features particles whose decay products are dealt with *MADSPIN*, one obtains (at least) one undecayed and one decayed hard-event files, for example:

```
MYPROC/Events/run_01/events.lhe.gz
```

```
MYPROC/Events/run_01_decayed_1/events.lhe.gz
```

only the latter of which is showered by default when *MADGRAPH5_AMC@NLO* steers the shower. In order to shower the former, one simply has to execute:

```
MG5_aMC> launch MYPROC -i
```

```
MYPROC> shower run_01
```

Namely, to access the running mode of the relevant process directory, and then execute the command `shower` followed by the name of the subdirectory of the `Events` directory where the events to be showered are stored. We point out that the shower command can be executed any number of times with the same argument, e.g. if one desires to change the seeds or the parameters in the PSMC.

B.2 Setting the hard scales at the NLO

The short distance NLO(+PS) cross sections in `MADGRAPH5_AMC@NLO` feature three hard scales: the renormalisation (μ_R), factorisation (μ_F), and Ellis-Sexton (Q_{ES}) scales. The latter appears only at the NLO and, at variance with the former two, its variations do not induce any changes in the cross sections. For this reason, Q_{ES} is only useful in the context of validation studies, performed by developers; regular users are recommended to always set it equal to the factorisation scale. In view of the standard way of performing scale variations, it is convenient to write the hard scales as follows:

$$\mu_R = f_R \mu_{R0}, \quad \mu_F = f_F \mu_{F0}, \quad Q_{\text{ES}} = f_{\text{ES}} Q_{\text{ES}0}, \quad (\text{B.5})$$

where μ_{R0} , μ_{F0} , and $Q_{\text{ES}0}$ are called *reference* scales.

Hard scales must be set by the user prior to compiling and running the code. They can be organised into two categories, typically called “fixed” and “dynamical”; the scales belonging to the former have constant values, independent of the event kinematics, while those belonging to the latter depend on the four-momenta of the final-state particles, and hence have values that change event-by-event during the course of the run. Whether a scale is fixed or dynamical is determined by an input parameter. For example, in the case of μ_R , the following setting in `run_card.dat`:

```
T = fixed_ren_scale ! if .true. use fixed ren scale
```

will instruct the code to use a fixed renormalisation scale. Such a fixed value is also given by the user in input by setting the pre-factor f_R and the reference scale μ_{R0} that appear in eq. (B.5). For example, the following entries in `run_card.dat`:

```
91.188 = muR_ref_fixed ! fixed ren reference scale
```

```
2      = muR_over_ref ! ratio of current muR over reference muR
```

set $\mu_{R0} = 91.188$ GeV and $f_R = 2$ respectively, and hence $\mu_R = 182.376$ GeV.

We now address the case of dynamical scales, again using the renormalisation scale to give definite examples. A dynamical μ_R is used when:

```
F = fixed_ren_scale ! if .true. use fixed ren scale
```

With this setting, one still has $f_R = \text{muR_over_ref}$. On the other hand, the input `muR_ref_fixed` is ignored, and the reference scale is defined as follows:

$$\mu_{R0} = \text{muR_ref_dynamic}. \quad (\text{B.6})$$

The quantity `muR_ref_dynamic` is a function of the four-momenta of the final-state particles; its body is found in the file `MYPROC/SubProcesses/set scales.f`, where the user

may include his/her definition of the dynamical scale best suited to the process of interest. Although a few examples of typical dynamical scales are given in the version of `setscales.f` which is included in the tarball of the package, we urge the user to study the structure of that file (which is amply commented – note, in particular, the role of the variable `temp_scale_id` in that file, which helps keep track of the functional forms used), and to change it if need be. It should be clear that `setscales.f` follows the same rules as all the other core files of the package (see sect. A). Hence, in order for any modifications to it to be taken into account in the current run, one must edit the file before the `launch` command is issued.

What said above for the renormalisation scale applies without changes to the factorisation and Ellis-Sexton scales; the relevant parameters and functions in `run_card.dat` and `setscales.f` have self-explanatory names. Note that, in the case of the factorisation scale, one can in principle assign two different values to the two incoming hadrons – hence, in the input cards one can find the variables `*_ref_fixed` and `*_over_ref`, with `*=muF1` and `muF2`, which are respectively relevant to the hadron coming from the left and the right. At the LO, this is unambiguous – the scales only enter the relevant PDFs. At the NLO, however, there are several ways to write the logarithmic terms whose arguments are ratios of scales. In order to avoid complications, at the NLO the two factorisation scales must always be chosen to be equal; when this is not the case, the code stops.

We point out that the structure outlined above will allow the user to choose one scale to be fixed and another one to be dynamical; however, in the vast majority of cases one will want the scales to be either all fixed (not necessarily to the same value), or all dynamical. In the latter case, the functions in `setscales.f` are such that different functional forms can be adopted for different scales. Again, this is a somehow infrequent situation. Having this in mind, the default version of `setscales.f` sets all `*_ref_dynamic` functions (with `*=muR`, `muF`, and `QES`) equal to the same function `scale_global_reference`, and one can limit oneself to modifying the latter for a standard usage.

We conclude this section by summarising schematically what has been described above.

1. Decide whether to use fixed (`fixed*_scale=T`) or dynamical (`fixed*_scale=F`) scales. This is done at runtime, either by editing `run_card.dat` before executing the `launch` command, or directly at the prompt after having executed it.
- 2a. If fixed scales are chosen: the relevant input parameters are `*_over_ref` (these are the f_* factors in eq. (B.5)) and `*_ref_fixed` (these are the reference scales μ_{*0} in eq. (B.5)). Both can be set at runtime in the same way as `fixed*_scale`.
- 2b. If dynamical scales are chosen: the relevant quantities are the input parameters `*_over_ref` as in case 2a., and the functions responsible for defining the reference scales, to be found in `setscales.f`. Modifications to the latter file must be carried out before executing the `launch` command (i.e., no modifications are possible at runtime); by default, the reference dynamical scales are set equal to $H_T/2$.

Note that the situation of FxFx-merged simulations is somewhat different, owing to the specific prescriptions for the settings of the scales which are inherent to the method; for more details, the user is encouraged to check http://amcatnlo.cern.ch/FxFx_merging.htm.

B.3 Scale and PDF uncertainties: the NLO case

Among all the dependencies of a cross section, those due to hard scales and PDFs are special, since it is always possible to write

$$\sigma = \sum_i w_i b_i, \quad (\text{B.7})$$

where the coefficients w_i (typically called “weights”) are independent of both scales and PDFs, while the “basis” members b_i contain all the information on scales and PDFs in simple forms such as:

$$b_i = f_{H_1}^{(i)} f_{H_2}^{(i)} \alpha_s^{k_i} \left\{ 1, \log \frac{\mu_R}{Q_{\text{ES}}}, \log \frac{\mu_F}{Q_{\text{ES}}} \right\}. \quad (\text{B.8})$$

The key point is that, while the weights might be very expensive to compute CPU-wise, the basis members are straightforward. A convenient strategy is therefore that of first evaluating the w_i ’s, and then of using them in eq. (B.7) for all the desired choices of scales and PDFs; each of these will therefore result in a basically instantaneous evaluation of the corresponding σ . In practice, what is done in MADGRAPH5_AMC@NLO is to compute σ for a given choice of scales and PDFs (the “central” or “default” choice), while at the same time storing the values of the w_i ’s (if this is required by the user in input – see later), in order to re-use them at a later stage, typically for the assessment of the theoretical uncertainties.

We stress that eq. (B.7) is exact⁶², and therefore so is the computation of a cross section starting from the weights for any given scale and PDF choice. A complete discussion, which includes all the relevant definitions of w_i and b_i for both fixed-order and MC@NLO cross sections, is given in ref. [122] and will not be repeated here. The aim of this appendix is rather that of giving some details on the way in which eq. (B.7) is exploited when computing scale and PDF uncertainties in the context of (N)LO+PS and f(N)LO simulations.

The basic idea relevant to (N)LO+PS is the following. In the LHE file and event-by-event, the values of σ will be stored that correspond to all the combinations of scales and PDFs selected by the user in input (we denote the numbers of these combinations by N_μ and N_{PDF} respectively). These σ ’s will have to be treated in the same way as the cross section associated with the central scales and PDFs (which is part of the standard LHE information, and corresponds to the variable **XWGTUP**); namely, each of them will constitute an entry in a histogram associated with that particular combination of scales and PDFs. In other words, for each observable of interest, one will have to fill $1 + N_\mu + N_{\text{PDF}}$ histograms (the “1” being for the central choices). At the end of the run, and for each observable, the envelope of the $1 + N_\mu$ histograms will give the scale uncertainty affecting that observable,

⁶²The dependence on PDFs of the (parton-shower) Sudakovs cannot be accounted for by eq. (B.7). However, this is expected to be rather small, and particularly so when computing PDF uncertainties. See ref. [122] for more details.

and the envelope of the $1 + N_{\text{PDF}}$ histograms will be the PDF uncertainty. The precise definition of these two envelopes is the user's responsibility. In the case of the scales, one will typically want to consider the largest and smallest cross sections bin-by-bin, possibly excluding from the computation of such extremes some of the (μ_R, μ_F) combinations (see e.g. [355] for a discussion on this point). In the case of the PDFs, the envelope must be defined following the prescription of the PDF authors.

We now show how the user can choose in input the scales and PDFs that will be used in the calculation of the uncertainties; we start from the former. In the present version of MADGRAPH5_AMC@NLO we have fixed $N_\mu = 8$, which corresponds to the following combinations:

$$(f_R^\downarrow, f_F^\downarrow), \quad (f_R^c, f_F^\downarrow), \quad (f_R^\uparrow, f_F^\downarrow), \quad (\text{B.9})$$

$$(f_R^\downarrow, f_F^c), \quad (f_R^\uparrow, f_F^c), \quad (\text{B.10})$$

$$(f_R^\downarrow, f_F^\uparrow), \quad (f_R^c, f_F^\uparrow), \quad (f_R^\uparrow, f_F^\uparrow), \quad (\text{B.11})$$

these being the pre-factors introduced in eq. (B.5) to define the renormalisation and factorisation scales given the reference scales:

$$(\mu_R^\alpha, \mu_F^\beta) = (f_R^\alpha \mu_{R0}, f_F^\beta \mu_{F0}), \quad \{\alpha, \beta\} \in \{\downarrow, c, \uparrow\}. \quad (\text{B.12})$$

The combination (f_R^c, f_F^c) missing in eqs. (B.9)–(B.11) is obviously that corresponding to the central scales, which is always computed. Equation (B.12) implies that scale variations are defined by choosing the reference renormalisation and factorisation scales (which is done as explained in sect. B.2), and by varying the pre-factors in front of them. Such prefactors are defined by means of some input parameters found in `run_card.dat`. More specifically, we have:

$$f_R^\downarrow = \text{muR_over_ref} \times \text{rw_Rscale_down}, \quad (\text{B.13})$$

$$f_R^c = \text{muR_over_ref}, \quad (\text{B.14})$$

$$f_R^\uparrow = \text{muR_over_ref} \times \text{rw_Rscale_up}, \quad (\text{B.15})$$

$$f_F^\downarrow = \text{muF_over_ref} \times \text{rw_Fscale_down}, \quad (\text{B.16})$$

$$f_F^c = \text{muF_over_ref}, \quad (\text{B.17})$$

$$f_F^\uparrow = \text{muF_over_ref} \times \text{rw_Fscale_up}. \quad (\text{B.18})$$

Given these inputs, MADGRAPH5_AMC@NLO will consider all the combinations given in eqs. (B.9)–(B.11), compute the corresponding b_i 's of eq. (B.8) *using the central PDFs*, and combine them with the weights according to eq. (B.7). The resulting σ (which could be denoted by $\sigma^{(\alpha, \beta)}$ for consistency with eq. (B.12)) will be stored in the LHE file, provided the user sets:

```
.true. = reweight_scale ! reweight to get scale dependence
in input.
```

As far as PDF uncertainties are concerned, we have assumed that one will use LHAPDF, where all members of an error set are identified by adjacent integer numbers. Using NNPDF 2.0 [356] as an example to be definite, one will have the following inputs:

```
lhapdf = pdlabel ! PDF set
90800 = lhaid ! if pdlabel=lhapdf, this is the lhapdf number
90801 = PDF_set_min ! First of the error PDF sets
90900 = PDF_set_max ! Last of the error PDF sets
```

The first two lines instruct the code to use LHAPDF and to choose the central NNPDF 2.0 set as the default. The last two lines will set $N_{\text{PDF}} = 100$; for each of these hundred NNPDF 2.0 error sets, MADGRAPH5_AMC@NLO will compute the b_i 's of eq. (B.8) *using the central scales*, and combine them with the weights according to eq. (B.7). The resulting σ will be stored in the LHE file, provided the user sets:

```
.true. = reweight_PDF ! reweight to get PDF uncertainty
in input.
```

For what concerns the storage in the LHE file of the σ 's computed as described above, we use a format which is fully compatible with the LHA v2.0 [92], and which is now officially adopted as v3.0 [215]. In the file header, there will be a part (which we call the reweight section) where a description is given of the meaning of the weights that will appear in each event. Its structure may read as follows:

```
<initrwgt>
  <weight id='1'> This is the central weight </weight>
  <weightgroup type='scale variation' combine='envelope'>
    <weight id='2'> muR=0.5 muF=0.5 </weight>
    <weight id='3'> muR=0.5 muF=1.0 </weight>
    ...
    <weight id='9'> muR=2.0 muF=2.0 </weight>
  </weightgroup>
  <weightgroup type='NNPDF20' combine='gaussian'>
    <weight id='10'> set001 </weight>
    ...
    <weight id='109'> set100 </weight>
  </weightgroup>
</initrwgt>
```

Thus, each choice of scales and of PDFs is uniquely identified by an ID number. For example, `id='1'` will correspond to the central scale and PDF choices, $(f_R, f_F) = (f_R^c, f_F^c)$ and PDF number 90800 in the examples given above (this is the same as `XWGTUP`, and hence is redundant, but it is convenient to include it in the reweight section as well). As far as `id='2'` to `id='9'` are concerned, these will correspond to the N_μ combinations given in eqs. (B.9)–(B.11), the numerical values reported in the header next to `muR` and `muF` being those of f_R^α and f_F^β respectively. Finally, `id='10'` to `id='109'` correspond to the N_{PDF} error sets 90801–90900.

In keeping with the reweight section in the LHE file header, there will be a reweight section event-by-event, which contains the actual numbers to be used to fill the histograms as described previously. Its structure will read as follows:

```
<event>
...
```

```

<rwgt>
  <weight id='1'> 3.905e+01</wgt>
  <weight id='2'> 4.142e+01</wgt>
  ...
  <weight id='109'> 3.876e+01</wgt>
</rwgt>
</event>

```

The presence of the ID numbers in the reweight section of each event facilitates debugging, does not require the weights to be always in the same order, and is especially convenient for on-the-fly manipulations (such as discarding some contributions, sorting them, and so forth).

We conclude this section with some general comments. The condition $N_\mu = 8$ can be trivially relaxed (which requires the inclusion of N_μ itself in the list of the inputs); we have refrained from doing so in the first public version of the code since three choices for each of the hard scales typically give a good estimate of the uncertainties. A more extended set of input parameters would also give one the possibility of performing scale variations by changing the functional forms of the reference scales w.r.t. those adopted for the central results. Finally, the complete generality could be achieved by storing in the LHE file the weights w_i 's. This would require, however, that additional information be stored as well (such as the values of the Bjorken x 's – more details can be found in ref. [122]). While this can be trivially done, it would render the computation of the basis members b_i 's of eq. (B.8), and their subsequent combination with weights according to eq. (B.7), a much more involved operation than the present one if performed by an external user⁶³. Such a possibility is left open for future developments.

In the case of f(N)LO runs, the information on scale and PDF variations is also available on an event-by-event basis. In keeping with the fact that here one cannot have unweighted events, MADGRAPH5_AMC@NLO will associate to each kinematic configuration an array of weights (rather than a single weight), each of which gives eq. (B.7) with the basis elements of eq. (B.8) recomputed for all desired scale and PDF choices. This implies that the second elements of the pairs in eqs. (3.4)–(3.6) will be turned into arrays, with dimensionality:

$$1 + (1 + N_\mu) + N_{\text{PDF}} \quad \text{reweight_scale} = \text{.true.} \quad \text{reweight_PDF} = \text{.true.} \quad (\text{B.19})$$

$$1 + (1 + N_\mu) \quad \text{reweight_scale} = \text{.true.} \quad \text{reweight_PDF} = \text{.false.} \quad (\text{B.20})$$

$$1 + N_{\text{PDF}} \quad \text{reweight_scale} = \text{.false.} \quad \text{reweight_PDF} = \text{.true.} \quad (\text{B.21})$$

The first entry thus always gives the value of the weight associated with central parameters. In the case of scale variations, this weight is present twice (the “1” in $(1 + N_\mu)$) essentially for reasons of backward compatibility which should not concern the user. The information of which weight is which is returned as the array of strings `weights_info` and made available to the user's initialisation routine `analysis_begin` – this is equivalent to the `id` number discussed before in the context of LHE files.

⁶³This *not* being the case at the LO, in LO-type generations we can adopt a different strategy – see appendix B.4.

B.4 Scale and PDF uncertainties: the LO case

At the LO, the structure of the cross section, eq. (B.7), is trivial – the sum contains one term $i = 1$ (see however footnote 8), which corresponds to the single PDF-and-coupling combination (i.e., to a single basis member, eq. (B.8)) relevant to this perturbative order: this is the reason for the simplicity of eq. (2.2). Thus here, at variance with the NLO case, from the user’s viewpoint it is therefore as simple to handle w_1 as is to handle σ . This suggests the following strategy: when unweighted events are produced, they are stored in an intermediate LHE file with a non-standard format, that features the weights w_1 . *After* the end of the run, this LHE file is read by a standalone module, dubbed `SysCALC`, that converts the weights w_1 into the corresponding cross sections σ , and stores them in a new LHE file, which has this time the standard format already described in appendix B.3. This procedure is advantageous because it allows one to run `SysCALC` as many times as desired using the same intermediate LHE file obtained at generation time; this implies that the type of scale or PDF variations need not be chosen before the event-generation phase, as is the case at the NLO. The `SysCALC` module can be installed⁶⁴ with:

```
MG5_aMC> install syscalc
```

from the `MADGRAPH5_AMC@NLO` shell. At runtime, `MADGRAPH5_AMC@NLO` is instructed to save the weights w_1 in the intermediate LHE file by setting

```
T = use_syst ! Enable systematics studies
```

in `run_card.dat`. When this is done, `SysCALC` is automatically called at the end of the run (although, as was said before, it can also be run independently afterwards). The type of scale and PDF variations considered are determined by the following entries in `run_card.dat`:

```
0.5 1 2 = sys_scalefact # Central scale factors
-1      = sys_scalecorrelation # for renormalization/scale variate
                                # -1: make all combination
                                # -2: only correlated variation
0.5 1 2 = sys_alpsfact # \alpha_s emission scale factors
30 50 = sys_matchscale # variation of merging scale
# PDF sets and number of members (0 or none for all members).
CT10nlo.LHgrid = sys_pdf #
```

The list of values to the left of `sys_scalefact` collects the multiplicative factors in front of the reference (fixed or dynamic⁶⁵) scales, and are thus analogous to the quantities f_R^α and f_F^β that appear in eq. (B.12); at variance with the current NLO implementation, such a list can contain more than three numbers. We stress that, when `use_syst=T`, the value of `scalefact` in `run_card.dat` is ignored. The flag `sys_scalecorrelation` allows one to choose which of the renormalisation/factorisation scale combinations are considered. When “-1” is entered, then all μ_R and μ_F values determined by the list `sys_scalefact` are taken into account, while with “-2” one restricts to code to dealing with $\mu_R = \mu_F$.

⁶⁴`SysCALC` requires that `LHAPDF` be installed as well.

⁶⁵Note that the `setscales.f` code relevant to LO calculations is different w.r.t that used in NLO ones.

More sophisticated options are also available (allowing one to select only some of the possible (μ_R, μ_F) combinations), which will be documented elsewhere. The entry `sys_pdf` is associated with the study of PDF systematics; if set equal to a PDF error set, all PDF members in that set will be considered. Alternatively, one can specify the individual PDF members to be taken into account. Finally, through `SysCALC` one can also investigate the systematics relevant to tree-level merging (see sect. 2.3.4), with `sys_alpsfact` and `sys_matchscale` corresponding to α_s -argument and Q_{match} variations respectively. More details on `SysCALC` can be found at:

<https://cp3.irmp.ucl.ac.be/projects/madgraph/wiki/SysCalc>

B.5 Other LO reweighting applications

In this appendix we comment in the briefest of manners on some technicalities relevant to the matrix-element reweighting (eq. (2.3)) and the matrix-element method (eq. (2.5)) discussed in sect. 2.3.3.

As was already mentioned in sect. 3.1, the former procedure is straightforwardly accessed through the `MADGRAPH5_AMC@NLO` shell, by simply setting `reweight=ON` in the interactive talk-to phase. By doing so, `MADGRAPH5_AMC@NLO` will use the file `reweight_card.dat` to modify the parameters (found in `param_card.dat`) used for the benchmark computation (that essentially corresponds to the denominator of eq. (2.3)). One may enter any number of such modifications, each of which may contain any number of parameter changes, to be done through the `set` command (see the comments inside the file `reweight_card.dat`). There are currently two main limitations to this procedure. Firstly, the changes must occur within one given model (i.e., one cannot reweight to matrix elements computed in a model different w.r.t. that adopted in the benchmark calculation). Secondly, the accessible kinematical region in the “new” hypothesis must be equal to or smaller than the original one. The interested reader can find more information by visiting:

<https://cp3.irmp.ucl.ac.be/projects/madgraph/wiki/Reweight>

The matrix-element method is handled by `MADWEIGHT`. As was discussed in sect. 3.1, the current version embedded in `MADGRAPH5_AMC@NLO` has vastly increased the speed of the previous version [133]. Such an increase is mainly due to a better combination of subprocesses, to a Monte-Carlo-type sum over jet-parton assignments (as opposed to an exact sum), and to the possibility of performing the simultaneous computation of $P(\mathbf{q}|\alpha)$ in the case of multiple choices of the transfer function. The `MADWEIGHT` executable specific to the process generated by the user simply corresponds to employing one of the reserved output keywords (see appendix B.6), namely to executing, after the generation phase, the command:

```
MG5_aMC> output madweight MYPROC
```

After that, one may continue with using the `MADGRAPH5_AMC@NLO` shell interface by executing:

```
MG5_aMC> launch MYPROC
```

Further details can be found at:

<https://cp3.irmp.ucl.ac.be/projects/madgraph/wiki/MadWeight>

B.6 Output formats and standalone libraries

The main purpose of MADGRAPH5_AMC@NLO is that of providing a self-contained framework where to compute cross sections and generate events at the desired level of perturbative accuracy, in both the SM and new-physics theories. On the other hand, the code may also be used to provide one with only a given ingredient of a calculation (e.g., a matrix element) which is to be performed elsewhere. This has been one of the defining characteristic of MADGRAPH, and has been wholly inherited by MADGRAPH5_AMC@NLO. Another example is the computation of a quantity which is not a cross section; a case in point is the likelihood dealt with by MADWEIGHT (see sect. 2.3.3 and appendix B.5).

All possible executables, libraries, or more elementary objects that can be produced by MADGRAPH5_AMC@NLO can simply be seen as *outputs* of the (meta-)code; they are in fact in one-to-one correspondence with the optional first keyword of the shell command:

```
MG5_aMC> output [OutputForm] [MYPROC]
```

The possible choices of *OutputForm* can be readily obtained by using the autocompletion <TAB> key in the shell after having typed `output` (or with `help output`). By doing so, one will notice that they all apply, bar one case (`standalone`, see below), to LO-type generations. Here we shall not list them all, but limit ourselves to commenting on those which are the most useful from the user's point of view. These are:

- **standalone**: self-contained Fortran77 library for the computation of either tree-level matrix elements (after an LO-type generation), or one-loop matrix elements (after an NLO-type generation with the keyword `virt=coupling1` ... – see appendix B.1). The directory structure thus created contains a simple program (`check_sa.f`) which allows one to evaluate the matrix elements pointwise for test purposes.
- **standalone_cpp**: the same as above, but in C++ rather than in Fortran77. Works only for tree-level matrix elements.
- **pythia8**: self-contained library for the computation of tree-level matrix elements, in a format which can be directly used in the PYTHIA8 PSMC. It includes a simple driver that one can employ to steer PYTHIA8 sample runs, and a `Processes_*` directory that contains the said matrix elements. More details can be found in sect. 3.2 of ref. [36].
- **madweight**: this output keyword allows one to set up a computation with MADWEIGHT (see appendix B.5).

We conclude this appendix by stressing that the above list (supplemented by that of the other output keywords not explicitly given here) is by no means all-inclusive. The reader who is interested in a particular output format specifically suited to his/her need is encouraged to contact us in order for that to be developed and included in future versions of MADGRAPH5_AMC@NLO. For instance, dedicated outputs for matrix elements to be used in the MATCHBOX [178] framework and by EVENTDECONSTRUCTION [357, 358] are being developed.

C. Features of one-loop computations

C.1 TIR and IREGI

The aim of this section is that of presenting the basic procedures used in TIR, and in particular by the program IREGI⁶⁶; more details on the latter will be given elsewhere [165]. IREGI computes the integral that appears as first element in the set of eq. (2.79); owing to the fact that we apply TIR to a given loop topology (see eq. (2.77)), we can exploit eq. (2.76) to simplify the notation here and drop the dependence on l_t . On the other hand, at variance with what was done in sect. 2.4.2, in order to make things more explicit it is convenient to insert in the notation the dependence on the external (four-dimensional, owing to the 't Hooft-Veltman scheme) four-momenta p_i and on the masses m_i that circulate in the loop (see eq. (2.60)), so that the integral we are interested in reads as follows:

$$I^{\mu_1 \dots \mu_r}(\{p_i\}, \{m_i\}) = \int d^d \bar{\ell} \frac{\ell^{\mu_1} \dots \ell^{\mu_r}}{\prod_{i=0}^{m-1} \bar{D}_i}. \quad (\text{C.1})$$

Lorentz-covariance then guarantees that eq. (C.1) can be re-written as follows:

$$I^{\mu_1 \dots \mu_r}(\{p_i\}, \{m_i\}) = \sum_{2j+i_0+i_1+\dots+i_{m-1}=r} \{[g]^j [p_0]^{i_0} \dots [p_{m-1}]^{i_{m-1}}\}^{\mu_1 \dots \mu_r} I_{ji_0 \dots i_{m-1}}(\{p_i\}, \{m_i\}), \quad (\text{C.2})$$

for certain scalar integrals $I_{ji_0 \dots i_{m-1}}$, and where the symmetric tensor form $\{[g]^j [p_0]^{i_0} \dots [p_{m-1}]^{i_{m-1}}\}^{\mu_1 \dots \mu_r}$ is defined in such a way that all non-equivalent permutations of the Lorentz indices μ_1, \dots, μ_r on j metric tensors g and i_s external momenta p_s contribute with weight one. For example:

$$\begin{aligned} \{[g]^2 [p_0]^0 [p_1]^0\}^{\mu_1 \dots \mu_4} &= g^{\mu_1 \mu_2} g^{\mu_3 \mu_4} + g^{\mu_1 \mu_3} g^{\mu_2 \mu_4} + g^{\mu_1 \mu_4} g^{\mu_2 \mu_3}, \\ \{[g]^1 [p_0]^0 [p_1]^2\}^{\mu_1 \dots \mu_4} &= g^{\mu_1 \mu_2} p_1^{\mu_3} p_1^{\mu_4} + g^{\mu_1 \mu_3} p_1^{\mu_2} p_1^{\mu_4} + g^{\mu_1 \mu_4} p_1^{\mu_2} p_1^{\mu_3}, \\ \{[g]^0 [p_0]^0 [p_1]^4\}^{\mu_1 \dots \mu_4} &= p_1^{\mu_1} p_1^{\mu_2} p_1^{\mu_3} p_1^{\mu_4}, \\ \{[g]^0 [p_0]^1 [p_1]^2\}^{\mu_1 \mu_2 \mu_3} &= p_0^{\mu_1} p_1^{\mu_2} p_1^{\mu_3} + p_0^{\mu_2} p_1^{\mu_1} p_1^{\mu_3} + p_0^{\mu_3} p_1^{\mu_1} p_1^{\mu_2}. \end{aligned} \quad (\text{C.3})$$

Given eq. (C.2), the computation of the original tensor integral of eq. (C.1) is reduced to that of the scalar integrals $I_{ji_0 \dots i_{m-1}}$. One starts by observing that the latter are independent of the number of dimensions used in the numerator of eq. (C.1), because the decomposition of eq. (C.2) would hold, with the formal replacement $g \rightarrow \bar{g}$, if one had replaced $\ell \rightarrow \bar{\ell}$ in eq. (C.1). Therefore, since working with the same number of dimensions in all parts of a computation is algebraically convenient, one determines the $I_{ji_0 \dots i_{m-1}}$ directly in d dimensions. This is done by recursively expressing such scalar integrals in terms of lower-point ones, till only integrals that cannot be further reduced are obtained – these are just a few and well known: IREGI makes use of those tabulated in ONELOOP [359] and QCDDLOOP [360].

One way of performing such recursive reduction stems from the pioneering work of Passarino and Veltman [151]: by contracting both sides of eq. (C.1) (in d -dimensions) with

⁶⁶The acronym stands for “Integral REduction with General positive propagator Indices”.

metric tensors and external four-momenta, one relates the $I_{j i_0 \dots i_{m-1}}$ integrals to lower-rank tensor or lower-point scalar integrals. This lowering is due to the fact that, when contracting, one obtains the scalar products $\bar{\ell}^2$ and $\bar{\ell} \cdot p_i$, which are then re-expressed as follows:

$$\bar{\ell}^2 = \bar{D}_0 + m_0^2, \quad (\text{C.4})$$

$$\bar{\ell} \cdot p_i = (\bar{D}_i - \bar{D}_0 + m_i^2 - m_0^2)/2, \quad (\text{C.5})$$

thus either cancelling some of the denominators or simplifying the dependence on $\bar{\ell}$ in the numerator. The procedure is algebraic, and one ends up with a system of equations where the unknowns are the scalar integrals, and the coefficients known functions of the kinematic variables. The solution of such a system is non-trivial, owing for example to the presence of special kinematic configurations; IREGI implements to a large extent the strategies proposed in ref. [361].

An alternative and independent way for performing the recursive reduction follows the work of Davydychev [152]. One introduces the generalised loop-tensor and basic-scalar integrals:

$$\bar{I}^{\mu_1 \dots \mu_r}(d, \{\nu_i\}, \{p_i\}, \{m_i\}) = \frac{(\mu^2)^{2-d/2}}{(2\pi)^d} \int d^d \bar{\ell} \frac{\bar{\ell}^{\mu_1} \dots \bar{\ell}^{\mu_r}}{\prod_{i=0}^{m-1} \bar{D}_i^{\nu_i}}, \quad (\text{C.6})$$

$$I_0(d, \{\nu_i\}, \{p_i\}, \{m_i\}) = \frac{(\mu^2)^{2-d/2}}{(2\pi)^d} \int d^d \bar{\ell} \frac{1}{\prod_{i=0}^{m-1} \bar{D}_i^{\nu_i}}, \quad (\text{C.7})$$

where the scale-dependent prefactor is conventional, and the indices $\nu_0, \nu_1, \dots, \nu_{m-1}$ are positive integers. By using a Feynman-parameter representation and the d -dimensional analogue of eq. (C.2):

$$\bar{I}^{\mu_1 \dots \mu_r}(d, \{\nu_i\}, \{p_i\}, \{m_i\}) = \frac{i}{(4\pi)} (4\pi\mu^2)^{2-d/2} \quad (\text{C.8})$$

$$\begin{aligned} & \times \sum_{2j+i_0+\dots+i_{m-1}=r} \{[\bar{g}]^j [p_0]^{i_0} \dots [p_{m-1}]^{i_{m-1}}\}^{\mu_1 \dots \mu_r} \\ & \times (-1)^{\sum_{i=0}^{m-1} \nu_i + r - j} \frac{\Gamma(\sum_{i=0}^{m-1} \nu_i - d/2 - j)}{2^j \prod_{i=0}^{m-1} \Gamma(\nu_i)} \int_0^1 \prod_{i=0}^{m-1} dy_i y_i^{\nu_i + i_i - 1} \\ & \times \delta\left(\sum_{i=0}^{m-1} y_i - 1\right) \left[-\sum_{i < j} y_i y_j (p_i - p_j)^2 + \sum_{i=0}^{m-1} y_i m_i^2 \right]^{j+d/2-\sum_{i=0}^{m-1} \nu_i}, \\ I_0(d, \{\nu_i\}, \{p_i\}, \{m_i\}) &= \frac{i}{(4\pi)} (4\pi\mu^2)^{2-d/2} \frac{\Gamma(\sum_{i=0}^{m-1} \nu_i - d/2)}{\prod_{i=0}^{m-1} \Gamma(\nu_i)} (-1)^{\sum_{i=0}^{m-1} \nu_i} \\ & \times \int_0^1 \prod_{i=0}^{m-1} dy_i y_i^{\nu_i - 1} \delta\left(\sum_{i=0}^{m-1} y_i - 1\right) \\ & \times \left[-\sum_{i < j} y_i y_j (p_i - p_j)^2 + \sum_{i=0}^{m-1} y_i m_i^2 \right]^{d/2-\sum_{i=0}^{m-1} \nu_i}, \quad (\text{C.9}) \end{aligned}$$

one arrives at:

$$\begin{aligned} \bar{I}^{\mu_1 \dots \mu_r}(d, \{\nu_i\}, \{p_i\}, \{m_i\}) &= \sum_{2j+i_0+\dots+i_{m-1}=r} \{[\bar{g}]^j [p_0]^{i_0} \dots [p_{m-1}]^{i_{m-1}}\}^{\mu_1 \dots \mu_r} \\ &\times \frac{(4\pi\mu^2)^{r-j}}{(-2)^j} \left(\prod_{i=0}^{m-1} \frac{\Gamma(\nu_i + i_i)}{\Gamma(\nu_i)} \right) \\ &\times I_0(d + 2(r-j), \{\nu_i + i_i\}, \{p_i\}, \{m_i\}). \end{aligned} \quad (\text{C.10})$$

By using eqs. (C.2) (in d dimensions) and (C.10), one finally obtains the relation:

$$\begin{aligned} I_{ji_0 \dots i_{m-1}}(\{p_i\}, \{m_i\}) &= \left[\frac{(\mu^2)^{2-d/2}}{(2\pi)^d} \right]^{-1} \frac{(4\pi\mu^2)^{r-j}}{(-2)^j} \left(\prod_{i=0}^{m-1} \frac{\Gamma(1 + i_i)}{\Gamma(1)} \right) \\ &\times I_0(d + 2(r-j), \{1 + i_i\}, \{p_i\}, \{m_i\})|_{d=4-2\epsilon}. \end{aligned} \quad (\text{C.11})$$

With eq. (C.9) one is also able to derive relationships among scalar integrals in different dimensions. For instance, eq. (6) of ref. [152] can be easily obtained:

$$I_0(d-2, \{\nu_i\}, \{p_i\}, \{m_i\}) = -4\pi\mu^2 \sum_{s=0}^{m-1} \nu_s I_0(d, \{\nu_i + \delta_{is}\}, \{p_i\}, \{m_i\}), \quad (\text{C.12})$$

where by δ_{is} we have denoted the Kronecker symbol. Furthermore, other recursion relations for the scalar integrals $I_0(d, \{\nu_i\}, \{p_i\}, \{m_i\})$ can be obtained with the help of the integration-by-parts method [362,363], which exploits the fact that integrals are translation-invariant in dimensional regularization. The practical implementation in IREGI of the method discussed here follows ref. [363].

IREGI can use either of the two methods presented above for the recursive reduction, the actual choice being made by the calling code (in our case, MADLOOP5). The current default in MADGRAPH5_AMC@NLO is the use of Passarino and Veltman; this is straightforward to change, since it is simply controlled by a parameter in an input card. IREGI has a minimal internal stability control: should e.g. Passarino and Veltman procedure be flagged unstable, the code will turn to using Davydychev's. We stress that this by no means replaces the stability control performed by MADLOOP5, described in sect. 2.4.2.

C.2 Quantitative profile of MadLoop performances

We have already stressed that the results presented in sect. 4.3 can be used as benchmarks for the validation of other codes. However, they reveal only one aspect of the performances of MADLOOP5, which we complement in this appendix by reviewing some quantitative characteristics of the handling of the scattering processes considered before. A summary of such characteristics is reported in table 15.

The number of topologies is the upper bound of the sum over the index t in eq. (2.77), and it corresponds to the number of independent loop reductions (i.e., of evaluations of the $\text{Red}[\]$ operator introduced in eq. (2.58)) for one kinematic configuration. As one can see from the table, such a number is much smaller than the number of Feynman diagrams, which emphasises the importance of the optimization induced by eq. (2.76). The quantity

	$gg \rightarrow d\bar{d}b\bar{b}t\bar{t}$	$u\bar{u} \rightarrow d\bar{d}t\bar{t}$	$u\bar{d} \rightarrow d\bar{d}W^+ZH$	$gg \rightarrow \tilde{t}_1\tilde{t}_1^*g$
# Feynman diagrams	54614	10947	187138	3952
# topologies	8190	811	8098	437
$\Delta(k_0)$	0	4	2	0
# non-zero hel. configs.	128	16	27	8
Generation time	15h	28min	25h	1min 38s
Running time	18.6s (19%)	895ms (72%)	26.4s (32%)	83.6ms (68%)
Output code size	600 Mb	20 Mb	700 Mb	6 Mb
Runtime RAM usage	3.6 Gb	152 Mb	8.3 Gb	81 Mb
Stability	$2 \cdot 10^{-8}$	$1 \cdot 10^{-7}$	$4 \cdot 10^{-7}$	$1 \cdot 10^{-7}$

Table 15: Performances of MADLOOP5 in the context of the computations presented in sect. 4.3. See the text for details.

$\Delta(k_0)$ is equal to the number of coupling-constant combinations, minus one, at the Born level, which is larger than zero in the case of a mixed-coupling expansion. See the beginning of sect. 2.4, and eqs. (2.17) and (2.22) in particular, for more details. The generation time includes the compilation of the source code. The running time corresponds to the time taken by the code output by MADLOOP5 to compute the one-loop squared matrix element summed over colours but for a single helicity configuration⁶⁷. The percentage in parenthesis specifies the fraction of the running time spent in the loop reduction which, we remind the reader, is independent of the number of non-zero helicity configurations considered. The complementary fraction of the time is spent in the computation of the coefficients $C_{\mu_1 \dots \mu_r; h, l}^{(r)}$ of eq. (2.79), and scales linearly with the number of helicity combinations. The size of the output code includes external data files (that essentially contain the colour coefficients Λ_{lb}) loaded by the library which is in itself much lighter. The RAM measure reported is the runtime peak of residential memory allocated. The figures given in the last row are the relative accuracies estimated by the MADLOOP5 internal stability tests in the context of double-precision computations that use the kinematic configurations considered in sect. 4.3 (however, we stress again that the matrix-element results have been obtained in quadruple precision); obviously, these pointwise accuracies have only an indicative value, since the real figure of merit necessitates averaging over a large statistical sample of independent kinematic configurations.

We conclude this appendix by stressing that the data reported in table 15 can be obtained by the user by using the command `check profile` in the MADGRAPH5_AMC@NLO shell. For example, one would have

```
MG5_aMC> check profile g g > t t~ z [virt=QCD]
```

in the case of the virtual corrections to $t\bar{t}Z$ production (i.e., process e.8 of table 6).

⁶⁷The timing indicated is for a single core of a 2.7 GHz i7 CPU, with the gfortran compiler v4.8.1 without optimization flags (which have been shown to have a negligible impact).

C.3 Computation of the integrand polynomial coefficients

We have discussed in section sect. 2.4.2 how the use of the loop-integrand representation of eq. (2.78) increases the speed of OPP-based integral reductions, as well as giving one the possibility of using TIR methods. This appendix elaborates on the techniques adopted in MADLOOP5 for the computation of the coefficients $C_{\mu_1 \dots \mu_r; h, l}^{(r)}$. The key fact is that such coefficients are fully symmetric tensors of rank r with only $\binom{3+r}{r}$ independent entries. In renormalisable theories and in the Feynman gauge the number of loop propagators sets the maximal rank in ℓ^μ of that loop-integrand numerator, so that the total number of coefficients necessary to express the numerator of any loop of a, say, $2 \rightarrow 6$ process, is at most $N_{coeff}(r_{\max} = 8) \equiv \sum_{r=0}^{r_{\max}=8} \binom{3+r}{r} = 495$ which is well within the reach of modern computers. We start by rewriting the analogue of eq. (2.78) for any polynomial $P^{(r_{\max})}(\ell^\mu)$ of maximal rank r_{\max} with the following shorthand and symbolic notation:

$$P^{(r_{\max})}(\ell^\mu) = C_{\dot{k}}^{(r_{\max})} \ell^{\dot{k}}, \quad (\text{C.13})$$

where \dot{k} takes values between 1 and $N_{coeff}(r_{\max})$, and effectively defines a map between the sets of Lorentz indices μ_i and integer numbers. The choice of such a map is arbitrary, and we use what follows:

$$C_{\mu_1, \dots, \mu_r}^{(r)}, \quad \mu_1 \leq \dots \leq \mu_r \quad \rightarrow \quad C_{\dot{k}(\mu_1, \dots, \mu_r)}^{(r_{\max})}, \quad (\text{C.14})$$

$$\dot{k}(\mu_1, \dots, \mu_r) = N_{coeff}(r-1) + \sum_{i=1}^r (1 - \delta_{0\mu_i}) \frac{(\mu_i + i - 1)!}{i!(\mu_i - 1)!}, \quad (\text{C.15})$$

where we define $N_{coeff}(-1) = 0$ (relevant to $r = 0$). To make things more explicit with one example, eq. (C.13) reads, with $r_{\max} = 2$:

$$\begin{aligned} C_{\dot{k}}^{(2)} \ell^{\dot{k}} \equiv & C_0^{(2)} + C_1^{(2)} \ell^0 + C_2^{(2)} \ell^1 + C_3^{(2)} \ell^2 + C_4^{(4)} \ell^3 \\ & + C_5^{(2)} \ell^0 \ell^0 + C_6^{(2)} \ell^0 \ell^1 + C_7^{(2)} \ell^1 \ell^1 + C_8^{(2)} \ell^0 \ell^2 + C_9^{(2)} \ell^1 \ell^2 \\ & + C_{10}^{(2)} \ell^2 \ell^2 + C_{11}^{(2)} \ell^0 \ell^3 + C_{12}^{(2)} \ell^1 \ell^3 + C_{13}^{(2)} \ell^2 \ell^3 + C_{14}^{(2)} \ell^3 \ell^3. \end{aligned} \quad (\text{C.16})$$

The computation of the coefficients $C_{\dot{k}}^{(r_{\max})}$ with MADLOOP5 is entirely numerical and follows the MADGRAPH procedure for evaluating Feynman diagrams. At tree level, the internal currents of a given Feynman diagram are denoted by $w_j^{(n)}$, with the integer n labeling them and the index j spanning the representation of the particle associated with the current. In MADLOOP5 the *loop* currents are promoted to more general objects embedding polynomials in ℓ^μ and they are denoted by $W_{i, r, \dot{k}, j}^{(n)}$, with the additional index i specifying the choice of the external current for the first L-cut particle (which is non-physical and whose only constraint is to reproduce the Lorentz trace when summed over). The index \dot{k} labels the coefficients of the polynomial of maximal rank r according to the convention of eq. (C.15). Figure 19 shows a complete example of the different numerical objects manipulated by MADLOOP5 in order to construct the polynomial coefficients for the integrand of a box loop diagram. Note that since the currents $w^{(\#)}$ attached to the loop are independent of the loop momentum ℓ^μ , it is irrelevant to know whether they are external currents or originate

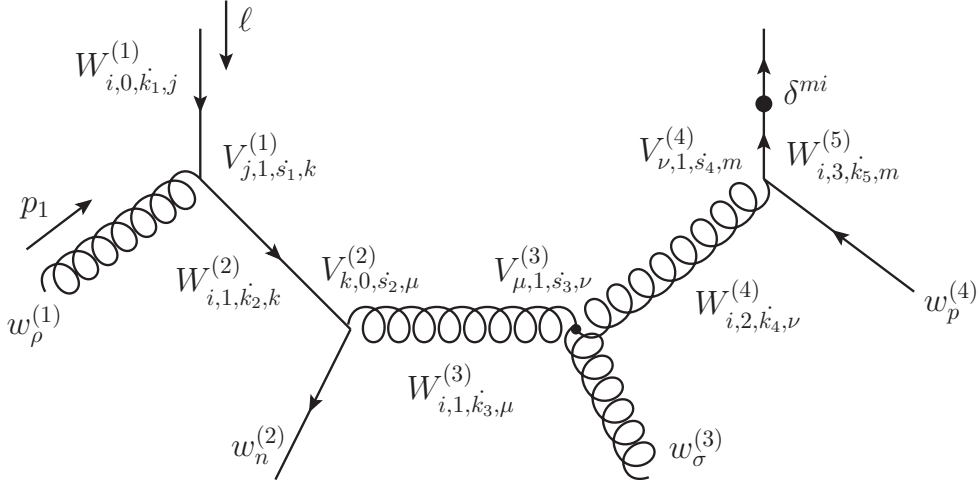


Figure 19: An example of the MADLOOP5 construction of the coefficients $C_k^{(r_{\max})}$. W denotes the loop currents and V the vertex polynomials (see the text). The figure depicts an L-cut diagram; the original box loop is obtained by sewing the two fermion lines at the top.

from larger trees. The starting loop current $W_{i,0,k_1,j}^{(1)}$ is a polynomial of rank 0 since it does not have any loop momentum dependence; its index k_1 can therefore only take the value 0. For all loop diagrams, the starting current is always $W_{i,0,k_1,j}^{(1)} = \delta_{ij}\delta_{k_1 0}$.

The objects $V_{a,r,s,b}^{(\#)}$ are the representations (polynomials of rank r in the loop momentum) of the vertex plus propagator structures, with a and b the incoming and outgoing loop current indices respectively. For example, the explicit expression of $V_{j,1,s_1,k}^{(1)}$ for a massless quark in fig. 19 reads:

$$V_{j,1,s_1,k}^{(1)} \ell^{s_1} = \underbrace{ig_s \gamma_{ji}^\rho w_\rho^{(1)}}_{\text{vertex}} \underbrace{\gamma_{ik}^\mu (\ell_\mu + p_{1\mu})}_{\text{propagator}}, \quad (\text{C.17})$$

where the denominator of the propagator is removed since it is already accounted for in the integral-reduction procedure. To be more definite, we show here the expression of each coefficient of the vertex polynomial of eq. (C.17):

$$V_{j,1,0,k}^{(1)} = ig_s (\psi^{(1)} p_1)_{jk}, \quad V_{j,1,s_1,k}^{(1)} = ig_s (\psi^{(1)} \gamma^{(s_1-1)})_{jk} \quad \text{for } s_1 = 1, \dots, 4. \quad (\text{C.18})$$

In renormalisable theories, the rank of the vertex polynomials is maximally equal to one as only one power of the loop momentum can arise from either the propagator or the vertex itself (but not from both). This constraint is not enforced by MADLOOP5, since it would make it impossible to compute one-loop diagrams in effective theories (such as HEFT). The numerical routines for the evaluation of vertex polynomials are generated automatically by ALOHA for each process, using the UFO model specifications; this is what renders the optimisation discussed in this appendix applicable to any model.

Each subsequent loop current $W^{(n+1)}$ is obtained from the previous one $W^{(n)}$ and the vertex polynomial $V^{(n)}$ placed in between via the defining implicit relation:

$$W_{i,r_1+r_2,\dot{k}_1,j}^{(n+1)} \ell^{\dot{k}_1} = (W_{i,r_1,\dot{k}_2,m}^{(n)} \ell^{\dot{k}_2})(V_{m,r_2,\dot{s},j}^{(n)} \ell^{\dot{s}}). \quad (\text{C.19})$$

The r.h.s. of eq. (C.19) is a multiplication of two polynomials and each coefficient of $W^{(n+1)}$ is obtained by summing the corresponding terms in the expanded product. This implies that a symmetrisation of the coefficients is performed after each loop vertex and this step is crucial in order to limit their proliferation and the resulting computing time. To illustrate this, eq. (C.19) is rewritten here for the case $r_1 = r_2 = 1$ with $\dot{k}_1 = 9$, corresponding to the term multiplying $\ell^1 \ell^2$ which can come either from $\dot{k}_2 = 2, \dot{s} = 3$ or $\dot{k}_2 = 3, \dot{s} = 2$:

$$W_{i,2,9,j}^{(n+1)} = W_{i,1,2,m}^{(n)} V_{m,1,3,j}^{(n)} + W_{i,1,3,m}^{(n)} V_{m,1,2,j}^{(n)}. \quad (\text{C.20})$$

Note the implicit summation on the index m which spans the representation of the particle circulating in the loop just before the vertex $V^{(n)}$. Eq. (C.19) is then iteratively used to compute all loop currents, until the second L-cut leg, which includes the last vertex and the L-cut propagator, is reached. The coefficients $C_{\dot{k}}$ of an n -point loop diagram are then simply obtained by *closing* the Lorentz trace:

$$C_{\dot{k}} = W_{i,r,\dot{k},i}^{(n+1)}. \quad (\text{C.21})$$

In the example of fig. 19, this translates into:

$$C_{\dot{k}} = W_{i,3,\dot{k},m}^{(5)} \delta^{mi} = \sum_{i=1}^4 W_{i,3,\dot{k},i}^{(5)}, \quad (\text{C.22})$$

with the sum written explicitly for clarity. It is clear that many loop diagrams can share some of their constituting loop currents; for example the L-cut box diagram of fig. 19 can be prolonged to form loops with more propagators. MADLOOP5 takes advantage of this and computes each loop current only once, for the first loop diagram in which it appears. An algorithm analogous to the one described in ref. [71] is used for choosing the L-cut location in order to maximise the number of loop currents recycled.

We conclude this appendix by stressing that all of the optimisations inherited from the integrand representation of eq. (2.78) can be turned off in MADGRAPH5_AMC@NLO via the option `loop_optimized_output` of the interactive interface and that, when this is done, the structure of the code output by MADLOOP5 is completely different. For this reason and despite being significantly slower, the non optimized output mode provides a powerful self-consistency check and is useful for debugging purposes.

D. Third-party codes included in MADGRAPH5_AMC@NLO

The tarball of MADGRAPH5_AMC@NLO is self-contained, and ready-to-run. This is also thanks to the fact that several third-party codes are included into it. We list all of them here: ALOHA [89], CUTTOOLS [153], FASTJET (CORE) [364], HELAS [88], HERWIG6 [139],

MINT [168], ONELOOP [359], PYTHIA6 [138], QCDLOOP [360], RAMBO [365], StdHEP [366], VEGAS [367, 368].

In the case of FASTJET, what is included in MADGRAPH5_AMC@NLO is a stripped version of that code (visit www.fastjet.fr for more details). For more extended jet-reconstruction capabilities, the user might want to install FASTJET proper (thus including all the relevant plugins).

References

- [1] D. J. Gross and F. Wilczek, *Ultraviolet Behavior of Nonabelian Gauge Theories*, *Phys.Rev.Lett.* **30** (1973) 1343–1346.
- [2] H. D. Politzer, *Reliable Perturbative Results for Strong Interactions?*, *Phys.Rev.Lett.* **30** (1973) 1346–1349.
- [3] T. Appelquist and H. Georgi, *e^+e^- annihilation in gauge theories of strong interactions*, *Phys.Rev.* **D8** (1973) 4000–4002.
- [4] G. F. Sterman and S. Weinberg, *Jets from Quantum Chromodynamics*, *Phys.Rev.Lett.* **39** (1977) 1436.
- [5] A. Buras, E. Floratos, D. Ross, and C. T. Sachrajda, *Asymptotic Freedom Beyond the Leading Order*, *Nucl.Phys.* **B131** (1977) 308.
- [6] W. A. Bardeen, A. Buras, D. Duke, and T. Muta, *Deep Inelastic Scattering Beyond the Leading Order in Asymptotically Free Gauge Theories*, *Phys.Rev.* **D18** (1978) 3998.
- [7] G. Altarelli, R. K. Ellis, and G. Martinelli, *Leptoproduction and Drell-Yan Processes Beyond the Leading Approximation in Chromodynamics*, *Nucl.Phys.* **B143** (1978) 521.
- [8] W. Celmaster and R. J. Gonsalves, *Fourth Order QCD Contributions to the e^+e^- Annihilation Cross-Section*, *Phys.Rev.* **D21** (1980) 3112.
- [9] R. K. Ellis, D. Ross, and A. Terrano, *The Perturbative Calculation of Jet Structure in e^+e^- Annihilation*, *Nucl.Phys.* **B178** (1981) 421.
- [10] S. Frixione, Z. Kunszt, and A. Signer, *Three jet cross-sections to next-to-leading order*, *Nucl.Phys.* **B467** (1996) 399–442, [[hep-ph/9512328](#)].
- [11] S. Catani and M. Seymour, *A General algorithm for calculating jet cross-sections in NLO QCD*, *Nucl.Phys.* **B485** (1997) 291–419, [[hep-ph/9605323](#)].
- [12] S. Frixione, *A General approach to jet cross-sections in QCD*, *Nucl.Phys.* **B507** (1997) 295–314, [[hep-ph/9706545](#)].
- [13] D. A. Kosower, *Antenna factorization of gauge theory amplitudes*, *Phys.Rev.* **D57** (1998) 5410–5416, [[hep-ph/9710213](#)].
- [14] J. M. Campbell, M. Cullen, and E. N. Glover, *Four jet event shapes in electron-positron annihilation*, *Eur.Phys.J.* **C9** (1999) 245–265, [[hep-ph/9809429](#)].
- [15] Z. Bern, L. J. Dixon, D. C. Dunbar, and D. A. Kosower, *One-loop n -point gauge theory amplitudes, unitarity and collinear limits*, *Nucl.Phys.* **B425** (1994) 217–260, [[hep-ph/9403226](#)].

- [16] F. del Aguila and R. Pittau, *Recursive numerical calculus of one-loop tensor integrals*, *JHEP* **0407** (2004) 017, [[hep-ph/0404120](#)].
- [17] Z. Bern, L. J. Dixon, and D. A. Kosower, *Bootstrapping multi-parton loop amplitudes in QCD*, *Phys.Rev.* **D73** (2006) 065013, [[hep-ph/0507005](#)].
- [18] G. Ossola, C. G. Papadopoulos, and R. Pittau, *Reducing full one-loop amplitudes to scalar integrals at the integrand level*, *Nucl.Phys.* **B763** (2007) 147–169, [[hep-ph/0609007](#)].
- [19] C. Anastasiou, R. Britto, B. Feng, Z. Kunszt, and P. Mastrolia, *D-dimensional unitarity cut method*, *Phys.Lett.* **B645** (2007) 213–216, [[hep-ph/0609191](#)].
- [20] C. Anastasiou, R. Britto, B. Feng, Z. Kunszt, and P. Mastrolia, *Unitarity cuts and Reduction to master integrals in d dimensions for one-loop amplitudes*, *JHEP* **0703** (2007) 111, [[hep-ph/0612277](#)].
- [21] R. K. Ellis, W. Giele, and Z. Kunszt, *A Numerical Unitarity Formalism for Evaluating One-Loop Amplitudes*, *JHEP* **0803** (2008) 003, [[arXiv:0708.2398](#)].
- [22] R. K. Ellis, W. T. Giele, Z. Kunszt, and K. Melnikov, *Masses, fermions and generalized D-dimensional unitarity*, *Nucl.Phys.* **B822** (2009) 270–282, [[arXiv:0806.3467](#)].
- [23] W. T. Giele, Z. Kunszt, and K. Melnikov, *Full one-loop amplitudes from tree amplitudes*, *JHEP* **0804** (2008) 049, [[arXiv:0801.2237](#)].
- [24] S. Frixione and B. R. Webber, *Matching NLO QCD computations and parton shower simulations*, *JHEP* **0206** (2002) 029, [[hep-ph/0204244](#)].
- [25] P. Nason, *A New method for combining NLO QCD with shower Monte Carlo algorithms*, *JHEP* **0411** (2004) 040, [[hep-ph/0409146](#)].
- [26] M. Dobbs, *Incorporating next-to-leading order matrix elements for hadronic diboson production in showering event generators*, *Phys.Rev.* **D64** (2001) 034016, [[hep-ph/0103174](#)].
- [27] Y.-j. Chen, J. Collins, and X.-m. Zu, *NLO corrections in MC event generator for angular distribution of Drell-Yan lepton pair production*, *JHEP* **0204** (2002) 041, [[hep-ph/0110257](#)].
- [28] Y. Kurihara, J. Fujimoto, T. Ishikawa, K. Kato, S. Kawabata, et al., *QCD event generators with next-to-leading order matrix elements and parton showers*, *Nucl.Phys.* **B654** (2003) 301–319, [[hep-ph/0212216](#)].
- [29] Z. Nagy and D. E. Soper, *Matching parton showers to NLO computations*, *JHEP* **0510** (2005) 024, [[hep-ph/0503053](#)].
- [30] C. W. Bauer and M. D. Schwartz, *Event Generation from Effective Field Theory*, *Phys.Rev.* **D76** (2007) 074004, [[hep-ph/0607296](#)].
- [31] Z. Nagy and D. E. Soper, *Parton showers with quantum interference*, *JHEP* **0709** (2007) 114, [[arXiv:0706.0017](#)].
- [32] W. T. Giele, D. A. Kosower, and P. Z. Skands, *A simple shower and matching algorithm*, *Phys.Rev.* **D78** (2008) 014026, [[arXiv:0707.3652](#)].
- [33] C. W. Bauer, F. J. Tackmann, and J. Thaler, *GenEvA. I. A New framework for event generation*, *JHEP* **0812** (2008) 010, [[arXiv:0801.4026](#)].
- [34] S. Hoeche, F. Krauss, M. Schonherr, and F. Siegert, *A critical appraisal of NLO+PS matching methods*, *JHEP* **1209** (2012) 049, [[arXiv:1111.1220](#)].

- [35] K. Hamilton, P. Nason, E. Re, and G. Zanderighi, *NNLOPS simulation of Higgs boson production*, *JHEP* **1310** (2013) 222, [[arXiv:1309.0017](#)].
- [36] J. Alwall, M. Herquet, F. Maltoni, O. Mattelaer, and T. Stelzer, *MadGraph 5 : Going Beyond*, *JHEP* **1106** (2011) 128, [[arXiv:1106.0522](#)].
- [37] T. Stelzer and W. Long, *Automatic generation of tree level helicity amplitudes*, *Comput.Phys.Commun.* **81** (1994) 357–371, [[hep-ph/9401258](#)].
- [38] F. Caravaglios and M. Moretti, *An algorithm to compute Born scattering amplitudes without Feynman graphs*, *Phys.Lett.* **B358** (1995) 332–338, [[hep-ph/9507237](#)].
- [39] F. Yuasa, J. Fujimoto, T. Ishikawa, M. Jimbo, T. Kaneko, et al., *Automatic computation of cross-sections in HEP: Status of GRACE system*, *Prog.Theor.Phys.Suppl.* **138** (2000) 18–23, [[hep-ph/0007053](#)].
- [40] A. Kanaki and C. G. Papadopoulos, *HELAC: A Package to compute electroweak helicity amplitudes*, *Comput.Phys.Commun.* **132** (2000) 306–315, [[hep-ph/0002082](#)].
- [41] M. Moretti, T. Ohl, and J. Reuter, *O’Mega: An Optimizing matrix element generator*, [hep-ph/0102195](#).
- [42] F. Krauss, R. Kuhn, and G. Soff, *AMEGIC++ 1.0: A Matrix element generator in C++*, *JHEP* **0202** (2002) 044, [[hep-ph/0109036](#)].
- [43] M. L. Mangano, M. Moretti, F. Piccinini, R. Pittau, and A. D. Polosa, *ALPGEN, a generator for hard multiparton processes in hadronic collisions*, *JHEP* **0307** (2003) 001, [[hep-ph/0206293](#)].
- [44] J. Fujimoto, T. Ishikawa, M. Jimbo, T. Kaneko, K. Kato, et al., *GRACE/SUSY automatic generation of tree amplitudes in the minimal supersymmetric standard model*, *Comput.Phys.Commun.* **153** (2003) 106–134, [[hep-ph/0208036](#)].
- [45] **CompHEP** Collaboration, E. Boos et al., *CompHEP 4.4: Automatic computations from Lagrangians to events*, *Nucl.Instrum.Meth.* **A534** (2004) 250–259, [[hep-ph/0403113](#)].
- [46] S. Tsuno, T. Kaneko, Y. Kurihara, S. Odaka, and K. Kato, *GR@PPA 2.7 event generator for pp / p \bar{p} collisions*, *Comput.Phys.Commun.* **175** (2006) 665–677, [[hep-ph/0602213](#)].
- [47] A. Cafarella, C. G. Papadopoulos, and M. Worek, *Helac-Phegas: A Generator for all parton level processes*, *Comput.Phys.Commun.* **180** (2009) 1941–1955, [[arXiv:0710.2427](#)].
- [48] W. Kilian, T. Ohl, and J. Reuter, *WHIZARD: Simulating Multi-Particle Processes at LHC and ILC*, *Eur.Phys.J.* **C71** (2011) 1742, [[arXiv:0708.4233](#)].
- [49] J. Alwall, P. Demin, S. de Visscher, R. Frederix, M. Herquet, et al., *MadGraph/MadEvent v4: The New Web Generation*, *JHEP* **0709** (2007) 028, [[arXiv:0706.2334](#)].
- [50] T. Gleisberg and S. Hoeche, *Comix, a new matrix element generator*, *JHEP* **0812** (2008) 039, [[arXiv:0808.3674](#)].
- [51] A. Belyaev, N. D. Christensen, and A. Pukhov, *CalcHEP 3.4 for collider physics within and beyond the Standard Model*, *Comput.Phys.Commun.* **184** (2013) 1729–1769, [[arXiv:1207.6082](#)].
- [52] T. Hahn and M. Perez-Victoria, *Automatized one loop calculations in four-dimensions and D-dimensions*, *Comput.Phys.Commun.* **118** (1999) 153–165, [[hep-ph/9807565](#)].

- [53] T. Hahn, *Generating Feynman diagrams and amplitudes with FeynArts 3*, *Comput.Phys.Commun.* **140** (2001) 418–431, [[hep-ph/0012260](#)].
- [54] T. Gleisberg and F. Krauss, *Automating dipole subtraction for QCD NLO calculations*, *Eur.Phys.J.* **C53** (2008) 501–523, [[arXiv:0709.2881](#)].
- [55] C. Berger, Z. Bern, L. Dixon, F. Febres Cordero, D. Forde, et al., *An Automated Implementation of On-Shell Methods for One-Loop Amplitudes*, *Phys.Rev.* **D78** (2008) 036003, [[arXiv:0803.4180](#)].
- [56] R. Frederix, T. Gehrmann, and N. Greiner, *Automation of the Dipole Subtraction Method in MadGraph/MadEvent*, *JHEP* **0809** (2008) 122, [[arXiv:0808.2128](#)].
- [57] W. Giele and G. Zanderighi, *On the Numerical Evaluation of One-Loop Amplitudes: The Gluonic Case*, *JHEP* **0806** (2008) 038, [[arXiv:0805.2152](#)].
- [58] M. Czakon, C. Papadopoulos, and M. Worek, *Polarizing the Dipoles*, *JHEP* **0908** (2009) 085, [[arXiv:0905.0883](#)].
- [59] R. Frederix, S. Frixione, F. Maltoni, and T. Stelzer, *Automation of next-to-leading order computations in QCD: The FKS subtraction*, *JHEP* **0910** (2009) 003, [[arXiv:0908.4272](#)].
- [60] K. Hasegawa, S. Moch, and P. Uwer, *AutoDipole: Automated generation of dipole subtraction terms*, *Comput.Phys.Commun.* **181** (2010) 1802–1817, [[arXiv:0911.4371](#)].
- [61] S. Hoche, F. Krauss, M. Schonherr, and F. Siegert, *Automating the POWHEG method in Sherpa*, *JHEP* **1104** (2011) 024, [[arXiv:1008.5399](#)].
- [62] S. Alioli, P. Nason, C. Oleari, and E. Re, *A general framework for implementing NLO calculations in shower Monte Carlo programs: the POWHEG BOX*, *JHEP* **1006** (2010) 043, [[arXiv:1002.2581](#)].
- [63] P. Mastrolia, G. Ossola, T. Reiter, and F. Tramontano, *Scattering Amplitudes from Unitarity-based Reduction Algorithm at the Integrand-level*, *JHEP* **1008** (2010) 080, [[arXiv:1006.0710](#)].
- [64] R. Frederix, T. Gehrmann, and N. Greiner, *Integrated dipoles with MadDipole in the MadGraph framework*, *JHEP* **1006** (2010) 086, [[arXiv:1004.2905](#)].
- [65] S. Becker, C. Reuschle, and S. Weinzierl, *Numerical NLO QCD calculations*, *JHEP* **1012** (2010) 013, [[arXiv:1010.4187](#)].
- [66] V. Hirschi, R. Frederix, S. Frixione, M. V. Garzelli, F. Maltoni, et al., *Automation of one-loop QCD corrections*, *JHEP* **1105** (2011) 044, [[arXiv:1103.0621](#)].
- [67] G. Bevilacqua, M. Czakon, M. Garzelli, A. van Hameren, A. Kardos, et al., *HELAC-NLO*, *Comput.Phys.Commun.* **184** (2013) 986–997, [[arXiv:1110.1499](#)].
- [68] S. Becker, D. Goetz, C. Reuschle, C. Schwan, and S. Weinzierl, *NLO results for five, six and seven jets in electron-positron annihilation*, *Phys.Rev.Lett.* **108** (2012) 032005, [[arXiv:1111.1733](#)].
- [69] G. Cullen, N. Greiner, G. Heinrich, G. Luisoni, P. Mastrolia, et al., *Automated One-Loop Calculations with GoSam*, *Eur.Phys.J.* **C72** (2012) 1889, [[arXiv:1111.2034](#)].
- [70] T. Binoth, D. Goncalves Netto, D. Lopez-Val, K. Mawatari, T. Plehn, et al., *Automized Squark-Neutralino Production to Next-to-Leading Order*, *Phys.Rev.* **D84** (2011) 075005, [[arXiv:1108.1250](#)].

- [71] F. Cascioli, P. Maierhofer, and S. Pozzorini, *Scattering Amplitudes with Open Loops*, *Phys.Rev.Lett.* **108** (2012) 111601, [[arXiv:1111.5206](#)].
- [72] S. Agrawal, T. Hahn, and E. Mirabella, *FormCalc 7*, *J.Phys.Conf.Ser.* **368** (2012) 012054, [[arXiv:1112.0124](#)].
- [73] Z. Bern, G. Diana, L. Dixon, F. Febres Cordero, S. Hoeche, et al., *Four-Jet Production at the Large Hadron Collider at Next-to-Leading Order in QCD*, *Phys.Rev.Lett.* **109** (2012) 042001, [[arXiv:1112.3940](#)].
- [74] S. Actis, A. Denner, L. Hofer, A. Scharf, and S. Uccirati, *Recursive generation of one-loop amplitudes in the Standard Model*, *JHEP* **1304** (2013) 037, [[arXiv:1211.6316](#)].
- [75] S. Badger, B. Biedermann, P. Uwer, and V. Yundin, *Numerical evaluation of virtual corrections to multi-jet production in massless QCD*, *Comput.Phys.Commun.* **184** (2013) 1981–1998, [[arXiv:1209.0100](#)].
- [76] D. Goncalves-Netto, D. Lopez-Val, K. Mawatari, T. Plehn, and I. Wigmore, *Automated Squark and Gluino Production to Next-to-Leading Order*, *Phys.Rev.* **D87** (2013) 014002, [[arXiv:1211.0286](#)].
- [77] S. Badger, B. Biedermann, P. Uwer, and V. Yundin, *Computation of multi-leg amplitudes with NJet*, [arXiv:1312.7140](#).
- [78] Z. Bern, L. Dixon, F. F. Cordero, S. Hoeche, H. Ita, et al., *The BlackHat Library for One-Loop Amplitudes*, [arXiv:1310.2808](#).
- [79] G. Cullen, H. van Deurzen, N. Greiner, G. Heinrich, G. Luisoni, et al., *GoSam-2.0: a tool for automated one-loop calculations within the Standard Model and beyond*, [arXiv:1404.7096](#).
- [80] E. Byckling and K. Kajantie, *Particle Kinematics*. Wiley, 1971.
- [81] N. D. Christensen and C. Duhr, *FeynRules - Feynman rules made easy*, *Comput.Phys.Commun.* **180** (2009) 1614–1641, [[arXiv:0806.4194](#)].
- [82] N. D. Christensen, P. de Aquino, C. Degrande, C. Duhr, B. Fuks, et al., *A Comprehensive approach to new physics simulations*, *Eur.Phys.J.* **C71** (2011) 1541, [[arXiv:0906.2474](#)].
- [83] N. D. Christensen, C. Duhr, B. Fuks, J. Reuter, and C. Speckner, *Introducing an interface between WHIZARD and FeynRules*, *Eur.Phys.J.* **C72** (2012) 1990, [[arXiv:1010.3251](#)].
- [84] C. Duhr and B. Fuks, *A superspace module for the FeynRules package*, *Comput.Phys.Commun.* **182** (2011) 2404–2426, [[arXiv:1102.4191](#)].
- [85] A. Alloul, N. D. Christensen, C. Degrande, C. Duhr, and B. Fuks, *FeynRules 2.0 - A complete toolbox for tree-level phenomenology*, [arXiv:1310.1921](#).
- [86] A. Alloul, J. D’Hondt, K. De Causmaecker, B. Fuks, and M. Rausch de Traubenberg, *Automated mass spectrum generation for new physics*, *Eur.Phys.J.* **C73** (2013) 2325, [[arXiv:1301.5932](#)].
- [87] C. Degrande, *Automated computation of the R_2 rational terms and ultraviolet counterterms by NLOCT : An illustration on the 2HDM, in preparation.*, .
- [88] H. Murayama, I. Watanabe, and K. Hagiwara, *HELAS: Helicity amplitude subroutines for Feynman diagram evaluations*. KEK-91-11, 1992.

- [89] P. de Aquino, W. Link, F. Maltoni, O. Mattelaer, and T. Stelzer, *ALOHA: Automatic Libraries Of Helicity Amplitudes for Feynman Diagram Computations*, *Comput.Phys.Commun.* **183** (2012) 2254–2263, [[arXiv:1108.2041](#)].
- [90] C. Degrande, C. Duhr, B. Fuks, D. Grellscheid, O. Mattelaer, et al., *UFO - The Universal FeynRules Output*, *Comput.Phys.Commun.* **183** (2012) 1201–1214, [[arXiv:1108.2040](#)].
- [91] J. Alwall, A. Ballestrero, P. Bartalini, S. Belov, E. Boos, et al., *A Standard format for Les Houches event files*, *Comput.Phys.Commun.* **176** (2007) 300–304, [[hep-ph/0609017](#)].
- [92] J. Butterworth, A. Arbey, L. Basso, S. Belov, A. Bharucha, et al., *The Tools and Monte Carlo working group Summary Report*, [arXiv:1003.1643](#).
- [93] E. N. Argyres, W. Beenakker, G. J. van Oldenborgh, A. Denner, S. Dittmaier, et al., *Stable calculations for unstable particles: Restoring gauge invariance*, *Phys.Lett.* **B358** (1995) 339–346, [[hep-ph/9507216](#)].
- [94] W. Beenakker, G. J. van Oldenborgh, A. Denner, S. Dittmaier, J. Hoogland, et al., *The Fermion loop scheme for finite width effects in e^+e^- annihilation into four fermions*, *Nucl.Phys.* **B500** (1997) 255–298, [[hep-ph/9612260](#)].
- [95] G. Passarino, *Unstable particles and nonconserved currents: A Generalization of the fermion loop scheme*, *Nucl.Phys.* **B574** (2000) 451–494, [[hep-ph/9911482](#)].
- [96] W. Beenakker, F. A. Berends, and A. Chapovsky, *An Effective Lagrangian approach for unstable particles*, *Nucl.Phys.* **B573** (2000) 503–535, [[hep-ph/9909472](#)].
- [97] W. Beenakker, A. Chapovsky, A. Kanaki, C. Papadopoulos, and R. Pittau, *Towards an effective Lagrangian approach to fermion loop corrections*, *Nucl.Phys.* **B667** (2003) 359–393, [[hep-ph/0303105](#)].
- [98] M. Beneke, A. Chapovsky, A. Signer, and G. Zanderighi, *Effective theory approach to unstable particle production*, *Phys.Rev.Lett.* **93** (2004) 011602, [[hep-ph/0312331](#)].
- [99] A. Denner, S. Dittmaier, M. Roth, and D. Wackeroth, *Predictions for all processes $e^+e^- \rightarrow 4$ fermions + γ* , *Nucl.Phys.* **B560** (1999) 33–65, [[hep-ph/9904472](#)].
- [100] A. Denner, S. Dittmaier, M. Roth, and L. Wieders, *Electroweak corrections to charged-current $e^+e^- \rightarrow 4$ fermion processes: Technical details and further results*, *Nucl.Phys.* **B724** (2005) 247–294, [[hep-ph/0505042](#)].
- [101] F. Staub, *SARAH 3.2: Dirac Gauginos, UFO output, and more*, *Computer Physics Communications* **184** (2013) pp. 1792–1809, [[arXiv:1207.0906](#)].
- [102] N. D. Christensen, P. de Aquino, N. Deutschmann, C. Duhr, B. Fuks, et al., *Simulating spin- $\frac{3}{2}$ particles at colliders*, *Eur.Phys.J.* **C73** (2013) 2580, [[arXiv:1308.1668](#)].
- [103] J. Alwall, C. Duhr, B. Fuks, O. Mattelaer, D. G. Ozturk, et al., *Computing decay rates for new physics theories with FeynRules and MadGraph5/aMC@NLO*, [arXiv:1402.1178](#).
- [104] F. A. Berends, R. Kleiss, P. De Causmaecker, R. Gastmans, and T. T. Wu, *Single Bremsstrahlung Processes in Gauge Theories*, *Phys.Lett.* **B103** (1981) 124.
- [105] P. De Causmaecker, R. Gastmans, W. Troost, and T. T. Wu, *Multiple Bremsstrahlung in Gauge Theories at High-Energies. 1. General Formalism for Quantum Electrodynamics*, *Nucl.Phys.* **B206** (1982) 53.

- [106] R. Kleiss and W. J. Stirling, *Spinor Techniques for Calculating $p\bar{p} \rightarrow W^\pm/Z^0 + \text{Jets}$* , *Nucl.Phys.* **B262** (1985) 235–262.
- [107] R. Gastmans and T. Wu, *The Ubiquitous photon: Helicity method for QED and QCD*, *Int.Ser.Monogr.Phys.* **80** (1990) 1–648.
- [108] Z. Xu, D.-H. Zhang, and L. Chang, *Helicity Amplitudes for Multiple Bremsstrahlung in Massless Nonabelian Gauge Theories*, *Nucl.Phys.* **B291** (1987) 392.
- [109] J. Gunion and Z. Kunszt, *Improved Analytic Techniques for Tree Graph Calculations and the $ggq\bar{q}l\bar{l}$ Subprocess*, *Phys.Lett.* **B161** (1985) 333.
- [110] K. Hagiwara and D. Zeppenfeld, *Helicity Amplitudes for Heavy Lepton Production in e^+e^- Annihilation*, *Nucl.Phys.* **B274** (1986) 1.
- [111] M. L. Mangano and S. J. Parke, *Multiparton amplitudes in gauge theories*, *Phys.Rept.* **200** (1991) 301–367, [[hep-th/0509223](#)].
- [112] V. Del Duca, L. J. Dixon, and F. Maltoni, *New color decompositions for gauge amplitudes at tree and loop level*, *Nucl.Phys.* **B571** (2000) 51–70, [[hep-ph/9910563](#)].
- [113] F. Maltoni, K. Paul, T. Stelzer, and S. Willenbrock, *Color flow decomposition of QCD amplitudes*, *Phys.Rev.* **D67** (2003) 014026, [[hep-ph/0209271](#)].
- [114] C. Duhr, S. Hoeche, and F. Maltoni, *Color-dressed recursive relations for multi-parton amplitudes*, *JHEP* **0608** (2006) 062, [[hep-ph/0607057](#)].
- [115] K. Hagiwara, J. Kanzaki, Q. Li, and K. Mawatari, *HELAS and MadGraph/MadEvent with spin-2 particles*, *Eur.Phys.J.* **C56** (2008) 435–447, [[arXiv:0805.2554](#)].
- [116] K. Hagiwara, J. Kanzaki, N. Okamura, D. Rainwater, and T. Stelzer, *Fast calculation of HELAS amplitudes using graphics processing unit (GPU)*, *Eur.Phys.J.* **C66** (2010) 477–492, [[arXiv:0908.4403](#)].
- [117] K. Hagiwara, J. Kanzaki, N. Okamura, D. Rainwater, and T. Stelzer, *Calculation of HELAS amplitudes for QCD processes using graphics processing unit (GPU)*, *Eur.Phys.J.* **C70** (2010) 513–524, [[arXiv:0909.5257](#)].
- [118] M. Bahr, S. Gieseke, M. Gigg, D. Grellscheid, K. Hamilton, et al., *Herwig++ Physics and Manual*, *Eur.Phys.J.* **C58** (2008) 639–707, [[arXiv:0803.0883](#)].
- [119] J. Bellm, S. Gieseke, D. Grellscheid, A. Papaefstathiou, S. Platzer, et al., *Herwig++ 2.7 Release Note*, [arXiv:1310.6877](#).
- [120] T. Sjostrand, S. Mrenna, and P. Z. Skands, *A Brief Introduction to PYTHIA 8.1*, *Comput.Phys.Comm.* **178** (2008) 852–867, [[arXiv:0710.3820](#)].
- [121] N. Arkani-Hamed, S. Dimopoulos, and G. Dvali, *The Hierarchy problem and new dimensions at a millimeter*, *Phys.Lett.* **B429** (1998) 263–272, [[hep-ph/9803315](#)].
- [122] R. Frederix, S. Frixione, V. Hirschi, F. Maltoni, R. Pittau, et al., *Four-lepton production at hadron colliders: aMC@NLO predictions with theoretical uncertainties*, *JHEP* **1202** (2012) 099, [[arXiv:1110.4738](#)].
- [123] J. Alwall, Q. Li, and F. Maltoni, *Matched predictions for Higgs production via heavy-quark loops in the SM and beyond*, *Phys.Rev.* **D85** (2012) 014031, [[arXiv:1110.1728](#)].
- [124] R. Frederix, S. Frixione, V. Hirschi, F. Maltoni, O. Mattelaer, et al., *Higgs pair production at the LHC with NLO and parton-shower effects*, [arXiv:1401.7340](#).

- [125] K. Kondo, *Dynamical Likelihood Method for Reconstruction of Events With Missing Momentum. 1: Method and Toy Models*, *J.Phys.Soc.Jap.* **57** (1988) 4126–4140.
- [126] R. Dalitz and G. R. Goldstein, *The decay and polarization properties of the top quark*, *Phys.Rev.* **D45** (1992) 1531–1543.
- [127] K. Kondo, *Dynamical likelihood method and top quark mass measurement at CDF*, *J.Phys.Conf.Ser.* **53** (2006) 202–213.
- [128] Y. Gao, A. V. Gritsan, Z. Guo, K. Melnikov, M. Schulze, et al., *Spin determination of single-produced resonances at hadron colliders*, *Phys.Rev.* **D81** (2010) 075022, [[arXiv:1001.3396](#)].
- [129] P. Avery, D. Bourilkov, M. Chen, T. Cheng, A. Drozdetskiy, et al., *Precision studies of the Higgs boson decay channel $H \rightarrow ZZ \rightarrow 4\ell$ with MEKD*, *Phys.Rev.* **D87** (2013), no. 5 055006, [[arXiv:1210.0896](#)].
- [130] J. M. Campbell, W. T. Giele, and C. Williams, *The Matrix Element Method at Next-to-Leading Order*, *JHEP* **1211** (2012) 043, [[arXiv:1204.4424](#)].
- [131] J. S. Gainer, J. Lykken, K. T. Matchev, S. Mrenna, and M. Park, *Geolocating the Higgs Boson Candidate at the LHC*, *Phys.Rev.Lett.* **111** (2013) 041801, [[arXiv:1304.4936](#)].
- [132] T. Plehn, P. Schichtel, and D. Wiegand, *MadMax, or Where Boosted Significances Come From*, [arXiv:1311.2591](#).
- [133] P. Artoisenet, V. Lemaître, F. Maltoni, and O. Mattelaer, *Automation of the matrix element reweighting method*, *JHEP* **1012** (2010) 068, [[arXiv:1007.3300](#)].
- [134] P. Artoisenet and O. Mattelaer, *MadWeight5.0, in preparation*, .
- [135] J. Alwall, A. Freitas, and O. Mattelaer, *The Matrix Element Method and QCD Radiation*, *Phys.Rev.* **D83** (2011) 074010, [[arXiv:1010.2263](#)].
- [136] P. Artoisenet, P. de Aquino, F. Maltoni, and O. Mattelaer, *Unravelling $t\bar{t}h$ via the Matrix Element Method*, *Phys.Rev.Lett.* **111** (2013), no. 9 091802, [[arXiv:1304.6414](#)].
- [137] T. Gleisberg, S. Hoeche, F. Krauss, A. Schalicke, S. Schumann, et al., *SHERPA 1. alpha: A Proof of concept version*, *JHEP* **0402** (2004) 056, [[hep-ph/0311263](#)].
- [138] T. Sjöstrand, S. Mrenna, and P. Z. Skands, *PYTHIA 6.4 Physics and Manual*, *JHEP* **0605** (2006) 026, [[hep-ph/0603175](#)].
- [139] G. Corcella, I. Knowles, G. Marchesini, S. Moretti, K. Odagiri, et al., *HERWIG 6: An Event generator for hadron emission reactions with interfering gluons (including supersymmetric processes)*, *JHEP* **0101** (2001) 010, [[hep-ph/0011363](#)].
- [140] G. Corcella, I. Knowles, G. Marchesini, S. Moretti, K. Odagiri, et al., *HERWIG 6.5 release note*, [hep-ph/0210213](#).
- [141] S. Catani, Y. L. Dokshitzer, M. Seymour, and B. Webber, *Longitudinally invariant k_t clustering algorithms for hadron hadron collisions*, *Nucl.Phys.* **B406** (1993) 187–224.
- [142] L. Lönnblad, *Correcting the color dipole cascade model with fixed order matrix elements*, *JHEP* **0205** (2002) 046, [[hep-ph/0112284](#)].
- [143] L. Lönnblad and S. Prestel, *Matching Tree-Level Matrix Elements with Interleaved Showers*, *JHEP* **1203** (2012) 019, [[arXiv:1109.4829](#)].

- [144] L. Lonnblad and S. Prestel, *Unitarising Matrix Element + Parton Shower merging*, *JHEP* **1302** (2013) 094, [[arXiv:1211.4827](#)].
- [145] J. Alwall, S. Hoche, F. Krauss, N. Lavesson, L. Lonnblad, et al., *Comparative study of various algorithms for the merging of parton showers and matrix elements in hadronic collisions*, *Eur.Phys.J.* **C53** (2008) 473–500, [[arXiv:0706.2569](#)].
- [146] J. Alwall, S. de Visscher, and F. Maltoni, *QCD radiation in the production of heavy colored particles at the LHC*, *JHEP* **0902** (2009) 017, [[arXiv:0810.5350](#)].
- [147] P. de Aquino, F. Maltoni, K. Mawatari, and B. Oehl, *Light Gravitino Production in Association with Gluinos at the LHC*, *JHEP* **1210** (2012) 008, [[arXiv:1206.7098](#)].
- [148] P. Artoisenet, P. de Aquino, F. Demartin, R. Frederix, S. Frixione, et al., *A framework for Higgs characterisation*, *JHEP* **1311** (2013) 043, [[arXiv:1306.6464](#)].
- [149] F. Maltoni and T. Stelzer, *MadEvent: Automatic event generation with MadGraph*, *JHEP* **0302** (2003) 027, [[hep-ph/0208156](#)].
- [150] R. Kleiss and R. Pittau, *Weight optimization in multichannel Monte Carlo*, *Comput.Phys.Commun.* **83** (1994) 141–146, [[hep-ph/9405257](#)].
- [151] G. Passarino and M. Veltman, *One Loop Corrections for e^+e^- Annihilation Into $\mu^+\mu^-$ in the Weinberg Model*, *Nucl.Phys.* **B160** (1979) 151.
- [152] A. I. Davydychev, *A Simple formula for reducing Feynman diagrams to scalar integrals*, *Phys.Lett.* **B263** (1991) 107–111.
- [153] G. Ossola, C. G. Papadopoulos, and R. Pittau, *CutTools: A Program implementing the OPP reduction method to compute one-loop amplitudes*, *JHEP* **0803** (2008) 042, [[arXiv:0711.3596](#)].
- [154] G. 't Hooft and M. Veltman, *Regularization and Renormalization of Gauge Fields*, *Nucl.Phys.* **B44** (1972) 189–213.
- [155] G. Ossola, C. G. Papadopoulos, and R. Pittau, *On the Rational Terms of the one-loop amplitudes*, *JHEP* **0805** (2008) 004, [[arXiv:0802.1876](#)].
- [156] P. Draggiotis, M. Garzelli, C. Papadopoulos, and R. Pittau, *Feynman Rules for the Rational Part of the QCD 1-loop amplitudes*, *JHEP* **0904** (2009) 072, [[arXiv:0903.0356](#)].
- [157] M. Garzelli, I. Malamos, and R. Pittau, *Feynman rules for the rational part of the Electroweak 1-loop amplitudes*, *JHEP* **1001** (2010) 040, [[arXiv:0910.3130](#)].
- [158] M. Garzelli, I. Malamos, and R. Pittau, *Feynman rules for the rational part of the Electroweak 1-loop amplitudes in the R_ξ gauge and in the Unitary gauge*, *JHEP* **1101** (2011) 029, [[arXiv:1009.4302](#)].
- [159] H.-S. Shao, Y.-J. Zhang, and K.-T. Chao, *Feynman Rules for the Rational Part of the Standard Model One-loop Amplitudes in the 't Hooft-Veltman γ_5 Scheme*, *JHEP* **09** (2011) 048, [[arXiv:1106.5030](#)].
- [160] R. Pittau, *Primary Feynman rules to calculate the epsilon-dimensional integrand of any 1-loop amplitude*, *JHEP* **1202** (2012) 029, [[arXiv:1111.4965](#)].
- [161] H.-S. Shao and Y.-J. Zhang, *Feynman Rules for the Rational Part of One-loop QCD Corrections in the MSSM*, *JHEP* **1206** (2012) 112, [[arXiv:1205.1273](#)].

- [162] B. Page and R. Pittau, R_2 vertices for the effective ggH theory, *JHEP* **1309** (2013) 078, [[arXiv:1307.6142](#)].
- [163] T. Binoth, J. P. Guillet, and G. Heinrich, Algebraic evaluation of rational polynomials in one-loop amplitudes, *JHEP* **0702** (2007) 013, [[hep-ph/0609054](#)].
- [164] S. Badger, Direct Extraction Of One Loop Rational Terms, *JHEP* **0901** (2009) 049, [[arXiv:0806.4600](#)].
- [165] H.-S. Shao, *Iregi user manual, unpublished*, .
- [166] J. Fleischer, T. Riemann, and V. Yundin, New developments in PJFry, *PoS LL2012* (2012) 020, [[arXiv:1210.4095](#)].
- [167] V. Yundin, *Massive loop corrections for collider physics*. PhD thesis, Humboldt-Universitat zu Berlin, 2012.
- [168] P. Nason, MINT: A Computer program for adaptive Monte Carlo integration and generation of unweighted distributions, [arXiv:0709.2085](#).
- [169] S. Frixione, P. Nason, and B. R. Webber, Matching NLO QCD and parton showers in heavy flavor production, *JHEP* **0308** (2003) 007, [[hep-ph/0305252](#)].
- [170] S. Frixione, E. Laenen, P. Motylinski, and B. R. Webber, Single-top production in MC@NLO, *JHEP* **0603** (2006) 092, [[hep-ph/0512250](#)].
- [171] P. Torrielli and S. Frixione, Matching NLO QCD computations with PYTHIA using MC@NLO, *JHEP* **1004** (2010) 110, [[arXiv:1002.4293](#)].
- [172] S. Frixione, F. Stoeckli, P. Torrielli, and B. R. Webber, NLO QCD corrections in Herwig++ with MC@NLO, *JHEP* **1101** (2011) 053, [[arXiv:1010.0568](#)].
- [173] L. Lonnblad, ARIADNE version 4: A Program for simulation of QCD cascades implementing the color dipole model, *Comput.Phys.Commun.* **71** (1992) 15–31.
- [174] Z. Nagy and D. E. Soper, A New parton shower algorithm: Shower evolution, matching at leading and next-to-leading order level, [hep-ph/0601021](#).
- [175] M. Dinsdale, M. Ternick, and S. Weinzierl, Parton showers from the dipole formalism, *Phys.Rev.* **D76** (2007) 094003, [[arXiv:0709.1026](#)].
- [176] S. Schumann and F. Krauss, A Parton shower algorithm based on Catani-Seymour dipole factorisation, *JHEP* **0803** (2008) 038, [[arXiv:0709.1027](#)].
- [177] J.-C. Winter and F. Krauss, Initial-state showering based on colour dipoles connected to incoming parton lines, *JHEP* **0807** (2008) 040, [[arXiv:0712.3913](#)].
- [178] S. Platzer and S. Gieseke, Dipole Showers and Automated NLO Matching in Herwig++, *Eur.Phys.J.* **C72** (2012) 2187, [[arXiv:1109.6256](#)].
- [179] M. Ritzmann, D. Kosower, and P. Skands, Antenna Showers with Hadronic Initial States, *Phys.Lett.* **B718** (2013) 1345–1350, [[arXiv:1210.6345](#)].
- [180] C. Friberg, G. Gustafson, and J. Hakkinen, Color connections in e^+e^- annihilation, *Nucl.Phys.* **B490** (1997) 289–305, [[hep-ph/9604347](#)].
- [181] W. Giele, D. Kosower, and P. Skands, Higher-Order Corrections to Timelike Jets, *Phys.Rev.* **D84** (2011) 054003, [[arXiv:1102.2126](#)].

- [182] S. Platzer and M. Sjodahl, *Subleading N_c improved Parton Showers*, *JHEP* **1207** (2012) 042, [[arXiv:1201.0260](#)].
- [183] Z. Nagy and D. E. Soper, *Parton shower evolution with subleading color*, *JHEP* **1206** (2012) 044, [[arXiv:1202.4496](#)].
- [184] G. Altarelli and G. Parisi, *Asymptotic Freedom in Parton Language*, *Nucl.Phys.* **B126** (1977) 298.
- [185] K. Odagiri, *Color connection structure of supersymmetric QCD ($2 \rightarrow 2$) processes*, *JHEP* **9810** (1998) 006, [[hep-ph/9806531](#)].
- [186] P. Nason and B. Webber, *Next-to-Leading-Order Event Generators*, *Ann.Rev.Nucl.Part.Sci.* **62** (2012) 187–213, [[arXiv:1202.1251](#)].
- [187] S. Hoeche, F. Krauss, and M. Schonherr, *Uncertainties in MEPS@NLO calculations of h +jets*, [arXiv:1401.7971](#).
- [188] R. Frederix and S. Frixione, *Merging meets matching in MC@NLO*, *JHEP* **1212** (2012) 061, [[arXiv:1209.6215](#)].
- [189] S. Catani, F. Krauss, R. Kuhn, and B. Webber, *QCD matrix elements + parton showers*, *JHEP* **0111** (2001) 063, [[hep-ph/0109231](#)].
- [190] F. Krauss, *Matrix elements and parton showers in hadronic interactions*, *JHEP* **0208** (2002) 015, [[hep-ph/0205283](#)].
- [191] S. Mrenna and P. Richardson, *Matching matrix elements and parton showers with HERWIG and PYTHIA*, *JHEP* **0405** (2004) 040, [[hep-ph/0312274](#)].
- [192] N. Lavesson and L. Lonnblad, *W +jets matrix elements and the dipole cascade*, *JHEP* **0507** (2005) 054, [[hep-ph/0503293](#)].
- [193] S. Hoeche, F. Krauss, S. Schumann, and F. Siegert, *QCD matrix elements and truncated showers*, *JHEP* **0905** (2009) 053, [[arXiv:0903.1219](#)].
- [194] K. Hamilton, P. Richardson, and J. Tully, *A Modified CKKW matrix element merging approach to angular-ordered parton showers*, *JHEP* **0911** (2009) 038, [[arXiv:0905.3072](#)].
- [195] N. Lavesson and L. Lonnblad, *Extending CKKW-merging to One-Loop Matrix Elements*, *JHEP* **0812** (2008) 070, [[arXiv:0811.2912](#)].
- [196] K. Hamilton and P. Nason, *Improving NLO-parton shower matched simulations with higher order matrix elements*, *JHEP* **1006** (2010) 039, [[arXiv:1004.1764](#)].
- [197] S. Hoeche, F. Krauss, M. Schonherr, and F. Siegert, *NLO matrix elements and truncated showers*, *JHEP* **1108** (2011) 123, [[arXiv:1009.1127](#)].
- [198] S. Alioli, K. Hamilton, and E. Re, *Practical improvements and merging of POWHEG simulations for vector boson production*, *JHEP* **1109** (2011) 104, [[arXiv:1108.0909](#)].
- [199] S. Hoeche, F. Krauss, M. Schonherr, and F. Siegert, *QCD matrix elements + parton showers: The NLO case*, *JHEP* **1304** (2013) 027, [[arXiv:1207.5030](#)].
- [200] S. Plaetzer, *Controlling inclusive cross sections in parton shower + matrix element merging*, *JHEP* **1308** (2013) 114, [[arXiv:1211.5467](#)].
- [201] S. Alioli, C. W. Bauer, C. J. Berggren, A. Hornig, F. J. Tackmann, et al., *Combining Higher-Order Resummation with Multiple NLO Calculations and Parton Showers in GENEVA*, *JHEP* **1309** (2013) 120, [[arXiv:1211.7049](#)].

- [202] L. Lonnblad and S. Prestel, *Merging Multi-leg NLO Matrix Elements with Parton Showers*, *JHEP* **1303** (2013) 166, [[arXiv:1211.7278](#)].
- [203] K. Hamilton, P. Nason, C. Oleari, and G. Zanderighi, *Merging $H/W/Z + 0$ and 1 jet at NLO with no merging scale: a path to parton shower + NNLO matching*, *JHEP* **1305** (2013) 082, [[arXiv:1212.4504](#)].
- [204] S. Alioli, C. W. Bauer, C. Berggren, F. J. Tackmann, J. R. Walsh, et al., *Matching Fully Differential NNLO Calculations and Parton Showers*, [arXiv:1311.0286](#).
- [205] G. Bozzi, S. Catani, D. de Florian, and M. Grazzini, *Transverse-momentum resummation and the spectrum of the Higgs boson at the LHC*, *Nucl.Phys.* **B737** (2006) 73–120, [[hep-ph/0508068](#)].
- [206] R. G. Stuart, *Gauge invariance, analyticity and physical observables at the Z^0 resonance*, *Phys.Lett.* **B262** (1991) 113–119.
- [207] A. Aeppli, G. J. van Oldenborgh, and D. Wyler, *Unstable particles in one loop calculations*, *Nucl.Phys.* **B428** (1994) 126–146, [[hep-ph/9312212](#)].
- [208] S. Frixione, E. Laenen, P. Motylinski, and B. R. Webber, *Angular correlations of lepton pairs from vector boson and top quark decays in Monte Carlo simulations*, *JHEP* **0704** (2007) 081, [[hep-ph/0702198](#)].
- [209] P. Richardson, *Spin correlations in Monte Carlo simulations*, *JHEP* **0111** (2001) 029, [[hep-ph/0110108](#)].
- [210] P. Artoisenet, R. Frederix, O. Mattelaer, and R. Rietkerk, *Automatic spin-entangled decays of heavy resonances in Monte Carlo simulations*, *JHEP* **1303** (2013) 015, [[arXiv:1212.3460](#)].
- [211] A. Papanastasiou, R. Frederix, S. Frixione, V. Hirschi, and F. Maltoni, *Single-top t -channel production with off-shell and non-resonant effects*, *Phys.Lett.* **B726** (2013) 223–227, [[arXiv:1305.7088](#)].
- [212] J. Conway, “Pretty Good Simulator.”
<http://www.physics.ucdavis.edu/~conway/research/software/pgs/pgs.html>.
- [213] J. de Favereau et al., *DELPHES 3, A modular framework for fast simulation of a generic collider experiment*, *JHEP* **1402** (2014) 057, [[arXiv:1307.6346](#)].
- [214] S. Ovyn, X. Rouby, and V. Lemaître, *DELPHES, a framework for fast simulation of a generic collider experiment*, [arXiv:0903.2225](#).
- [215] **SM Working group** Collaboration, *Proceedings of the workshop physics at tev colliders, les houches, 2013, to appear*, .
- [216] A. Martin, W. Stirling, R. Thorne, and G. Watt, *Parton distributions for the LHC*, *Eur.Phys.J.* **C63** (2009) 189–285, [[arXiv:0901.0002](#)].
- [217] M. Cacciari, G. P. Salam, and G. Soyez, *The anti- k_t jet clustering algorithm*, *JHEP* **0804** (2008) 063, [[arXiv:0802.1189](#)].
- [218] S. Frixione, *Isolated photons in perturbative QCD*, *Phys.Lett.* **B429** (1998) 369–374, [[hep-ph/9801442](#)].
- [219] R. Frederix, E. Re, and P. Torrielli, *Single-top t -channel hadroproduction in the four-flavour scheme with POWHEG and aMC@NLO*, *JHEP* **1209** (2012) 130, [[arXiv:1207.5391](#)].

- [220] J. M. Campbell and R. K. Ellis, *Next-to-leading order corrections to W^+ 2 jet and Z^+ 2 jet production at hadron colliders*, *Phys.Rev.* **D65** (2002) 113007, [[hep-ph/0202176](#)].
- [221] J. M. Campbell, R. K. Ellis, and D. L. Rainwater, *Next-to-leading order QCD predictions for $W + 2$ jet and $Z + 2$ jet production at the CERN LHC*, *Phys.Rev.* **D68** (2003) 094021, [[hep-ph/0308195](#)].
- [222] J. M. Campbell, R. K. Ellis, P. Nason, and G. Zanderighi, *W and Z bosons in association with two jets using the POWHEG method*, *JHEP* **1308** (2013) 005, [[arXiv:1303.5447](#)].
- [223] J. M. Campbell, R. K. Ellis, F. Febres Cordero, F. Maltoni, L. Reina, et al., *Associated Production of a W Boson and One b Jet*, *Phys.Rev.* **D79** (2009) 034023, [[arXiv:0809.3003](#)].
- [224] J. M. Campbell, R. K. Ellis, F. Maltoni, and S. Willenbrock, *Associated production of a Z Boson and a single heavy quark jet*, *Phys.Rev.* **D69** (2004) 074021, [[hep-ph/0312024](#)].
- [225] J. M. Campbell, R. K. Ellis, F. Maltoni, and S. Willenbrock, *Production of a Z boson and two jets with one heavy-quark tag*, *Phys.Rev.* **D73** (2006) 054007, [[hep-ph/0510362](#)].
- [226] J. M. Campbell, R. K. Ellis, F. Maltoni, and S. Willenbrock, *Production of a W boson and two jets with one b-quark tag*, *Phys.Rev.* **D75** (2007) 054015, [[hep-ph/0611348](#)].
- [227] J. Campbell, F. Caola, F. Febres Cordero, L. Reina, and D. Wackerroth, *NLO QCD predictions for $W + 1$ jet and $W + 2$ jet production with at least one b jet at the 7 TeV LHC*, *Phys.Rev.* **D86** (2012) 034021, [[arXiv:1107.3714](#)].
- [228] S. Alioli, P. Nason, C. Oleari, and E. Re, *NLO vector-boson production matched with shower in POWHEG*, *JHEP* **0807** (2008) 060, [[arXiv:0805.4802](#)].
- [229] S. Alioli, P. Nason, C. Oleari, and E. Re, *Vector boson plus one jet production in POWHEG*, *JHEP* **1101** (2011) 095, [[arXiv:1009.5594](#)].
- [230] E. Re, *NLO corrections merged with parton showers for $Z+2$ jets production using the POWHEG method*, *JHEP* **1210** (2012) 031, [[arXiv:1204.5433](#)].
- [231] R. K. Ellis, K. Melnikov, and G. Zanderighi, *Generalized unitarity at work: first NLO QCD results for hadronic W^+ 3jet production*, *JHEP* **0904** (2009) 077, [[arXiv:0901.4101](#)].
- [232] K. Melnikov and G. Zanderighi, *$W+3$ jet production at the LHC as a signal or background*, *Phys.Rev.* **D81** (2010) 074025, [[arXiv:0910.3671](#)].
- [233] C. Berger, Z. Bern, L. J. Dixon, F. Febres Cordero, D. Forde, et al., *Precise Predictions for $W + 3$ Jet Production at Hadron Colliders*, *Phys.Rev.Lett.* **102** (2009) 222001, [[arXiv:0902.2760](#)].
- [234] C. Berger, Z. Bern, L. J. Dixon, F. Febres Cordero, D. Forde, et al., *Next-to-Leading Order QCD Predictions for $W+3$ -Jet Distributions at Hadron Colliders*, *Phys.Rev.* **D80** (2009) 074036, [[arXiv:0907.1984](#)].
- [235] C. Berger, Z. Bern, L. J. Dixon, F. Febres Cordero, D. Forde, et al., *Next-to-Leading Order QCD Predictions for $Z, \gamma^* + 3$ -Jet Distributions at the Tevatron*, *Phys.Rev.* **D82** (2010) 074002, [[arXiv:1004.1659](#)].
- [236] C. Berger, Z. Bern, L. J. Dixon, F. Febres Cordero, D. Forde, et al., *Precise Predictions for $W + 4$ Jet Production at the Large Hadron Collider*, *Phys.Rev.Lett.* **106** (2011) 092001, [[arXiv:1009.2338](#)].

- [237] H. Ita, Z. Bern, L. Dixon, F. Febres Cordero, D. Kosower, et al., *Precise Predictions for $Z + 4$ Jets at Hadron Colliders*, *Phys.Rev.* **D85** (2012) 031501, [[arXiv:1108.2229](#)].
- [238] S. Hoeche, F. Krauss, M. Schonherr, and F. Siegert, *$W+n$ -jet predictions at the Large Hadron Collider at next-to-leading order matched with a parton shower*, *Phys.Rev.Lett.* **110** (2013) 052001, [[arXiv:1201.5882](#)].
- [239] S. Catani, M. Fontannaz, J. Guillet, and E. Pilon, *Cross-section of isolated prompt photons in hadron hadron collisions*, *JHEP* **0205** (2002) 028, [[hep-ph/0204023](#)].
- [240] Z. Bern, G. Diana, L. Dixon, F. Febres Cordero, S. Hoche, et al., *Driving Missing Data at Next-to-Leading Order*, *Phys.Rev.* **D84** (2011) 114002, [[arXiv:1106.1423](#)].
- [241] K. Arnold, J. Bellm, G. Bozzi, M. Brieg, F. Campanario, et al., *VBFNLO: A Parton Level Monte Carlo for Processes with Electroweak Bosons – Manual for Version 2.5.0*, [arXiv:1107.4038](#).
- [242] B. Jager, S. Schneider, and G. Zanderighi, *Next-to-leading order QCD corrections to electroweak Zjj production in the POWHEG BOX*, *JHEP* **1209** (2012) 083, [[arXiv:1207.2626](#)].
- [243] B. Mele, P. Nason, and G. Ridolfi, *QCD radiative corrections to Z boson pair production in hadronic collisions*, *Nucl.Phys.* **B357** (1991) 409–438.
- [244] J. Ohnemus and J. Owens, *An $O(\alpha_s)$ calculation of hadronic ZZ production*, *Phys.Rev.* **D43** (1991) 3626–3639.
- [245] S. Frixione, P. Nason, and G. Ridolfi, *Strong corrections to WZ production at hadron colliders*, *Nucl.Phys.* **B383** (1992) 3–44.
- [246] J. Ohnemus, *An $O(\alpha_s)$ calculation of hadronic W^-W^+ production*, *Phys.Rev.* **D44** (1991) 1403–1414.
- [247] J. Ohnemus, *An $O(\alpha_s)$ calculation of hadronic $W^\pm Z$ production*, *Phys.Rev.* **D44** (1991) 3477–3489.
- [248] S. Frixione, *A Next-to-leading order calculation of the cross-section for the production of W^+W^- pairs in hadronic collisions*, *Nucl.Phys.* **B410** (1993) 280–324.
- [249] J. M. Campbell and R. K. Ellis, *An update on vector boson pair production at hadron colliders*, *Phys.Rev.* **D60** (1999) 113006, [[hep-ph/9905386](#)].
- [250] L. J. Dixon, Z. Kunszt, and A. Signer, *Vector boson pair production in hadronic collisions at order α_s : Lepton correlations and anomalous couplings*, *Phys.Rev.* **D60** (1999) 114037, [[hep-ph/9907305](#)].
- [251] D. De Florian and A. Signer, *$W\gamma$ and $Z\gamma$ production at hadron colliders*, *Eur.Phys.J.* **C16** (2000) 105–114, [[hep-ph/0002138](#)].
- [252] J. M. Campbell, R. K. Ellis, and C. Williams, *Vector boson pair production at the LHC*, *JHEP* **1107** (2011) 018, [[arXiv:1105.0020](#)].
- [253] P. Nason and G. Ridolfi, *A Positive-weight next-to-leading-order Monte Carlo for Z pair hadroproduction*, *JHEP* **0608** (2006) 077, [[hep-ph/0606275](#)].
- [254] T. Melia, P. Nason, R. Rontsch, and G. Zanderighi, *W^+W^- , WZ and ZZ production in the POWHEG BOX*, *JHEP* **1111** (2011) 078, [[arXiv:1107.5051](#)].

- [255] P. Nason and G. Zanderighi, W^+W^- , WZ and ZZ production in the POWHEG-BOX-V2, *Eur.Phys.J.* **C74** (2014) 2702, [[arXiv:1311.1365](#)].
- [256] V. Del Duca, F. Maltoni, Z. Nagy, and Z. Trocsanyi, *QCD radiative corrections to prompt diphoton production in association with a jet at hadron colliders*, *JHEP* **0304** (2003) 059, [[hep-ph/0303012](#)].
- [257] T. Gehrmann, N. Greiner, and G. Heinrich, *Precise QCD predictions for the production of a photon pair in association with two jets*, *Phys.Rev.Lett.* **111** (2013) 222002, [[arXiv:1308.3660](#)].
- [258] S. Badger, A. Guffanti, and V. Yundin, *Next-to-leading order QCD corrections to di-photon production in association with up to three jets at the Large Hadron Collider*, *JHEP* **1403** (2014) 122, [[arXiv:1312.5927](#)].
- [259] Z. Bern, L. Dixon, F. Febres Cordero, S. Hoeche, H. Ita, et al., *Next-to-leading order diphoton+2-jet production at the LHC*, [arXiv:1312.0592](#).
- [260] Z. Bern, L. Dixon, F. Febres Cordero, S. Hoeche, H. Ita, et al., *Next-to-Leading Order $\gamma\gamma + 2$ -Jet Production at the LHC*, [arXiv:1402.4127](#).
- [261] T. Melia, K. Melnikov, R. Rontsch, and G. Zanderighi, *Next-to-leading order QCD predictions for W^+W^+jj production at the LHC*, *JHEP* **1012** (2010) 053, [[arXiv:1007.5313](#)].
- [262] F. Campanario, M. Kerner, L. D. Ninh, and D. Zeppenfeld, *Next-to-leading order QCD corrections to W^+W^+ and W^-W^- production in association with two jets*, *Phys.Rev.* **D89** (2014) 054009, [[arXiv:1311.6738](#)].
- [263] J. M. Campbell, H. B. Hartanto, and C. Williams, *Next-to-leading order predictions for $Z\gamma$ +jet and $Z\gamma\gamma$ final states at the LHC*, *JHEP* **1211** (2012) 162, [[arXiv:1208.0566](#)].
- [264] F. Campanario, M. Kerner, L. D. Ninh, and D. Zeppenfeld, *Next-to-leading order QCD corrections to $W\gamma$ production in association with two jets*, [arXiv:1402.0505](#).
- [265] F. Campanario, M. Kerner, L. D. Ninh, and D. Zeppenfeld, *NLO QCD corrections to $WZjj$ production at the LHC*, [arXiv:1310.4369](#).
- [266] F. Campanario, C. Englert, M. Spannowsky, and D. Zeppenfeld, *NLO-QCD corrections to $W\gamma j$ production*, *Europhys.Lett.* **88** (2009) 11001, [[arXiv:0908.1638](#)].
- [267] F. Campanario, C. Englert, and M. Spannowsky, *Precise predictions for (non-standard) $W\gamma + jet$ production*, *Phys.Rev.* **D83** (2011) 074009, [[arXiv:1010.1291](#)].
- [268] F. Campanario, C. Englert, S. Kallweit, M. Spannowsky, and D. Zeppenfeld, *NLO QCD corrections to $WZ+jet$ production with leptonic decays*, *JHEP* **1007** (2010) 076, [[arXiv:1006.0390](#)].
- [269] B. Jager and G. Zanderighi, *Electroweak W^+W^-jj production at NLO in QCD matched with parton shower in the POWHEG-BOX*, *JHEP* **1304** (2013) 024, [[arXiv:1301.1695](#)].
- [270] F. Schissler and D. Zeppenfeld, *Parton Shower Effects on W and Z Production via Vector Boson Fusion at NLO QCD*, *JHEP* **1304** (2013) 057, [[arXiv:1302.2884](#)].
- [271] B. Jger, A. Karlberg, and G. Zanderighi, *Electroweak $ZZjj$ production in the Standard Model and beyond in the POWHEG-BOX V2*, *JHEP* **1403** (2014) 141, [[arXiv:1312.3252](#)].

- [272] G. Bozzi, F. Campanario, M. Rauch, and D. Zeppenfeld, *$Z\gamma\gamma$ production with leptonic decays and triple photon production at next-to-leading order QCD*, *Phys.Rev.* **D84** (2011) 074028, [[arXiv:1107.3149](#)].
- [273] G. Bozzi, F. Campanario, M. Rauch, and D. Zeppenfeld, *$W^\pm\gamma\gamma$ production with leptonic decays at NLO QCD*, *Phys.Rev.* **D83** (2011) 114035, [[arXiv:1103.4613](#)].
- [274] G. Bozzi, F. Campanario, M. Rauch, H. Rzehak, and D. Zeppenfeld, *NLO QCD corrections to $W^\pm Z\gamma$ production with leptonic decays*, *Phys.Lett.* **B696** (2011) 380–385, [[arXiv:1011.2206](#)].
- [275] G. Bozzi, F. Campanario, V. Hankele, and D. Zeppenfeld, *NLO QCD corrections to $W^+W^-\gamma$ and $ZZ\gamma$ production with leptonic decays*, *Phys.Rev.* **D81** (2010) 094030, [[arXiv:0911.0438](#)].
- [276] F. Campanario, V. Hankele, C. Oleari, S. Prestel, and D. Zeppenfeld, *QCD corrections to charged triple vector boson production with leptonic decay*, *Phys.Rev.* **D78** (2008) 094012, [[arXiv:0809.0790](#)].
- [277] J. M. Campbell and C. Williams, *Triphoton production at hadron colliders*, [arXiv:1403.2641](#).
- [278] M. Mandal, P. Mathews, V. Ravindran, and S. Seth, *Three photon production to NLO+PS accuracy at the LHC*, [arXiv:1403.2917](#).
- [279] A. Lazopoulos, K. Melnikov, and F. Petriello, *QCD corrections to tri-boson production*, *Phys.Rev.* **D76** (2007) 014001, [[hep-ph/0703273](#)].
- [280] F. Campanario, C. Englert, M. Rauch, and D. Zeppenfeld, *Precise predictions for $W\gamma\gamma$ +jet production at hadron colliders*, *Phys.Lett.* **B704** (2011) 515–519, [[arXiv:1106.4009](#)].
- [281] S. Hoeche, F. Krauss, S. Pozzorini, M. Schoenherr, J. Thompson, et al., *Triple vector boson production through Higgs-Strahlung with NLO multijet merging*, [arXiv:1403.7516](#).
- [282] P. Nason, S. Dawson, and R. K. Ellis, *The Total Cross-Section for the Production of Heavy Quarks in Hadronic Collisions*, *Nucl.Phys.* **B303** (1988) 607.
- [283] W. Beenakker, H. Kuijf, W. van Neerven, and J. Smith, *QCD Corrections to Heavy Quark Production in $p\bar{p}$ Collisions*, *Phys.Rev.* **D40** (1989) 54–82.
- [284] P. Nason, S. Dawson, and R. K. Ellis, *The One Particle Inclusive Differential Cross-Section for Heavy Quark Production in Hadronic Collisions*, *Nucl.Phys.* **B327** (1989) 49–92.
- [285] W. Beenakker, W. van Neerven, R. Meng, G. Schuler, and J. Smith, *QCD corrections to heavy quark production in hadron hadron collisions*, *Nucl.Phys.* **B351** (1991) 507–560.
- [286] M. L. Mangano, P. Nason, and G. Ridolfi, *Heavy quark correlations in hadron collisions at next-to-leading order*, *Nucl.Phys.* **B373** (1992) 295–345.
- [287] S. Frixione, P. Nason, and G. Ridolfi, *A Positive-weight next-to-leading-order Monte Carlo for heavy flavour hadroproduction*, *JHEP* **0709** (2007) 126, [[arXiv:0707.3088](#)].
- [288] S. Dittmaier, P. Uwer, and S. Weinzierl, *NLO QCD corrections to $t\bar{t}$ + jet production at hadron colliders*, *Phys.Rev.Lett.* **98** (2007) 262002, [[hep-ph/0703120](#)].
- [289] K. Melnikov, A. Scharf, and M. Schulze, *Top quark pair production in association with a jet: QCD corrections and jet radiation in top quark decays*, *Phys.Rev.* **D85** (2012) 054002, [[arXiv:1111.4991](#)].

- [290] S. Alioli, S.-O. Moch, and P. Uwer, *Hadronic top-quark pair-production with one jet and parton showering*, *JHEP* **1201** (2012) 137, [[arXiv:1110.5251](#)].
- [291] G. Bevilacqua, M. Czakon, C. Papadopoulos, and M. Worek, *Dominant QCD Backgrounds in Higgs Boson Analyses at the LHC: A Study of $pp \rightarrow t\bar{t} + 2 \text{ jets}$ at Next-To-Leading Order*, *Phys.Rev.Lett.* **104** (2010) 162002, [[arXiv:1002.4009](#)].
- [292] M. Schonherr, S. Hoeche, J. Huang, G. Luisoni, and J. Winter, *NLO merging in $t\bar{t}$ -jets*, [arXiv:1311.3621](#).
- [293] S. Hoeche, F. Krauss, P. Maierhoefer, S. Pozzorini, M. Schonherr, et al., *Next-to-leading order QCD predictions for top-quark pair production with up to two jets merged with a parton shower*, [arXiv:1402.6293](#).
- [294] Z. Nagy, *Next-to-leading order calculation of three jet observables in hadron hadron collision*, *Phys.Rev.* **D68** (2003) 094002, [[hep-ph/0307268](#)].
- [295] S. Badger, B. Biedermann, P. Uwer, and V. Yundin, *NLO QCD corrections to multi-jet production at the LHC with a centre-of-mass energy of $\sqrt{s} = 8 \text{ TeV}$* , *Phys.Lett.* **B718** (2013) 965–978, [[arXiv:1209.0098](#)].
- [296] S. Badger, B. Biedermann, P. Uwer, and V. Yundin, *Next-to-leading order QCD corrections to five jet production at the LHC*, *Phys.Rev.* **D89** (2014) 034019, [[arXiv:1309.6585](#)].
- [297] S. Alioli, K. Hamilton, P. Nason, C. Oleari, and E. Re, *Jet pair production in POWHEG*, *JHEP* **1104** (2011) 081, [[arXiv:1012.3380](#)].
- [298] A. Kardos, P. Nason, and C. Oleari, *Three-jet production in POWHEG*, *JHEP* **1404** (2014) 043, [[arXiv:1402.4001](#)].
- [299] N. Greiner, A. Guffanti, T. Reiter, and J. Reuter, *NLO QCD corrections to the production of two bottom-antibottom pairs at the LHC*, *Phys.Rev.Lett.* **107** (2011) 102002, [[arXiv:1105.3624](#)].
- [300] G. Bevilacqua, M. Czakon, M. Krämer, M. Kubocz, and M. Worek, *Quantifying quark mass effects at the LHC: A study of $pp \rightarrow b\bar{b}b\bar{b} + X$ at next-to-leading order*, *JHEP* **1307** (2013) 095, [[arXiv:1304.6860](#)].
- [301] G. Bevilacqua, M. Czakon, C. Papadopoulos, R. Pittau, and M. Worek, *Assault on the NLO Wishlist: $pp \rightarrow t\bar{t}b\bar{b}$* , *JHEP* **0909** (2009) 109, [[arXiv:0907.4723](#)].
- [302] A. Bredenstein, A. Denner, S. Dittmaier, and S. Pozzorini, *NLO QCD corrections to $pp \rightarrow t\bar{t}b\bar{b} + X$ at the LHC*, *Phys.Rev.Lett.* **103** (2009) 012002, [[arXiv:0905.0110](#)].
- [303] A. Bredenstein, A. Denner, S. Dittmaier, and S. Pozzorini, *NLO QCD Corrections to Top Anti-Top Bottom Anti-Bottom Production at the LHC: 2. full hadronic results*, *JHEP* **1003** (2010) 021, [[arXiv:1001.4006](#)].
- [304] G. Bevilacqua and M. Worek, *Constraining BSM Physics at the LHC: Four top final states with NLO accuracy in perturbative QCD*, *JHEP* **1207** (2012) 111, [[arXiv:1206.3064](#)].
- [305] R. K. Ellis and S. Veseli, *Strong radiative corrections to $Wb\bar{b}$ production in $p\bar{p}$ collisions*, *Phys.Rev.* **D60** (1999) 011501, [[hep-ph/9810489](#)].
- [306] S. Badger, J. M. Campbell, and R. Ellis, *QCD corrections to the hadronic production of a heavy quark pair and a W-boson including decay correlations*, *JHEP* **1103** (2011) 027, [[arXiv:1011.6647](#)].

- [307] R. Frederix, S. Frixione, V. Hirschi, F. Maltoni, R. Pittau, et al., *W and Z/ γ^* boson production in association with a bottom-antibottom pair*, *JHEP* **1109** (2011) 061, [[arXiv:1106.6019](#)].
- [308] C. Oleari and L. Reina, *$W^\pm b\bar{b}$ production in POWHEG*, *JHEP* **1108** (2011) 061, [[arXiv:1105.4488](#)].
- [309] J. M. Campbell and R. K. Ellis, *Radiative corrections to $Zb\bar{b}$ production*, *Phys.Rev.* **D62** (2000) 114012, [[hep-ph/0006304](#)].
- [310] K. Melnikov, M. Schulze, and A. Scharf, *QCD corrections to top quark pair production in association with a photon at hadron colliders*, *Phys.Rev.* **D83** (2011) 074013, [[arXiv:1102.1967](#)].
- [311] A. Lazopoulos, T. McElmurry, K. Melnikov, and F. Petriello, *Next-to-leading order QCD corrections to $t\bar{t}Z$ production at the LHC*, *Phys.Lett.* **B666** (2008) 62–65, [[arXiv:0804.2220](#)].
- [312] M. Garzelli, A. Kardos, C. Papadopoulos, and Z. Trocsanyi, *$t\bar{t}W^\pm$ and $t\bar{t}Z$ Hadroproduction at NLO accuracy in QCD with Parton Shower and Hadronization effects*, *JHEP* **1211** (2012) 056, [[arXiv:1208.2665](#)].
- [313] J. M. Campbell and R. K. Ellis, *$t\bar{t}W^\pm$ production and decay at NLO*, *JHEP* **1207** (2012) 052, [[arXiv:1204.5678](#)].
- [314] T. Stelzer and S. Willenbrock, *Single top quark production via $q\bar{q} \rightarrow t\bar{b}$* , *Phys.Lett.* **B357** (1995) 125–130, [[hep-ph/9505433](#)].
- [315] T. Stelzer, Z. Sullivan, and S. Willenbrock, *Single top quark production via W - gluon fusion at next-to-leading order*, *Phys.Rev.* **D56** (1997) 5919–5927, [[hep-ph/9705398](#)].
- [316] J. M. Campbell, R. K. Ellis, and F. Tramontano, *Single top production and decay at next-to-leading order*, *Phys.Rev.* **D70** (2004) 094012, [[hep-ph/0408158](#)].
- [317] J. M. Campbell, R. Frederix, F. Maltoni, and F. Tramontano, *NLO predictions for t-channel production of single top and fourth generation quarks at hadron colliders*, *JHEP* **0910** (2009) 042, [[arXiv:0907.3933](#)].
- [318] J. M. Campbell, R. Frederix, F. Maltoni, and F. Tramontano, *Next-to-Leading-Order Predictions for t-Channel Single-Top Production at Hadron Colliders*, *Phys.Rev.Lett.* **102** (2009) 182003, [[arXiv:0903.0005](#)].
- [319] J. M. Campbell and F. Tramontano, *Next-to-leading order corrections to Wt production and decay*, *Nucl.Phys.* **B726** (2005) 109–130, [[hep-ph/0506289](#)].
- [320] S. Frixione, E. Laenen, P. Motylinski, B. R. Webber, and C. D. White, *Single-top hadroproduction in association with a W boson*, *JHEP* **0807** (2008) 029, [[arXiv:0805.3067](#)].
- [321] S. Alioli, P. Nason, C. Oleari, and E. Re, *NLO single-top production matched with shower in POWHEG: s- and t-channel contributions*, *JHEP* **0909** (2009) 111, [[arXiv:0907.4076](#)].
- [322] E. Re, *Single-top Wt -channel production matched with parton showers using the POWHEG method*, *Eur.Phys.J.* **C71** (2011) 1547, [[arXiv:1009.2450](#)].
- [323] J. Campbell, R. K. Ellis, and R. Rontsch, *Single top production in association with a Z boson at the LHC*, *Phys.Rev.* **D87** (2013) 114006, [[arXiv:1302.3856](#)].

- [324] **LHC Higgs Cross Section Working Group** Collaboration, S. Dittmaier et al., *Handbook of LHC Higgs Cross Sections: 1. Inclusive Observables*, [arXiv:1101.0593](#).
- [325] S. Dittmaier, S. Dittmaier, C. Mariotti, G. Passarino, R. Tanaka, et al., *Handbook of LHC Higgs Cross Sections: 2. Differential Distributions*, [arXiv:1201.3084](#).
- [326] **LHC Higgs Cross Section Working Group** Collaboration, S. Heinemeyer et al., *Handbook of LHC Higgs Cross Sections: 3. Higgs Properties*, [arXiv:1307.1347](#).
- [327] J. Baglio, A. Djouadi, R. Gröber, M. Mühlleitner, J. Quevillon, et al., *The measurement of the Higgs self-coupling at the LHC: theoretical status*, *JHEP* **1304** (2013) 151, [[arXiv:1212.5581](#)].
- [328] T. Plehn, M. Spira, and P. Zerwas, *Pair production of neutral Higgs particles in gluon-gluon collisions*, *Nucl.Phys.* **B479** (1996) 46–64, [[hep-ph/9603205](#)].
- [329] S. Dawson, S. Dittmaier, and M. Spira, *Neutral Higgs boson pair production at hadron colliders: QCD corrections*, *Phys.Rev.* **D58** (1998) 115012, [[hep-ph/9805244](#)].
- [330] A. Signer and L. J. Dixon, *Electron - positron annihilation into four jets at next-to-leading order in α_s* , *Phys.Rev.Lett.* **78** (1997) 811–814, [[hep-ph/9609460](#)].
- [331] A. Signer, *Next-to-leading order corrections to $e^+e^- \rightarrow$ four jets*, [hep-ph/9705218](#).
- [332] Z. Nagy and Z. Trocsanyi, *Four jet production in e^+e^- annihilation at next-to-leading order*, *Nucl.Phys.Proc.Suppl.* **64** (1998) 63–67, [[hep-ph/9708344](#)].
- [333] Z. Nagy and Z. Trocsanyi, *Next-to-leading order calculation of four jet shape variables*, *Phys.Rev.Lett.* **79** (1997) 3604–3607, [[hep-ph/9707309](#)].
- [334] R. Frederix, S. Frixione, K. Melnikov, and G. Zanderighi, *NLO QCD corrections to five-jet production at LEP and the extraction of $\alpha_s(M_Z)$* , *JHEP* **1011** (2010) 050, [[arXiv:1008.5313](#)].
- [335] M. S. Bilenky, G. Rodrigo, and A. Santamaria, *Three jet production at LEP and the bottom quark mass*, *Nucl.Phys.* **B439** (1995) 505–535, [[hep-ph/9410258](#)].
- [336] C. R. Schmidt, *Top quark production and decay at next-to-leading order in e^+e^- annihilation*, *Phys.Rev.* **D54** (1996) 3250–3265, [[hep-ph/9504434](#)].
- [337] C. Oleari, *Next-to-leading order corrections to the production of heavy flavor jets in e^+e^- collisions*, [hep-ph/9802431](#).
- [338] P. Nason and C. Oleari, *Next-to-leading order corrections to the production of heavy flavor jets in e^+e^- collisions*, *Nucl.Phys.* **B521** (1998) 237–273, [[hep-ph/9709360](#)].
- [339] W. Bernreuther, A. Brandenburg, and P. Uwer, *Next-to-leading order QCD corrections to three jet cross-sections with massive quarks*, *Phys.Rev.Lett.* **79** (1997) 189–192, [[hep-ph/9703305](#)].
- [340] A. Brandenburg and P. Uwer, *Next-to-leading order QCD corrections and massive quarks in $e^+e^- \rightarrow$ three jets*, *Nucl.Phys.* **B515** (1998) 279–320, [[hep-ph/9708350](#)].
- [341] A. Brandenburg, *The Reaction $e^+e^- \rightarrow t\bar{t}g$ at next-to-leading order in α_s* , [hep-ph/9908383](#).
- [342] S. Dittmaier, M. Kramer, Y. Liao, M. Spira, and P. Zerwas, *Higgs radiation off top quarks in e^+e^- collisions*, *Phys.Lett.* **B441** (1998) 383–388, [[hep-ph/9808433](#)].

- [343] S. Frixione, P. Torrielli, and M. Zaro, *Higgs production through vector-boson fusion at the NLO matched with parton showers*, *Phys.Lett.* **B726** (2013) 273–282, [[arXiv:1304.7927](#)].
- [344] **ATLAS** Collaboration **ATLAS-CONF-2013-099** .
- [345] **CMS** Collaboration, S. Chatrchyan et al., *Measurement of differential top-quark pair production cross sections in pp collisions at $\sqrt{s} = 7$ TeV*, *Eur.Phys.J.* **C73** (2013) 2339, [[arXiv:1211.2220](#)].
- [346] **CMS** Collaboration **CMS-TOP-12-027** .
- [347] **CMS** Collaboration **CMS-TOP-12-028** .
- [348] **ATLAS** Collaboration, G. Aad et al., *Measurement of $t\bar{t}$ production with a veto on additional central jet activity in pp collisions at $\sqrt{s} = 7$ TeV using the ATLAS detector*, *Eur.Phys.J.* **C72** (2012) 2043, [[arXiv:1203.5015](#)].
- [349] **CMS** Collaboration **TOP-12-023** .
- [350] **CMS** Collaboration **TOP-12-041** .
- [351] S. Dittmaier and M. Kramer, *Electroweak radiative corrections to W boson production at hadron colliders*, *Phys.Rev.* **D65** (2002) 073007, [[hep-ph/0109062](#)].
- [352] A. Denner, *Techniques for calculation of electroweak radiative corrections at the one loop level and results for W physics at LEP-200*, *Fortsch.Phys.* **41** (1993) 307–420, [[arXiv:0709.1075](#)].
- [353] W. Beenakker, S. Dittmaier, M. Kramer, B. Plumper, M. Spira, et al., *NLO QCD corrections to $t\bar{t}H$ production in hadron collisions*, *Nucl.Phys.* **B653** (2003) 151–203, [[hep-ph/0211352](#)].
- [354] M. Whalley, D. Bourilkov, and R. Group, *The Les Houches accord PDFs (LHAPDF) and LHAGLUE*, [hep-ph/0508110](#).
- [355] M. Cacciari, S. Frixione, M. L. Mangano, P. Nason, and G. Ridolfi, *Updated predictions for the total production cross sections of top and of heavier quark pairs at the Tevatron and at the LHC*, *JHEP* **0809** (2008) 127, [[arXiv:0804.2800](#)].
- [356] R. D. Ball, L. Del Debbio, S. Forte, A. Guffanti, J. I. Latorre, et al., *A first unbiased global NLO determination of parton distributions and their uncertainties*, *Nucl.Phys.* **B838** (2010) 136–206, [[arXiv:1002.4407](#)].
- [357] D. E. Soper and M. Spannowsky, *Finding top quarks with shower deconstruction*, *Phys.Rev.* **D87** (2013), no. 5 054012, [[arXiv:1211.3140](#)].
- [358] D. E. Soper and M. Spannowsky, *Finding physics signals with event deconstruction*, [arXiv:1402.1189](#).
- [359] A. van Hameren, *OneLoop: For the evaluation of one-loop scalar functions*, *Comput.Phys.Commun.* **182** (2011) 2427–2438, [[arXiv:1007.4716](#)].
- [360] R. K. Ellis and G. Zanderighi, *Scalar one-loop integrals for QCD*, *JHEP* **0802** (2008) 002, [[arXiv:0712.1851](#)].
- [361] A. Denner and S. Dittmaier, *Reduction schemes for one-loop tensor integrals*, *Nucl. Phys.* **B734** (2006) 62–115, [[hep-ph/0509141](#)].

- [362] O. Tarasov, *Connection between Feynman integrals having different values of the space-time dimension*, *Phys.Rev.* **D54** (1996) 6479–6490, [[hep-th/9606018](#)].
- [363] G. Duplancic and B. Nizic, *Reduction method for dimensionally regulated one-loop N-point Feynman integrals*, *Eur.Phys.J.* **C35** (2004) 105–118, [[hep-ph/0303184](#)].
- [364] M. Cacciari, G. P. Salam, and G. Soyez, *FastJet User Manual*, *Eur.Phys.J.* **C72** (2012) 1896, [[arXiv:1111.6097](#)].
- [365] R. Kleiss, W. J. Stirling, and S. Ellis, *A New Monte Carlo Treatment of Multiparticle Phase Space at High-energies*, *Comput.Phys.Commun.* **40** (1986) 359.
- [366] L. Garren and P. Lebrun, *StdHEP v5 manual*, <http://cepa.fnal.gov/psm/stdhep/>.
- [367] G. P. Lepage, *A New Algorithm for Adaptive Multidimensional Integration*, *J.Comput.Phys.* **27** (1978) 192.
- [368] G. P. Lepage, *VEGAS: an adaptive multidimensional integration program*. CLNS-80/447, 1980.